Supergene enrichment and exotic mineralization at Chuquicamata, Chile

Pinget, Marie-Caroline

UNIVERSITE DE GENEVE
Section des Sciences de la Terre et de l'Environnement
Département des Sciences de la Terre
Mineral Resources and Geofluids

FACULTE DES SCIENCES

Professeur Lluís Fontboté
Professeur Bernhard Dold

Supergene enrichment and exotic mineralization at Chuquicamata, Chile

THÈSE

soumise à la Faculté des sciences de l'Université de Genève pour obtenir le grade de Docteur ès Sciences, mention Sciences de la Terre

par

Marie-Caroline Pinget
de
Carouge (GE)

Thèse N° 5003

Genève
2016

Contents

UNIVERSITÉ DE GENÈVE

FACULTÉ DES SCIENCES

Doctorat ès sciences
Mention sciences de la Terre

Thèse de *Madame Marie-Caroline PINGET MORALES OPAZO*

intitulée :

"Supergene Enrichment and Exotic Mineralization at Chuquicamata, Chile"

La Faculté des sciences, sur le préavis de Monsieur L. FONTBOTE, professeur ordinaire et directeur de thèse (Département des sciences de la Terre), Monsieur B. DOLD, professeur et codirecteur de thèse (Luleå Technical University, Sweden), Monsieur M. ZENTILLI, professeur (Dalhousie University, Nova Scotia, Canada), autorise l'impression de la présente thèse, sans exprimer d'opinion sur les propositions qui y sont énoncées.

Genève, le 25 octobre 2016

Thèse - 5003 -

Le Doyen

N.B. - La thèse doit porter la déclaration précédente et remplir les conditions énumérées dans les "Informations relatives aux thèses de doctorat à l'Université de Genève".

Acknowledgements

I would like to thank B. Dold and L. Fontboté who let me the opportunity to work on this thesis, and help me to bring it to a successful conclusion, and to Marcos Zentilli (Dalhousie University) for his kind review. The constructive collaboration with the geologic team of the Chuquicamata mine (CODELCO) made this work possible; I specially thank Manuel Vergara, Fernando Ramirez, Victorino Moyano, and their collaborators, and specially Carlos Barrios, for their inestimable help, and for their very friendly reception. I also thank, at the University of Geneva, A. Martigner for the SEM analyses, K. Kouzmanov for the QEMSCAN® analyses, R. Spikings for the $^{39}Ar/^{40}Ar$ datations, J. Poté for the ICP analyses, D. Ariztegui, S. Castelltort, and R. Cerny for their helpful advises, F. Capponi for the XRF analyses and J.-M. Boccard and Frederic Arlaud for the technical support. The project was financed by the Swiss National Science Foundation Project FN129988.

Abstract

The Chuquicamata giant porphyry copper deposit, located north of Chile in the Atacama Desert, 20 km to the North of the city of Calama, is part of the Eocene-Oligocene Porphyry copper belt extending in northern Chile and southern Peru. The Chuquicamata district, estimated to contain more than >130 Mt Cu, includes four porphyry copper deposits, i.e., Chuquicamata deposit (100 Mt Cu including reserves and extracted), Radomiro Tomic deposit, Ministro Hales mine and Toki cluster, and two exotic copper oxide deposits, to the north and to the south of the Chuquimata deposit. The latter one, Exótica deposit with a resource of 6 Mt Cu that was mined between the 1960's and 2015, is located directly south of the Chuquimata deposit, and is eponym for secondary oxide deposits formed by lateral flux of supergene solutions. Published studies dated the emplacement of the Chuquicamata porphyry system between 35.2±0.2 Ma and 32.8±0.2 Ma (U/Pb on zircon). The hypogene hydrothermal alteration is constituted by early "potassic" and "chloritic" hydrothermal stages and a late "quartz-sericite" (may also be termed argillic) hydrothermal stage. The potassic hydrothermal alteration zone, with little pyrite and mineral associations containing mainly chalcopyrite - bornite, bornite - digenite - chalcopyrite, some coarse grained covellite, and abundant digenite - covellite, was dated between 33.9±0.3 Ma and 30.9±0.3 Ma ($^{40}Ar/^{39}Ar$ on biotite and K-feldspar). The chloritic hydrothermal alteration zone, with pyrite - chalcopyrite (in propylitically altered rocks containing chlorite and epidote) was dated between 33.7±0.2 Ma and 35.2±0.2 Ma ($^{40}Ar/^{39}Ar$ on biotite and K-feldspar). The late quartz-sericite hydrothermal alteration stage, with pyrite - chalcopyrite - bornite, pyrite - bornite - digenite - enargite, and pyrite - digenite - covellite – enargite, was dated between 31.1±0.2 Ma and 32.1±0.2 Ma ($^{40}Ar/^{39}Ar$ on biotite, sericite and K-feldspar). The hypogene copper grades varies with the hydrothermal alteration zone, with mean copper grades of 0.72 wt%, 0.63wt% and 0.24wt% in the quartz-sericite, potassic and chloritic hydrothermal alteration zone. Hydrothermal alteration zones have a roughly vertical orientation.

A well developed supergene profile of up to 1 km depth is observed in the Chuquicamata porphyry copper deposit. The oxidation zone has a more or less constant thickness of around 200 m, and presents copper grades that largely but not exclusively depend on the preexisting hypogene copper grade and hydrothermal alteration zone. Calculated mean copper grades are of 0.42, 1.08 and 0.50 wt%, in the present quartz-sericite, potassic and chloritic hydrothermal alteration zones respectively.

The copper amount contained in the oxidation zone is mainly present as copper minerals and mineraloids, including mainly anthlerite, brochantite, copper wad, and chrysocolla. Element mapping shows also that part of the copper is present in Fe oxides and hydroxides. Previous studies described, in the nowadays totally mined central part of the Chuquicamata deposit, a perched chalcocite blanket. The latter, combined with the high mean copper grade in the oxidation zone, has been interpreted as an immature oxidation zone, consequence of the Middle-Late Miocene Andean uplift, and of the subsequent rapid drop of the oxidation front in the supergene profile. The arid to hyperarid climatic conditions at least occuring after 15 Ma, even if wetter periods surly occurred, allowed the preservation of the supergene profile.

The supergene sulfide enriched zone is constituted by a chalcocite blanket, mostly developed in the quartz-sericite hydrothermal zone, overlying a covellite dominated supergene sulfide enriched zone. Mean copper grades in the chalcocite blanket and in the covellite dominated supergene sulfide enriched zone are of 2.44 and 1.00 wt% in the quartz-sericite hydrothermal alteration zone, 1.73 and 0.82 wt% in the potassic hydrothermal alteration zone and of 1.00 and

0.72 wt% in the chloritic hydrothermal alteration zone. Previously published supergene alunite K/Ar ages in the oxidation zone of Chuquicamata span between 19.0±0.7 Ma and 15.2±0.7 Ma. Geological constraints suggest that supergene processes were mainly active during the Late Oligocene - Early Miocene Andean uplift. A mass balance model, based on 40 W-E vertical sections using CODELCO Cu grade data, has shown north-south, and also in a lesser extent west-east transport of supergene solutions yielding a 0.5 Mt of "copper excess" in the southern part of the deposit. According this model, erosion of thickness of around 900 m of hydrothermal altered porphyry is necessary to provide the copper today contained in the different parts of the supergene profile of Chuquicamata and in the Exótica deposit.

A detailed mineralogical study has been carried out along three representative vertical W-E sections using largely legacy material archived at the Chuicamata deposit. The principal supergene sulfide in the lower part of the supergene sulfide enriched zone is covellite, progressively replaced by chalcocite dominating in the higher part and almost totally replacing the hypogene sulfides. In the upper part of the supergene sulfide enriched zone in the northern extent of the deposit, chalcocite presents rims of covellite indicating a subsequent oxidation processes, probably related with the Middle-Late Miocene Andean uplift. The sulfide textures were used to discriminate between supergene and hypogene origin, and use to determine the lower limit of the supergene processes.

Sphalerite rimming copper sulfides that in previous studies was proposed to be of supergene origin has been reinterpreted as belonging to a late hydrothermal stage, using microscopic observations and scanning electronic microscope (SEM) backscattered electron imaging and electron microprobe analyses on samples from a central and a southern vertical section. The following scenario is proposed to explain the formation of the peculiar “sphalerite rims”: (1) precipitation of chalcopyrite, typical of the early and main hydrothermal stages; (2) precipitation of sphalerite rimming chalcopyrite and in voids and in weakness sites during the late hydrothermal stage; (3) partial or total replacement of chalcopyrite by chalcocite-digenite during the late hydrothermal stage; and (4) formation of lamellar covellite, principally at the expense of chalcopyrite, suggesting increasingly oxidizing and/or acidic conditions. This covellite may be linked to supergene processes and/or to the late hydrothermal stage.

The lower limit of the supergene profile obtained in the present work based on the study of the sulfide textures is significantly higher than the lower limit of the supergene processes obtained in the CODELCO 3D mine model that uses the presence of anhydrite as indicator of absence of supergene processes and the presence of gypsum and porosity due to dissolution of anhydrite to identify circulation of supergene solutions. In the quartz-sericite zone, the CODELCO model places the lower limit for the supergene sulfide enrichment zone up to 800 m deeper than the limit revcognized in the present study. Recognition of these disparities is of importance for the estimation of the copper resource of the deposit, as the sectors with the largest differences between the two methods are the ones with the strongest the supergene sulfide enrichment.

The copper bearing phases in the Exótica deposit are mainly chrysocolla, copper wad and copper pitch, all the three phases showing high composition variability. Sequential extraction combined with sequential X-ray diffraction and inductively coupled plasma spectrometry (ICP) analyses on solutions applied to copper pitch samples from the Exótica deposit show the presence of crystalline birnessite containing main of the manganese, together with other crystalline phases as libethenite, atacamite, and gypsum. Small amounts of phyllosilicates (smectite and kaolinite groups) are also detected. An important pseudo amorphous component

is present too, with a behavior during sequential extraction very similar to the behavior observed in chrysocolla.

Contemporaneously with the sulfide oxidation occurring at the Chuquicamata main ore, the mineralization sequence in the Exótica deposit develops by the lateral flow of acidic solutions (acid rock drainage, ARD). They form first by interaction of rainwater with soluble salts at the surface of the Chuquicamata oxidation zone, which results in a decrease of the pH (1-3) and increase of the Eh (>1 [V]). Interaction of these solutions with the oxidation zone of the Chuquicamata deposit results in a slight increase of pH (around 2-4) and a slightly more reducing environment (Eh around 0.5 - 1 [V]) and increase of the Cu and Mn concentration. Due to water-rock interactions, the solutions, which were flowing latterly south will increase pH, triggering chrysocolla precipitation. If the pH increases more due to neutralization reactions, birnessite becomes oversaturated and copper wad can form further south of the source. As a constant ARD supply during a long time frame can be assumed, acid solutions consumed the neutralization potential of the gangue mineralogy along the flow path, altering through dissolution and precipitation to the final altered (kaolinitized) tube present in the center of the Exótica deposit. This explains also the present dominance of chrysocolla at the end of the tube and at the base of the ore, as well the presence of copper wad at the further southern part of Exótica. While chrysocolla /copper pitch massive veins have to form under low flow regime, in desiccation cracks or even in surface ponds, the precipitation of copper wad should be mainly controlled by the local Eh-pH and chemical composition of the solution due to water-rock interaction.

The Exótica deposit rests on the southern end of the supergene profile of the Chuquicamata deposit suggesting that if the Exótica deposit was formed during the main Late Oligocene - Early Miocene supergene stage, it should have been at the end of the event. Alternatively, the Exótica deposit could result from leaching of exposed immature supergene profile because of a subsequent Middle - Late Miocene Andean uplift and, consequently, a rapid drop of the oxidation front. According the second hypothesis, copper contained in the oxidation zone, partly as soluble salts, and in relictic sulfides including the chalcocite blanket "perched" in the oxidation zone, could be leached. The soluble salts, mainly acid-bearing sulfates, would trigger the acidity necessary to explain strong acidic alteration observed in parts of Exótica deposit. In both alternatives, i.e., formation at the end of the 19-15 Ma main supergene enrichment event at Chuquicamata, or during the subsequent Middle - Late Miocene Andean uplift, onset of hyperaride would strongly slow down supergene processes. The second alternative would therefore imply either a delayed onset of hyperarid conditions, or the existence of important wet episodes during a general hyperarid climate climate.

Résumé en français

Le gisement de type porphyre cuprifère de Chuquicamata est situé au nord du Chili, dans le désert d'Atacama, à 20 km au nord de la ville de Calama et à 200 km au nord-est de celle d'Antofagasta. Le district minier de Chuquicamata (>130 Mt de cuivre), est constitué de quatre porphyres cuprifères (gisements de Chuquicamata, Radomir Tomic, Ministro Hales et Toki) et de deux gisements de type exotiques, situés au nord et au sud de Chuquicamata. Le second, le gisement Exótica (6 Mt de cuivre), est éponyme pour les gisements d'oxydes secondaires provenant de l'écoulement de solutions supergènes à l'extérieur du gisement primaire. Il a été exploré et exploité entre les années 1960 et 2015, et s'étend sur plus de 7 km, au-dessus du profil supergène de Chuquicamata dans son extrémité sud, et au sud de celui-ci.

Des études antérieures ont daté la mise en place du système porphyrique de Chuquicamata entre 35.2±0.2 Ma et 32.8±0.2 Ma (U/Pb sur zircon). L'altération hydrothermale hypogène est principalement constituée de deux évènements précoces, les altérations hydrothermales potassique et chloritique, et d'un évènement tardif acide, l'altération hydrothermale quartz-séricite. L'altération hydrothermale potassique (contenant typiquement peu de pyrite, et des assemblages de sulfures digénite-covellite, chalcopyrite-bornite, bornite-digénite-chalcopyrite, et quelques grains grossiers de covellite) a été datée entre 33.9±0.3 Ma et 30.9±0.3 Ma ($^{40}Ar/^{39}Ar$ sur biotite et feldspath potassique). L'altération hydrothermale chloritique (contenant comme sulfures principaux des assemblages pyrite-chalcopyrite dans une roche présentant une altération propylitique, avec de la chlorite et de l'épidote), a été située entre 33.7±0.2 Ma et 35.2±0.2 Ma ($^{40}Ar/^{39}Ar$ sur biotite et feldspath potassique). L'altération hydrothermale quartz-séricite (contenant typiquement des associations de sulfures telles que pyrite - chalcopyrite - bornite, pyrite - bornite - digénite - énargite, et pyrite - digénite - covellite - énargite), a été datée entre 31.1±0.2 Ma et 32.1±0.2 Ma ($^{40}Ar/^{39}Ar$ sur biotite, séricite et feldspath potassiques). Les teneurs en cuivre hypogène varient en fonction de la zone d'altération hydrothermale concernée, avec des valeurs moyennes de 0.72 %pds, 0.63 %pds et 0.24 %pds respectivement dans les zones quartz-séricite, potassique et chloritique. Les zones d'altération hydrothermales ont une orientation générale verticale.

Un profil supergène bien développé, d'une extension verticale atteignant jusqu'à 1 km, est observé dans tout le gisement. La zone d'oxydation a une épaisseur constante d'environ 200 m sur tout le gisement; la teneur en cuivre dépend en grande partie de l'altération hydrothermale, notamment en raison de différences du potentiel de neutralisation et d'acidification de l'assemblage minéralogique hypogène. Les teneurs moyennes en cuivre dans la zone d'oxydation sont de 0.42, 1.08 et 0.50 %pds respectivement dans les zones d'altération hydrothermales quartz-sericite, potassique et chloritique.

Le cuivre de la zone d'oxydation est principalement contenu sous la forme d'anthlérite et de brochantite, et de minéraloïdes tels que le copper wad et la chrysocolle. La cartographie des éléments chimiques, obtenue grâce au QEMSCAN indique que le cuivre est également présent associé à des oxydes et hydroxydes de cuivre. Des études préalables ont également montré la présence d'un niveau de chalcocite perché dans la zone d'oxydation, dans la partie aujourd'hui entièrement excavée de la mine. Cette dernière observation, en plus de la teneur anormalement élevée en cuivre dans la zone d'oxydation, est interprétée comme la conséquence du soulèvement andin ayant eu lieu entre le milieu et la fin du Miocène, et de la conséquente rapide descente du front d'oxydation. La préservation du profil supergène a été permise par les conditions climatiques arides à hyperarides dans le bassin de Calama, en place depuis environ 15 Ma, même si des périodes plus humides ont sûrement existé.

La zone d'enrichissement en sulfures supergènes est constituée par un niveau de chalcocite, principalement développé dans la zone d'altération hydrothermale quartz-séricite, et d'un niveau sous-jacent dans lequel le sulfure supergène principal est la covellite. Les teneurs en cuivre moyennes dans ces deux niveaux sont de 2.44 et 1.00 %pds dans la zone d'altération quartz-séricite, de 1.73 et 0.82 %pds dans la zone d'altération potassique, et de 1.00 et 0.72 %pds dans la zone d'altération chloritique. Des études antérieures ont daté les processus supergènes entre 19.0±0.7 Ma et 15.2±0.7 Ma (K/Ar sur alunite supergène). Le contexte géologique et tectonique de la région suggèrent que l'épisode supergène principal a probablement eu lieu pendant le soulèvement andin de la fin de l'Oligocène - début du Miocène. Un modèle de balance de masse, basé sur 40 sections verticales couvrant tout le gisement a montré un transport de cuivre supergène du nord vers le sud, et dans de moindre mesures d'ouest en est, et un excès de cuivre de 0.5 Mt dans la partie sud du gisement. En accord avec ce modèle, l'épaisseur de porphyre minéralisé nécessaire pour fournir le cuivre supergène aujourd'hui contenu dans le profil supergène et dans le gisement exotique a été estimée de 900 m.

Une étude minéralogique a été menée sur trois section verticales orientées est-ouest, en utilisant principalement le matériel d'archive conservé sur le site de la mine. La texture des sulfures a été utilisée pour différencier les sulfures d'origine supergène de ceux d'origine hypogène, et ainsi définir une limite inférieure pour les processus supergènes. Des grains de sulfures de cuivre entourés d'une bordure de sphalérite, qui avaient été préalablement publiés comme étant d'origine supergène, ont été réinterprétés dans cette étude comme étant d'origine hypogène. La limite inférieure des processus supergènes, obtenue sur la base des textures des sulfures a été comparée avec celle définie dans le modèle 3D de la mine de CODELCO, basée sur la présence d'anhydrite comme indicateur d'une absence de processus supergène, et sur la présence de gypse et/ou de porosité comme indicateur du passage de solutions supergènes.

Dans la zone d'altération hydrothermale quartz-séricite, le modèle de CODELCO place la limite inférieure des processus supergènes jusqu'à 800 m plus bas que la limite définie dans cette étude. Les disparités entre ces deux méthodes doivent être prises en compte lors de l'estimation des ressources en cuivre d'un gisement, en particulier parce que ces différences sont plus importantes dans les zones les plus riches du gisement.

Dans le gisement Exótica, le cuivre est principalement présent sous forme de chrysocolle, copper pitch et copper wad, trois phases pseudo-amorphes et de composition chimique variable. L'extraction séquentielle combinée à la diffraction de rayons X et à la spectrométrie à plasma à couplage inductif (ICP) sur les solutions, appliquées à des échantillons de copper pitch et chrysocolle, montrent que ces deux matériaux sont principalement constitués d'une fraction pseudo-amorphe identique, combinée dans le cas de la chrysocolle avec de la libéthénite, et dans le cas du copper pitch avec de l'atacamite et de la birnessite, ainsi que dans les deux cas, de gypse et d'une petite quantité de phyllosilicates.

Un model conceptuel est proposé pour expliquer la formation du gisement Exótica en quatre étapes: (1) interaction de l'eau de pluie avec les sulfates acides solubles présents dans la partie supérieure de la zone d'oxydation, provocant une baisse du pH (1-3) et une augmentation du Eh (>1 [V]); (2) interaction de la solution avec la zone d'oxydation du gisement de Chuquicamata, pH autours de 2-3 et Eh autours de 1 [V]; (3) interaction de la solution avec le tube altéré (kaolinitisé) au centre du gisement Exótica, pH 2-3, Eh autours de 0.7 [V]; (4) interaction de la solution avec sédiments non altéré et du substratum rocheux, propagation du tube altéré, augmentation du pH, précipitation de chrysocolle et copper pitch / wad. La chrysocolla et le

copper pitch forment des veines massives, et précipitent dans des fissures de dessiccation et même dans des plans d'eau de surface temporaire, en régime de basse énergie. Le copper wad, qui précipite sous forme de patine et de ciment, a une précipitation largement contrôlée par les interactions eau-roche, qui induisent des changements locaux de Eh, pH et composition chimique des solutions, et a de ce fait une nature plus inhomogène.

Le gisement Exótica est sus-jacent à l'extension sud du profil supergène de Chuquicamata, ce qui suggère que si la formation du gisement exotique a également eu lieu pendant l'épisode de soulèvement andin de la fin de l'Oligocène - début du Miocène, cela a du avoir lieu à la fin de celui-ci. Un scénario alternatif est proposé, dans lequel la formation du gisement exotique est principalement relié à l'épisode de soulèvement andin ayant eu lieu entre le milieu et la fin du Miocène, en conséquence des changements hydrogéologiques induits par cet épisode. Quel que soit le scénario considéré, le climat joue un rôle déterminant, et une mise en place plus récente que celle proposée au plus tard autours de 15 Ma par certains auteurs, ou des évènements plus humides au sein de ce climat hyperaride, doivent être envisagés.

Introduction

The general aim of the project was to understand qualitatively and, as far as possible, quantitatively the supergene processes (leaching and mineralization) at the giant porphyry copper of Chuquicamata, one of the largest ore deposits in the world, including those leading to the formation of a downstream exotic deposit.

The project received four years funding from SNF and logistic support of CODELCO. The field work was carried out between May 10th, and August 29th 2010, and between 2011, September 9th and October 6th, 2011. During the first field campaign a comprehensive image of the deposit was obtained using the 3D CODELCO mine model processed with Vulcan Mining Software, and to the best vertical profiles to study the supergene and exotic processes were selected. Material for this study was sampled in the pits of the Mina Sur (Exótica deposit) and Chquicamata mines mines, in drill cores, and in the CODELCO archives. The field work of a complementary Master Thesis (Lambiel, 2014), focused on gel-like precipitates occurring at Mina Sur considered to be potential precursors of crhysocolla and other Cu supergene minerals, partly coincided with the second field campaign.

The Thesis manuscript consists of following three chapters and five Annexes:

1) "Supergene profile of the Chuquicamata porphyry deposit (northern Chile): mineralogy, textural characteristics, and mass balance"

2) "Mineralogical and geochemical characterization of “Copper wad”, “Copper pitch”, and chrysocolla at Chuquicamata, Chile: Implications for the genesis of the Exótica Deposit"

3) "Reported "supergene" sphalerite rims at the Chuquicamata porphyry deposit (northern Chile) revisited: evidence for a hypogene origin". (already published in Economic Geology, Pinget et al., 2015)

The present Thesis leaves several open questions. A stable isotopic study that should help to trace the principal oxidants implied in the oxidation processes was not performed. In addition, the results obtained in the present work suggest that the waters that migrated laterally and formed the Exótica deposit were not purely meteoric but that in the late stages included basinal brines. A chlorine isotope study of atacamite and other Cl-bearing minerals, together with sulfur and oxygen isotope data, would contribute to solve this question. Finally, the timing of the formation of the Exótica Deposit was only bracketed by geological constraints as $^{40}Ar/^{39}Ar$ dating on alunite failed and a new dating attempt was not finished before completion of the Thesis manuscript.

Lambiel, F., 2014, New insights into the ore genesis of the Exótica deposit at Chuquicamata (Northern Chile) through the neoformation of Cu-oxide minerals from gel-like precursors. Master thesis, University of Geneva, 96 p.

Pinget M., M.C., Dold, B., Zentilli, M. and Fontboté, L., 2015, Reported supergene sphalerite rims at the Chuquicamata porphyry deposit (northern Chile) revisited: evidence for a hypogene origin: Economic Geology, v. 110, pp. 253–262.

Chapter 1

Supergene profile of the Chuquicamata porphyry deposit (northern Chile): mineralogy, textural characteristics, and mass balance

Marie-Caroline Pinget M.[1]

Department of Earth Sciences, University of Geneva, rue de Maraîchers 13, Geneva, Switzerland

Lluís Fontboté

Department of Earth Sciences, University of Geneva, rue de Maraîchers 13, Geneva, Switzerland

Bernhard Dold

Division of Geosciences and Environmental Engineering, Luleå University of Technology, Luleå, Sweden.

[1] Corresponding author: marie-caroline.pinget@unige.ch

Abstract

The Chuquicamata giant porphyry copper deposit is part of the Eocene-Oligocene Porphyry copper belt extending in northern Chile and southern Peru and was emplaced between 35.2±0.2 Ma and 32.8±0.2 Ma (U/Pb on zircon). An up to 1 km deep well developed supergene profile is observed at Chuquicamata. The oxidation zone has a more or less constant thickness of around 200 m and mean copper grades of 0.42, 1.08 and 0.50 wt%, in the quartz-sericite, potassic and chloritic hydrothermal alteration zones respectively. The high mean total copper grade in the oxidized hydrothermal potassic alteration zone reflects its higher neutralization potential. Copper is mainly contained in anthlerite, brochantite, chrysocolla and copper wad, in iron oxides and hydroxides, and as in relictic sulfides including a perched chalcocite blanket described previously. The supergene sulfide enriched zone is constituted by (i) a chalcocite blanket, mostly developed in the quartz-sericite alteration zone, and (ii) a covellite dominated supergene sulfide enriched zone underlying the chalcocite blanket. Mean copper grades in the chalcocite blanket and in the covellite dominated supergene sulfide enriched zone are of 2.44 and 1.00 wt% in the quartz-sericite hydrothermal alteration zone, 1.73 and 0.82 wt% in the potassic alteration zone and of 1.00 and 0.72 wt% in the chloritic alteration zone.

A detailed mineralogical study has been carried out along three representative vertical W-E sections largely using legacy material. In the lower part of the supergene sulfide enriched zone the main mineral is covellite, progressively replaced by chalcocite, mineral that dominates the higher part by almost totally replacing the hypogene sulfides. In the upper part of the supergene sulfide enriched zone, in the northern part of the deposit, chalcocite presents rims of covellite indicating a subsequent oxidation processes. Sulfide textures were used to discriminate between supergene and hypogene origin, and used to determine the lower limit of the supergene processes.

A mass balance model, based on 40 W-E vertical sections using CODELCO Cu grade data, has shown north-south, and also in a lesser extent east-west transport of supergene solutions yielding a 0.5 Mt of "copper excess" in the southern part of the deposit. According this model, erosion of a around 900 m thick portion of hydrothermal altered porphyry is necessary to provide the copper today contained in the different parts of the supergene profile of Chuquicamata and in the Exótica deposit.
Previously published supergene alunite K/Ar ages in the oxidation zone of Chuquicamata span between 19.0±0.7 Ma and 15.2±0.7 Ma. Geological constraints suggest that supergene processes were mainly active during the Late Oligocene - Early Miocene Andean uplift. The distinguishing character of the oxidation zone is a relatively high copper contents, which may result form the Middle-Late Miocene Andean exhumation, and of the subsequent rapid drop of the oxidation front in the supergene profile, oxidation that could also explain the rims of covellite on chalcocite. The arid to hyperarid climatic conditions occuring after 15 Ma, even if wetter periods possibly occurred, allowed the preservation of the supergene profile.

1.1. Introduction

Supergene enrichment may significantly increase the grade of low grade ores to economic interesting ore deposits, and has been extensively studied (e.g., Gottschalk and Buehler, 1912; Schwartz, 1934; Brimhall et al., 1985; Ague, 1989; Alpers and Brimhall, 1989; Sato, 1992; Plumlee, 1999; Sillitoe, 2005). An important stage of supergene enrichment in the porphyry copper deposits of the northern Chile took place between 22 and 15 Ma, with some younger ages in the southern Atacama desert, and has been studied in several works, also for the paleoclimatic implications (e.g., Sillitoe and McKee, 1996; Perelló et al., 2010; Alpers and Brimhall, 1988; Arancibia et al., 2006). In the giant porphyry copper deposit of Chuquicamata, Chile (> 130 Mt Cu resources and past production for the whole Chuquicamata district including Radomiro Tomic and Ministro Hales Mine (Fig. 1), Rivera et al., 2012, and 98.4 Mt Cu for the Chuquicamata deposit, Ossandón and Zentilli, 1997) the supergene processes are very important, leading to a more than 1 km deep supergene profile in the richest part of the deposit. In addition exotic deposits occur both north and south of the Chuquicamata deposit, the latter constitutes the Exótica deposit (Newberg, 1967; Mortimer, 1978; Chapter 2 of this work), where the exotic model was defined (Münchmeyer, 1996) and represents one of the known largest deposits of this type (5.1 MT Cu, Ossandón and Zentilli, 1997). Its genesis will be discussed in detail in Chapter 2 (Pinget et al., in prep.)

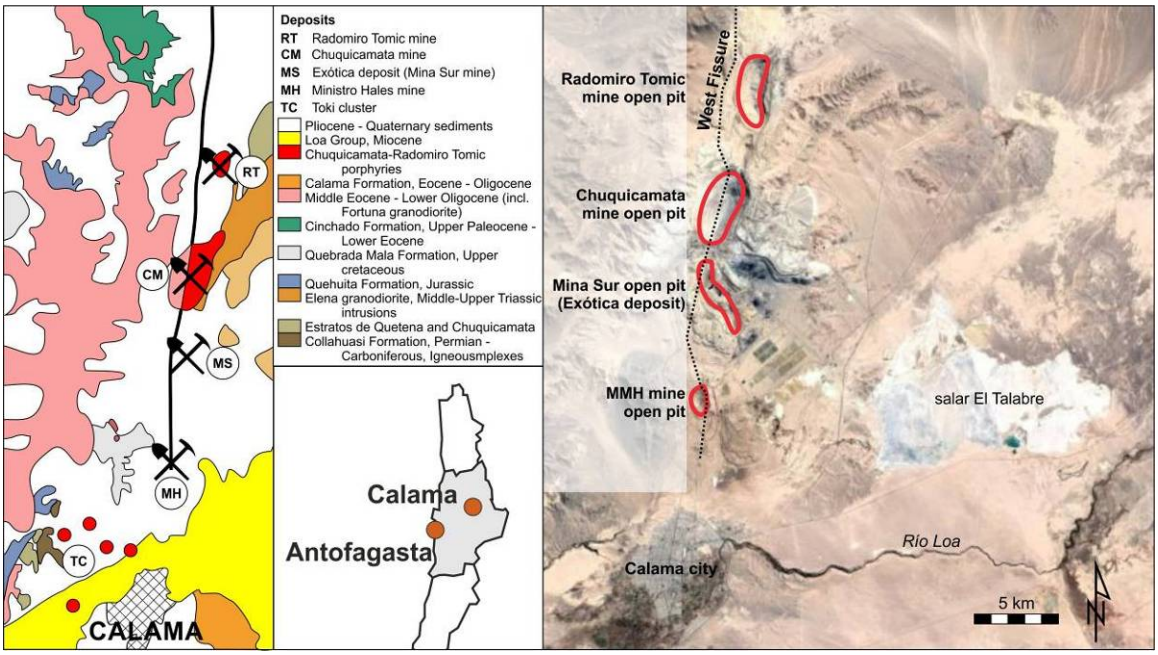

Figure 1: General geography of the Chuquicamata district (Image Google© 2016).

Mineralogical and geological descriptions of supergene alteration and enrichment at the porphyry copper deposit of Chuquicamata, were provided by Bandy (1938), López (1939) and Jarrell (1944). Ossandón et al. (2001), in their general description of the deposit, summarize also the main available data on supergene processes at Chuquicamata. A modern detailed description of the supergene alteration profile at Chuquicamata was lacking in order to get a deeper insight into the genesis of the deposit, and this constitutes the first part of the present paper. The investigation is based on microscopic observation, presented in abundant graphic illustrations, as there are virtually no published pictures of supergene textures at Chuquicamata, on scanning electron microscope, element mapping using QEMSCAN®, X-ray fluorescence chemical analyses, and sequential extraction analysis. The detailed study has been

performed in three vertical sections perpendicular to the roughly North-South trending hydrothermal alteration zones (Fig. 2). The investigation makes also use of legacy data archived at the mine site including, in places, detailed logs of parts of the deposit, which were mined during the past century (Fig. 3).

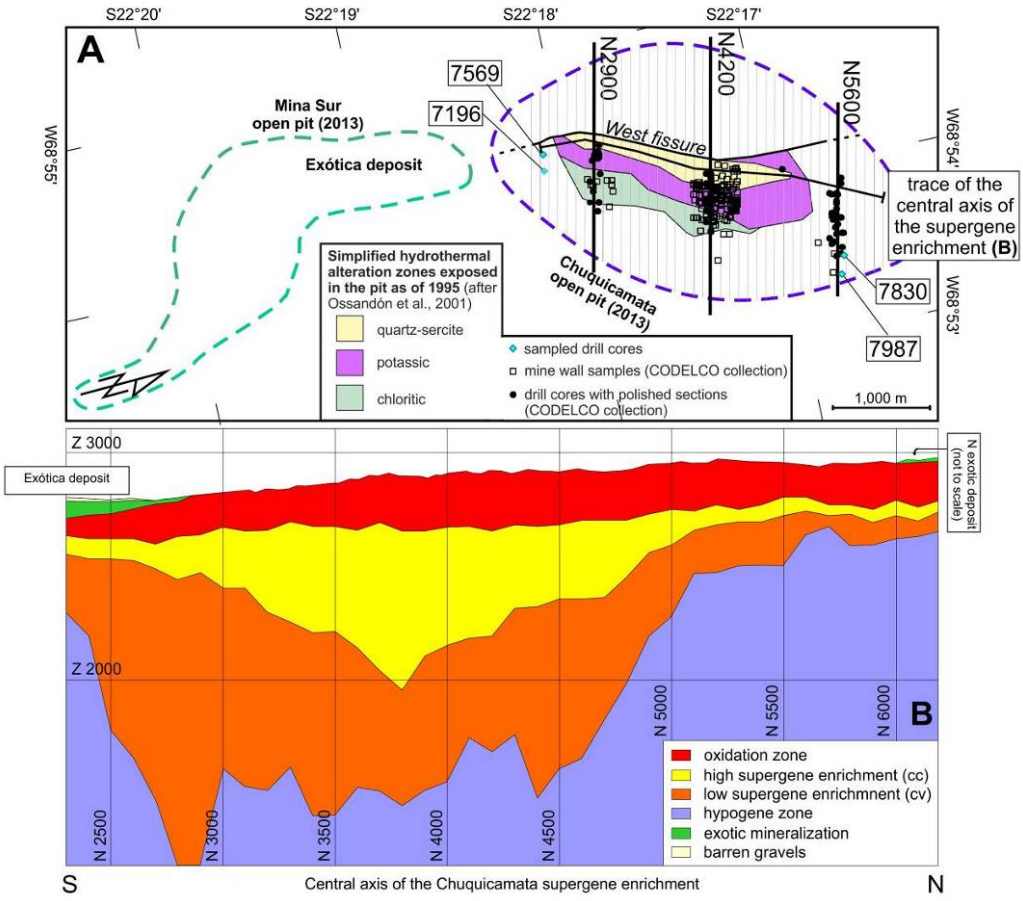

Figure 2: A. Outline of the Chuquicamata and Mina Sur open pits and location of the sections used for the mass balance calculations. B. Vertical roughly S-N section along the central axis of the supergene enrichment profile. Note also position of the extoci deposits (green).

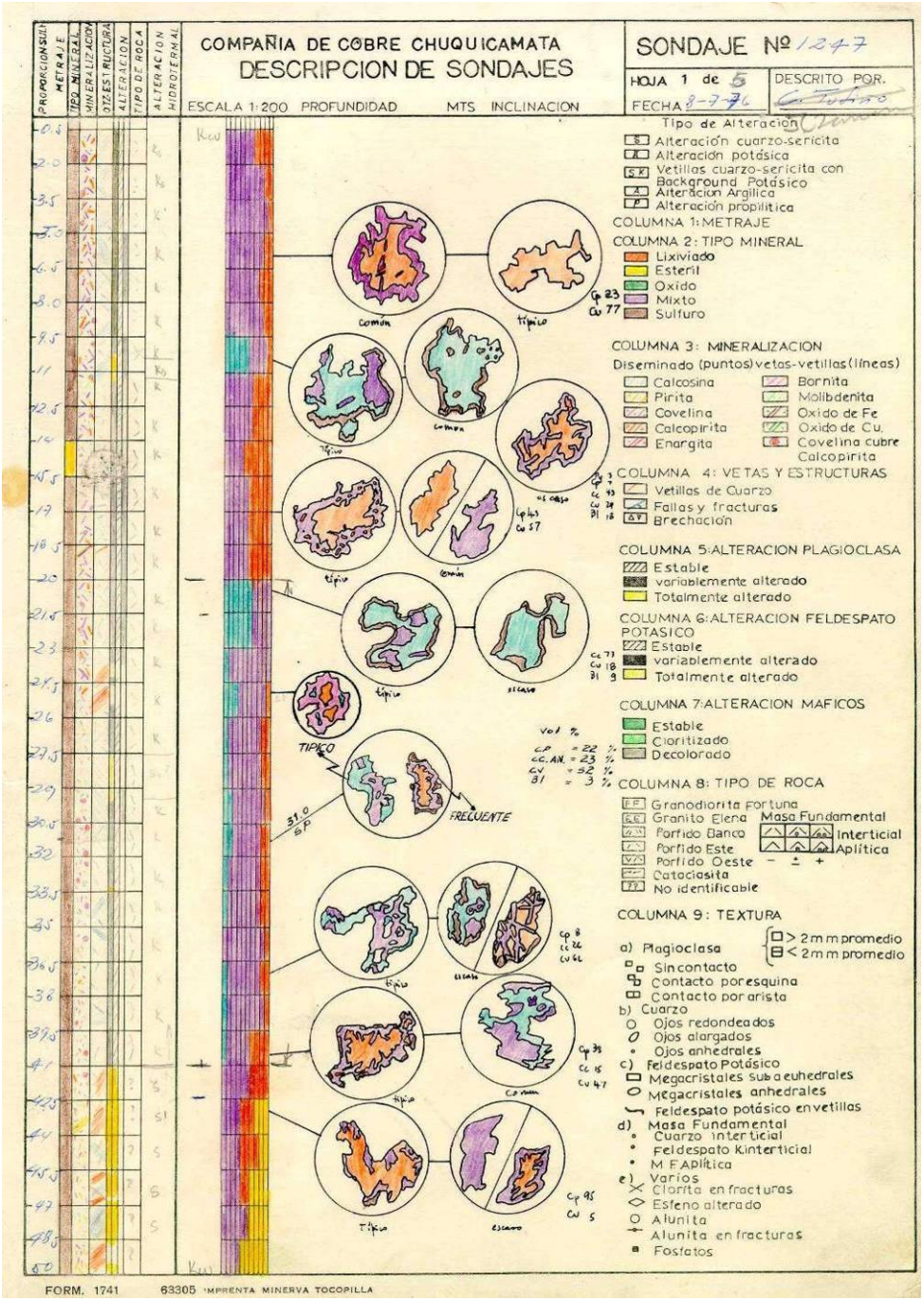

Figure 3: Example of the archived drillcore log (CHDD1247, 0 to 50 meters depth, CODELCO staff 1976, unpublished) used to reconstruct the supergene alteration

The general principles of supergene enrichment in copper deposits are well known and supergene enrichment in the porphyry environment is one of the few ore-making processes, where mass balance calculations have been applied successfully at the deposit scale (e.g., Brimhall et al. 1985, Alpers and Brimhall, 1989). In this study, a mass balance model has been developed at Chuquicamata to evaluate the vertical and lateral fluxes and the amount of copper mobilized during the supergene processes. This constitutes the second part of the study.

Although an attempt to $^{40}Ar/^{39}Ar$ date supergene alunite from the Exótica deposit and so complement the existing K/Ar ages on supergene alunite from Chuquicamat obtained by

Sillitoe and McKee (1996), was not successful, the new mineralogic data and the mass balance combined to previous geochronological and geological data put constraints on the evolution of the supergene profile in Chuquicamata and on the Exótica Deposit. The obtained results have been compared with published data on the regional geology, tectonics, geomorphology, and climate, with the aim of identifing a temporal window favorable to the development of the supergene profile.

The present work is part of a more comprehensive study of supergene processes at Chuquicamata, that includes a detailed characterization of assemblages typical for the Exótica deposit containing chrysocolla, copper pitch, and copper wad, and a model for their formation (Chapter 2 of this work). In addition, in the companion paper Pinget et al. (2015, Chapter 3 of this work) sphalerite that was originally interpreted as supergene (Aracena et al., 1997) is reinterpreted as belonging to a late acidic, oxidizing hypogene stage of the porphyry system evolution at Chuquicamata.

1.1.2 Geological setting

The Chuquicamata giant porphyry copper deposit, located north of Chile in the Atacama desert, is part of the Eocene-Oligocene Porphyry copper belt, present in the northern Chile and southern Peru. General descriptions of the deposit are presented by Bandy (1938), Jarrell (1944), Ossandón et al. (2001), and Rivera et al. (2012).

The emplacement of the Chuquicamata Porphyry Complex, including the hydrothermal alteration events, is well constrained (e.g., Sillitoe et al., 1968; Zentilli et al., 1994; Zentilli et al., 1995; Cuadra et al., 1997; Reynolds et al., 1998; Mathur et al., 2000; Ballard et al., 2001; Ossandón et al., 2001; Müller and Quiroga, 2003; Campbell et al., 2006; and Barra et al., 2013). The obtained ages for the Chuquicamata Porphyry Complex emplacement are between 35.2±0.2 Ma and 32.8±0.2 Ma (U/Pb on zircon), and the different steps of hydrothermal alteration are included in this age range (Fig. 4). The Chuquicamata deposit was cut in two parts by the ca 35 km post-mineralization sinistral displacement of the West Fissure (Dilles et al., 1997; Tomlinson and Blanco, 1997a), which constitutes nowadays the western limit of the deposit (Ossandón et al., 2001). The location of the "missing part" of Chuquicamata located on the West side of the West Fissure has been the object of several hypothesis (e.g., Tomlinson and Blanco 1997; Dilles et al. 1997). Recently Zentilli et al. (2015) proposed that the Ministro Hales Mine (MMH), located on the west side of the West Fissure 6 km south of the Chuquicamata deposit, could represent this part that was wedged in a fault loop and had spared the full 35 km displacement of the West Fissure. The end of the sinistral movement of the West Fissure is known to have taken place after the end of the hypogene mineralization (~33 Ma, Fig. 4), as no mineralization is observed in the Fortuna granodiorite occurring in Chuquicamata on the west side of the West Fissure (Lindsay, 1998).

Potassic, quartz-sericite, and chloritic alteration were distinguished by Ossandón et al. (2001). They occur in three roughly longitudinal vertical bands, whereby the westernmost band is dominated by quartz-sericite alteration and the eastern most by chloritic alteration (Fig. 2).

Porphyry copper deposits, when exposed to oxidizing conditions by uplift and erosion (atmospheric oxygen or water with high partial pressure of oxygen), develop a typical oxidation zone (Gottschalk and Buehler, 1912; Field and Gustafson, 1976; Bladh, 1982; Whiteside, 1986; Alpers and Brimhall, 1989; Sikka et al., 1991; Sato, 1992; Sillitoe et al., 1996; Plumlee, 1999; Enders, 2000; Dold, 2003; Sillitoe, 2005; Hartley and Rice, 2005). In the

oxidation zone, most of the primary minerals formed under reduced conditions are more or less quickly destroyed, starting with the sulfides. Oxidation of copper sulfides liberates copper, which is transported by solutions and can precipitate as copper oxides in the oxidation zone, or in less oxidizing conditions as supergene sulfides, developing the supergene sulfide enriched zone.

The supergene profile at Chuquicamata is constituted by an oxidation zone around 200 meters thick developed over the quartz-sericite, potassic, and chloritic alteration zone. The vertical extent of the supergene sulfide enriched zone varies depending on the hydrothermal alteration zone, and on the position of preferential flux pathways; it is specially well developed in the quartz-sericite alteration zone and in the southern sector of the deposit, where it is more than 1 km deep (Fig. 2). Typical copper oxides minerals in the oxidation zone of Chuquicamata are chalcantite, antlerite, chrysocolla, and copper pitch / copper wad, while atacamite occurs only in the upper 30 meters of the deposit (Bandy, 1938; Jarrell, 1944). In the CODELCO 3D mine model, the supergene sulfide enriched zone is divided into low supergene sulfide enrichment, in which covellite is the principal supergene sulfide, and high supergene sulfide enrichment, in which chalcocite is the principal supergene sulfide. This distinction was kept in this study, and specifically for the mass balance calculations, in order to obtain a more detailed estimation of the copper grades.

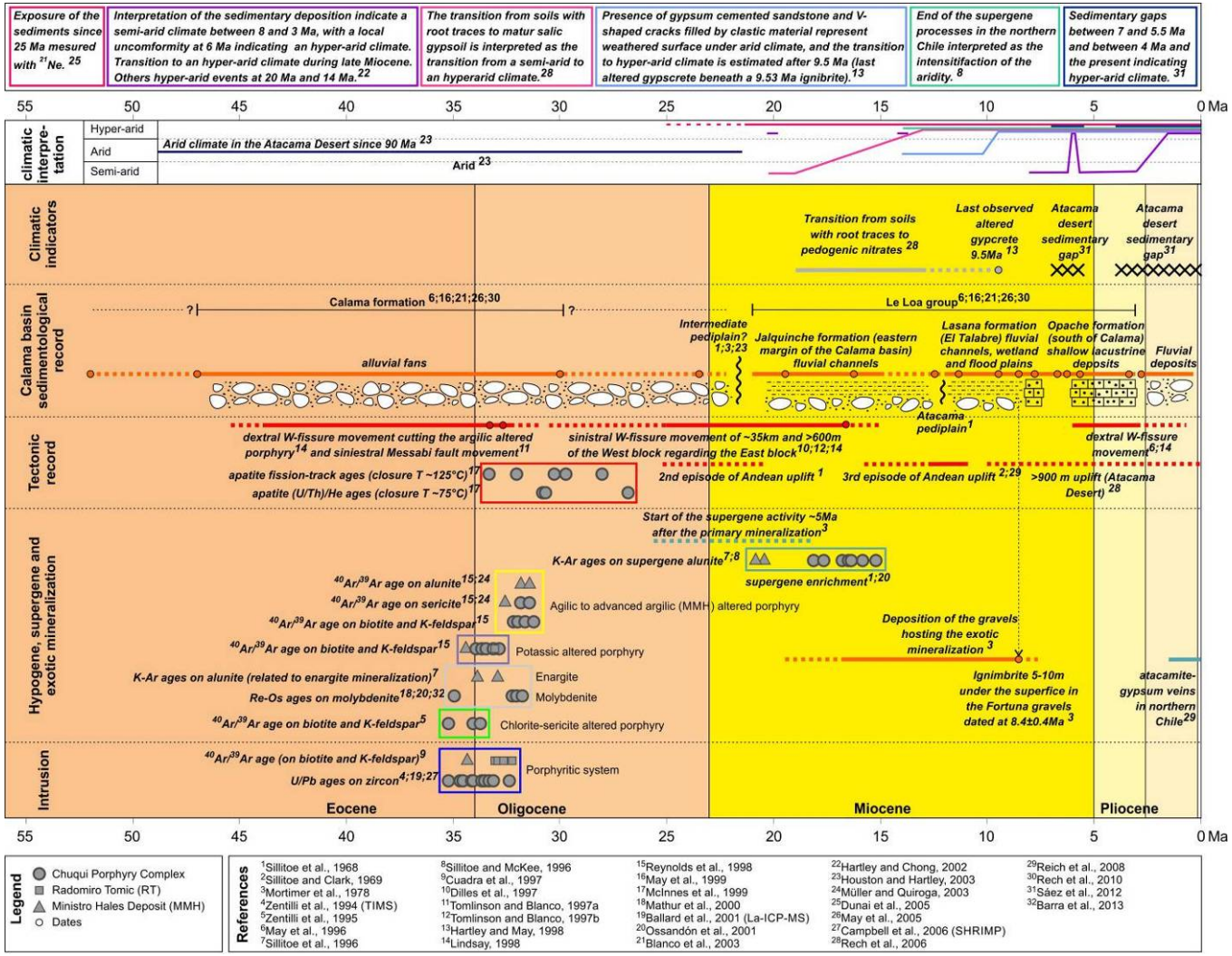

Figure 4: Compilation of the chronological, tectonic, sedimentological and climatologic data on the Calama Basin. Points represent geochronological data, full lines represent event durations considered to be confirmed, and dotted lines the possible events.

1.2. Methodology

For the first part of this study presenting detailed description of the supergene alteration profile at Chuquicamata, three representative vertical West - East sections (Fig 2) were selected from the CODELCO 3D mine model. They are located on the local coordinates N5600 (northern limit of the Chuquicamata open pit, Fig. 7), N4200 (central part of the open pit of the deposit, Fig. 6), and N2900 (southern part of the open pit, northern limit of the exotic mineralization, Fig. 5). The sections, in addition to their representativeness, were chosen according a maximum data density and availability of samples.

For the mass balance model that constitutes the second part of the study, data contained in CODLECO database, including copper grades, was considered for 40 vertical transversal cross sections, for local coordinate N2100 to N6000. Details on the methodology used are given in the results section.

1.2.1 Available samples

Most of the oxidation zone and a significant portion of the other parts of the deposit affected by supergene processes has been removed during mine operation that started in 1879 (Ossandón et al., 2001). Although almost all drill cores extracted since the beginning of mining activity at Chuquicamata were kept, most of them are in a outdoor site and their long exposition to weathering makes difficult distinguishing between features due to the supergene alteration and those that have taken place during storage, as both types of alteration develop at similar physico-chemical conditions. The drill cores are always accompanied by a more or less detailed description. The rhythm of drilling increased with time, as illustrated in Fig. 8. Part of the drill hole logs, in addition of macroscopic observations, also contain microscopic descriptions of polished sections (generally around 4x2x2 cm) that are conserved in the "CODELCO collection" on the mine site. Polished section descriptions are especially abundant for drill cores extracted between 1970 and 1990 (an example of original log is presented in Fig. 3).

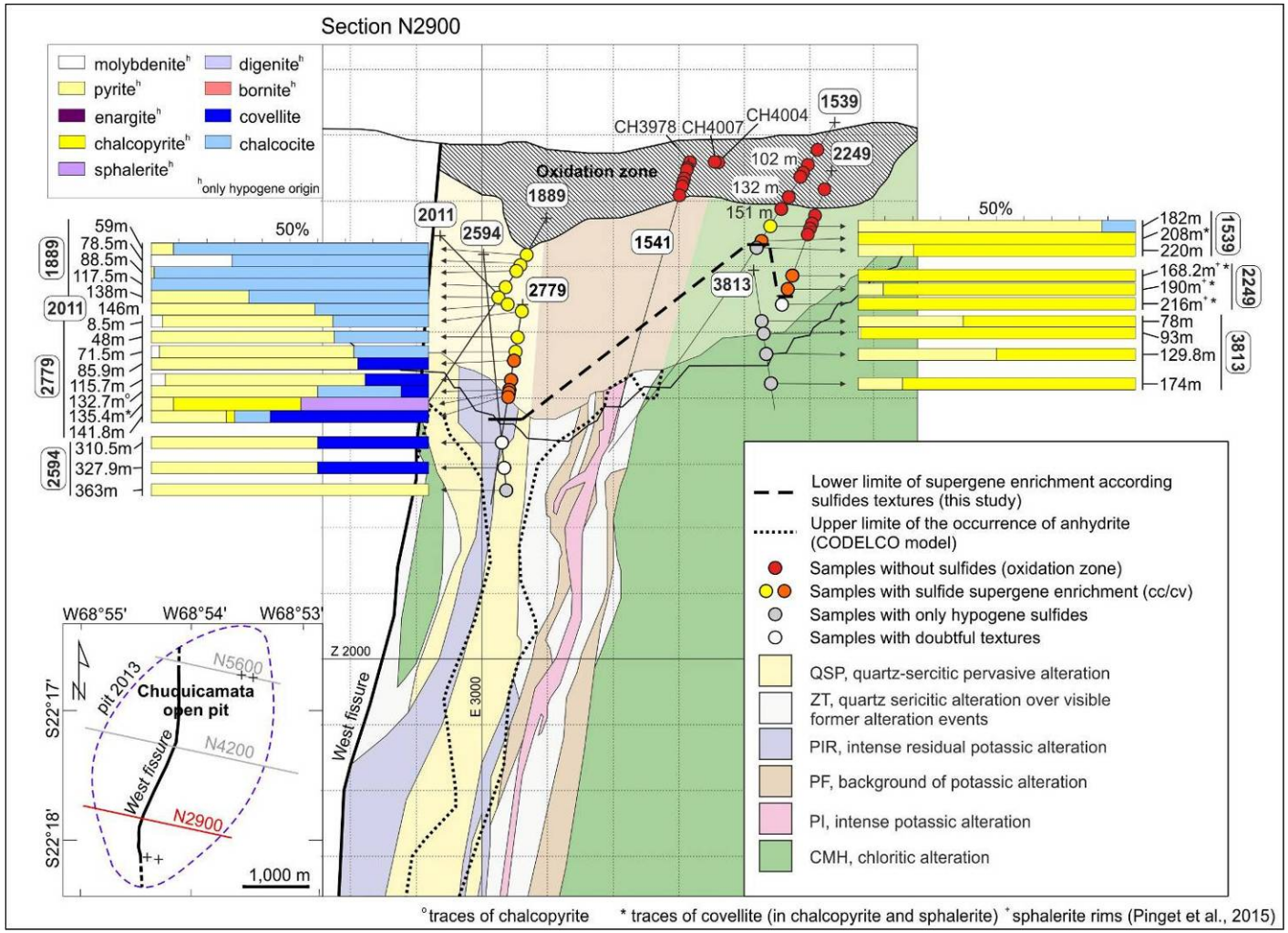

Figure 5: Sulfide percentage of selected samples in section N2900. (legend in upper left inset). Total sulfide content of each sample is given in Table 1. The lower limit of supergene alteration determined in the present study on the basis of sulfide textures is indicated by a discontinuous line. The upper limit of the occurrence of anhydrite is shown by a dotted line. Hydrothermal alteration zones according the CODELCO mine model (legend in bottom right inset).

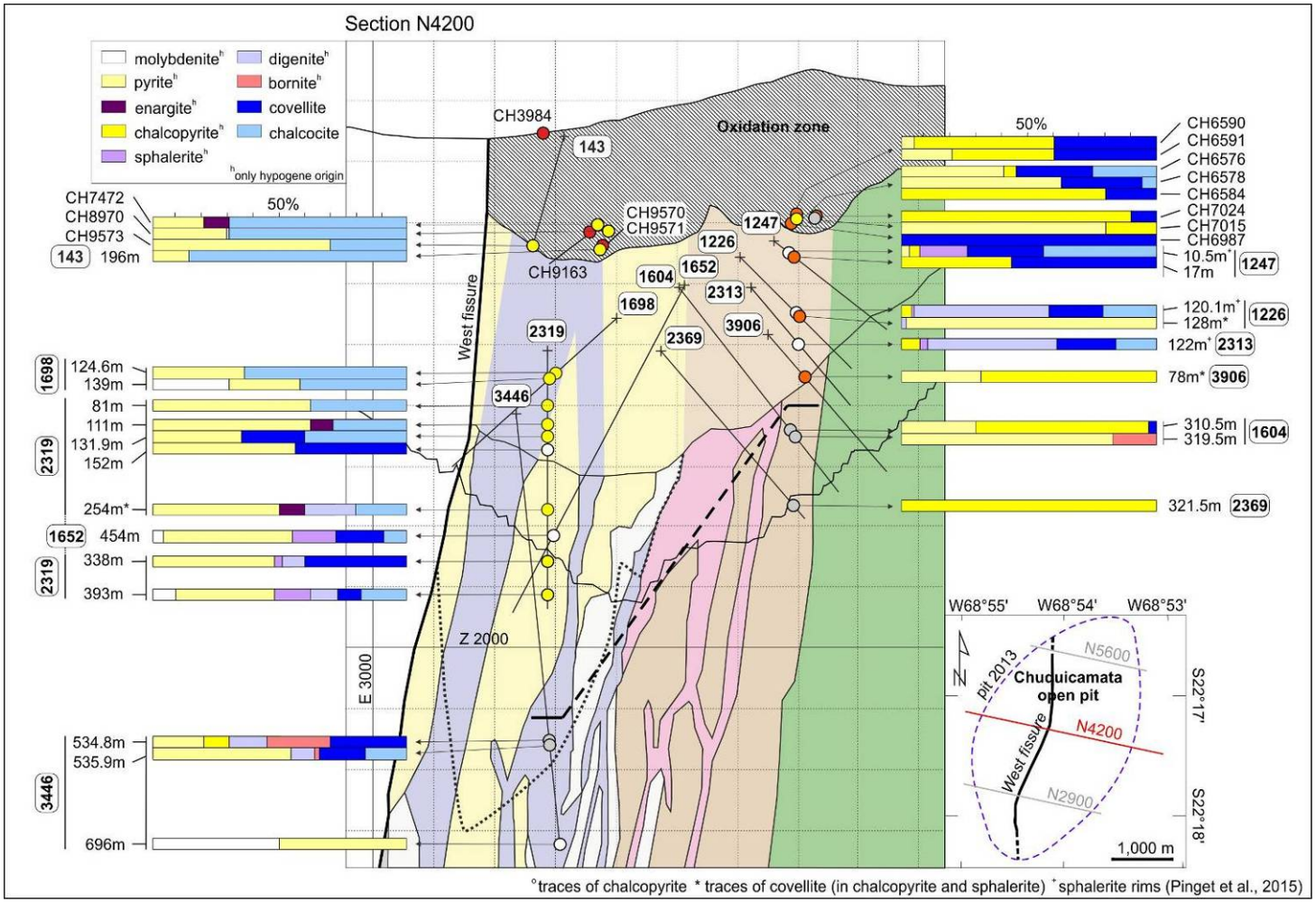

Figure 6: Section N4200 (position is indicated in the bottom right map). The hydrothermal alteration zones are from the CODELCO mine model (see legend of Fig. 5). The sulfide percents observed in each sample are indicated in graphs on the right and on the left of the section (colors in the up left legend).

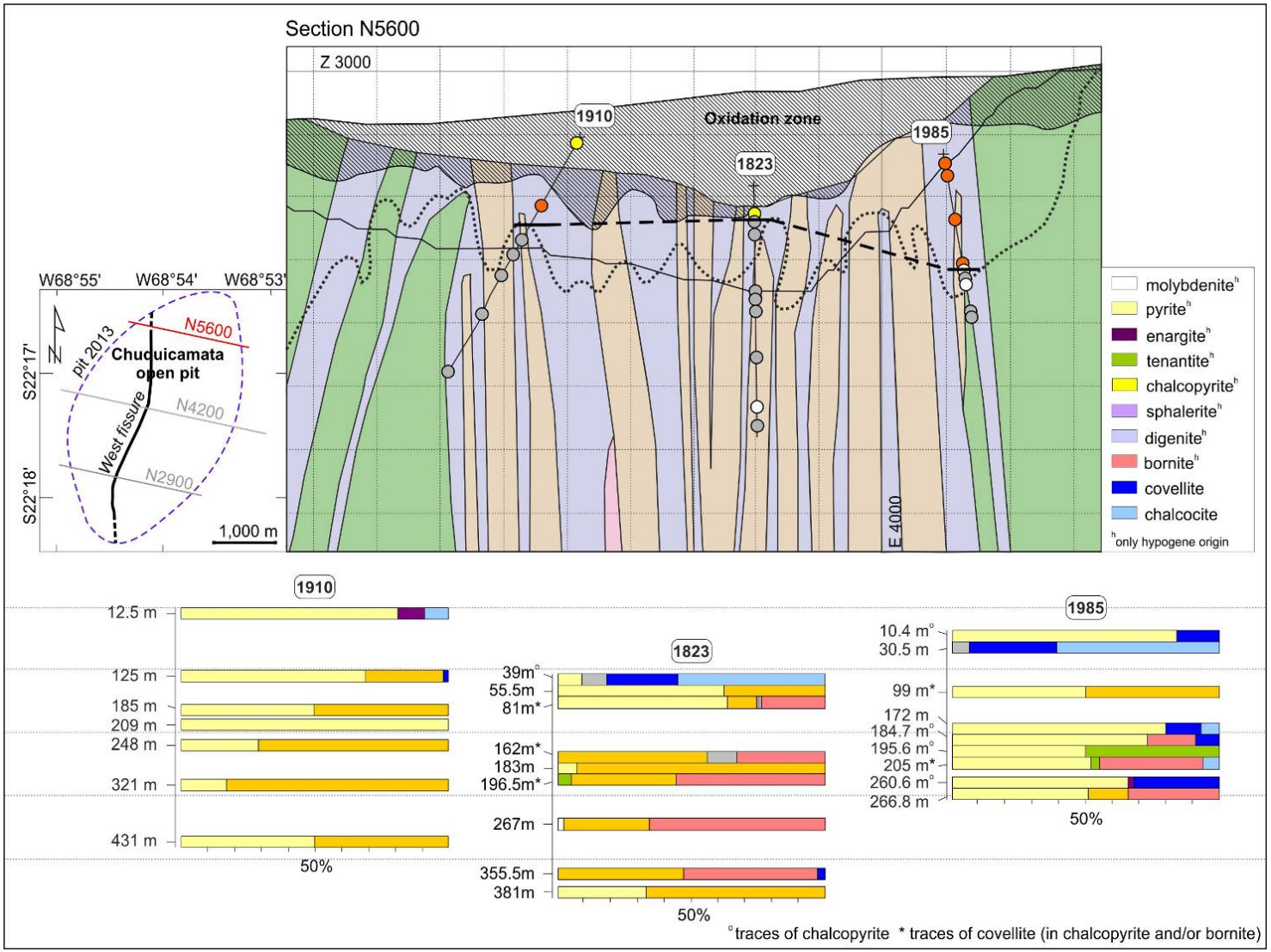

Figure 7: Section N5600 (position is indicated in the left map). The hydrothermal alteration zones are from the CODELCO mine model (see legend of Fig. 5). The sulfide percents observed in each sample are indicated in graphs below the section (colors in the right legend).

Table 1: List of the studied samples and summary of microscopical observations.

section	drill core	depth	hydrothermal alteration / hypogene zone according CODELCO model	supergene zone / hypogene according CODELCO model	supergene zone hypogene accrding present study	sulfide percent	Observed supergene textures					
							massive cc / cc rounding py/en	cc(dg?)-cv grains	cv replacing cp	cv grains with py	"rims of sl"	cv replacing py/en
N2300	7196	11	chloritic	oxidation	oxidation	0						
N2300	7196	28.5	chloritic	oxidation	oxidation	0						
N2300	7196	44.5	chloritic	oxidation	oxidation	0						
N2300	7569	33.5	quartz-sericite	oxidation	oxidation	0						
N2300	7569	43.2	quartz-sericite	supergene enrichment	supergene enrichment	13	x		x			
N2300	7569	72	quartz-sericite	hypogene	hypogene	5						
N2300	7569	92	quartz-sericite	hypogene	hypogene	5						
N2900	2011	146	quartz-sericite	supergene enrichment	supergene enrichment	11	x					
N2900	1889	59	quartz-sericite	supergene enrichment	supergene enrichment	4.3	x					
N2900	1889	78.5	potassic	supergene enrichment	supergene enrichment	2.5	x					
N2900	1889	88.5	quartz-sericite	supergene enrichment	supergene enrichment	8	x					
N2900	1889	117.5	quartz-sericite	supergene enrichment	supergene enrichment	traces	x					
N2900	1889	138	quartz-sericite	supergene enrichment	supergene enrichment	16	x					
N2900	2779	8.5	quartz-sericite	supergene enrichment	supergene enrichment	3	x					
N2900	2779	48	quartz-sericite	supergene enrichment	supergene enrichment	5	x					
N2900	2779	71.5	quartz-sericite	supergene enrichment	supergene enrichment	5	x					
N2900	2779	85.9	quartz-sericite	supergene enrichment	supergene enrichment	20	x	x				
N2900	2779	115.7	quartz-sericite	supergene enrichment	supergene enrichment	10	x	x				
N2900	2779	132.7	quartz-sericite	supergene enrichment	supergene enrichment	7	x	x	x (+cc)			
N2900	2779	135.4	quartz-sericite	supergene enrichment	supergene enrichment	3			x			
N2900	2779	141.8	quartz-sericite	supergene enrichment	supergene enrichment	7		x	x			
N2900	2594	310.5	quartz-sericite	supergene enrichment	?	3				x		
N2900	2594	327.9	silicification	supergene enrichment	?	6				x		
N2900	2594	362.5	breccia	supergene enrichment	hypogene	1						
N2900	1539	102	breccia	?	no sufides	0						
N2900	1539	132.2	breccia	?	no sufides	0						

section	drill core	depth	hydrothermal alteration / hypogene zone according CODELCO model	supergene zone / hypogene according CODELCO model	supergene zone hypogene accrding present study	sulfide percent	Observed supergene textures					
							massive cc / cc rounding py/en	cc(dg?)-cv grains	cv replacing cp	cv grains with py	"rims of sl"	cv replacing py/en
N2900	1539	151.2	breccia	?	no sufides	0						
N2900	1539	182.2	propylitic	?	supergene enrichment	5						x
N2900	1539	208.5	propylitic	?	supergene enrichment	traces			x			
N2900	1539	221.5	propylitic	?	hypogene	1						
N2900	2249	168.2	propylitic	?	?	2.5					x	
N2900	2249	190	propylitic	?	?	12					x	
N2900	2249	216	propylitic	?	?	9					x	
N2900	3813	78	potassic	hypogene	hypogene							
N2900	3813	93	potassic	hypogene	hypogene	2						
N2900	3813	130	potassic	hypogene	hypogene	traces						
N2900	3813	174	potassic	hypogene	hypogene	1						
N2900	CH3978	bench		?	no sufides	0						
N2900	CH4004	bench		?	no sufides	0						
N2900	CH4007	bench		?	no sufides	0						
N4200	143	196	quartz-sericite	supergene enrichment	supergene enrichment	6	x					
N4200	2319	81	quartz-sericite	supergene enrichment	supergene enrichment	7	x					
N4200	2319	111	quartz-sericite	supergene enrichment	supergene enrichment	8	x (py and en)					
N4200	2319	131.9	quartz-sericite	supergene enrichment	supergene enrichment	57	x			x		
N4200	2319	152	quartz-sericite	supergene enrichment	?	8				x		
N4200	2319	254	quartz-sericite	supergene enrichment	supergene enrichment	7	x (py and en)					x (en)
N4200	2319	338	quartz-sericite	supergene enrichment	supergene enrichment	14	x					
N4200	2319	393	quartz-sericite	supergene enrichment	supergene enrichment	20	x					
N4200	1698	124.6	quartz-sericite	supergene enrichment	supergene enrichment	4.8	x					
N4200	1698	139	quartz-sericite	supergene enrichment	supergene enrichment	8.9	x					
N4200	3446	534.8	potassic	supergene enrichment	hypogene	8						
N4200	3446	535.9	potassic	supergene enrichment	hypogene	80						
N4200	3446	696	quartz-sericite	hypogene	hypogene	2						
N4200	1652	454	quartz-sericite	supergene enrichment	?	5.5				x		

section	drill core	depth	hydrothermal alteration / hypogene zone according CODELCO model	supergene zone / hypogene according CODELCO model	supergene zone hypogene accrding present study	sulfide percent	Observed supergene textures					
							massive cc / cc rounding py/en	cc(dg?)-cv grains	cv replacing cp	cv grains with py	"rims of sl"	cv replacing py/en
N4200	1247	10	potassic	hypogene	?	3		x		x (without py)	x	
N4200	1247	17	potassic	hypogene	supergene enrichment	7			x			
N4200	1226	120.1	quartz-sericite	hypogene	supergene enrichment	5			x		x	
N4200	1226	128	silicification	hypogene	supergene enrichment	8	x					
N4200	2313	122	potassic	hypogene	supergene enrichment	0			x		x	
N4200	3906	78	potassic	hypogene	supergene enrichment	8			x			
N4200	1604	310.5	potassic	hypogene	hypogene	3.6						
N4200	1604	319	potassic	hypogene	hypogene	1.2						
N4200	2369	321.5	propylitic	hypogene	hypogene	6						
N4200	CH3984	bench		?	no sulfides	0						
N4200	CH7472	bench		?	supergene enrichment	5	x (en)					
N4200	CH8970	bench		?	supergene enrichment	5	x					
N4200	CH9163	bench		?	no sufides	0						
N4200	CH9570	bench		?	no sufides	0						
N4200	CH9571	bench		?	no sufides	0						
N4200	CH9573	bench		?	supergene enrichment	95	x					
N4200	CH6590	bench		?	supergene enrichment	5			x	x		
N4200	CH6591	bench		?	supergene enrichment	3			x	x		
N4200	CH6987	bench		?	supergene enrichment	1				x (without py)		
N4200	CH6576	bench		?	supergene enrichment	5	x	x		x		
N4200	CH6578	bench		?	supergene enrichment	15	x	x				
N4200	CH6584	bench		?	supergene enrichment	2			x			
N4200	CH7024	bench		?	?	2				x		
N4200	CH7015	bench		?	hypogene	6						
N5600	1910	12.5	silicification	?	supergene enrichment	11	x	x				
N5600	1910	125	potassic	supergene enrichment	supergene enrichment	4			x			
N5600	1910	185	potassic	hypogene	hypogene	3						
N5600	1910	209	potassic	hypogene	hypogene	3						

section	drill core	depth	hydrothermal alteration / hypogene zone according CODELCO model	supergene zone / hypogene according CODELCO model	supergene zone hypogene accrding present study	sulfide percent	Observed supergene textures					
							massive cc / cc rounding py/en	cc(dg?)-cv grains	cv replacing cp	cv grains with py	"rims of sl"	cv replacing py/en
N5600	1910	248	potassic	hypogene	hypogene	traces						
N5600	1910	321	potassic	hypogene	hypogene	traces						
N5600	1910	431	potassic	hypogene	hypogene	4						
N5600	1823	39	quartz-sericite	supergene enrichment	supergene enrichment	1		x				
N5600	1823	55.5	quartz-sericite	supergene enrichment	hypogene	7						
N5600	1823	81.2	quartz-sericite	supergene enrichment	hypogene	15			x (bn)			
N5600	1823	162	potassic	hypogene	hypogene	1			x (bn)			
N5600	1823	183	potassic	hypogene	hypogene	3						
N5600	1823	196.5	potassic	hypogene	hypogene	5						
N5600	1823	267	potassic	hypogene	hypogene	9						
N5600	1823	355.5	potassic	hypogene	?	5			x (and bn)			
N5600	1823	381	potassic	hypogene	hypogene	6						
N5600	1985	10.4	quartz-sericite	supergene enrichment	supergene enrichment				x			
N5600	1985	30.5	silicification	supergene enrichment	supergene enrichment	3		x				
N5600	1985	99	potassic	supergene enrichment	supergene enrichment	3			x			
N5600	1985	172	silicification	supergene enrichment	supergene enrichment			x		x (with cc)		
N5600	1985	184.7	silicification	supergene enrichment	?	10			x (and bn)			
N5600	1985	195.6	silicification	supergene enrichment	hypogene	4						
N5600	1985	205	quartz-sericite	supergene enrichment	?	6		x	x (replacing bn)			
N5600	1985	260.6	silicification	hypogene	hypogene	20		x				
N5600	1985	266.8	silicification	hypogene	hypogene	8						
N5600	7830	14.5	potassic	oxidation	oxidation	0						
N5600	7830	28.7	potassic	supergene enrichment	supergene enrichment	10	x					
N5600	7987	27	chloritic	oxidation	oxidation	0						
N5600	7987	31.5	chloritic	oxidation	oxidation	0						
N5600	7987	49	chloritic	supergene enrichment	supergene enrichment	0						
N5600	7987	64.5	chloritic	supergene enrichment	supergene enrichment	0						

The polished samples from the CODELCO collection were the only ones adequate for studying the central and richest supergene sulfide enriched zone of the deposit, given the previously mentioned oxidized state of the stored cores; however they cover only fragmentary the oxidation zone. Polished samples from the past mine walls are also available in the collection, some on them located in the oxidation zone of the supergene profile, principally in the central part of the deposit. The coordinates and altitude of these samples are known, but original descriptions and year of sampling could not be found. From the CODELCO collection, 1215 polished sections from drill cores and 194 from the mine walls are located on or near the three vertical sections used for the present study, 90 of them were selected for a detailed description, after study of the archived logs. Additionally, 72 samples were obtained from four recent drill cores, which cover well the complete supergene profile. They are located in the northern part (section N5600) and southern part (section N2300) of the deposit (Fig. 2). Twenty-five of these recent drill cores samples were used for detailed observation, including microscopic observations on polished sections and sequential extraction.

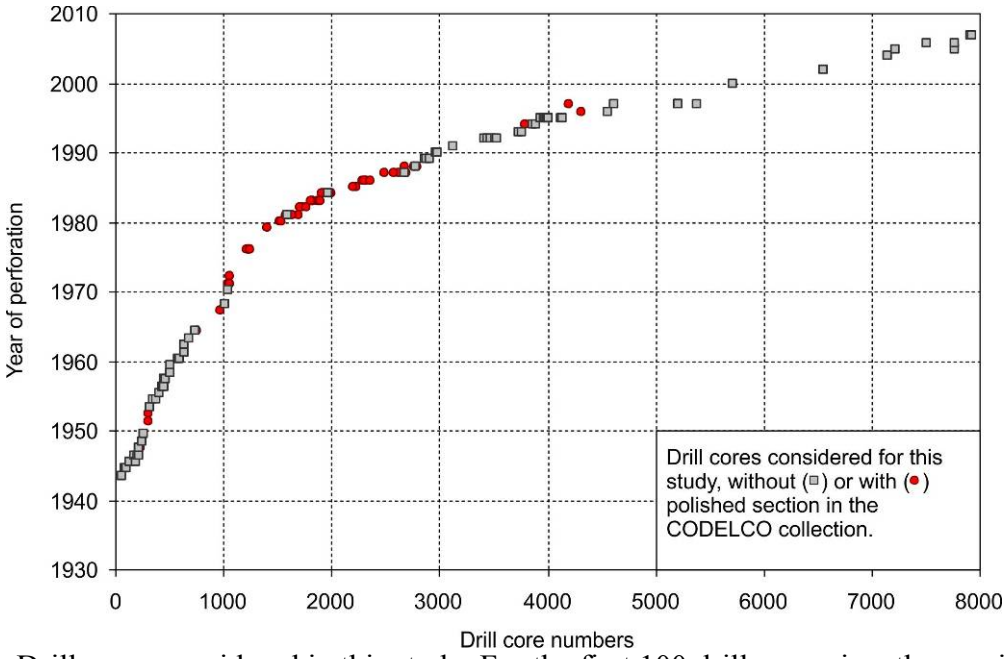

Figure 8: Drill cores considered in this study. For the first 100 drill cores, i.e., those prior to 1943, no date was indicated.

These 115 samples studied in detail are listed in Table 1, that also indicates the geographic provenance, and their position is shown in Figs. 5, 6, and 7 for section N2900 (34 samples), section N4200 (31 samples) and section N5600 (25 samples), respectively, and in Fig. 9 for the four sampled drill cores. The list of all the samples considered for this study is presented in Annex 2.1.

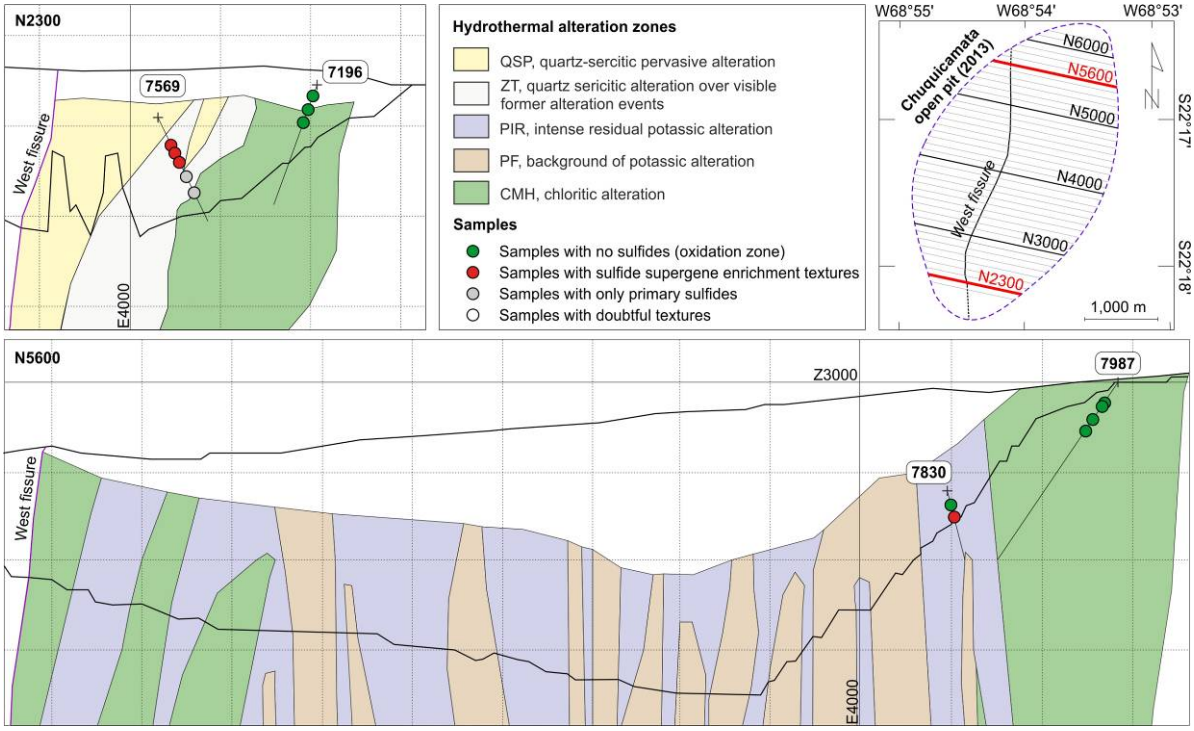

Figure 9: Sections N2300 and N5600 with the location of the sampled drill cores, and of the samples used for sequential extraction.

1.2.2 Analytical methods

In addition to the microscopical studies on 115 polished sections obtained from the CODELCO mine collection (90) and from the samples drill cores (25), various analytical methods were used, including Scanning Electron Microscope, element mapping using QEMSCAN®, X-ray fluorescence standard-less methodology (UniQuant®), and $^{39}Ar/^{40}Ar$ dating on alunite samples.

Seventeen thin sections were selected for backscattered electron imaging (SEI) and energy-dispersive X-ray spectrometry (EDS) semi-quantitative chemical analyses with a Jeol JSM 7001F Scanning Electron Microscope (SEM) at the Department of Earth Sciences, University of Geneva. The 17 thin sections were covered with an ultra-thin coating (ca 10 nm) of carbon by low vacuum sputter coating.

Table 2: X-ray fluorescence on bulk samples.

section	drill core	depth	hydrothermal alteration / hypogene zone accroding CODELCO model	supergene zone / hypogene according CODELCO model	Al2O3 %	CaO %	Fe2O3 %	K2O %	MgO %	Na2O %	P2O5 %	S %	SiO2 %	TiO2 %	As mg/kg	Ba mg/kg	Cu mg/kg	Mn mg/kg	Mo mg/kg	Pb mg/kg	Rb mg/kg	Sr mg/kg	V mg/kg	Zn mg/kg	Zr mg/kg	Sum %	LOI %
N2300	7196	11.0	chloritic	oxidation	21.51	1.18	18.39	2.27	0.75	1.03	0.09	1.38	44.02	0.22	42	750	7510	424	1570	29	124	256	24	131	102	91.9	7.66
N2300	7196	28.5	chloritic	oxidation	16.14	0.11	13.90	5.21	0.76	3.26	0.06	0.04	58.74	0.18	n.d.	1090	279	59	185	n.d.	219	249	18	43	118	98.6	1.32
N2300	7196	44.5	chloritic	oxidation	11.73	0.52	25.34	0.74	n.d.	6.72	0.19	0.66	49.93	0.09	11	122	1810	40	2050	22	31	550	n.d.	810	97	96.5	3.32
N2300	7196	46.5	chloritic	oxidation	16.14	0.72	5.04	4.79	0.75	4.15	0.18	0.83	64.40	0.21	n.d.	930	338	61	249	15	210	273	16	57	147	97.4	2.50
N2300	7196	63.0	chloritic	oxidation	6.73	7.63	5.14	0.76	n.d.	3.70	0.17	5.62	62.20	0.11	n.d.	16	830	n.d.	830	24	32	255	n.d.	180	87	92.3	7.55
N2300	7196	94.2	chloritic	supergene enrichment	16.91	0.68	2.99	6.74	0.95	3.59	0.10	0.84	63.93	0.26	n.d.	1540	10600	47	13	22	275	400	11	83	139	98.3	1.36
N2300	7569	13.3	quartz sericite	oxidation	23.89	0.02	1.64	7.83	1.51	n.d.	0.03	0.14	60.31	0.30	36	269	459	94	49	20	283	101	74	30	156	95.8	4.12
N2300	7569	33.5	quartz sericite	oxidation	14.98	0.09	2.78	5.83	0.49	1.76	0.07	1.74	64.81	0.22	n.d.	1350	1510	99	136	33	200	570	28	37	147	93.2	6.71
N2300	7569	43.2	quartz sericite	supergene enrichment	12.68	0.59	1.81	5.57	0.73	1.84	0.01	1.48	68.69	0.25	n.d.	1080	14100	110	15	42	227	208	26	63	158	95.3	4.31
N2300	7569	46.0	quartz sericite	supergene enrichment	18.90	0.28	2.46	7.02	1.60	n.d.	0.02	1.45	61.51	0.21	76	185	13100	99	96	28	272	56	43	10	89	94.9	4.77
N2300	7569	54.5	quartz sericite	supergene enrichment	16.50	0.10	1.38	8.66	0.78	2.08	0.12	0.59	66.50	0.24	n.d.	1290	5840	49	48	15	263	650	20	265	104	97.8	1.98
N2300	7569	72.0	quartz sericite	hypogene	16.07	0.25	0.99	6.58	0.57	4.32	n.d.	0.44	66.50	0.27	n.d.	n.d.	0.368	n.d.	n.d.	1400	n.d.	n.d.	n.d.	n.d.	n.d.	96.1	n.d.
N2300	7569	87.0	quartz sericite	hypogene	17.04	0.46	2.23	6.25	1.15	3.57	0.05	0.99	64.74	0.26	n.d.	690	1610	86	105	28	262	304	41	530	151	97.1	2.74
N2300	7569	92.0	quartz sericite	hypogene	17.43	n.d.	4.05	8.16	0.80	2.81	n.d.	0.77	69.64	0.23	n.d.	n.d.	n.d.	n.d.	n.d.	2040	n.d.	n.d.	n.d.	n.d.	n.d.	104.1	n.d.
N5600	7830	14.5	potassic	oxidation	20.00	0.58	4.55	5.93	1.56	2.22	0.05	1.46	58.23	0.22	23	530	1190	166	n.d.	24	328	244	54	105	165	95.1	4.81
N5600	7830	25.0	potassic	oxidation	16.71	0.29	1.63	2.34	0.77	6.74	0.02	1.00	67.04	0.20	n.d.	30	288	43	n.d.	43	111	228	33	28	142	96.8	3.13
N5600	7830	27.5	potassic	oxidation	16.66	0.27	5.79	3.53	1.18	3.96	0.01	1.04	63.66	0.20	n.d.	47	630	121	n.d.	30	170	103	35	44	144	96.4	3.53
N5600	7830	28.7	potassic	oxidation	19.32	0.16	1.37	3.74	1.05	4.09	0.02	1.24	61.93	0.15	n.d.	55	20000	63	n.d.	13	151	116	25	29	111	95.1	4.33
N5600	7830	37.5	potassic	oxidation	13.96	0.20	1.78	0.50	n.d.	8.48	0.13	1.19	70.90	0.19	22	n.d.	254	n.d.	n.d.	32	15	175	8	17	155	97.4	2.57
N5600	7830	4.7	potassic	oxidation	15.88	0.44	1.39	1.20	0.30	6.55	0.11	0.14	71.59	0.28	n.d.	148	471	30	11	33	59	700	37	47	161	98.0	1.89
N5600	7987	27.0	chloritic	oxidation	19.91	1.45	4.86	6.10	1.32	2.63	0.21	1.32	57.43	0.28	n.d.	880	2210	488	394	n.d.	262	272	47	810	180	96.1	3.70
N5600	7987	31.5	chloritic	oxidation	15.36	0.82	1.66	5.34	1.11	5.93	0.08	0.77	66.75	0.25	n.d.	1420	1350	360	65	30	196	375	43	750	215	98.6	1.23
N5600	7987	49.0	chloritic	oxidation	15.35	1.07	1.93	4.90	0.98	5.46	0.13	0.01	68.02	0.26	n.d.	1430	2580	512	15	27	155	630	25	370	175	98.7	1.17
N5600	7987	64.5	chloritic	oxidation	15.14	0.85	2.50	4.88	1.26	5.72	0.17	0.19	67.28	0.26	n.d.	1610	328	1400	26	22	151	540	28	1110	138	98.8	1.04
N5600	7987	89.5	chloritic	oxidation	14.87	4.44	10.00	6.46	0.91	3.78	0.32	3.94	47.29	0.26	n.d.	1860	1150	214	259	45	260	362	21	2660	158	93.0	6.80

Element mapping with was performed at the Department of Earth Sciences, University of Geneva at the QEMSCAN® facility to obtain elements maps of two thin sections of samples from the oxidation zone, in order to identify to which mineral phases copper is associated.

X-ray fluorescence (XRF) methodology (UniQuant®) was used to chemically characterize 25 selected samples (Philips PW2400 vacuum X-ray fluorescence spectrometer of the Department of Earth and Environmental Sciences, University of Lausanne). This method gives chemical compositions of strongly mineralized samples with reasonable accuracy on powder samples (Table 2), and the copper values obtained by XRF are consistent with those of the CODELCO data base used for the mass balance model.

Four samples containing supergene alunite coming from the exotic mineralization were used for $^{39}Ar/^{40}Ar$ dating. They were packed in glass tubes and irradiated in the CLICIT facility of the TRIGA reactor at Oregon State University for 4 hours. Samples were degassed by step-heating with a 55W CO_2-IR laser (Photon Machines Inc.) that was rastered over the samples to provide even-heating of the grains, and the extracted gas was gettered (SAES GP50 ST101 and AP10) in a stainless steel UHV line, after passing through a cold trap chilled to ~150 Kelvin. Fish Canyon Tuff sanidine was used as a fluence monitor, with an age of 28.20±0.05 Ma (Kuiper et al., 2008). Argon isotopes were analyzed at the University of Geneva using a multi-collector GV Instruments Argus mass spectrometer equipped with four high-gain (10^{12} Ω) Faraday detectors, and a single 10^{11} Ω Faraday detector (^{40}Ar). Time-zero regressions were fitted to data collected from twelve cycles and ages were calculated using the ^{40}K decay constant of Steiger and Jaeger (1977). Age plateaus were determined using the criteria of Dalrymple and Lanphere (1974), and data reduction utilized ArArCalc (Koppers 2002). The complete data set, along with additional analytical information is presented in Annex 2.2.

Sequential extractions were used as an indirect way to determine the mineralogical composition of poorly crystallized and/or fined grained phases. Step by step dissolution and analysis of the chemical elements liberated during each step allow in the ideal case to reconstruct the minerals constitutive of the rock. Selected samples from the oxidation zone (9 samples), from the sulfide enrichment zone (2 samples), and from the hypogene zone (2 samples), coming from drill cores 7196 and 7569 (section N2300) and drill cores 7830 and 7987 (section N5600), were submitted to the seven steps of sequential dissolution listed in Table 3, according the protocol described by Dold (2003). Solutions resulting of each dissolution step, were analyzed by ICP for 33 elements (see Annex 2.3 for complete results). The sequential extractions and the ICP chemical analyses were performed by SGS Minerals Services (Toronto, Canada).

Table 3: Steps of the sequential extraction protocol (after Dold, 2003)

Step	Solvent	Objective
1	deionized water	water-soluble fraction
2	ammonium acetate	carbonates and adsorbed ions
3	oxalic acid	reactive Fe(III) hydroxides
4	heated oxalic acid	Fe(III) oxides
5	H_2O_2	organic matter and supergene sulfides
6	$KClO_4$	primary sulfides
7	HNO_3, HF and $HClO_4$	residual fraction (principally silicates)

For the mass balance model, the copper grades of 437 drill cores selected from CODELCO data bases that contain also logging of the drill cores, and an assignment to a particular

hydrothermal and supergene zone. Analyzed segments are generally 1.5 m long. For certain drill cores, mainly the recent ones, contents of other elements are also given and could be used for better mineralogical determination.

1.3. Results

1.3.1 Oxidation zone

Mineralogy and fabrics of the oxidation zone

Samples used for the oxidation zone are mainly from the four drill cores sampled during this study (Fig. 10). The characteristic red to brown to light pink coloration of the oxidized samples is largely due to the presence of a fine mixture of mainly Fe (III) oxides and hydroxides (Fig. 11 C-D-E-F). In samples, like in Fig. 11 G, where the fine mixture is wide and homogenous enough to obtain representative EDS chemical analyses, they yielded iron oxide contents over 50wt%, copper oxide around 6 wt%, as well as around 1 wt% of molybdenum, silica and aluminum oxides. In most cases, the intergrowths are too fine and inhomogenous to obtain chemical values for single grains. EDS bulk analyses of these fine-grained mixtures reveal the presence of Cu, Mo, Si, Al, Zn, Mn, S and P suggesting, in addition to the main Fe oxides and hydroxides, the presence of minor amounts of phosphates, silicates, and sulfates (Fig. 12).

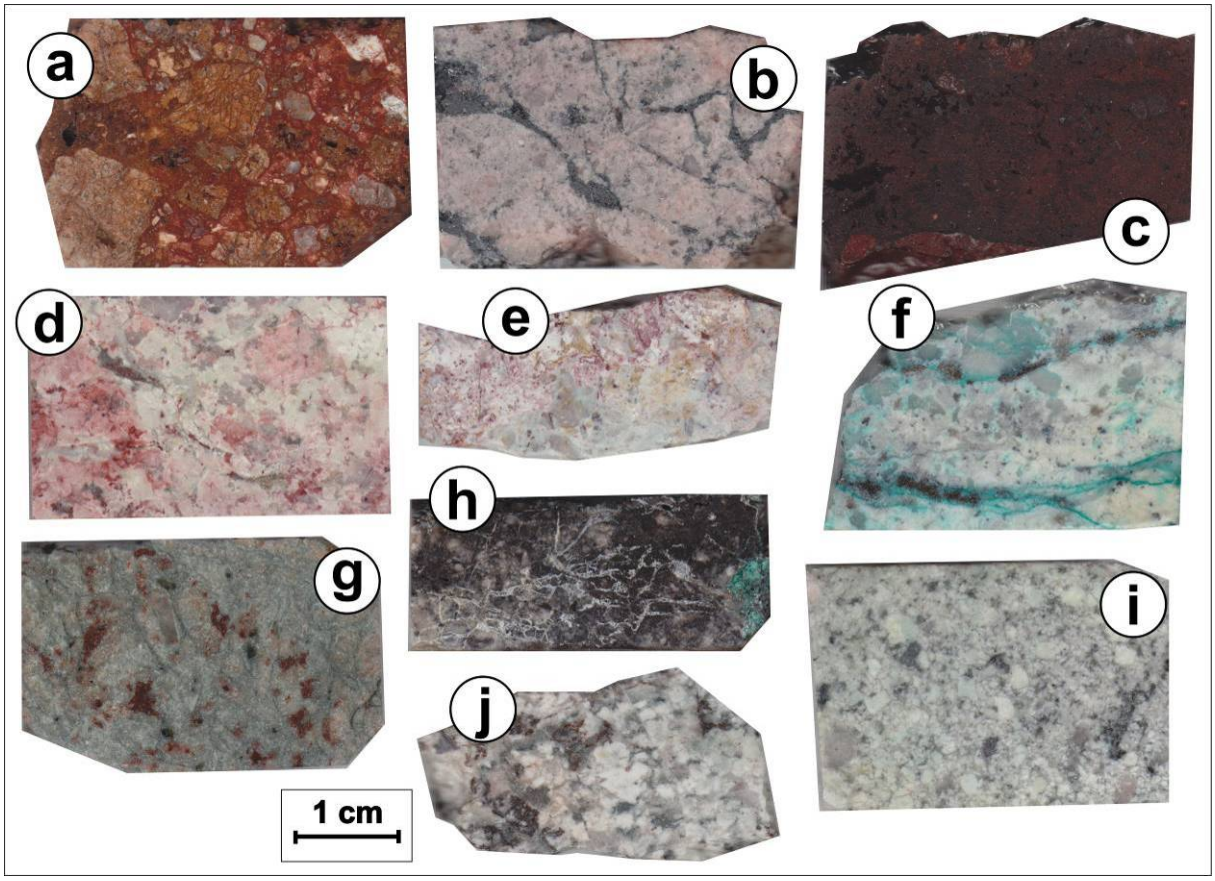

Figure 10: Pictures of the 10 selected samples for textural observations (Microscope and MEB). A. CHDD7196 at 11 m, highly porous (>40%) gossan sample with quartz, sericite and oxide/hydroxides minerals; B. CHDD7196 at 28.5 m, sample from the oxidation zone displaying a well preserved texture, with quartz, highly seritized feldspar, muscovite, and hematite as specularite in veins; C. CHDD7196 at 44.5 m, gossan sample containing quartz, altered plagioclases, goethite and some hematite as specularite; D. CHDD7569 at 33.5 m, sample from the oxidation zone containing coarse grains of quarz, sericitized feldspar and iron oxides concentrated on the red spots visible on the scan of the section; E. CHDD7830 at 14.5 m, sample from the oxidation zone displaying highly altered feldspars in a fine matrix, the former crystals of pyrite are totally replaced by sulfates and oxides conserving the pyrite shape (see Fig. 11); F. CHDD7830 at 28.7 m, sample from te mixed zone, pyrite is present rimed by chalcocite in certain places, in others it is totally replaced by antlerite and cubic Al-Fe sulfates; G. CHDD7987 at 27 m, sample from the oxidation zone, displaying quartz and highly sericitized feldspars, oxidation is present as spots, probably related with the position of sulfides before the oxidation processes, containing copper wad, iron oxides and hydroxides, and sericite, frequently with concretional textures; H. CHDD7987 at 31.5 m, sample from the oxidation zone containing copper wad and atacamite, and sulfates and phosphates replacing pyrite totally destroyed by oxidation processes (see Fig. 11); I. CHDD7987 at 49 m. sample from the oxidation zone displaying quartz, some biotite, and highly seritized plagioclase and orthoclase, hematite and titanite are the observed oxides; J. CHDD7987 at 64.5 m, sample from the oxidation zone, rock has a very well preserved texture with quartz, feldspar, sericite and chlorite in veins, magnetite crystals are martitized, copper wad concretions replace oxidized formed minerals.

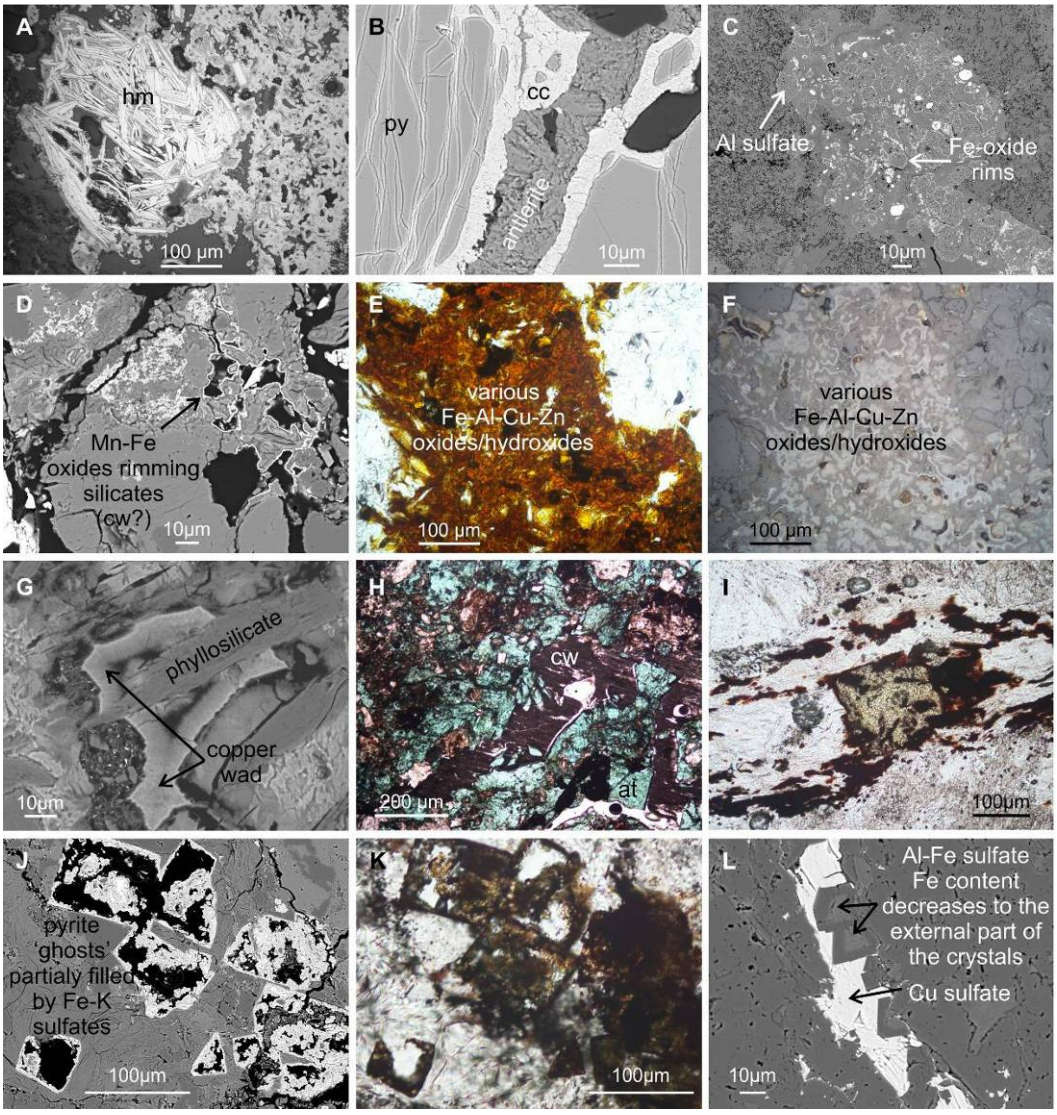

Figure 11: A. CHDD7196 at 11 m, reflected light, plane-polarized, hematite as specularite; B. CHDD7830 at 28.7 m, SEM BEI, pyrite replaced on borders and cracks by supergene chalcocite, antlerite vein betweem two pyrite crystals; C. CHDD7569 at 33.5, SEM BEI, concretions of Al sulfates rimed by iron oxides or hydroxides; D. CHDD7987 at 31.5 m, SEM BEI, view of a copper wad spot identified on the polished section as a black spot, constituted by Mn-Fe oxides or hydroxides rimming silicates; E. CHDD7987 at 27 m, transmitted light, plane-polarized, "oxidation spot" made of a concretion of various Fe-Al-Cu-Zn oxides or hydroxides; F. CHDD7987 at 27 m, reflected light, plane-polarized, same zone than (E.); G. CHDD7987 at 27 m, SEM BEI, copper wad concretion with phyllosilicate crystals; H. CHDD7987 at 31.5 m, transmitted light, plane-polarized, copper wad - atacamite mineralization; I. CHDD7830 at 14 m, transmitted light, plane-polarized, yellowish Fe-Al-K sulfate replacing a totally oxidized crystal of pyrite, regarding aspect and composition it could voltaite, spacially associated with a dark red Fe-Ti oxide or hydroxide; J. CHDD7987 at 31 m, SEM BEI, ghosts of pyrite partially filled byFe-K sulfates, which could be voltaite, such as in sample CHDD7830 at 14 m; K. CHDD7987 at 31 m, transmitted light, plane-polarized, idem than (K.); L. CHDD7830 at 28 m, SEM BEI, antlerite vein containing cubic Al-Fe sulfate, whom Fe content decreases to the external part of the crystals, the vein was probably filled by pyrite before the oxidation processes.

Some oxidation zone samples contain copper wad (Fig. 11 H) with compositions of 30 to 35 wt% MnO, 7 to 10 wt% CuO, in places up to 16 to 17 wt% ZnO, 1 to 3 wt% SiO_2 and around 1 wt% Al_2O_3 (Fig. 12), i.e., similar compositions than those obtained for copper wad in the Exótica deposit (Chapter 2), apart from Zn, which is present only as trace element in the Exótica deposit.

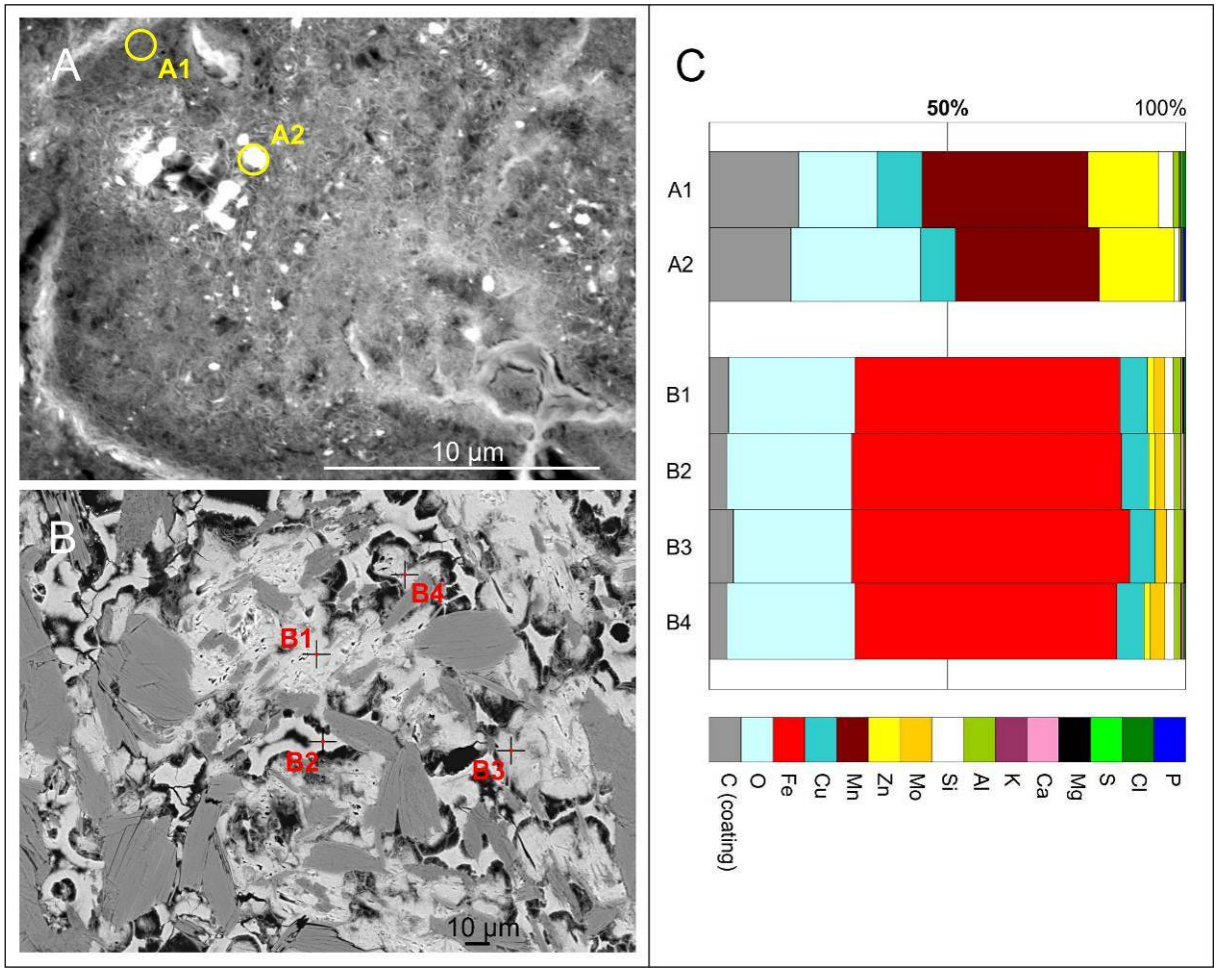

Figure 12: Examples of the importance of texture to interpret the EDS chemical results. A. Sample 7987 at 64 m, SEM BEI, fine grained "copper wad" mineralization (brown to black patches in transmitted light), with the two EDS analyses presented in (C) (1µm approx. spots); B. Sample 7987 at 27 m, SEM BEI, complex texture made of various generations of iron oxides/hydroxides, with the four EDS analyses presented in (C) (1µm approx. spots are represented by the cross centers). Analyzed carbon comes principally from the sample coating.

There is a great variety in the textures and composition of supergene minerals in the oxidation zone. In Fig. 11 C, Fe(III) oxides/hydroxides rim Al-sulfates, indicating larger mobility of iron (most possibliy as ferrous iron) than of aluminum during the oxidation process and consequently pH over 4 (to avoid the mobility of aluminum, diagram obtained with Medusa KTM software) and Eh around 0 (to allow the mobility of iron, Dill et al., 2010). Under these conditions, iron in solution is mainly in the form of Fe^{2+}, easily mobilized by aqueous solutions. Under more oxidizing conditions, Fe^{2+} is oxidized into Fe^{3+}, iron requiring therefore very low pH to be mobile (pH below 3 as $Fe(OH)^{2+}$ and below 2 as Fe^{3+}, Dill et al., 2010; Salgado et al., 2013). Thus, the described iron hydroxide rims record a pH increase (and maybe also of Eh), probably due to a neutralizing water-rock reaction.

The texture of Fig. 11 D showing Fe-Mn oxides rimming supergene silica bearing minerals suggest a difference of mobility during the oxidation processes between silica (less mobile) and ferrous iron-manganese (more mobile), and consequently probably also Eh around 0 allowing the transport of iron, at least at a small scale (Dill et al., 2010). The gradation in the chemical composition of certain minerals may reflect the evolution of the chemical composition of the solution during the precipitation. Figure 11 L show an example of zoned composition of aluminum-iron sulfates with iron content decrease and aluminum increase to the external parts of the crystals (iron from around 15% to around 3%, aluminum from around 15% to around 22% from core to border).

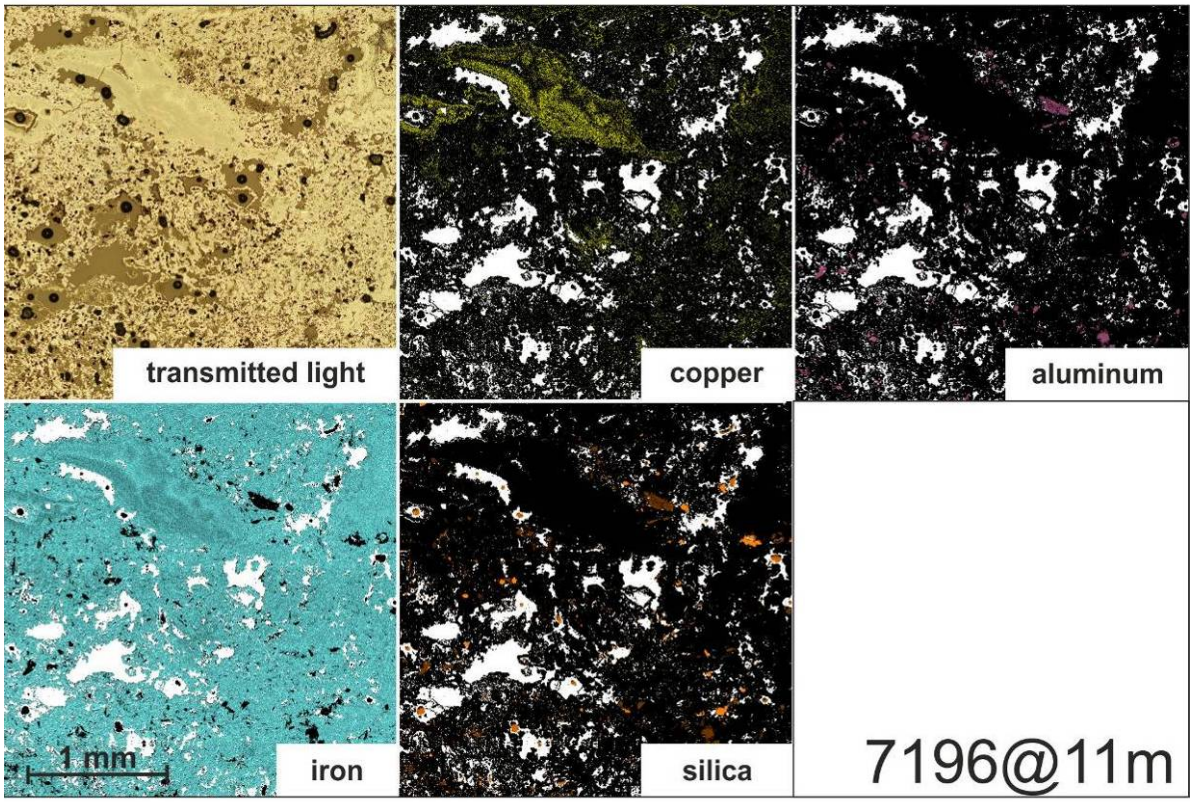

Figure 13: Reflected light picture and chemical elements repartition (Cu, Fe, Al, Si) obtained with QEMSCAN on sample 7196@11m. Copper is mainly in a banded iron hydroxide grain.

Examples of material consisting almost exclusively of Fe(III) oxide and hydroxides with partly concretional texture is shown in Figs. 10 A (sample 7196@11m) and C (sample 7196@44.5m). Under the microscope, well formed hypogene specularite crystals up to 150 µm in length are also distinguished (Figs. 11 A). Element mapping using QEMSCAN® on sample 7196@11m, with a bulk copper content of 7510 mg/kg (XRF analyses, Table 2) show the association of copper with Fe(III) hydroxides (Fig. 13). In this sample, no Cu sulfate or phosphate is evidenced, suggesting a coprecipitation of copper with the Fe(III) hydroxides.

Other samples, like sample 7569@33.5 m, are poor in Fe(III) oxides and hydroxides (Fe_2O_3=2.78%, Table 2) and show under the microscope an important fraction of preserved hypogene minerals, mainly quartz grains and feldspar. The observations made under the microscope are confirmed by element mapping using QEMSCAN® (Fig. 14) showing that the

original texture and mineralogy of the sample is partly preserved, and evidences the important sericitization of feldspars. This is consistent also with high Al_2O_3 (14.98%), K_2O (5.83%) and SiO_2 (64.81%) bulk analysis (Table 2). In this sample 7569@33.5 m, the bulk copper content is 1510 mg/kg (XRF analyses, Table 2). Element mapping indicates that Cu is contained in the red spots visible in the rock slab (Fig. 10 D), that are sulfates containing also Al, K, and Fe (Fig. 14. The Cu-Al-K-Fe bearing sulfates show a border of iron oxide minerals (Fig. 14 F) and are probably relicts of former sulfides, possibly chalcopyrite. The sulfates and their iron oxide borders illustrate the differences of mobility of the different elements liberated during the oxidation processes, oxidized forms of iron remain on site, while the probably associated copper was almost totally removed by the supergene solutions.

Relictic pyrite frequently rimmed by supergene chalcocite has been observed (Fig. 11 B) in the lower part of the oxidation zone in all three vertical sections where polished were studied. Antlerite veins are occasionally recognized (Figs. 10 F and 11 B). Atacamite is only observed in samples without sulfide relicts and is frequently spatially associated with copper wad (Fig. 10 H, 11 D and 11 H). No other chloride mineral was identified.

EDS analyses show that sulfates frequently replace pyrite, the crystalline shape of which is still present as ghosts partly or totally filled (Figs. 11 I-J-K). Those sulfates contain principally iron (around 25%), aluminum and potassium (both around 5%), and might by minerals from the jarosite-alunite group.

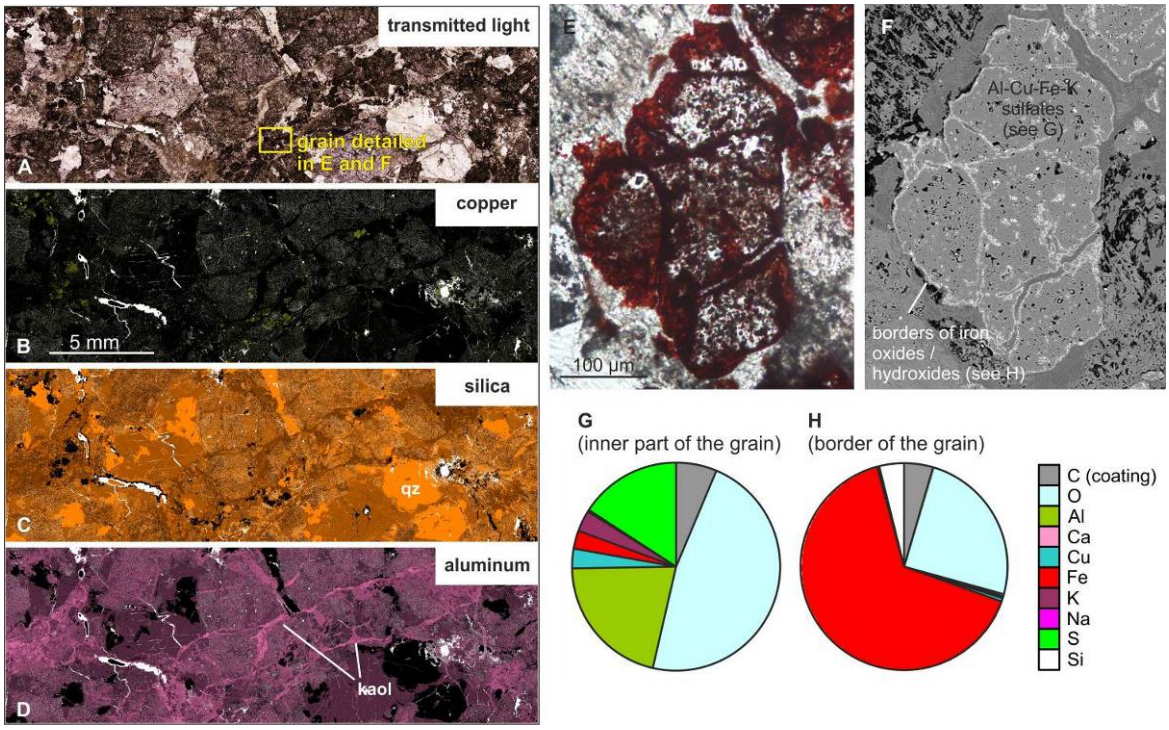

Figure 14: Sample 7569 at 33m. A. Transmitted light, plane-polarized, box indicate the location of the grain detailed in (E) and (F); B. to D. relative repartition map of copper, silica and aluminum obtained with the QEMSCAN®; B. light yellow patches indicate the presence of copper, and microscope and SEM observations indicate that they are related with sulfate grains as detailed in (E) to (H); C. Orange scale indicate the relative concentration of silica, bright orange representing pure quartz grains; D. Violet scale indicate the relative concentration of aluminum, the grains presenting silica and aluminum are aluminum bearing

silicates (like the two kaolinite veins crossing the sample), while others with aluminum and without silica are the aluminum-copper-iron sulfates as presented in (E) to (H); E. Transmitted light, plane-polarized view of a sulfate grain (boxwork texture), whom chemical composition obtained with EDS is detailed in (G) and (H); F. Same grain as (E) with SEM BEI, the variation of chemical composition between the center and the border of the grain is illustrated by the changes in grey scale intensities; G. chemical composition of the center of the sulfate grain obtained with EDS, showing the presence of sulfate (16%), aluminum (21%), and little amounts copper (3.1%), iron (2.6%) and potassium (3.4%) ; H. chemical composition of the border of the sulfate grain obtained with EDS, showing the presence of iron (65%), and little amount of silica (3.8%) and copper (0.7%).

The pale green to yellow color of these sulfates in transmitted light microscopy and the frequently observed cubic fabrics correspond to the characteristics of voltaite ($K_2Fe^{2+}_5(Fe^{3+}$, $Al)_4(SO_4)_{12} \bullet 18H_2O$, Fig. 11 I-J-K-L). They are frequently spatially associated with iron oxides and/or hydroxides (Fig. 11 I). Bandy (1938), who had access to larger examples, describes metavoltine, ferrinatrine, metasideronatrite, ungemachite and alums. Nevertheless, no one of these minerals has optical characteristics and/or chemical composition similar to those of voltaite.

Bulk analyses

The copper contents in the oxidation zone (Table 4) depend largely on the hydrothermal alteration zone in which the oxidation zone develops. Samples from the quartz-sericite hydrothermal alteration zone have averages of 0.46 wt% in Cu in the N2900 and N4200 sections (in the N5600 section this alteration zone is not represented); those of the potassic hydrothermal alteration zone averages of 1.03 wt%, 2.2 wt% and 0.6 wt% Cu in the, respectively, N2900, N4200, and N5600 sections; and those from the chloritic hydrothermal alteration zone averages of 0.58 wt%, 0.78 wt%, and 0.14 wt% in the same sections (Table 2).

Iron values in the oxidation zone are highly variable (Table UNIQUAN_DATA, no iron content is available in the CODELCO database). The richest in iron, with values up to 25 wt% Fe_2O_3 are gossan samples from the chloritic hydrothermal alteration zone in the section N2300 of the deposit; they display reddish to pinkish colors and in part bear fine grained specularite in veinlets (section N2300, drill core 7196, Figs. 10 A to C). In most studied samples, iron values range between 1.37% and 5.14% Fe_2O_3.

Obtained manganese values in the oxidation zone lie between 424 and 40 mg/kg in section N2300 and between 30 and 1400 mg/kg in section N5600 (semi-quantitative XRF analysis, Table 2). These relatively low values contrast with the frequent hypogene rhodocrosite veins observed in the open pit. It can be derived that most Mn was mobilized and not retained during the oxidation processes in the oxidation zone of Chuquicamata.

High contents in Al, Si, K, and Mg indicate that in most samples the rock forming and hypogene alteration minerals are the main constituents. (Table 2).

Table 4: Copper grade values used for the mass balance. Bold values are estimated from the adjacent. Each mean copper value has been obtained using the grades of the CODELCO data base for the drill hole intersections in each "cell" defined by the roughly vertical hydrothermal and the roughly horizontal supergene alteration zones in each of the 40 vertical sections. Data of 437 drill hole cores and more than 70.000 analyses have been used.

		N2200	N2300	N2400	N2500	N2600	N2700	N2800	N2900	N3000	N3100	N3200	N3300	N3400	N3500	N3600	N3700	N3800	N3900
Oxidation zone Cu_{ox}	qs	0.03	0.16	0.3	0.3	0.11	0.09	0.62	0.46	0.18	0.26	**0.22**	0.18	0.18	0.63	0.2	0.05	0.04	0.73
	zt/pot		0.16	0.72	0.76	0.99	0.27	0.42	1.03	0.62	1.05	0.32	2.47	0.92	0.69	1.13	1.01	1.64	2.11
	chl	0.48	0.12	0.12	0.18	**0.255**	0.33	0.16	0.58	0.71	0.57	0.88	0.24	1.75	0.33	0.1	0.55	0.42	0.11
Supergene 1 (cc) Cu_{sup1}	qs	**2.44**	2.24	2.8	2.3	2.85	2.67	3.16	3.7	2.47	1.31	1.16	1.34	2.7	1.32	2.14	2.18	2.85	2.33
	zt/pot		1.33	**1.58**	1.83	**2.26**	1.34	1.27	2.64	0.8	2.41	1.66	0.85	1.81	1.99	0.82	1.72	1.08	1.83
	chl	1.25			**0.7**	1.83	0.7	**0.7**	**0.7**	**0.99**	1.28	**1.14**	1	0.75					
Supergene 2 (cv) Cu_{sup2}	qs	**0.35**	**0.35**	0.35	0.96	0.44	0.67	1.53	0.94	0.96	0.72	0.96	1.09	1.03	0.84	1.88	0.92	1.2	1.26
	zt/pot		0.66	0.7	0.71	0.55	**0.81**	0.81	0.92	0.69	1.17	0.86	0.8	0.73	0.72	0.55	1.48	0.77	0.84
	chl	0.13	0.27	0.16	0.3	0.14	0.28	0.22	0.54	0.56	0.53	1.5	0.44	0.56	0.62		0.83	**1.145**	
Primary Cu_{prim}	qs		**0.39**	**0.39**	**0.39**	0.39	0.37	0.86	0.5	0.55	0.49	0.6	0.52	**0.725**	**0.725**	0.93	0.84	1.61	0.62
	zt/pot		0.22	0.56	**0.65**	0.74	0.75	0.69	0.69	0.53	0.89	0.69	0.68	0.71	0.98	0.92	0.98	0.45	0.94
	chl	**0.28**	0.28	0.14	0.17	0.14	**0.175**	0.21	0.22	0.36	0.15	0.25	0.23	0.15	0.2	0.09	0.46	0.21	0.33

		N4000	N4100	N4200	N4300	N4400	N4500	N4600	N4700	N4800	N4900	N5000	N5100	N5200	N5300	N5400	N5500	N5600	N5700	N5800	N5900	N6000	N6100	N6200
Oxidation zone Cu_{ox}	qs	0.46	1.46	0.46	0.55	0.39	0.8	0.35	1.35	0.36	0.79													
	zt/pot	2.1	1.25	2.2	0.69	2.65	0.95	1.62	2.43	2.32	2.74	1.49	0.68	1.36	0.53	0.61	0.57	0.6	0.22	0.25	0.37	0.5	0.42	0.31
	chl	0.24	0.31	0.78	0.61	0.95	0.53	0.75	0.99	0.75	1.75	1.23	0.88	0.78	0.17	0.65	0.22	0.14	0.09	0.03	0.18	0.18	0.14	0.15
Supergene 1 (cc) Cu_{sup1}	qs	3.08	3.02	2.8	3.1	2.94	2.92	2.42	1.95	0.97	3.08													
	zt/pot	1.23	1.05	**2.1**	3.15	**2.725**	2.3	1.96	2.21	2.82	2.07	1.76	1.67	2.27	**1.86**	1.45	0.4	0.7						
	chl											0.91	2.13	**1.68**	1.23	0.95	0.98	**0.98**						
Supergene 2 (cv) Cu_{sup2}	qs	1.31	1.66	1.12	1.07	1.29	0.83	0.95	1.27	1.03	0.92													
	zt/pot	1.1	1.59	1.14	1.43	1.26	1.28	0.85	0.98	0.9	1.08	0.81	1	0.79	0.69	0.51	0.37	0.45	0.42	0.4	0.23	0.78	0.32	0.52
	chl	**1.145**	1.46	0.64	0.51	**0.51**			0.94	0.18	0.22	0.5	0.44	0.46	0.45	0.47	0.74	0.21	0.25	0.19	0.19	0.22	0.33	0.24
Primary Cu_{prim}	qs	1.2	1.27	1.02	**0.875**	0.73	0.7	0.83	0.77	0.5	0.7													
	zt/pot	0.89	0.71	0.74	0.77	0.81	0.8	0.72	0.8	0.76	0.62	0.43	0.63	0.86	0.51	0.49	0.5	0.3	0.24	0.34	0.42	0.36	0.32	0.24
	chl	0.4	0.42	0.3	0.23	0.16	0.17	0.25	0.11	0.08	0.58	0.26	0.32	0.31	0.13	0.55	0.27	0.32	0.12	0.17	0.17	0.26	0.09	0.09

Sequential extraction

Nine samples from the oxidation zone were analyzed with sequential extraction (Fig. 15, Table 5). Microscopic and MEB descriptions, combined with XRF bulk chemical analyses were used to select the samples for sequential extraction.

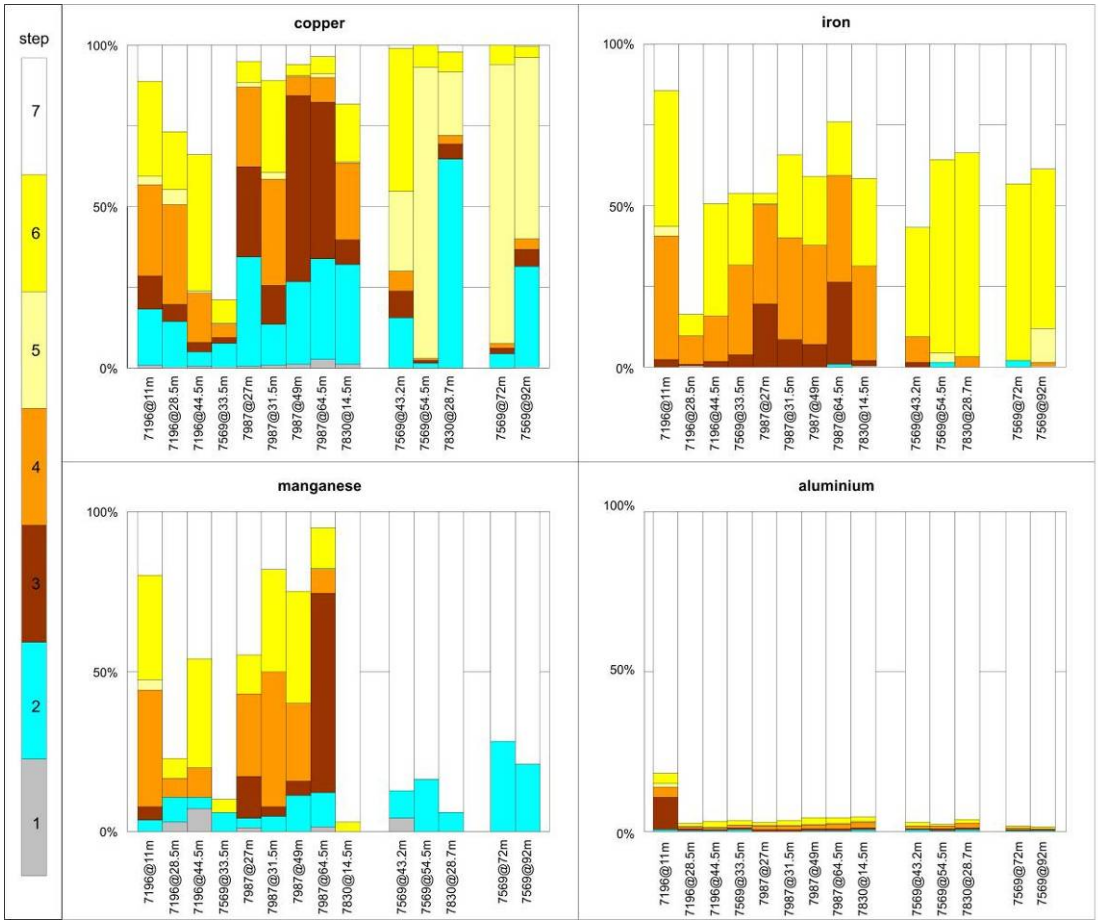

Figure 15: Percent of Cu, Fe, Mn and Al contained in each analyzed sample liberated during each sequential extraction step. The amounts are given in Table 5.

Table 5: Results of the sequential extraction for Cu, Fe, Mn and Zn, presented as mg/kg and as percent of the total of the element liberated during each step.

drill core	depth m	step	Cu mg/kg	Cu % of the tot Cu	Fe mg/kg	Fe % of the tot Fe	Mn mg/kg	Mn % of the total Mn	Zn mg/kg	Zn % of the total Zn
7196	11	1	41.9	0.76		0.00	0	0.0	2.5	2.7
7196	11	2	967	17.52		0.00	10	3.7	17	18.0
7196	11	3	567	10.27	2300	2.38	11	4.0	6.2	6.6
7196	11	4	1560	28.26	37000	38.22	99	36.4	14.5	15.4
7196	11	5	149	2.70	2800	2.89	9	3.3	3.2	3.4
7196	11	6	1620	29.34	40700	42.05	89	32.7	24.5	26.0
7196	11	7	616	11.16	14000	14.46	54	19.9	26.3	27.9
7196	28.5	1	0.7	0.24		0.00	2	3.0	0.6	1.3
7196	28.5	2	41.6	14.28	100	0.16	5	7.6	18.9	39.6
7196	28.5	3	15.2	5.22	500	0.80	0	0.0	2	4.2
7196	28.5	4	90.1	30.93	5400	8.63	4	6.1	3.8	8.0
7196	28.5	5	13.1	4.50	100	0.16	0	0.0	2.1	4.4
7196	28.5	6	52.8	18.13	4100	6.55	4	6.1	3.3	6.9
7196	28.5	7	77.8	26.71	52400	83.71	51	77.3	17	35.6
7196	44.5	1	9.3	0.58		0.00	6	7.1	7.6	1.0

drill core	depth m	step	Cu mg/kg	Cu % of the tot Cu	Fe mg/kg	Fe % of the tot Fe	Mn mg/kg	Mn % of the total Mn	Zn mg/kg	Zn % of the total Zn
7196	44.5	2	70.1	4.38		0.00	3	3.5	7	0.9
7196	44.5	3	48.9	3.06	2600	1.70	0	0.0	7.3	1.0
7196	44.5	4	242	15.12	21400	14.00	8	9.4	63.9	8.6
7196	44.5	5	10	0.62	200	0.13	0	0.0	4.1	0.6
7196	44.5	6	677	42.30	53300	34.86	29	34.1	396	53.2
7196	44.5	7	543	33.93	75400	49.31	39	45.9	259	34.8
7569	33.5	1	2.3	0.19		0.00	0	0.0	3.3	8.7
7569	33.5	2	89.5	7.56		0.00	3	6.0	14.6	38.6
7569	33.5	3	19.6	1.66	600	3.95	0	0.0	1.1	2.9
7569	33.5	4	49.9	4.22	4200	27.63	0	0.0	1.5	4.0
7569	33.5	5	1.3	0.11		0.00	0	0.0	0	0.0
7569	33.5	6	87.2	7.37	3400	22.37	2	4.0	2.4	6.3
7569	33.5	7	934	78.90	7000	46.05	45	90.0	14.9	39.4
7569	43.2	1	6.3	0.04		0.00	2	4.3	1.9	2.9
7569	43.2	2	2560	15.46		0.00	4	8.5	22.2	34.3
7569	43.2	3	1370	8.28	200	1.55	0	0.0	0.9	1.4
7569	43.2	4	1040	6.28	1000	7.75	0	0.0	1.7	2.6
7569	43.2	5	4060	24.52		0.00	0	0.0	1.3	2.0
7569	43.2	6	7360	44.46	4400	34.11	0	0.0	6.1	9.4
7569	43.2	7	159	0.96	7300	56.59	41	87.2	30.6	47.3
7569	54.5	1	1.6	0.03		0.00	0	0.0	3.3	1.4
7569	54.5	2	91.5	1.59	100	1.43	6	16.2	79.3	34.3
7569	54.5	3	37.3	0.65		0.00	0	0.0	9.6	4.2
7569	54.5	4	36.5	0.63		0.00	0	0.0	14.7	6.4
7569	54.5	5	5200	90.29	200	2.86	0	0.0	78.6	34.0
7569	54.5	6	386	6.70	4200	60.00	0	0.0	12.6	5.5
7569	54.5	7	6.4	0.11	2500	35.71	31	83.8	33	14.3
7569	72	1	4.9	0.14		0.00	0	0.0	6.6	0.7
7569	72	2	154	4.35	100	1.96	13	28.3	167	17.0
7569	72	3	56.9	1.61		0.00	0	0.0	37	3.8
7569	72	4	54.3	1.53		0.00	0	0.0	83.1	8.5
7569	72	5	3070	86.63		0.00	0	0.0	522	53.2
7569	72	6	200	5.64	2800	54.90	0	0.0	97.9	10.0
7569	72	7	3.6	0.10	2200	43.14	33	71.7	68.5	7.0
7569	92	1	0.7	0.31		0.00	0	0.0	0.8	0.7
7569	92	2	71.3	31.11		0.00	9	20.9	28.7	23.8
7569	92	3	12.1	5.28	100	0.30	0	0.0	4.9	4.1
7569	92	4	7.5	3.27	400	1.22	0	0.0	8.8	7.3
7569	92	5	129	56.28	3400	10.37	0	0.0	26.3	21.8
7569	92	6	7.8	3.40	16200	49.39	0	0.0	3.6	3.0
7569	92	7	0.8	0.35	12700	38.72	34	79.1	47.4	39.3
7987	27	1	8.5	0.55		0.00	4	1.3	28.6	5.0
7987	27	2	522	33.88		0.00	9	3.0	130	22.7
7987	27	3	431	27.97	4400	19.56	39	12.8	98.2	17.2
7987	27	4	378	24.53	6900	30.67	79	26.0	132	23.1
7987	27	5	26.4	1.71	100	0.44	0	0.0	16.6	2.9
7987	27	6	96.8	6.28	700	3.11	37	12.2	69.5	12.1
7987	27	7	78.2	5.07	10400	46.22	136	44.7	97.3	17.0
7987	31.5	1	8.4	0.97		0.00	0	0.0	5.7	1.1
7987	31.5	2	109	12.61		0.00	9	4.6	53.6	10.5
7987	31.5	3	105	12.15	600	8.57	6	3.1	26.2	5.1
7987	31.5	4	283	32.74	2200	31.43	82	42.3	125	24.5
7987	31.5	5	19.3	2.23		0.00	0	0.0	19.4	3.8
7987	31.5	6	245	28.34	1800	25.71	62	32.0	197	38.6
7987	31.5	7	94.8	10.97	2400	34.29	35	18.0	83.6	16.4
7987	49	1	19.3	1.10		0.00	0	0.0	2.1	0.8
7987	49	2	448	25.64		0.00	36	11.4	51.4	18.7
7987	49	3	1010	57.81	700	7.14	14	4.4	27.3	9.9
7987	49	4	101	5.78	3000	30.61	77	24.3	60.2	21.8
7987	49	5	6.6	0.38		0.00	0	0.0	6.1	2.2
7987	49	6	59.3	3.39	2100	21.43	111	35.0	68.6	24.9
7987	49	7	103	5.90	4000	40.82	79	24.9	59.9	21.7
7987	64.5	1	6.7	2.64		0.00	13	1.6	19.4	2.3
7987	64.5	2	78.8	31.10	100	0.75	90	10.8	166	20.1
7987	64.5	3	123	48.54	3400	25.56	520	62.1	276	33.3

drill core	depth m	step	Cu mg/kg	Cu % of the tot Cu	Fe mg/kg	Fe % of the tot Fe	Mn mg/kg	Mn % of the total Mn	Zn mg/kg	Zn % of the total Zn
7987	64.5	4	19.9	7.85	4400	33.08	62	7.4	132	15.9
7987	64.5	5	2.9	1.14		0.00	3	0.4	20.5	2.5
7987	64.5	6	12.8	5.05	2200	16.54	107	12.8	123	14.9
7987	64.5	7	9.3	3.67	3200	24.06	42	5.0	91	11.0
7830	14.5	1	9	1.05		0.00	0	0.0	1.9	2.9
7830	14.5	2	265	31.02	100	0.41	0	0.0	7.2	10.9
7830	14.5	3	65.8	7.70	400	1.65	0	0.0	0.8	1.2
7830	14.5	4	202	23.65	7100	29.22	0	0.0	4	6.1
7830	14.5	5	2.4	0.28		0.00	0	0.0	1.4	2.1
7830	14.5	6	153	17.91	6600	27.16	3	2.8	9.7	14.7
7830	14.5	7	157	18.38	10100	41.56	103	97.2	41.1	62.2
7830	28.7	1	15.7	0.10		0.00	0	0.0	0.8	2.5
7830	28.7	2	10000	64.69		0.00	2	6.1	11.2	35.4
7830	28.7	3	725	4.69		0.00	0	0.0	0.6	1.9
7830	28.7	4	416	2.69	400	3.28	0	0.0	1.6	5.1
7830	28.7	5	3050	19.73		0.00	0	0.0	0	0.0
7830	28.7	6	916	5.93	7700	63.11	0	0.0	2.4	7.6
7830	28.7	7	336	2.17	4100	33.61	31	93.9	15	47.5

The nature of the oxide minerals is variable, including iron oxide and hydroxides, sulfates, phosphates and silicates, as described in detail below for some examples. In samples 7196@11m and 7196@44.5m, supergene iron oxides and hydroxides are the principal minerals (almost 90% of the sample, the rest being principally quartz and fine sericite). In the other seven samples, the original textures are recognized, oxide minerals are less abundant and occur as reddish to dark brown disseminate grains or in veins. In sample 7987@31.5m (Fig. 10 H), a black copper wad impregnation is observed. No relict sulfides were found in the selected samples. Relict feldspar crystals were commonly strongly sericitized.

During step 1 (deionized water), gypsum is the only mineral that dissolves (sample 7987@27m). During step 2 (ammonium acetate), atacamite is dissolved. The results for steps 1 and 2 are consistent with tests made on pure copper pitch that confirm that atacamite doesn't dissolve during step 1, and almost totally disappears during step 2 (Chapter 2). Copper wad seems to start dissolving during step 3 (oxalic acid) as illustrated by the results of the two samples with this mineral (Fig. 10 G, 7987@27m and Fig. 10 H, 7987@64.5m) that partly dissolve during this step and release principally Mn, Cu, Al, Fe, P. Step 4 (heated oxalic acid) partly dissolves the iron oxides and/or hydroxides (principally hematite and goethite). Step 5 (oxygen peroxide) has no impact on the samples of the oxidation zone. Step 6 (KClO3, HCl and HNO3) continues dissolving the iron oxides and hydroxides; no sulfide, originally targeted by this step, is present in the selecte samples of the oxidation zone. Finally, step 7 dissolves the residual fraction, principally silicates of hypogene and supergene origin (probably principally amorphous fraction contained in chrysocolla and copper wad mineralization). In samples from section N5600, most copper is adsorbed (liberated during step 2, ammonium acetate) or part of copper wad and/or iron oxides or hydroxides mineralization (steps 3, oxalic acid, and 4, heated oxalic acid). This is not the case in the section N2300, where most copper appears to be linked to more resistant phases, including well crystallized iron oxides and hydroxides (copper liberated during steps 6, $KClO_4$, and 7, HNO_3, HF and $HClO_4$). In some samples of this section, and principally in sample 7569@33.5m, an important fraction of the total copper in the sample is liberated during these steps (Table 5).

1.3.2 Supergene sulfide enriched zone and hypogene zone

The supergene sulfide enriched zone is defined by the presence of new sulfides formed from supergene solutions. At Chuquicacamata, the supergene enrichment zone is best developed in

the southern and western part of the deposit as shown in Figs. 5, 6, 7, illustrating the three studied sections, with the position of the described samples, and their sulfide composition. This gradation of the mineralization corresponds to the distribution of the mineralization intensity in the deposit, the lower neutralization potential in the western part of the deposit owing the widespread acidic alteration at the vicinity of the West Fissure (Ossandón et al. 2001). Chalcocite is the dominant sulfide in the upper supergene sulfide enrichment. A chalcocite blanket of around 300 m is recognized in the sections N4200 and N2900, and roughly corresponds to the high supergene sulfide enrichment zone. Microprobe analyses (disscused in Chapter 3) show that the chemical composition field of this chalcocite corresponds to djurleite, but chalcocite name was conserved as a general term for supergene copper sulfide with the optical characteristics of chalcocite; no XRD analyses were carried out to prove or disprove the presence of djurleite. Downwards the ratio covellite/chalchocite increases. In the less developed eastern and northern sections, chalcocite is almost absent and covellite is the dominant supergene sulfide. This chalcocite versus covellite distribution is typical for supergene profiles in porhypry deposits as covellite forms before chalcocite during sulfide enrichment, at more oxidizing conditions (Sillitoe, 2005; Brimhall et al., 1985; Sato, 1992).

Both chalcocite and covellite can be of hypogene as well as supergene origin. As already noted by Ossandón et al. (2001) supergene chalcocite, massive or rimming pyrite, is found at highest elevation, (Figs. 16 A-G, Figs. 17 A-C). Microprobe analyses on hypogene copper sulfides (dissused in Chapter 3) show compositions for hypogene covellite between CuS and $Cu_{1.08}S_{0.92}$ and compositions of supergene chalcocite between $Cu_{1.85}S_{1.12}$ and $Cu_{1.99}S_{1.01}$, crossing the chemical composition fields of anilite, djurleite, digenite and chalcocite. As no microscopic criteria was possible to be apply, the term chalcocite-digenite is used in this study, taking in account the stability field of these copper sulfides (Vaughan et al., 1997; Evans, 1981). Analyses on supergene chalcocite are included in the same range of composition. Downward and to the east of the supergene sulfide enrichment, fine-grained covellite becomes more abundant, mainly rimming hypogene chalcopyrite. Coarse grains (0.5 to 2 mm) of covellite occur deeper in the oxidation profile together with digenite and/or bornite, and locally with anhydrite.

The presence of anhydrite not hydrated to gypsum is interpreted as an indication of hypogene origin for this type of covellite. Coarse grained covellite together with pyrite is interpreted by Rivera et al. (2013) as formed by sulfidation of bornite during the late sericitic hydrothermal alteration.

The copper content in the sulfide supergene enriched zone also depends largely upon the hydrothermal alteration zone in which they occur. Samples in the low and high supergene sulfide enriched zone from the quartz-sericite hydrothermal alteration zone have averages of 0.94% and 3.7% copper in the N2900 section, and 1.12% and 2.8% in the N4200 section. Those of the potassic hydrothermal alteration zone contain 0.92% and 2.6% copper in the N2900 section, 1.14% and 2.1% in the N4200 section and 0.45%, and 0.7% in the N5600 section. Those of the chloritic hydrothermal alteration zone contain 0.54% and 0.7% copper in the section N2900, 0.64% in the section N4200, and 0.21% in the section N5600 (no high supergene sulfide enriched zone is observed in sections N4200 and N5600). The semi-quantitative XRF analyses (UniQuant®) copper concentrations range between 5840 and 10600 mg/kg in the supergene sulfide enrichment zone. The sequential extraction results show that, as expected, most copper is present as sulfides (liberated during step 5, H_2O_2, and step 6, $KClO_4$), even if a fraction of copper is also liberated during step 2 (ammonium acetate), what should liberate the adsorbed fraction of copper and/or associated with atacamite (Table 5).

At Chuquicamata, as in many other deposits (e.g., Ramdohr, 1980), covellite replaces mainly chalcopyrite. Covellite replacing sphalerite (Fig. 16 K) and enargite (Fig. 17 F) is also observed.

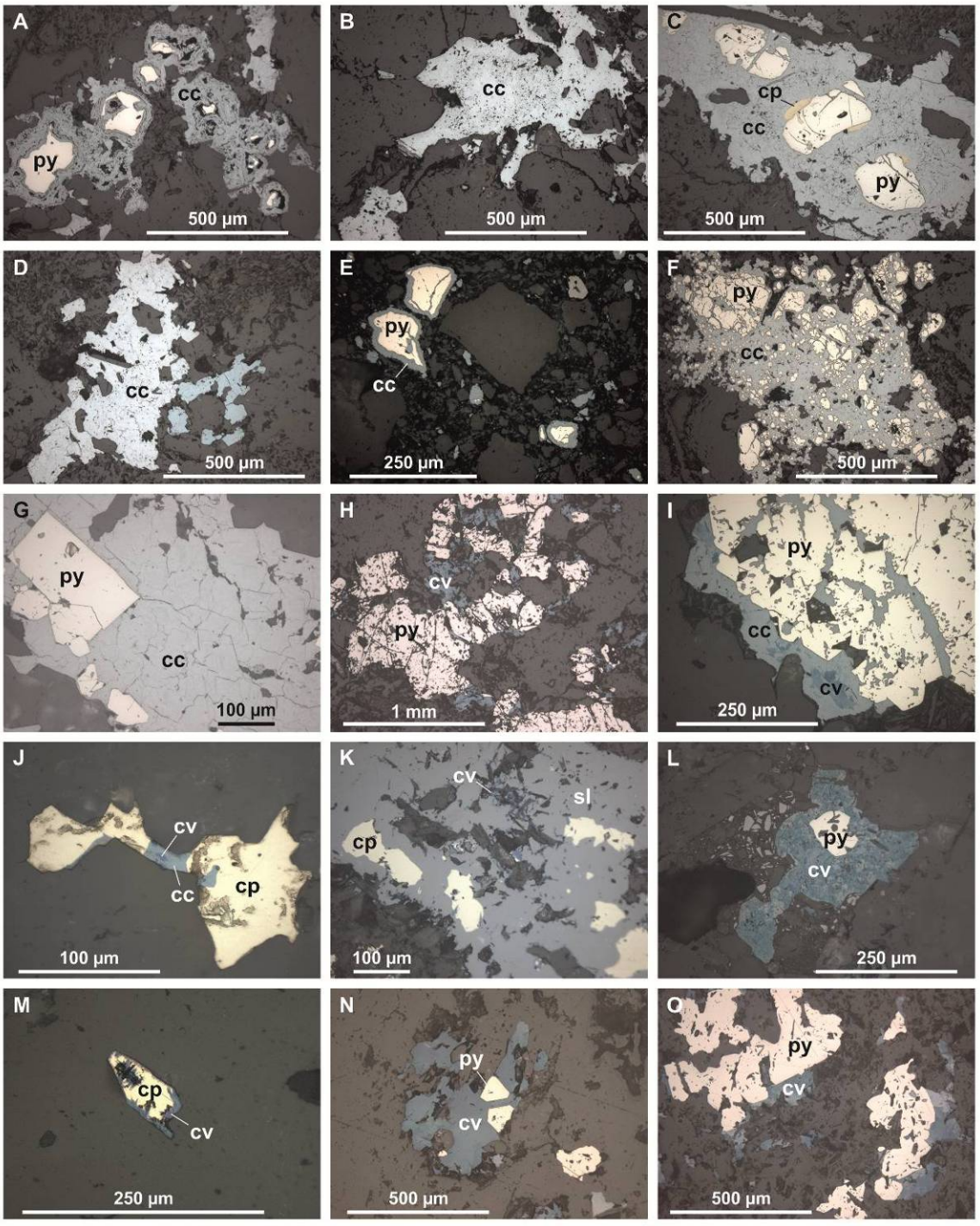

Figure 16: Photomicrographs of sulfides from section N2900, western vertical profile, reflected light, plane-polarized. cc = chalcocite, cp = chalcopyrite, cv = covellite, sl =sphalerite, py = pyrite.
A. CHDD1889 at 59 m, supergene chalcocite with concretional aspect riming pyrite relicts ; B. CHDD1889 at 59 m, supergene chalcocite with a typical mosaic-like aspect; C. CHDD1889 at 88.5 m, supergene chalcocite with concretional aspect riming pyrite-chalcopyrite relicts; D.

CHDD1889 at 88.5 m, supergene chalcocite with a typical mosaic-like aspect; E. CHDD 2011 at 146 m, pyrite grains with supergene chalcocite on porders and cracks; F. CHDD 2779 at 48 m, chalcocite grain with rounded pyrite relicts; G. CHDD2779 at 71.5 m, supegene chalcocite containing a preserved crystal of pyrite, this texture could indicate that pyrite was previously surrounded by chalcopyrite, whom oxidation and replacement by chalcocite is easier; H. CHDD 2779 at 115.7 m, pyrite spacially associated with supergene covellite, which can be the result of the supergene enrichment of pyrite itself, but more probably of chalcopyrite; I. CHDD2779 at 132.7 m, pyrite grain spacially associated with supergene chalcocite contining supergene covellite, covellite has probably replaced chalcopyrite, and has itself been enriched to chalcocite during the ongoing supergene processes; J. CHDD2779 at 132.7 m, chacopyrite grain enriched with the same process as presented in (I.); K. CHDD 2779@135.4 m, sphalerite replacing chalcopyrite during the late hydrothermal stage, replaced itself in small zones by supergene covellite; L. CHDD2779 at 142 m, supergene covellite together with iron oxides replacing pyrite; M. CHDD2779 at 142 m, chalcopyrite grain replaced by supergene covellite on borders and cracks; N. CHDD 2594 at 311 m, supergene covellite grain containing preserved pyrite crystals, which could indicate that covellite replaced chalcopyrite previously spacially associated with pyrite (see G.); O. CHDD 2594 at 328 m, supergene covellite spacially associated with pyrite, probably replacing previously present chalcopyrite.

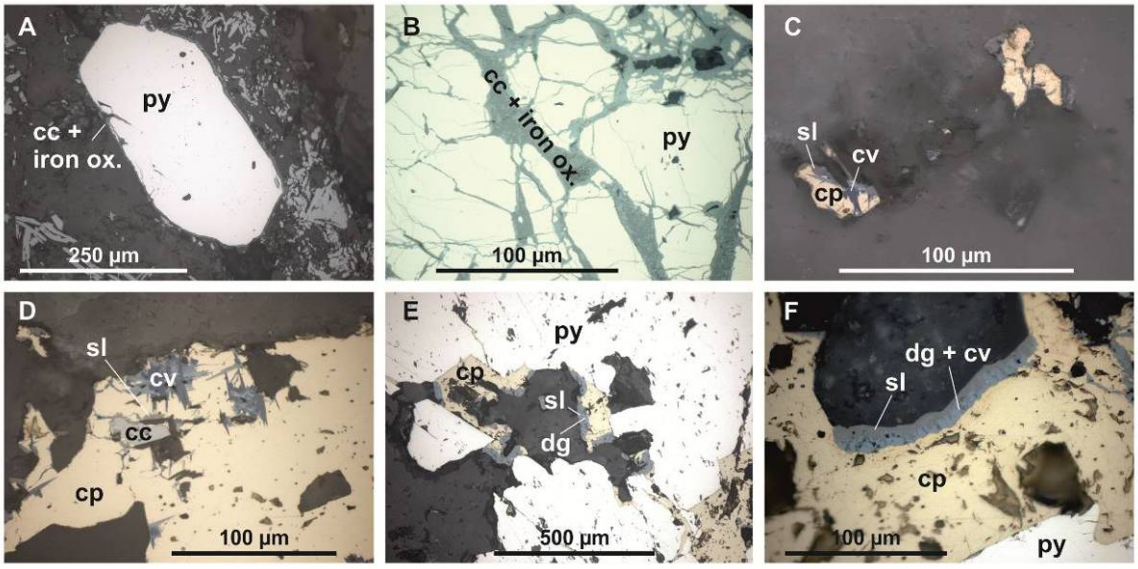

Figure 18: Photomicrographs of sulfides from section N2900, eastern vertical profile, reflected light, plane-polarized. cc = chalcocite, cp = chalcopyrite, cv = covellite, dg = digenite, sl =sphalerite, py = pyrite.
A. CHDD 1539 at 182.2 m, pyrite grain with thin supergene repacement by chalcocite and iron oxides on the border; B. CHDD 1539 at 182.2 m, pyrite grain replacecd in border and cracks by supergene chalcocite and iron oxides; C. CHDD 1539 at 208.5 m, hypogene chalcopyrite-sphalerite grain partly replaced by supergene lamellar covellite; D. CHDD 2249 at 168.2 m, chalcocite with supergene covellite; E. CHDD 2249 at 190 m, hypogene pyrite and chalcopyrite, with small borders of sphalerite on the chalcopyrite, and digenite formed at the contact between chalcopyrite and sphalerite. Supergene covellite is observed in the chalcopyrite; F. CHDD 2249 at 190 m., closer view of the texture described in (E).

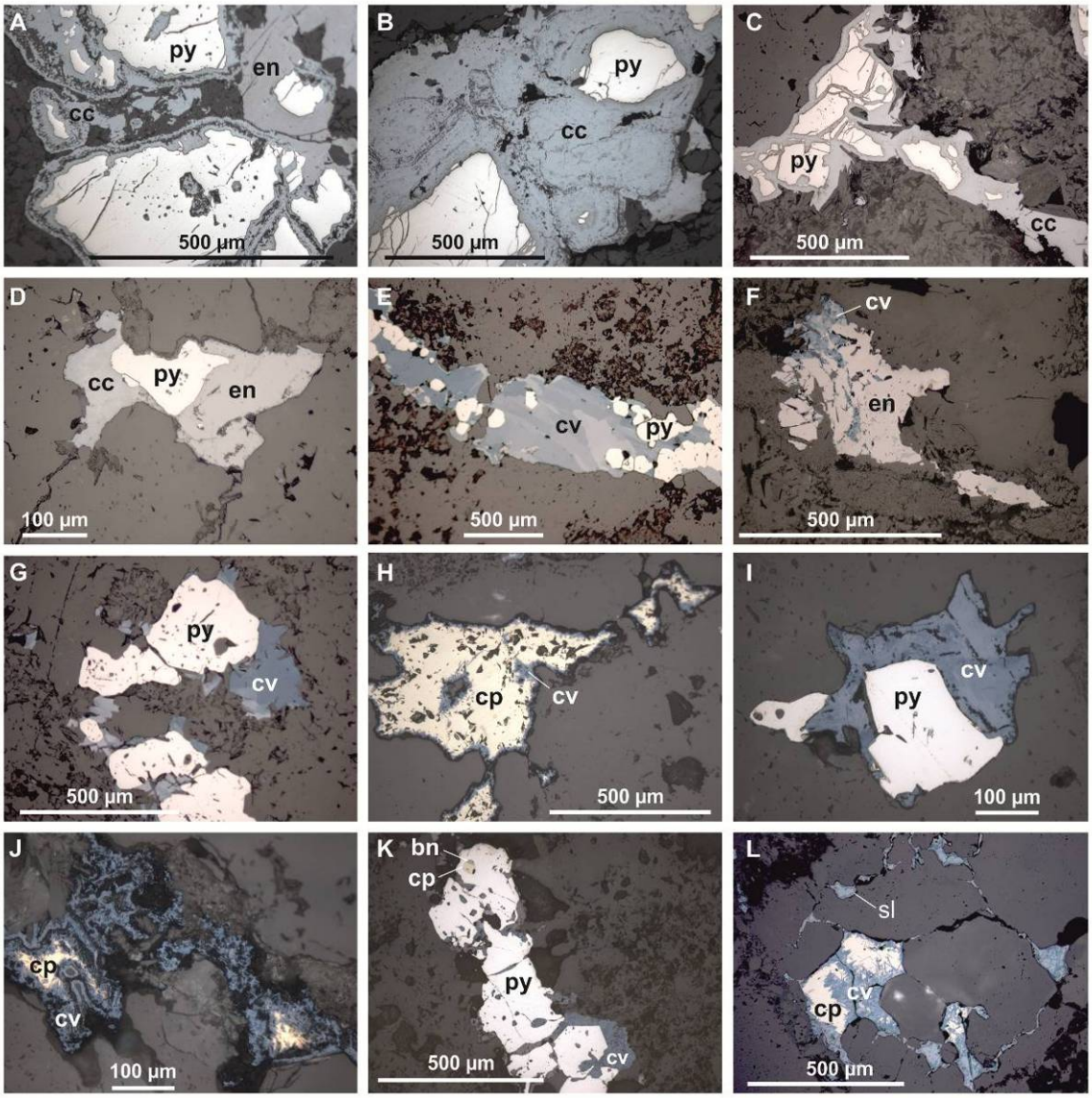

Figure 17: Photomicrographs of sulfides from section N4200, reflected light, plane-polarized. bn = bornite, cc = chalcocite, cp = chalcopyrite, cv = covellite, en = enargite, sl =sphalerite, py = pyrite.

A. bench sample CH7472, hypogene pyrite and enarigite with concretional borders of supergene chalcocite; B. bench sample CH8970, concretional chalcocite containing relictic grains of hypogene pyrite; C. CHDD 1698 at 124.6 m, supergene chalcocite with relictic hypogene pyrite; D. CHDD 2319 at 111 m, hypogene pyrite and enargite with supergene chalcocite; E. CHDD 2319 at 152, supergene covellite containing unaltered pyrite grains. It could indicate that covellite replaced another hypogene mineral, like chalcopyrite; F. CHDD 2319 at 254 m, hypogene enargite with supergene covellite; G. CHDD 1652 at 454 m, hypogene pyrite spatially associated with supergene covellite, which could be the product of chalcopyrite replacement; H. bench sample CH6590, chalcopyrite with borders of supergene coellite; I. bench sample CH6591, same texture than in sample (G); J. bench sample CH6591, concretional supergene covellite containing chalcopyrite relicts; K. bench sample CH6576, same texture than in sample (G); L. CHDD 1226 at 120.1 m, supergene covellite replacing chalcopyrite.

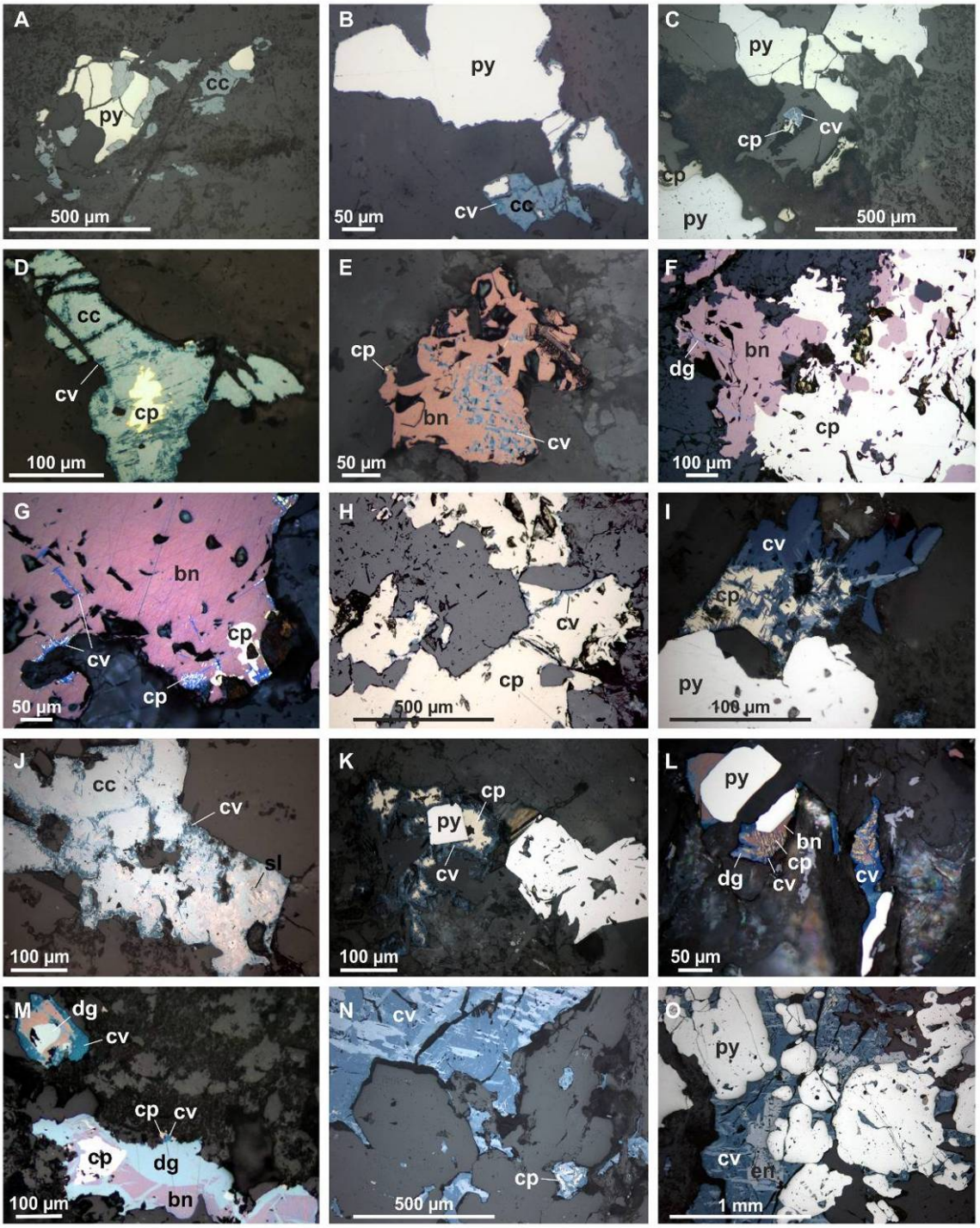

Figure 19: Photomicrographs of sulfides from section N5600, reflected light, plane-polarized. bn = bornite, cc = chalcocite, cp = chalcopyrite, cv = covellite, dg = digenite; en = enargite, sl = sphalerite, py = pyrite.

A. CHDD 1910 at 12.5 m, hypogene pyrite with supergene chalcocite; B. CHDD 1910 at 12.5 m, hypogene pyrite with borders of supergene covellite and chalcocite, spacially associated with a supergene chalcocite-covellite grain; C. CHDD 1910 at 185; 5 m, unaltered pyrite grains and chalcocite grains partly replaced by supergene covellite; D. CHDD 1823 at 39 m, supergene chalcocite containing relict of chalcopyrite, oxidized to covellite on its borders and cracks; E. CHDD 1823 at 196.5 m, hypogene bornite with inclusions of supergene covellite, probably replacing chalcopyrite; F. CHDD 1823 at 196.5 m, hypogene chalcopyrite-bornite

grain with small veins of digenite; G. CHDD 1823 at 355.5 m, bornite-chalcopyrite grain with supergene covellite replacing the chalcopyrite; H. CHDD 1823 at 355.5 m, chalcopyrite grains with borders of supergene covellite; I. CHDD 1985 at 10.4 m, chalcopyrite partly replaced by supergene covellite; J. CHDD 1985 at 30.5 m, supergene chalcocite oxidized to covellite; K. CHDD 1985 at 99 m, chalcocite replaced by supergene covellite, pyrite remains unaltered; L. CHDD 1985 at 184.5 m, unaltered pyrite together with covellite-digenite-chalcopyrite-bornite grains; M. CHDD 1985 at 205 m, hypogene chalcopyrite-bornite-digenite-covellite grains, part of the covellite, replacing chalcopyrite, could be of supergene origine; N. CHDD 1985 at 260.6 m, supergene (?) covellite grains, with some chalcopyrite relicts; O. CHDD 1985 at 260.6 m, supergene covellite partly replacing enargite.

In the studied samples, supergene covellite appears (a) as needles replacing hypogene chalcopyrite, (b) as small grains in chalcocite, and (c) as monomineral grains frequently spatially associated with pyrite.

(a) Covellite needles in chalcopyrite
Needles of covellite in hypogene chalcopyrite are shown in Figs. 16 M, 18 C, 18 D, 17 H, 17 J, 17 L, 19 C, 19 H, 19 I and 19 K. This texture is the result of replacement of chalcopyrite by covellite. In the studied supergene vertical sequences, the occurrence of covellite needles is often the first supergene feature observed; their abundance increase when rising in the supergene profile (section N2900, in the eastern and western vertical sequences, Fig. 16 and 18, in the section N4200, in the eastern and western vertical sequences, Fig. 17, and in the drill cores 1910, at 125 m, Fig. 19, and 1985, at 99 m, Fig. 19, of the section N5600).

All covellite needles in chalcopyrite have been observed in section portions clearly identified as belonging to the supergene sulfide enriched zone; this supports their supergene origin. Therefore, the minor lamellar covellite found in the the lower part of the supergene sulfide enriched zone at the western side of the deposit presenting chloritic alteration (section N2900, Fig. 5), have been used to draw the lower limit of the supergene sulfide enrichment zone.

(b) Small grains of covellite in chalcocite
Small grains of covellite in chalcocite are shown in Figs. 16 I, 16 J, 18 E, 18 F, 19 B, 19 D, 19 J. Figures 16 I, 16 J, 18 E, 18 F give examples of grains of covellite only partly replaced by chalcocite. In the supergene environment, replacement of covellite by chalcocite generally is interpreted to indicate a change to more reducing conditions (Sato, 1992; Enders, 2000). The reverse process, i.e., chalcocite replaced by covellite is observed too (Figs. 19 B, 19 D, 19 J), and suggests that conditions become more oxidizing. In this case, the covellite grains are preferentially located on the borders and fractures of chalcocite.

(c) Covellite as monomineral grains frequently spatially associated with pyrite
Textural differences give in certain cases indications about the origin of monomineral grains of covellite. Supergene covellite is generally fine grained (Fig. 16 H, 16 L), while hypogene covellite shows larger and elongated lamellar crystals (Fig. 16 N, 16 O, 17 E, 19 N, 19 O) (Koski, 2012). The location in the supergene vertical sequence in relation to sulfides identified as supergene by other means, gives also indications on the origin of covellite grains. For instance, supergene covellite in Fig. 17 I does not present a typical fine grained texture but is clearly supergene because of its position on top of the supergene vertical sequence. Nevertheless, there are always samples showing doubtful textures, where covellite could be interpreted as hypogene or as supergene. It is the case for the covellite of Fig. 17 G, showing a

texture very similar to the supergene covellite of sample 17 I, and located at the bottom of the supergene vertical sequence.

In all supergene vertical sequences described in this study, the ratio chalcocite versus covellite increases upwards.

Roughly at the same depth as the covellite replacing chalcopyrite or in samples located just above the samples with covellite replacing chalcopyrite, chalcocite appears rimming hypogene pyrite grains (Figs. 16 E, 16 I, 19 B), in places together with iron oxides (Figs. 18 B, 17 D). In section N4200, chalcocite appears first as grains spatially associated with pyrite and/or enargite. Rising in the supergene vertical sequence, the ratio chalcocite versus pyrite increases (Figs. 16 A, 16 F, 16 G, 17 A, 17 B, 17 C). In samples with pyrite relicts in chalcocite grains, only few samples present relicts of chalcopyrite and enargite (Figs. 16 C, 19 D). In the uppermost samples of section N2900, chalcocite appears as monomineral grains (Figs. 16 B, 16 D). Supergene chalcocite often shows a typical "crackled porcelain" texture (Ramdohr, 1980, Fig. 16 B and 16 D).

Presence of chalcocite in the supergene vertical sequence can be explained by the in situ replacement of hypogene sulfides, following the electromotive series of Schürmann (1888), starting from the mineral boundaries and fissures. Current knowledge shows that the reduction of sulfate is not a significant source of sulfur for the supergene sulfides (Sillitoe, 2005), and would only be possible in the presence of sulfate-reducing bacteria and of significant amount of organic matter (Sillitoe et al., 1996; Enders, 2000; Dold, 2014). Chalcocite is not directly formed as replacement of primary sulfides, but is the final product of a series of copper sulfides. Intermediate products, principally covellite, can be observed when descending the supergene vertical sequence.

Pyrite is frequently the only remaining hypogene sulfide, because of its resistance to the supergene processes (Sikka, 1990; Sato, 1992). There are indications for the former presence of other hypogene sulfides presently totally replaced. In certain samples, pyrite inside chalcocite grains is not rounded but euhedral (Fig. 16 G). In this case, chalcocite may not replace pyrite, as the original shape of pyrite grains is preserved, but another mineral which was spatially associated with pyrite in the hypogene mineralization, likely chalcopyrite, bornite or enargite.

Four samples containing supergene alunite coming from the exotic mineralization were used for $^{39}Ar/^{40}Ar$ dating. Unfortunately, no conclusive results were obtained (Fig. 20). Two types of samples were analyzed. Sample 1 is a pure alunite sample, but the analysis of this sample gave no plateau age. The three other samples are mixed samples from the central strongly acidic altered tube in the central part of the Exótica Deposit. In these samples, XRD analyses show principally the presence of quartz, sanidine and kaolinite in addition to alunite. Separation of the alunite fraction being not possible because of the fine grained texture, it was hoped that the different fusion temperature of the mineral constituting the samples would yield several plateau ages. Unfortunately, only mixed ages, impossible to interpret accurately, were obtained.

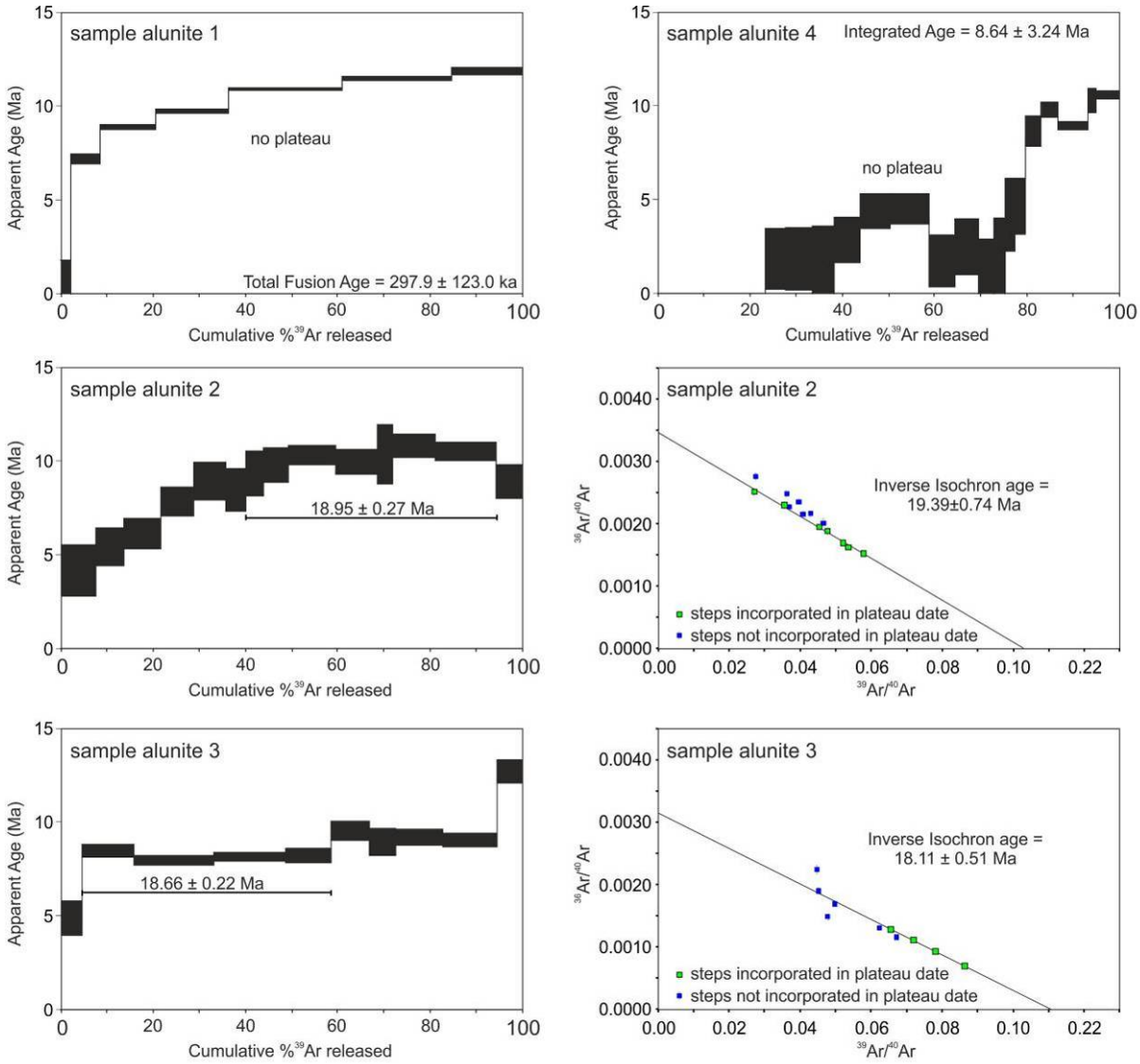

Figure 20: Conventional age spectra and inverse isochron plots for supergene alunite samples.

1.3.3 Mass balance model

A mass balance model based on the copper grades was developed through 40 west-northwest to east-southeast oriented sections between the local coordinates N2300 and N6200, being each section located each one hundred meters apart (Fig. 21). The limits of the hydrothermal alteration zones and of the supergene zones (Fig. 22), and the corresponding copper grades (Fig. 23) are based on the CODELCO mine mode and on a detailed analysis of the logging and metal contents of 437 drill cores of those existing in the CODELCO archives.

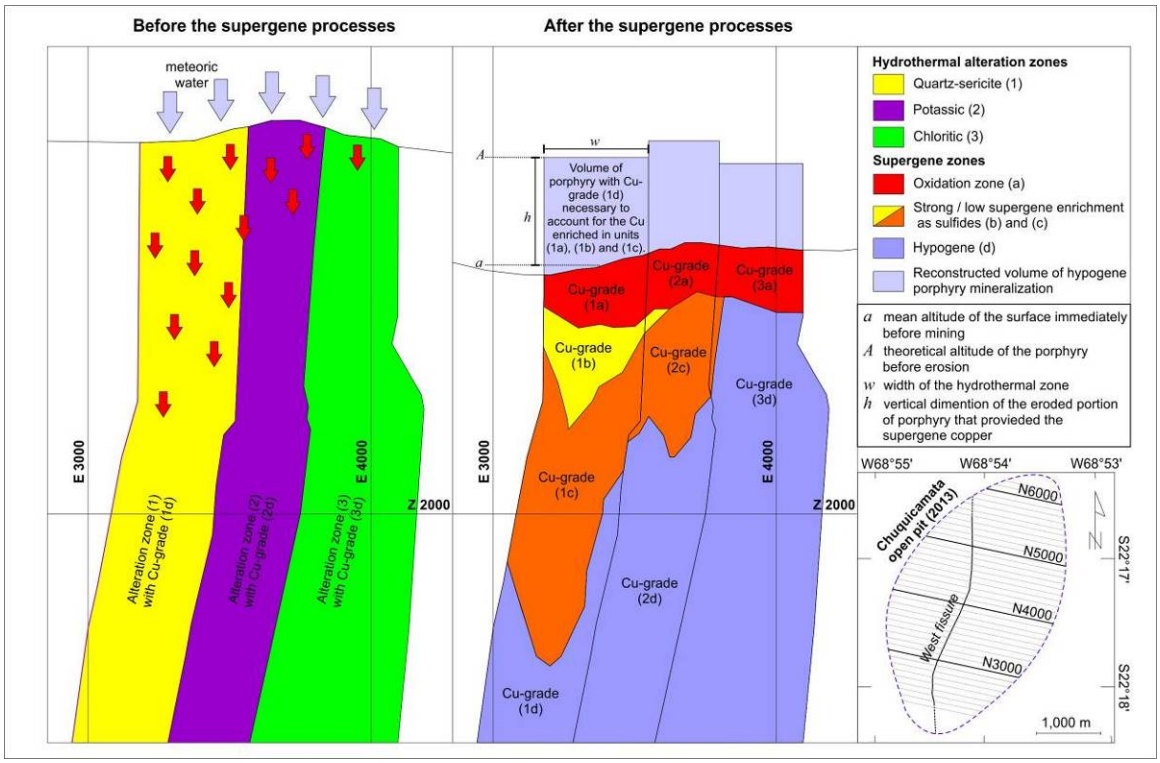

Figure 21: Section N4300 as example of the simplified hydrothermal alteration and supergene zones used for the mass balance calculations. **A.** The left section shows the simplified hydrothermal alteration zones before onset of supergene alteration, arrows symbolizing the infiltrating supergene solutions. **B.** The right section shows the present supergene zones and topography. The size of the light blue columns over the present topography has been obtained with the mass balance model and represents the amount of leached primary porphyry mineralization required to account for the copper enrichment or loss in each supergene profile part. The cells defined by the intersections of the supergene and hydrothermal alteration zones used for the mass balance were measured with ArcGIS on section like part "B" of the figure.

For the purpose of the mass balance model, the roughly vertical alteration zones were simplified into (1) quartz-sericite hydrothermal alteration (*qz-ser*), (2) potassic hydrothermal alteration (*pot*, various grades of potassic alteration), and (3) chloritic hydrothermal alteration zone (*chl*, Fig. 22). From the southern limit of the deposit to the local coordinate N4900, the quartz-sericite hydrothermal alteration zone is located on the western margin of the deposit along the West Fissure, the potassic hydrothermal alteration zone in the central part, and the chloritic hydrothermal alteration zone on the eastern margin (Fig. 22). Further north, the quartz-sericite alteration zone disappears, and the chloritic hydrothermal alteration appears east of the potassic hydrothermal alteration zone (Fig. 22).

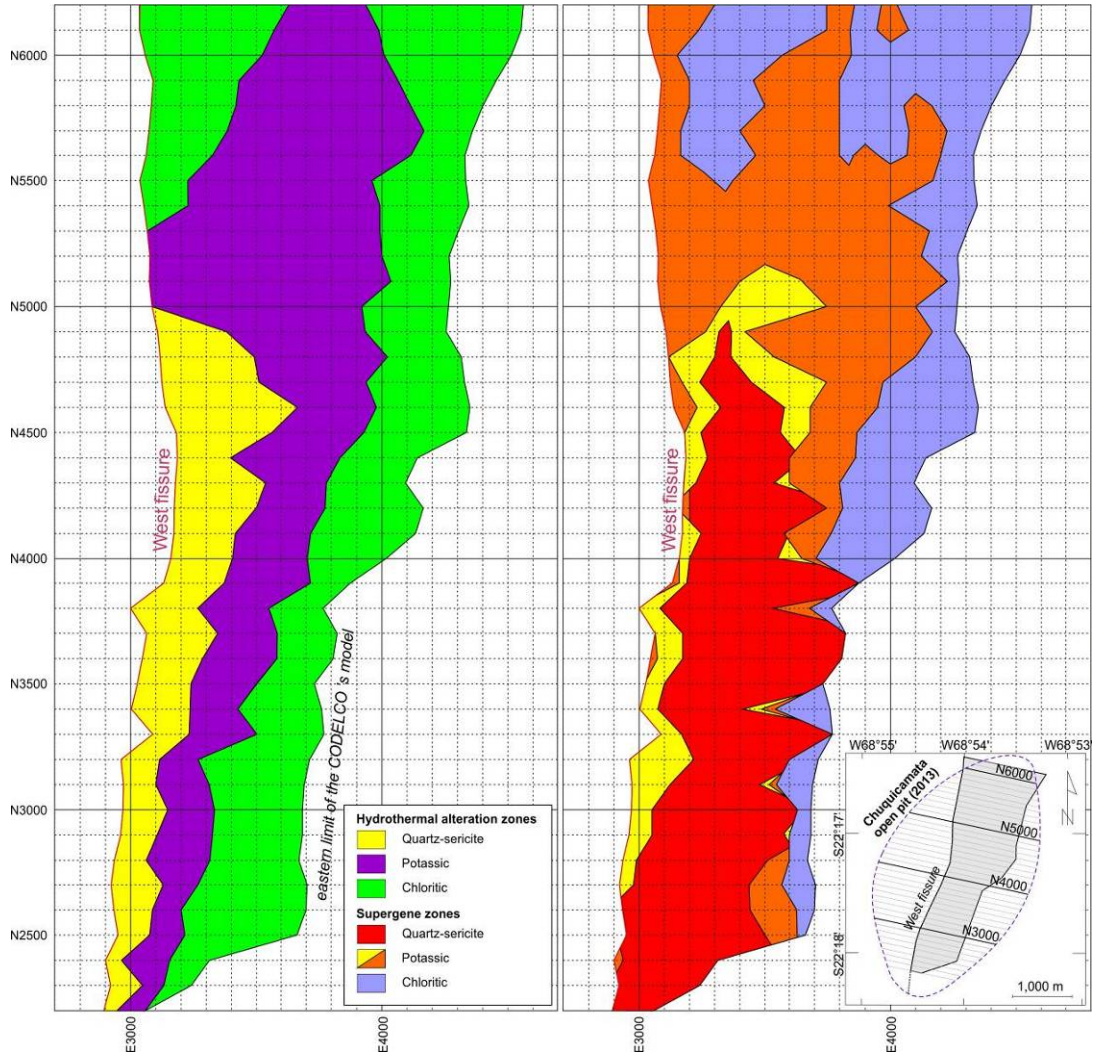

Figure 22: Simplified hydrothermal alteration and supergene zones used for the mass balance calculation in plan view at the 2,700 meters altitude.

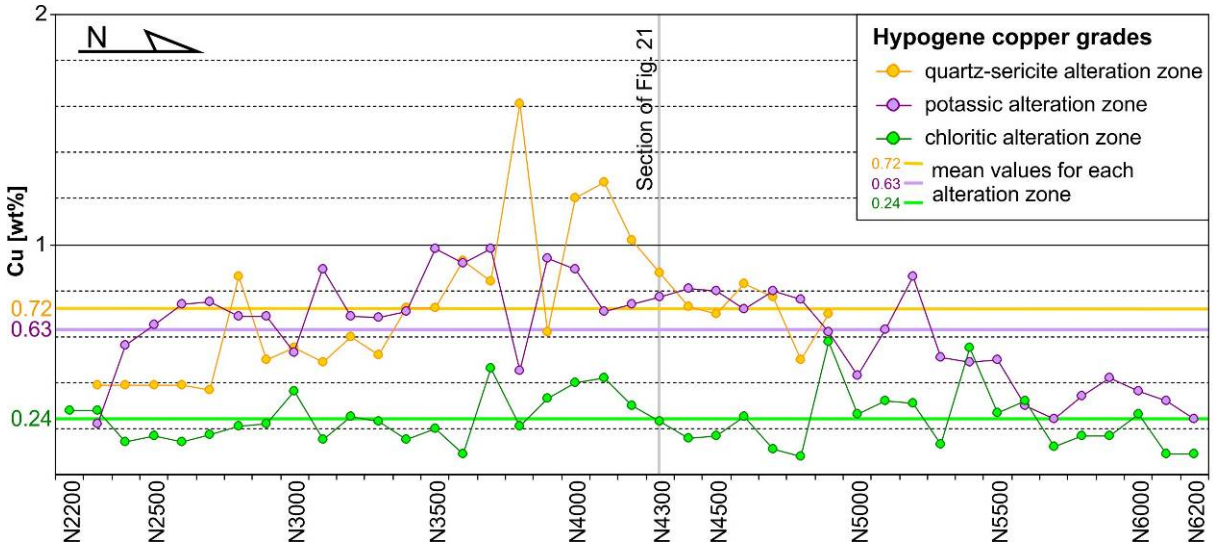

Figure 23: Hypogene copper grades in the quartz-sericite, potassic and chloritic hydrothermal alteration zones used for the mass balance calculations.

Four roughly horizontal supergene zones were defined for the scope of the mass balance model (Fig. 21). The uppermost one is the oxidation zone (*ox*). Below the oxidation zone, the sulfide cementation zone has been subdivided into "strongly enriched supergene sulfide zone" (*strong_sup*) and "low enriched sulfide zone" (*low_sup*) following the CODELCO model classification, based on the replacement ratio of hypogene sulfides. Observations made during this study show that the strongly enriched sulfide zone is chalcocite-dominated and the low enriched sulfide zone is covellite dominated. Strongly enriched supergene sulfide zone is chiefly observed in the quartz-sericite and potassic hydrothermal alteration zones (Fig. 22). The copper contents of portions of the profile not affected by supergene processes, i.e., the hypogene zone (*hyp*), are used for the protore values in the mass balance model.

Mean copper content values obtained from the drill core analyses available at the CODELCO data base were assigned to each hydrothermal alteration zone for each supergene zone (Fig. 21 B). In certain sections, the information was incomplete and copper grades were estimated from the adjacent sections. The primary and supergene copper grades (Cu_{ox}, Cu_{sup1}, Cu_{sup2}, Cu_{prim}) used for each of the 40 sections were calculated from more than 70.000 analyses contained in the CODELCO data base in the way explained in Table 4.

The area of each hydrothermal alteration zone and supergene alteration zone in each of the 40 vertical sections were obtained with the *calculate area* tool of ArcGIS (Annex 2.4). Density (d) has been considered to be homogeneous at the value of 2650 [kg/m^3] in all the deposit.
The copper enrichment or loss in the supergene zones (ε) is defined as the difference between the hypogene and the supergene copper. Equation (1) gives an example how the enrichment in the oxidation zone of the quartz-sericite alteration zone in a particular section is obtained. The copper balance can be negative if the supergene processes removed Cu. The enrichment (ε) allows calculating directly the mass of supergene copper ($[Cu_{sup}]$) removed or added during the supergene processes (2), whereas the total copper present in the supergene zone ($[Cu_{tot}]$) is given in equation (3).

$$\varepsilon_{ox}^{qz-ser} = Cu_{ox}^{qz-ser} - Cu_{hyp}^{qz-ser} \quad (1)$$

$$\left[Cu_{\sup}\right]_{ox}^{qz-ser} = V_{ox}^{qz-ser} \cdot d \cdot \varepsilon_{ox}^{qz-ser} \quad (2)$$

$$\left[Cu_{tot}\right]_{ox}^{qz-ser} = V_{ox}^{qz-ser} \cdot d \cdot Cu_{ox}^{qz-ser} \quad (3)$$

The superposition of the roughly vertical hydrothermal zones and the roughly horizontal supergene zones is taken in account in equation (4) that gives the total mass of copper added or removed by supergene processes in a vertical hydrothermal alteration zone. The total copper in the supergene zones of a single hydrothermal alteration zone is given by equation (5). The difference between the results of (4) and (5) represents the copper already present in the supergene zone before the supergene processes. The result of (4) was used to calculate (6), the vertical dimension (h) of the eroded portion of mineralized porphyry required to explain the copper added to each hydrothermal zone during supergene processes (Fig. 21), being w the width of the hydrothermal zone (obtained from the CODELCO model).

The L factor in equation (6) represents the leaching efficiency in the eroded portion of the oxidation zone. The paramter L equals 1 when all copper contained in the protore has been leached before erosion and is lower than 1 if part of the copper is retained in the oxidation zone. The neutralization potential of the hydrothermal altered rock influences the L factor, as Cu needs pH below 4 to remain in solution. A high neutralization potential of the hydrothermaly altered porphyry will slow down or even prevent the development of a

supergene profile. As a consequence, the oxidation zone will have a pH high enough to cause precipitation of copper in oxide minerals. The ratio hpogene py:cp is also important, as it mainly control the acidification of the supergene solutions.

As it will be explained in the discussion section, the preserved portions of oxidation zone (formed during a period of hyperaditiy and therefore with low supergene activity) are not representative for the previous, now eroded, oxidation zone that was formed in a period with more precipitation and in which leaching efficiency was higher. Therefore, to obtain the parameter of leaching efficiency *L* is not possible to merely calculate the present Cu sup/Cu hyp ratio. Instead, the L values have to be estimated.

The parameter *L* was fixed at 0.9 for the quartz-sericite hydrothermal alteration zone, which because its pyrite abundance relative to chalcopyrite and chalcocite, and scarcity of neutralizing minerals has good conditions for acidic copper mobilization and transport during the supergene processes. This value is close to the 96% efficiency estimated Brimhall et al. (1985) for the "superleached" area at La Escondida. In the potassic and chloritic hydrothermal alteration zones, *L* was fixed, respectively, at 0.7 and 0.5, to take in account the increased neutralization potential of these hydrothermal alteration zones compared to the quartz-sericite hydrothermal alteration zone. Even if these L values are rough approximations, it should be noted the *L* factor value does not impact much the general conclusions of the mass balance model as it will be discussed below.

The parameters and the results of the mass balance model calculations for the 40 sections and rock volume (50 m apart each section) are given in Annex 2.4.

The hypothetical altitude of the porphyry before erosion (*A*) is given by (7), being *a* the mean altitude of the surface immediately before mining (Fig. 21).

$$\left[Cu_{\text{sup}}\right]_{tot}^{qz-ser} = \left[Cu_{\text{sup}}\right]_{ox}^{qz-ser} + \left[Cu_{\text{sup}}\right]_{strong\_\text{sup}}^{qz-ser} + \left[Cu_{\text{sup}}\right]_{low\_\text{sup}}^{qz-ser} \quad (4)$$

$$\left[Cu_{tot}\right]_{tot}^{qz-ser} = \left[Cu_{tot}\right]_{ox}^{qz-ser} + \left[Cu_{tot}\right]_{strong\_\text{sup}}^{qz-ser} + \left[Cu_{tot}\right]_{low\_\text{sup}}^{qz-ser} \quad (5)$$

$$h^{qz-ser} = \frac{\left[Cu_{\text{sup}}\right]_{tot}^{qz-ser}}{w^{qz-ser} \cdot 100 \cdot d \cdot Cu_{hyp}^{qz-ser} \cdot L} \quad (6)$$

$$A = h + a \quad (7)$$

Figure 24 illustrates the ratio of supergene over hypogene copper grades for each supergene zone of each hydrothermal alteration zone. Copper enrichment is given by the Cu_{sup}/Cu_{hyp} ratios and the inverse ratios (Cu_{hyp}/Cu_{sup}) represent copper depletion. Figure 25 shows enrichment and depletion for the oxidation zone (A), the low sulfide enriched zone (B), and the strongly enriched sulfide supergene zone (C).

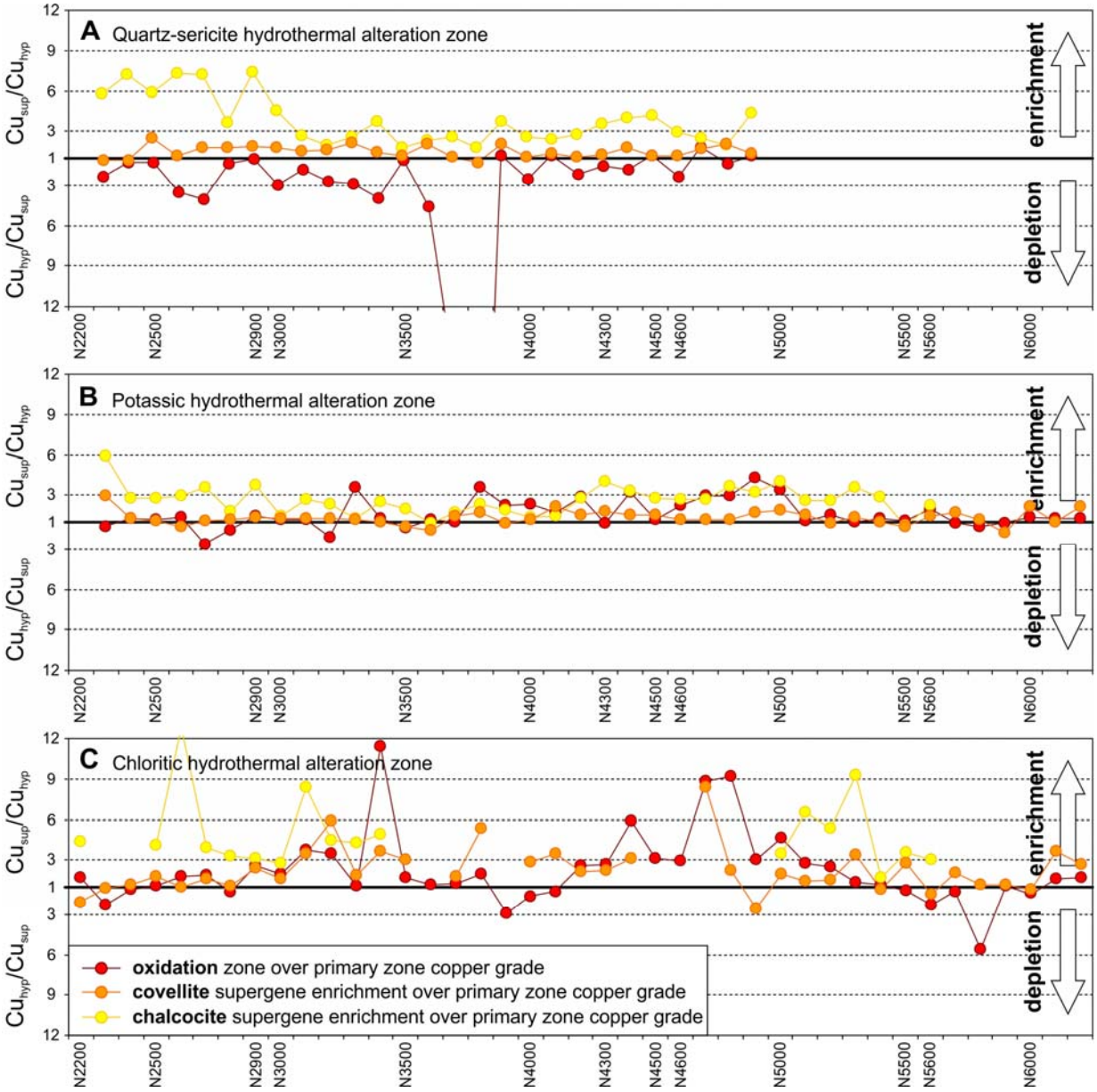

Figure 24: Ratio of copper contents of strong supergene enrichment zone versus hypogene zone for the enriched cells (Cu_{sup}/Cu_{hyp}) and of copper contents of hypogene zone versus strong supergene enrichment zone for the depleted cells (Cu_{hyp}/Cu_{sup}) for oxidation zone (red), low supergene sulfide enrichment (orange) and strong supergene sulfide enrichement (yellow), in the (A) quartz-sericite, (B) potassic and (C) chloritic hydrothermal zones. Each point represents the mean value of a vertical section (same values as used of the mass balance model, see Table 4).

1.4. Discussion

1.4.1 Evolution of a high ore grade oxidation zone

In a typical well developed supergene profile, copper in the oxidation zone should be virtually completely leached ("leached capping", e.g. Brimhall et al, 1985; Sillitoe, 2005, as shown also in the leached oxidation zones of porphyry copper mine tailings Dold and Fontboté, 2001; Dold, 2014). This is not the case at Chuquicamata as showed by the copper contents in the oxidation zone from the CODELCO data base used in the present study. Mean copper grades for single alteration zones and vertical sections are frequently in the range of 0.2% to 1%, in places they surpass 2% Cu, in particular in the oxidation zone developed on rocks affected by potassic and chloritic hydrothermal alteration (Table 4). Figures 24 and 25 A show that for a given vertical section, the copper values in the oxidation zone may even be higher than in the corresponding hypogene zone.

Unlike the copper grades that cover the integrality of the 40 considered vertical sections, the mineralogical observations are fragmentary because of the sampling limitations explained above. The available information indicates a high variability of textures and chemical composition and suggests that these high copper contents occur mainly not as discrete minerals but contained in parts of concretional, fine "oxide" material. Observations with SEM and element mapping (made with QEMSCAN®) on this Cu-bearing "oxide" material allow to distinguish Fe oxides and hydroxides, Mn±Fe±Zn oxides and hydroxides (when macroscopically distinguishable and black in color, called copper wad), and Al-Fe-K-bearing sulfates (possibly from the jarossite-alunite group). The relictic supergene copper sulfides occurring in parts of the oxidation zone developed in the quartz-sericite hydrothermal zone contribute also to the unusually high copper contents for an oxidation zone. In addition, minor amounts of antlerite and atacamite have been found in the studied samples, that as indicated above, were obtained from the external parts of the deposit because no samples of the main part of the oxidation zone were available, as it was mined long ago.

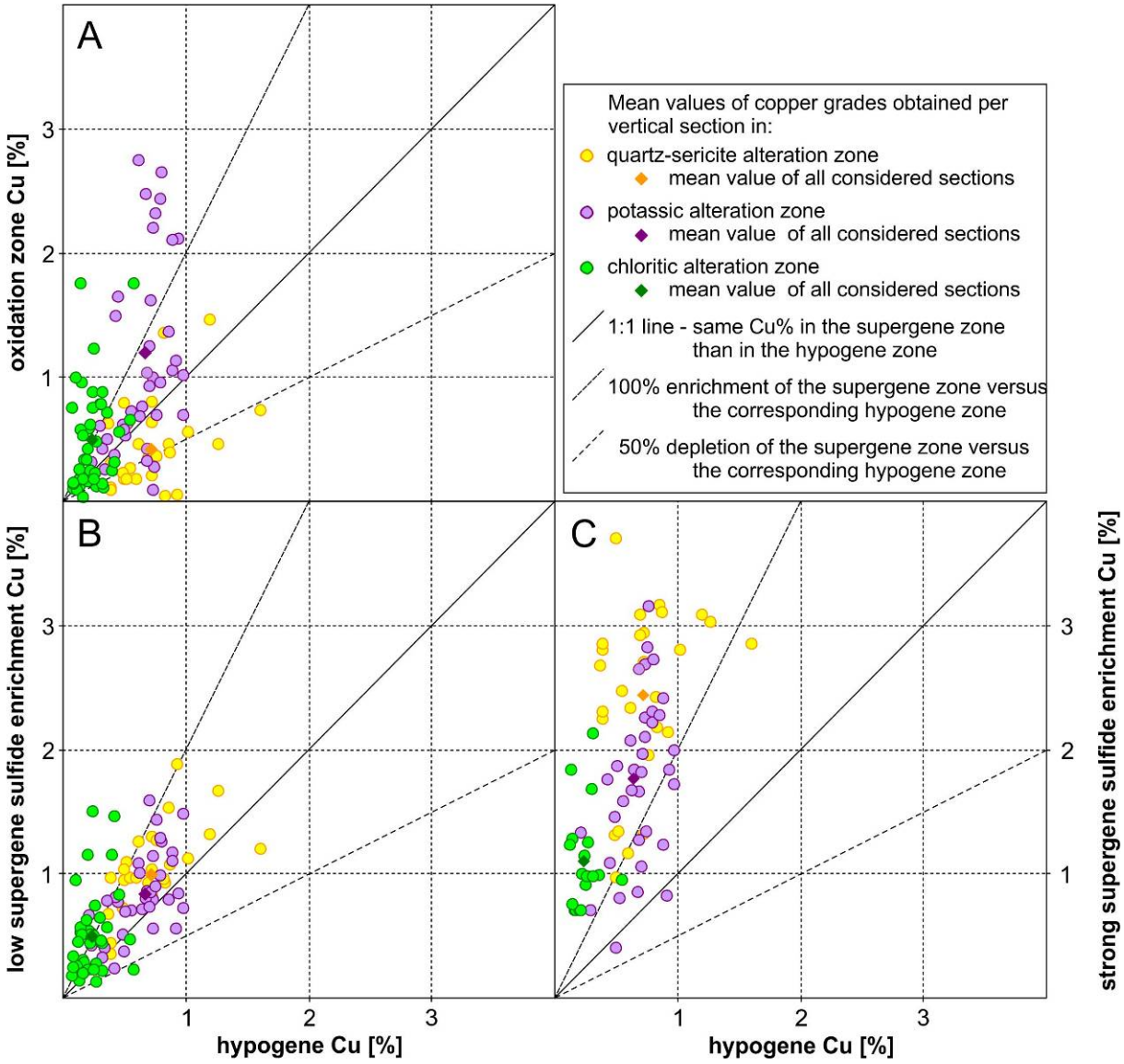

Figure 25: Supergene copper grades versus hypogene copper grades in the oxidation (A) , low supergene sulfide enrichment (B), and strong supergene sulfide enrichment (C) zones. Each round point represents the mean value of a vertical section (same values as used of the mass balance model, see Table 4). The colors indicate the different hydrothermal alteration zones. Discontinuous lines represnet the 100% enrichment and 50% depletion of the supergene versus the hypogene values.

For the mineralogy of the central part we have to refer to observations of Bandy (1938) and Jarrell (1944) that were summarized above. Of great importance for the further discussion is the reported occurrence of abundant copper rich soluble salts and other sulfates in the upper part of the oxidation zone, formed by capilar transport back to the surface of infiltrating water due to the arid and hot climate (Bandy, 1938; Chapter 2).

The existence of a partly oxidized supergene chalcocite enrichment blanket "perched" within the oxidation zone within the oxidation zone (Ossandon et al. 2001) suggest that the supergene profile has undergone a complex history. It is discussed below in the frame of the tectonic and climatic evolution of the area.

1.4.2 Sulfide textures, development of a chalcocite blanket, and lower limit of the supergene sulfide enrichment zone

A chalcocite blanket was evidenced in the quartz-sericite hydrothermal alteration zone (between coordinates N5000 and N2700). It roughly corresponds to the high supergene sulfide enrichment zone defined in the CODELCO 3D mine model characterized by copper grades around 2.5%, in place up to more than 3%. Figures 5 and 6 illustrate, from top to down, the mineralogical transition, occurring at around 300 m below surface, from the high to the low supergene sulfide enrichment zones. In high supergene sulfide enriched zone, hypogene pyrite and enargite are partially or totally replaced by chalcocite (e.g. Fig. 16 A-I). In these sections, it corresponds to the chalcocite blanket. Covellite is only present in traces, mostly on the external part of chalcocite grains (e.g. Fig. 16 K), and could indicate a change to more oxidizing conditions (Sato, 1992; Enders, 2000). In the northern part of the deposit, north to the section N5000, the quartz-sericite hydrothermal alteration zone does not exist and a chalcocite blanket is not observed in section N5600.

Below the chalcocite blanket and in the potassic and chloritic hydrothermal alteration zones, i.e., in the zone called low supergene sulfide enrichment in the CODELCO 3D mine model, characterized by copper grades around 1%, 0.8% and 0.5%, respectively in the quartz sericite, potassic and chloritic hydrothermal alteration zones, covellite is the principal supergene sulfide. In general, it is less abundant than chalcocite in the chalcocite blanket. It presents generally a needle texture on the border of chalcopyrite grains (e.g. Fig. 17 H), but supergene covellite can also be present as massive grains (Fig. 16 N-O).

The sulfide textures in the Chuquicamata deposit were interpreted to obtain the position of the lower limit of the supergene sulfide enrichment processes. The lower limit so determined, varies depending on the hydrothermal alteration zone in which it occurs (Figs. 5, 6, 7), and on the neutralization potential of the hypogene mineralogy. It is lower in the quartz-sericite hydrothermal alteration zone, and in the central sector of the mine. Lowering of the limit indicates increased drainage in these sectors, favored by increased permeability of the rock and/or by the paleotopography.

The approach used in the present study to determine the lower limit of the supergene sulfide enrichment processes, based on the observation of the sulfide mineralogy and textures, gives depth far above the depth of the limit of occurrence of anhydrite, specially in the quartz-sericite hydrothermal alteration zone.

Recognition that supergene solutions reach deeper depth than the maximal depth observed for the supergene sulfides is of importance for the estimation of the copper resource of the deposit, as the sectors with the largest differences between he two methods are also the sectors with the strongest the supergene sulfide enrichment.

The disparity results from the fact that each method detects different processes. The method applied in this study, based on the actual presence of supergene sulfides, reflects the redox boundary where Cu-bearing oxidized supergene fluids are reduced and enter in contact with the hypogene sulfides. In contrast, hydration and dissolution of sulfates, essentially hypogene anhydrite, may just reflect waters descending to deeper levels, possibly at a subsequent stage, without formation of supergene sulfides. The steep morphology of the limit in the quartz-sericite zone determined by hydration and dissolution of sulfates indicates, illustrate an increased permeability (or at least more abundant soluble minerals, i.e., essentially anhydrite),

resulting in a preferential flux pathway in the fractured aquifer system, probably associated to more oxidizing conditions than in the surrounding saturated fractured rocks presenting less water movement. It is especially obvious in section N2900 (Fig. 5), were the difference of level between the lower supergene sulfide and the lower hydrated anhydrite is at least of 800 m.

It is hypothesized that hydration and dissolution of anhydrite partly occurred during an oxidation stage postponing the main supergene sulfide enrichment, possibly resulting from an uplift of the area. The above mentioned transition from chalcocite to covellite in the chalcocite blanket supports this hypothesis.
The neutralization potential of the host porphry influences the nature and extension of the supergene zone. Low pH is necessary to allow the mobilization of copper in aquous solution. If the interaction water-rock increases the pH, copper tends to precipitate, either as oxide minerals or as sulfides, depending on the Eh conditions (e.g. Alpers and Brimhall, 1989; Plumlee, 1999; Sillitoe, 2005). The quartz-sericite hydrothermal altered zone has low neutralization potential (e.g., Alpers and Brimhall, 1989) and in this zone, a well developed supergene profile with a thick chalcocite blanket is observed; in this zone, in almost all setions copper depletion has been registered in the oxidation zone compared with the hypogene grades. In the potassic, and even more in the chloritic hydrothermal alteration zones, the neutralization potential of the host rock is higher, copper grades in the oxidation zones are frequently higher than in the hypogene zone, and the amount of supergene chalcocite is low. Similar phenomena have been described in the oxidation profile of mine tailings (Dold, 2014).

1.4.3 Mass balance model

The results of the mass balance calculations allow an estimation of the copper mobilized during the supergene processes (without taking in account the copper transported outside of the limit of the model by lateral migration). Using the calculations of the copper contained in the 40 vertical sections of the mass balance model (Fig. 26 and Annex 2.4), it results that from the 50 Mt of copper present in the actual supergene profile of the Chuquicamata deposit, 21.6 Mt were added from parts of the supergene profile now eroded. These values are consistent with the total supergene copper (sulfides and oxides) resource given by Ossandón and Zentilli (1997) of 30 Mt for the supergene copper with a cutoff grade of 0.2 wt%.

Figure 26A shows the total amount of copper in the supergene zone of each vertical section compared to the calculated on the basis of the hypogene copper grades (Fig. 26B) added or removed copper during supergene processes (Annex 2.4). Figure 26C gives the vertical extension of the supergene zones along the central axis of the deposit. It highlights that whereas the central part of the deposit (N4000 to N5000) contains most of the total copper, it is in the southern part (between local coordinate N2200 and N3500) where the proportion of copper supergenically added to total copper is higher. This is shown in detail in Fig. 24.

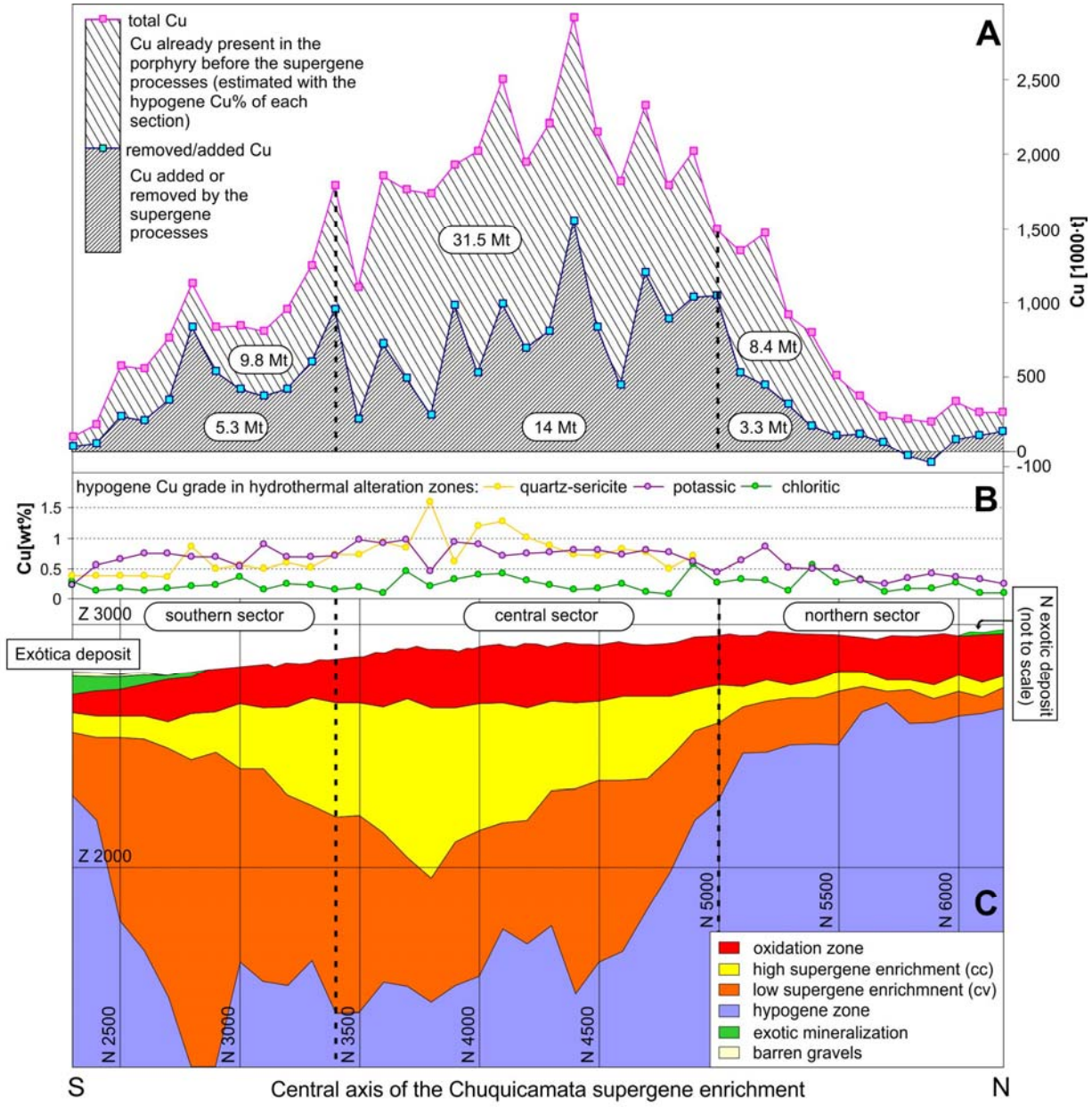

Figure 26: Section along the axis of maximum development of supergene enrichment with (A) amount of total copper present before supergene processes (upper line) and copper added or removed during supergene processes (lower line), amounts refer to 100 m wide slices; (B) hypogene Cu grades used for the calculation in the three hydrothermal zones; and (C) vertical extension of the considered supergene zones.

The high Cu_{sup}/Cu_{hyp} ratios (values over 6) of the south western part of the deposit (N3000 to the South, developed out quartz-sericite hydrothermal alteration, Fig. 24) indicate strong copper enrichment impossible to explain only by a vertical migration of the supergene solutions, and could indicate a lateral north-south (and to a lesser extent east-west) copper transport. An alternative explanation is that the hypogene copper grades of sections N3000 to the south used for the model are too low Table 4). This second possibility may have played only a subordinate role, because even if the retained hypogene values (Table 4) used for the section sections N2900 to the south were underestimated by 50%, the Cu_{sup}/Cu_{hyp} ratios would still be in the range of 3.8 to 4.9, i.e., clearly higher than the ratios found in the sections north

of N3000 that are mostly below 3. Similar increases of the Cu_{sup}/Cu_{hyp} ratios in sections N2900 to the south, weaker than those noted in the quartz-sericite hydrothermal alteration zone, are recognized in the potassic and chloritic hydrothermal alteration zones (Figs. 24). The copper migration from north to south and from east to west is consistent with the pre-mining topography of the deposit (Figs. 5 and SECTION_4200) that had a general slope to the south and to the west, the latter partly controlled by the West Fissure fault on the west side of the deposit. Between sections N3100 and N3800, a less enriched portion is observed, especially in the quartz-sericite and potassic hydrothermal alteration zones. It could represent the source area of the supergene solutions enriching the southern part of the deposit. Inhomogenous Cu_{sup}/Cu_{hyp} ratios in the sulfide supergene enrichment zones in the chloritic hydrothermal alteration zone all over the deposit, partly due to the less abundant data of copper grades in the eastern margin of the deposit, are difficult to interpret in terms of lateral transport of copper.

The values of leached and eroded mineralized porphyry height obtained with equations (1) to (7), depend on the enrichment factors (L) used in each case. To reconstruct the topography before erosion the barren rock overlying the porphyry should be added. Figure 27A shows the theoretical value of eroded mineralized material that would have been necessary to explain the supergene copper present in each section assuming a hundred percent leaching efficiency (L= 1) and only vertical transport. The results obtained with the lower, more realistic values of $L_{qz\text{-}ser} = 0.9$, $L_{pot}=0.7$ and $L_{chl}=0.5$ are shown in (Fig. 27B). Fig. 27C illustrates the effect of using the different values of L for the representative section N3700. It can be recognized that the overall picture does not significantly change by using the different L values. In the following, the more realistic values $L_{qz\text{-}ser} = 0.9$, $L_{pot}=0.7$ and $L_{chl}=0.5$ are used.

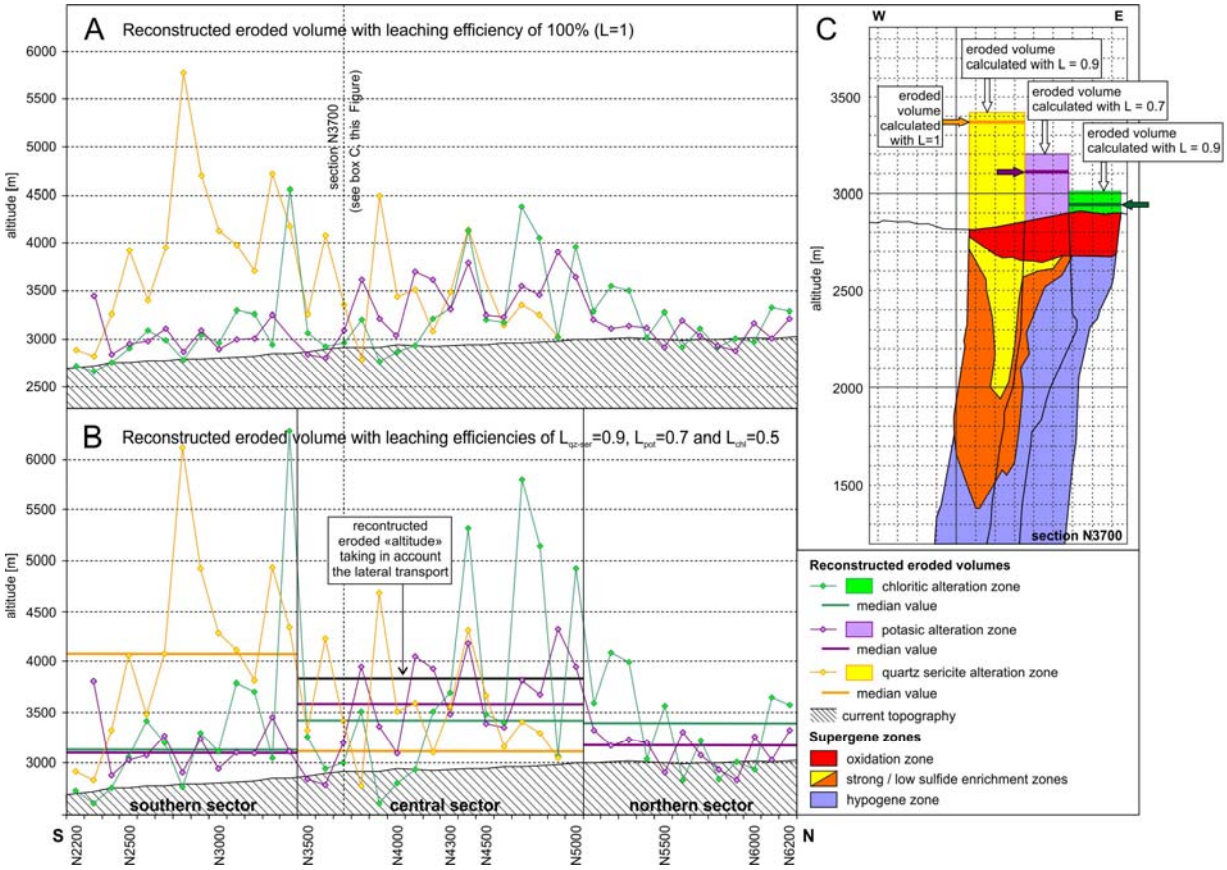

Figure 27: Reconstruction of the topography of the Chuquicamata Deposit based on the mass balance model A. Reconstration along along axes parallel to the hydrothermal alteration zones using a leaching efficiency of 100% for all the hydrothermal alteration zones (L=1); B. Reconstruction using L=0.9 for the quartz-sericite hydrothermal alteration zone, L=0.7 for the potassic hydrothermal alteration zone, and L=0.5 for the chloritic hydrothermal alteration zone (inset B); C. Reconstruction of the section N3700 as an example.

In general terms, the obtained results, summarized in Figs. 26 and 27, allow dividing the North-South Chuquicamata profile into a southern part (between coordinates N2200 and N3400), a central part (between coordinates N3500 and N5000) and a northern part (from coordinate N5100 to N6000). In the northern part of the profile, the total amount of copper is mostly lower than the expected copper in the leached hypogene zone and therefore the calculated altitude values for the porphyry before erosion are generally lower or very near to those of the present topography (median altitude values of 3363 and 3393 m.o.s.l in the chloritic hydrothermal alteration zone, and of 3132 and 3184 m.o.s.l. in the potassic hydrothermal alteration zone, Fig. 27). These values are not considered as realistic and rather reflect lateral copper transport (due to erosion and/or supergene solutions).

In contrast, in the southern part of the deposit (Fig. 27), and more specifically in the high supergene sulfide enrichment zone of the quartz-sericite hydrothermal alteration zone (Fig. 24) ratios of Cu_{sup}/Cu_{hyp} as high as 7 are registered. If the copper enrichment in the southern part of the deposit was only due to vertical mass transfer, unrealistically high vertical columns of leached and subsequently eroded mineralized porphyry would be necessary. The copper enrichment of the quartz-sericite hydrothermal alteration zone in the southern sector of the N-S profile would require the leaching of a mineralized column of almost 1300 m above the present topography (median value around 4100 m.o.s.l., Fig. 27, Table 6). Lateral flux from North (and

to a lesser extent from East) have to be considered to explain the large copper excess recognized in the southern part of the deposit.

Table 6: Mean and median altitude values in meters over sea level obtained in the southern (local coordinate between N2200 and N3400), central (between N3500 and N5000) and northern (between N5100 and N6000) sections.

		mean value	median value
chloritic hydrothermal alteration zone	southern zone	3367	3120
	central zone	3713	3436
	northern zone	3363	3393
potassic hydrothermal alteration zone	southern zone	3159	3102
	central zone	3585	3580
	northern zone	3132	3184
quartz-sericite hydrothermal alteration zone	southern zone	4094	4079
	central zone	3538	3109

In contrast, in the central part of the deposit, for the quartz -sericite hydrothermal zone, the Cu_{sup}/Cu_{hyp} ratios are around 3 (Fig. 24) and the obtained mean altitude value of the mineralized porphyry paleo surface is of only 200 m above the present topography (Fig. 27, Table 6). This value is considered to be unrealistically low and can be explained because of a significant copper lateral transfer to the southern part. The copper transfer southwards appears to be stronger in the quartz-sericite than in the potassic and chloritic hydrothermal zones that yield theoretical altitudes of the mineralized porphyry paleo surface of 3580 m.o.s.l. and 3436 m.o.s.l., respectively, it averages around 700 m over the present topography. The fact that the latter two values have similar magnitudes adds credibilty to them as, originally, the mineralization top in a given section should show a certain continuity. In other words, if the top of the mineralized quartz-sericite zone was at a similar altitude than the contiguous potassic and chloritic hydrothermal zones, the copper contained in a 500 m high column of quartz-sericite altered porphyry was transported away, probably to the south. For the further discussion, this amount of copper is termed $[Cu]_{transported\_1}$.

To estimate the "copper excess", the actual copper content in the southern sector of the deposit (that yields the obtained Cu_{sup}/Cu_{hyp} ratio around 7) was compared with the copper that the high supergene sulfide enriched zone would have been if it had a Cu_{sup}/Cu_{hyp} ratio of 3 for each section. The difference, the "copper excess" amounts to 0.5 Mt. In addition, the copper contained in the Exótica deposit has been estimated to be of 5.1 Mt with a cutoff of 0.2% Cu (Ossandón & Zentilli, 1997). Adding to the Exótica resource calculation around 20 % of not minable Cu, it can be assumed that a minimum of 6 Mt of Cu have been transported from the Chuquicamata ore deposit to the South. Assuming that all this copper (0. 5 Mt and 6 Mt) has been transported from the central part of the deposit, the required column of mineralized porphyry to provide this amount of copper was calculated in two steps.

First, it has been estimated the $[Cu]_{transported\_1,}$ i.e, the copper contained in the 500 m high column of quartz-sericite altered porphyry as defined above. For each section of the central part of the deposit (sections N3100 to N5000) equation (8) has been applied. In this equation, $w_{qz\text{-}ser}$ is the width of the quartz-sericite hydrothermal alteration zone un the section, h is the considered high of porphyry (in this case 500 m), t is the thickness of the section (100 m in this model), and d is the density of the porphyry (2650 kg/m^3). The result obtained for $[Cu]_{transported\_1,}$ is 1.3 Mt of copper.

$$[Cu]_{transported\_1} = w_{qz-ser} \cdot h \cdot t \cdot d \cdot Cu_{hyp}^{qz-ser} \quad (8)$$

The second part of the calculation consist in the estimation of the column height of porphyry necessary to provide the remaining 5.2 Mt (6.5 Mt Cu $_{South}$-1.3 Mt $[Cu]_{transported\_1,}$) of copper transported to the South. Taking in account that the mineralized parts of the sections have similar extension, the 5.2 Mt of copper was evenly distributed into the 16 sections of the central part of the deposit, with an homogenous high for each section. The height h of mineralized porphyry column required to obtain 1/16 of 5.2 Mt Cu in each vertical section has been calculated with equations (9) and (10), $[Cu]_{south}$ being the total copper transported to the South (6.5 Mt), *w* the width of each hydrothermal alteration zones, Cu_{hyp} the copper grade in the hypogene zone of each hydrothermal alteration zone, *h* the considered high of porphyry (to be calculated), *t* is the thickness of the section (100 m in this model), and *d* is the density of the porphyry (2650 kg/m^3).

$$\frac{1}{16} \cdot \left([Cu]_{south} - [Cu]_{transoprted\_1}\right) = \frac{d \cdot h \cdot t}{100} \cdot \left[\left(w_{qz-ser} \cdot Cu_{hyp}^{qz-ser}\right) \cdot \left(w_{pot} \cdot Cu_{hyp}^{pot}\right) \cdot \left(w_{chl} \cdot Cu_{hyp}^{chl}\right)\right] \quad (9)$$

$$h = \frac{\left([Cu]_{south} - [Cu]_{transoprted\_1}\right) \cdot 100}{16 \cdot d \cdot t \cdot \left[\left(w_{qz-ser} \cdot Cu_{hyp}^{qz-ser}\right) \cdot \left(w_{pot} \cdot Cu_{hyp}^{pot}\right) \cdot \left(w_{chl} \cdot Cu_{hyp}^{chl}\right)\right]} \quad (10)$$

The median and mean values calculated for this data set are respectively 192 and 196 m, which means that the copper of a column around 200 m high of mineralized porphyry was transported to the south. Considering the 700 m calculated above to account for the copper existing in the supergene profile, a minimum total of 900 m of leached and eroded mineralized column in the central part of the deposit is necessary. Transport of the northern sector, although possible is neglected in this estimation as this sector is less mineralized and a significant part of the copper was transported northwards as indicated by exotic mineralization north of Chuquicamata open pit (Section N6000 in 26).

1.4.2 Genetic model of supergene enrichment at Chuquicamata and Exótica Deposits

Figure 4 presents the available data on dating, tectonic records, sedimentological records and climatic indicators concerning the Chuquicamata area. The principal steps necessary for the formation of the supergene enrichement and a exotic deposits are (1) emplacement of the porphyry, (2) various stages of hypogene hydrothermal alteration and mineralization, (3) deposition of the gravels hosting the exotic deposit, (4) exposure of the porphyry to oxidation (beginning of the supergene processes), and (5) vertical and lateral migration of supergene solutions downstream to form the supergene enriched and the exotic mineralization; various steps being possible to occur simultaneously. Tectonic evolution and climate are of key importance in the accomplishment of this series of events, and must be taken in account to understand the conditions of formation of the supergene and exotic mineralization.

Tectonic, exhumation and cooling rates

With the mass balance performed in the present study, a column of mineralized porphyry around 900 m high was estimated to be necessary to provide the copper added in the supergene profile and contained in the Exótica deposit located south of Chuquicamata. Fission track data and (U/Th)/He ages on apatite from the Fortuna granodiorite and the Chuquicamata porphyry complex obtained by McInnes et al. (1999) suggest a rapid cooling rate after the emplacement of the Chuquicamata Porphyry Complex (~100°C/Ma), and an emplacement depth of less than

4 km for porphyry samples located at the present surface. Combining this result with those of the mass balance calculation of the present study, a maximum depth of the upper part of the porphyry mineralization of 3 km can be proposed, i.e., in the range of typical depths for porphyry systems in the Andes (e.g., Sillitoe, 2010). The exhumation could result from the Late Oligocene- Early Miocene Andean uplift event (Sillitoe et al., 1968; Mortimer et al., 1978), at the origin of a pediplain described in the southern Atacama desert (Sillitoe et al.,1968). There, Riquelme et al. (2010) describe the Upper to Middle Miocene Sierra Checos del Cobre surface (between 30 and 20 Ma) and the overlying Asientos pediplain (around 20 Ma). These pediplains have not been described in the Calama basin. Contemporaneously with the exhumation, the West Fissure had a sinistral offset estimated around 35 km (Tomlinson and Banco, 1997; Dilles et al. 1997). According Lindsay (1998), the displacement took place before 19 to 15 Ma. The results obtained by McInnes et al. (1999) on the Fortuna granodiorite suggest that the west side of the West Fissure was exhumed at least 600±100 m more than the East side. These different exhumation amounts are in agreement with only 50 m alluvial gravel cover west side of the West Fissure at the Ministro Hales Mine (MMH, 6 km south of Chuquicamata), while east of it a 500 m thick sequence of sediments is recognized (Sillitoe et al., 1996).

Age of supergene mineralization at Chuquicamata

Sillitoe and McKee (1996), dated (K/Ar) seven supergene alunite samples near the surface (between 50 and 100 m) from an hematitic leached capping and from antlerite ore of Chuquicamata. The ages are comprised between 19.0±0.7 Ma and 15.2±0.7 Ma (Fig. 4). At Mina Ministro Hales (MMH), located 6 km south of Chuquicamata and that according to Zentilli et al. (2015) represents a portion of Chuquicamata displaced sinistraly along the West Fissure), two supergene alunite samples from the jarositic leached caping (55 and 93 m depth) were dated at 20.8±0.6 Ma and 20.4±0.6 Ma, K/Ar (Sillitoe and McKee, 1996). The erosion of the mineralization at MMH was most likely less important than in Chuquicamata as indicated by the fact that advanced argillic alteration is preserved in MMH, while it has been removed in the Chuquicamata deposit. It is likely, therefore, that the dated alunite samples at Chuquicamata represent originally deeper and therefore younger parts of the supergene alteration profile than at MMH, and for this reason the oldest supergene ages found in Chuquicamata are slightly younger than those in MMH. Thus, the existing oldest K/Ar ages on the supergene alunite at Chuquicamata and at MMH have to be considered as a minimum age for the start of the supergene processes, older, shallower supergene horizons may have been eroded.

These ages are consistent with other obtained in supergene zones from deposits of northern Chile including Collahuasi (15.2 ± 0.5 Ma, K-Ar on alunite, Sillitoe and McKee, 1996), Centinela (Telégrafo 21.49± 0.36, Polo Sur 21.2± 0.2 and 19.2± 0.2, $^{40}Ar/^{39}Ar$ on alunite, Perelló et al., 2010), La Escondida (18 ± 0.7 to 14.7 ± 0.5 Ma, K-Ar on alunite, Alpers and Brimhall, 1988). At El Peñon Au-Ag epithermal deposit, south of Escondida, $^{40}Ar/^{39}Ar$ ages on alunite and Mn-oxide by Arancibia et al. (2006) suggest relatively continuous supergene processes between 29 and 9 Ma.

The ages on supergene enrichment partly coincide with the Late Oligocene - Early Miocene Andean uplift, believed to have favored development of supergene oxidation and enrichment northern Chile (e.g., Sillitoe et al., 1968, Sillitoe and McKee, 1996, Alpers and Brimhall, 1988).

Taking in account that hypogene mineralization at Chuquicamata took place between 35 and 31 Ma (see geological setting above), and that the obtained alunite ages at Chuquicamata are minimum ages, it is possible that supergene processes at Chuquicamata started 5-10 Ma after hypogene mineralization, giving sufficient time to uncover the around 3 km of unmineralized rocks on top of the deposit. This time range is in agreement with the observations on the Late Eocene to Early Oligocene porphyry cooper belt in Northern Chile done by several authors (Gustafson and Hunt, 1975, Alpers and Brimhall, 1988, Sillitoe and McKee, 1996**),** who have placed the beginning of supergene enrichment around 5 to 15 Ma after hypogene mineralization.

The above discussed ages of supergene alunite from Chuquicamata and in general in Northern Chile indicate that the conditions for formation of well developed supergene profiles were fulfilled at least until around 15 Ma (e.g. Sillitoe et al., 1996; Bissig and Riquelme, 2010). Taking in account the absence of younger ages. The gross of the supergene enrichment was supposed to take place during the Late Oligocene - Early Miocene uplift, before an onset of hyperarid climatic conditions. Hyperarid conditions during Late Miocene and Pliocene in the Atacama Desert have also been documented by several authors. As illustrated in Fig. 4, different ages for the onset of hyperaridity have been obtained using different climatic proxies. Rech et al. (2006) on the basis of a soil study of the Atacama Desert, including the Calama basin, placed the transition to hyperaridity between 21 and 9.5 Ma. Dunai et al. (2005) proposed that the hyperaridity period started at 25 Ma on the basis of cosmogenic ^{21}Ne analyses in clasts from erosion-sensitive sediment surfaces. Hartley and May (1998) placed the onset of hyperaridity at 9.5 Ma by correlating weathered surfaces with dated ash layers. Hartley and Chong (2002) propose a semi-arid climate between 8 and 3 Ma, with a period of hyperaridiy around 6 Ma, and Saez et al. (2012) hyperarid conditions between 7 and 5.5 Ma and between 4 Ma and the present, with wetter period during the interval, both studies being based on the sedimentary gaps and sedimentation rates. According Hartley and Chong (2002), onset of hyperaditiy was only in the Pliocene, these authors explain the cessation of supergene activity around 15 Ma, because of tectonic reasons instead of climatic changes. Works of Reich et al. (2009 and 2013) describe how the climatic changes affected the supergene mineralization, allowing the preservation of atacamite. In addition, it is known from recent paleoclimatic records, that even under hyperarid climates, wetter periods may occur. For instance, Latorre et al. (2002 and 2006) describe a wetter phase at 11.8 and 10.5 ka in the Salar de Atacama region. Several of these studies show that local relief conditions, in turn controlled by local tectonic parameters introduce complexity to the climate and the hydrological conditions.

In the Chuquicamata area, wetter periods may have relatively easily mobilized copper precisely because hyperarid climate allows precipitation of copper rich soluble salts and acid bearing soluble sulfates in the upper part of the supergene profile (Bandy, 1938, Chapter 2). Therefore, it can not be excluded that the supergene profile at Chuquicamata could be partly active after 15 Ma during the Middle-Late Miocene Andean uplift episode evidenced by the Atacama pediplain (12.6±0.5 Ma and 11.5±0.5 Ma, Sillitoe and Clark, 1969; between 14 and 10 Ma, Bissig and Riquelme, 2010). The existence of the "perched" chalcocite blanket within the oxidation zone described by Ossandon et al. (2001) indicating a rapid drop of the oxidation front in the supergene profile, could be the consequence of this uplift. The replacement patterns of chalcocite by covellite described above (Figs. 19 B, 19 D, 19 J) may illustrate this phenomenon that is accompanied by copper release. A similar "reverse sequence" has been described in the supergene profile of the Malanjkhand porphyry deposit (India) and interpreted to document a transition to more oxidizing conditions (Sikka, 1991). Hydration and dissolution

of anhydrite used in the CODELCO 3D mine model to define the lower depth reached by supergene solutions could also have been occured during this oxidation stage.

The rapid descent of the oxidation front could be based on local block faulting related or not to the regional Middle-Late Miocene Andean uplift episode. The Estanques Blancos-Portezuelo northeast-southwest trending fault system in the Chuquicamata open pit, and other subparallel faults north and south of it, have a normal component which gave rise to "en échelon" block structure, the northern blocks being raised relative to the southern ones (CODELCO, unpublished report, 2006). The "en échelon" block structure is observed from the Radomiro Tomic mine to south of Chuquicamata and down to the El Loa river. It can also explain the erosion of several hundred of meters of the upper part of the porphyry system in the Radomiro Tomic mine, where only traces of phyllic alteration and no advanced argillic alteration is observed. This normal movement is not dated, but is partly synmineral (faults of the Estanques Blancos fault systems served as conduits for the hydrothermal fluids, Lindsay, 1998), and partly concordant with the deposition of the Exótica gravels (Mortimer et al., 1978).

Age of the Exótica Deposit

As reported above, the attempt to $^{40}Ar/^{39}Ar$ date supergene alunite in exotic mineralization in Mina Sur in this study failed. In the absence of other absolute ages, the chronology of the formation of the exotic deposit is difficult to establish precisely and it is necessary to rely on geological constraints.

The maximum age of the exotic deposit is the age of the host sedimentary units, named by Mortimer et al. (1978) Fortuna and the Exótica Gravels. The Fortuna gravels consist of slope talus deposits with principally angular to sub-rounded clasts, up to 2 m in diameter, derived mainly from the Fortuna granodiorite, located west of the West Fissure. The provenance of the Fortuna clasts indicate that deposition took place after the ~35 km sinistral strike-slip displacement along the West fissure so that the Fortuna granodiorite was adjacent to the gravels. According Lindsay, 1998, this displacement took place before 19 to 15 Ma. The Exótica gravels are mud flow deposits made of coarse sand and small angular clasts up to 5 cm diameter, derived from Chuquicamata granodiorite and from areas located to the North (Mortimer et al., 1978). In its lower part, the Exótica gravels contain clasts derived from the Chuquicamata oxidation zone. The Fortuna and the Exótica gravels are intercalated in the northern part of the Exótica deposit. The (unmineralized) top of the gravels has been approximately dated with an ignimbrite bed (8.4±0.4 Ma, Mortimer et al., 1978) located 5 to 10 meters below the present surface.

The Jalquinche Formation at the base El Loa Group in the Calama area is, like le Exótica gravels, made up of fluvial channels (May et al. 1999, 2005). May et al., (2005, p. 45) dated an ash tuff at the base of the Jalquinche Formation $^{40}Ar/^{39}Ar$ at 19.62±0.36 Ma and propose that "from 22 Ma to 10 Ma sedimentation was continuous throughout […] the central Calama basin". Blanco (2008) and Rech et al. (2010) also tentatively place the base of the El Loa sediments at around 22 Ma in the Calama area. If the Exótica gravels can be correlated with these El Loa Group sediments in the Calama area, a maximum age of around 22 Ma for the exotic mineralization could be proposed.

As described in Pinget et al. (Chapter 3), and schematically represented in Fig. 26, in the northern part of the Exótica deposit, the Exótica and the Fortuna gravels, partly altered and mineralized by supergene fluids, overly a relatively thin but complete supergene alteration

profile developed in the Chuquicamata porphyry deposit (comprising 60 m of oxidation zone, and 140 m of supergene sulfide enrichment). This shows that exotic mineralization took place when the supergene profile of Chuquicamata had already achieved an advanced stage.

As indicated above, at least 6 Mt Cu were transported from the oxidation zone of the Chuquicamata deposit southwards, from which 5.1 Mt Cu constituted the Exótica deposit resource before exploitation. This represents around 10% of the total copper in the supergene zones of the Chuquicamata deposit. Taking in account the "late" character of the exotic mineralization relative to the evolution of the supergene profile, the question may be arisen where this large amount of copper comes from.

The above mentioned rapid exhumation that resulted in a perched chalcocite blanket in the oxidation zone of the Chuquicamata deposit could have exposed to leaching an immature oxidation zone providing a copper source easy to mobilize. As explained above, the oxidation zone of the Chuquicamata deposit present in places unusually high copper contents, and is often enriched in a comparison with the hypogene copper grades of the same section (Fig. 25), documenting the immature character of the oxidation zone. Moreover, it is known to contains abundant copper rich soluble salts and other sulfates abundant in its upper part, able to easily provide not only a copper but also acidic (pH<2) fluids required to produce the conspicuous alteration of the Exótica deposit (Pinget, Chapter 2).

At the Exótica deposit, the morphology of the central strong acidic alteration and low copper zone and of the surrounding alteration zone suggests that the principal axis of circulation of the supergene solutions essentially did not migrate during the formation of the exotic deposit (Chapter 2). This may suggest that at least the main part of Exótica deposit was formed in a period of time short enough to not have been subjected to significant changes of the hydrological pattern.

In summary, the exotic mineralization appears to has taken place in a relatively short period of time when the supergene profile of Chuquicamata had already achieved an advanced stage. This period can be placed at the end of the formation of the supergene mineralization dated in Chuquicamata, i.e., at the end of the Late Oligocene- Early Miocene or at a later stage, during Middle to Late Miocene uplift. The latter possibility would require enough precipitation events in a dominantly hyperarid period.

As described in Pinget (Chapter 2), minor but significant atacamite occurs together with gypsum. It is located mainly in late crosscutting veins. Reich et al. (2008) place at "< 1.5 Ma" this final episode of exotic mineralization. This implies that supergene and exotic processes continued until recent times. The predominance of atacamite may require a change in the hydrological system allowing increasing input of chlorides. It can be connected to the salar appearance after 3 Ma in the Calama basin (May et al., 1999; Hartley and Chong, 2002; Fig 4).

1.5 Conclusion

For the first time mineralogy and textures of the supergene sulfide enrichement zone of the Chuquicamata porphyry copper ore deposit have been documented in detail. The study, based on archival material located along three representative vertical sections complemented by some recent drill holes, has allowed distinguishing characteristic hypogene and supergene sulfide textures, in particular for chalcocite and covellite, minerals forming both under hypogene and supergene conditions at Chuquicamata. The chalcocite blanket corresponding in the

CODELCO 3D model to the high supergene enrichment zone (with typical grades in the range of 2.5%), occurs only in the quartz-sericite hydrothermal alteration zone, between coordinates N5000 and N2700 with a thickness around 300 m. In the chalcocite blanket, covellite is uncommon, and occurs or as relict in the chalcocite grains, or at the chalcocite grain border, indicating a change to more oxidizing conditions. Below the chalcocite blanket, and laterally of it, in the potassic and chloritic alteration zones, in the "low supergene sulfide enrichment zone" of the CODELCO 3D model, the main supergene copper sulfide is covellite, presenting frequently needle textures on the border of hypogene sulfides.

The oxidation zone at Chuquicamata is unusually copper-rich, indicating an immature supergene profile. In the oxidation zone of the external parts of the deposit, the only areas where material from this zone was available for mineralogical and geochemical study, most copper is contained in poorly defined, very fine-grained material, in places concretional, that when is black in color can be termed copper wad. This Cu-bearing fine-grained material includes oxides/hydroxides, sulfates, phosphates, also containing Fe, Mn, K, Al and K, in varying proportions. Crystalline copper minerals (antlerite, atacamite) are also observed. These characteristics contrast with those of the oxidation zone in the central parts of the deposit, where according the descriptions published when these parts were mined (Bandy, 1938; Jarrell, 1944), copper occurred mainly as chalcantite, antlerite, chrysocolla, and copper pitch / copper wad, as well as, in the upper 30 meters of the supergene profile, atacamite.

A lower limit of the supergene sulfide enrichment was determined, on the basis of textural and mineralogical analysis.

A mass balance calculation based on 40 vertical cross sections has shown a copper excess of around 0.5 Mt of copper in the southern part of the deposit (N2100-N3400), mainly contained in the supergene sulfide enrichement zone. This copper was transported from the central part (N5400-N6200) to the South during the main stage of supergene processes. Considering also the around 6 Mt of copper transported to the south to form the Exótica deposit and comparing with the pre-mine topography, it has been estimated that around 900 m of mineralized porphyry was leached and subsequently eroded in the central part of the deposit.

At least part these 900 m of mineralized porphyry were leached and eroded concomitantly with the Late Oligocene - Early Miocene Andean uplift considered by various authors to trigger the main stage of supergene enrichment in Northern Chile. This hypothesis is supported by supergene Ar/Ar alunite ages at Chuquicamata between 19 and 15 Ma and at the near Ministro Hales Mine (MMH) around 21 Ma (Sillitoe and McKee (1996). These ages do not correspond to the eroded upper parts of the oxidation profile, so that the age of the beginning of this main event of supergene enrichment is not known.

The Exótica deposit rests on the southern end of the supergene profile of the Chuquicamata deposit suggesting that if the Exótica deposit was formed during the main Late Oligocene - Early Miocene supergene stage, it should have been at the end of the event. Alternatively, the Exótica deposit could result from leaching of exposed immature supergene profile because of a subsequent Middle - Late Miocene Andean uplift. Copper contained in the oxidation zone (including as soluble salts) and in a chalcocite blanket "perched" in the oxidation zone, indicating a rapid drop of the oxidation front and supporting therefore an uplift, could be leached. The soluble salts, mainly acid-bearing sulfates, could trigger the acidity necessary to explain strong acidic alteration observed in parts of Exótica deposit. In both alternatives, i.e., formation at the end of the 19-15 Ma main supergene enrichment event at Chuquicamata, or

during the subsequent Middle - Late Miocene Andean uplift, the Exótica deposit the water amount necessary to its formation has to be taken in account. A latter formation of the Exótica deposit would imply eihter a delayed onset of hyperarid conditions, or important wet episode during the a general hyperarid climate.

1.6 Acknowledgements

The constructive collaboration with the geologic team of the Chuquicamata mine (CODELCO) made this work possible. We specially thank Manuel Vergara, Fernanado Ramirez, Victorino Moyano, and their collaborators, and Carlos Barrios for his inestimable help. We thank A. Martigner for the SEM analyses, K. Kouzmanov for the QEMSCAN® analyses, R.Spikings for the $^{39}Ar/^{40}Ar$ datations, F. Capponi for the XRF analyses and J.-M. Boccard for the technical support, University of Geneva, Switzerland. The project was financed by the Swiss National Science Foundation Project FN129988.

Chapter 2

Mineralogical and geochemical characterization of "copper wad", "copper pitch", and chrysocolla at Chuquicamata, Chile: Implications for the genesis of the Exótica Deposit

Marie-Caroline Pinget M.[1]

Department of Earth Sciences, University of Geneva, rue de Maraîchers 13, Geneva, Switzerland

Bernhard Dold

Division of Geosciences and Environmental Engineering, Luleå University of Technology, Luleå, Sweden.

Lluís Fontboté

Department of Earth Sciences, University of Geneva, rue de Maraîchers 13, Geneva, Switzerland

[1] Corresponding author: marie-caroline.pinget@unige.ch

Abstract

The Exótica deposit, with a resource of 6 Mt Cu, was mined between the 1960's and 2015. It extends, with a slope of 3 to 7 degrees, for more than 7 km south of the Chuquicamata porphyry copper deposit. The oxidation of the Chuquicamata ore is the source for the acid rock drainage solution and gives origin of the exotic mineralization. The principal copper bearing minerals of the deposit are chrysocolla, copper pitch and copper wad, which are mainly located as a halo around an altered "tube" and south of the end of the paleochannel, were the main mineralization took place.

Copper wad and copper pitch have variable mineralogical and chemical compositions. Sequential extraction combined with sequential X-ray diffraction and ICP analyses on solutions applied to copper pitch samples from the Exótica deposit show the presence of crystalline birnessite in the copper pitch/wad material, together with other crystalline phases as libethenite, atacamite, and gypsum. An important pseudo amorphous component is present too, behaving similarly to chrysocolla during sequential extraction. Manganese contained in copper pitch/wad is distributed between the crystalline birnessite and the chrysocolla-like pseudo amorphous fraction. The chemical composition and texture of copper wad is more variable than the composition of copper pitch. This variability is interpreted to be mainly related to the precipitation mode of copper wad that is principally controled by water-rock interaction, and therefore, by the type of rock on which the copper wad coatings from. In contrast, chrysocolla / copper pitch massive veins are thought to form under low flow regime, in desiccation cracks or even in surface ponds, and composition depends mainly of that of the fluid.

The formation of the mineral assemblage observed at Exótica was investigated using geochemical modeling to determine the thermodynamic stability fields of chrysocolla, copper pitch/wad (i.e. chrysocolla and birnessite). It was found that these phases precipitated mainly at oxidizing conditions above 0.5 V and pH > 4.7. At lower redox conditions only chrysocolla can precipitate.

The available data allow to propose the following conceptual model for the genesis of the Exótica Deposit. The Exótica mineralization developed by lateral flow of acidic solutions (acid rock drainage, ARD) originated in the oxidation profile of the Chuquicamata ore deposit. There, interaction of rainwater with soluble salts at the surface of the oxidation zone results in a decrease of the pH (1-3) and increase of the Eh (>1 [V]). Interaction of these solutions with the oxidation zone of the Chuquicamata deposit resulted in a slight pH increase to 2-4 and a slightly more reducing environment (Eh around 0.5 - 1 [V]) and increase of the Cu and Mn concentrations. Water-rock interactions increased pH of the solutions flowing south, and lead to chrysocolla precipitation. The modelling shows that if the pH increases more due to neutralization reactions, birnessite becomes oversaturated and copper wad can form further south of the source. As a constant ARD supply during a long time frame can be assumed, acid solutions consumed the neutralization potential of the gangue mineralogy along the flow path, altering through dissolution and precipitation to the final altered (kaolinitized) tube or conduit present in the center of the Exótica deposit. This explains also today's dominance of chrysocolla at the end of the tube and at the base of the ore, as well as the presence of copper wad at the further southern part of Exótica. Periodic flushing of the oxidation zone of Chuquicamata during strong rain events most likely have led also to acidic, Cu-Mn rich surface runoff, which, in very oxidizing conditions formed close to the source and in a more superficial environment copper pitch – chrysocolla intercalations. The atacamite-gypsum mineralization is

the latest mineralization event, most likely associated to inflow of saline groundwater due to changed tectonic setting and temporal wet seasons resulting in a temporal rise of the groundwater levels in the Calama basin.

Keywords: Chuquicamata, Exótica deposit, Mina Sur, chrysocolla, copper pitch, copper wad, birnessite, atacamite, solubility, acid rock drainage, exotic mineralization

2.1 Introduction

Porphyry copper deposits, when exposed to oxidizing conditions by exhumation and erosion (atmospheric oxygen or water with high partial pressure of oxygen), develop charactersitic oxidation profiles (e.g., Brimhall et al., 1985; Ague and Brimhall, 1989; Sillitoe, 2005). In the oxidation zone, primary sulfide minerals are oxidized, resulting in acidification (acid rock drainage, ARD) and formation of a secondary mineral assemblage typical for this environment (e.g., Alpers and Brimhall, 1989). The development of the oxidation zone depends principally on the sulfide mineralogy of the porphyry and on the neutralization potential of the gangue minerals and requires the formation of an unsaturated zone; therefore, tectonics, climate and erosion are also key parameters (Alpers and Brimhall, 1989; Brimhall et al., 1985; Sillitoe, 2005; Hartley and Rice, 2005).

In these conditions, the resulting ARD, which is rich in dissolved metals, can mobilize vertically copper and lead to supergene enrichment by precipitation of covellite, chalcocite-digenite in a more reducing environment. It is generally believed that the groundwater level is responsible for this redox change (e.g. Ague and Brimhall, 1989). However, in-situ measurements of the geochemical parameters during ARD formation in oxidizing porphyry copper mine tailings, suggest that the reducing environment is mainly controlled by the oxidation front in the profile. At this geochemical interface, oxygen is depleted by the (microbiologically catalyzed) sulfide oxidation, and the Fe(II)/Fe(III) redox couple controls the reducing conditions, defining together with the pH conditions, where Cu enrichment can take place (Dold, 2003b; Dold et al. 2005). If the solutions are drained laterally, and maintain their oxidizing conditions, they can lead to the formation of a new "exotic" copper deposit due to water-rock interactions with the bedrock, containing typically chrysocolla and copper wad and pitch, and in certain cases atacamite (Newberg, 1967; Münchmeyer, 1996; Dold, 2006b; Tapia et al. 2012), known as copper oxide mineralization. In southern Peru and northern Chile, conditions were favorable for the formation of exotic deposits, which prevailed at least during late Oligocene and early Miocene (Münchmeyer, 1996), and probably later, as exotic mineralization processes were evidence even until the Pleistocene (Reich et al., 2008, 2009; Chapter 1). Such deposits were for example described in Cerro Indio Muerto (El Salvador porphyry copper deposit), forming the exotic deposit Damiana, in the Collahuasi porphyry copper district, with the exotic deposit of Huinquintipa, or in the Sierra Gorda district, with the El Tesoro exotic deposit (Münchmeyer, 1996; Tapia et al., 2012).

Exotic deposits have been described also in different parts of the world (e.g. Oyu Tolgoi porphyry Cu-Au(-Mo) deposit in Mongolia, Perelló et al., 2001; Bayugo porphyry copper-gold deposit in Philippines, Braxton and Mathur, 2011; Chagai Cu-porphyry belt in Pakistan, Perelló et al., 2008). The term exotic is nowadays used in a more general way to define deposits resulting from the lateral migration of metal bearing solutions from a primary deposit (e.g. Boni and Mondillo, 2015).

Table 1: Typical copper oxides of a porphyry copper oxidation zone.

Mineral / descriptive term	**Formula**
Antlerite	$Cu_3SO_4(OH)_4$
Atacamite	$Cu_2(OH)_3Cl$
Azurite	$Cu_3(CO_3)_2(OH)_2$
Brochantite	$Cu_4(SO_4)(OH)_6$

Mineral / descriptive term	Formula
Chrysocolla	$Cu_{2-x}Al_x(H_{2-x}Si_2O_5)(OH)_4 \bullet nH_2O$, $x < 1$
Copper pitch	Mn-rich chrysocolla (Throop and Buseck, 1971)
Copper wad	Black copper silicate containing principally Cu, Mn, Fe, Al and Si (Pincheira et al., 2003)
Cuprite / chalcotrichite	Cu_2O
Limonite	Fine mixture of Fe(III) and Al(III) oxides and hydroxides, principally goethite, hematite, jarosite-alunite, and schwertmannite
Malachite	$Cu_2(CO_3)(OH)_2$
Native Cu	Cu^0
Neotocite	$(Mn,Fe,Mg)SiO_3 \bullet H_2O$
Tenorite	CuO

In the oxidation zone, copper can be transported in solution and can precipitate as "copper oxides", depending on physico-chemical parameters largely controlled by tectonics, climate, water, and rock composition (Hartley and Rice, 2005; Dold, 2006a). The term "copper oxide" refers in this context to non sulfide minerals and includes oxides, hydroxides, silicates, sulfates, and carbonates (Brimhall et al., 1985; Padilla Garza et al., 2001). The main copper oxides observed in porphyry copper oxidation zones are presented in Table 1. As shown by (Anderson, 1982; Sillitoe, 2005), pH controls largely precipitation of copper minerals in the oxidation zone. From acidic to neutral conditions, the following sequence is typically observed: chalcanthite, antlerite, brochantite, tenorite (Anderson, 1982; Sillitoe, 2005). Chrysocolla can precipitate instead of brochantite in presence of silica, malachite in presence of carbonate, and atacamite in the presence of chloride.

The Exótica Deposit south of Chuquicamata (Fig. 1), also known as Mina Sur mine, is the product of such laterally migrating acid rock drainage from the sulfide oxidation zone of the Chuquicamata porphyry copper deposit. (Mortimer et al., 1978; Münchmeyer, 1996).

Copper wad and copper pitch are frequent phases in the mineralogical assemblages of the oxidation zone of porphyry copper deposits, and in the related exotic deposits (Sillitoe, 2005; Münchmeyer, 1996). However, their mineralogical characterization is poorly documented. The present study aims to characterize copper pitch and copper wad using new mineralogical and chemical data collected on samples from the Exótica deposit, Chuquicamata district. A genetic model for the formation of chrysocolla, copper pitch, and copper wad at Exótica is proposed based on the interpretation of the collected data set and on the already published data. This work falls within a more general project aiming studying the supergene and exotic mineralization at Chuquicamata (Pinget et al., 2015; Chapter 1)

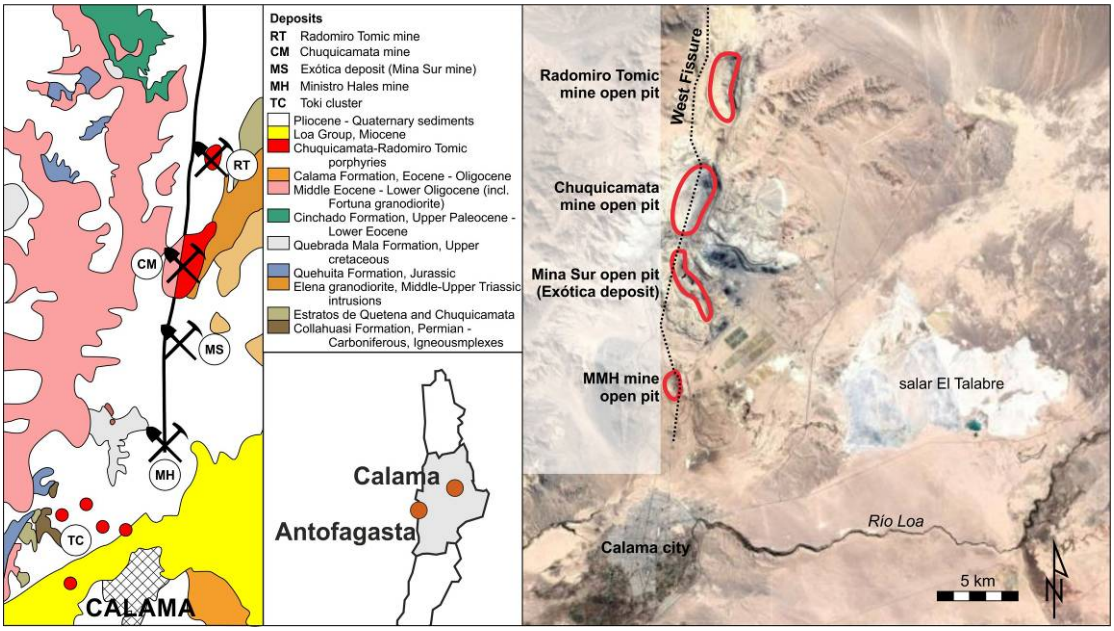

Figure 1: General geography and geology of the Chuquicamata district. Geological map after Rivera et al., 2014. Satellite picture GoogleEarth©.

2.1.2. Geological settings at Exótica (Mina Sur) deposit

The Exótica deposit or Mina Sur mine is the product of acid rock drainage formation in the oxidation zone of the Chuquicamata porphyry copper deposit and the lateral migration of supergene solutions to the South (Fig. 2). The Exótica Deposit was mined between 1957 and 2015. According to Ossandón and Zentilli (1997), around 300 Mt @ 1.17 wt.% Cu were mined.

Downstream of the Chuquicamata deposit, along a gravel-filled channel, supergene solutions interacted with Miocene gravel units and the underlying bedrock (Newberg, 1967; Mortimer et al. 1978; Münchmeyer, 1996; Fam and Rojas, 1997; Dold, 2006a; Chapter 1). Gravels are divided into two units, the Fortuna gravels, that are slope talus deposits with angular to sub-rounded clasts up to 2 meters in diameter, mainly from the adjacent Fortuna granodiorite, and the Exótica gravels consisting mainly of mud flow deposits including coarser intercalations of sand and small angular clasts up to 5 cm in diameter. Based on tectonic considerations, Mortimer et al. (1978) proposed a Middle Miocene age for both gravel units, i.e., contemporaneous to the El Loa Group in the Calama Basin (May et al., 1999; May et al., 2005). An ash tuff intercalated in the gravels, 5 to 10 meters below the present surface, was dated at 8.4 ±0.4 Ma (K/Ar, Mortimer et al., 1978).

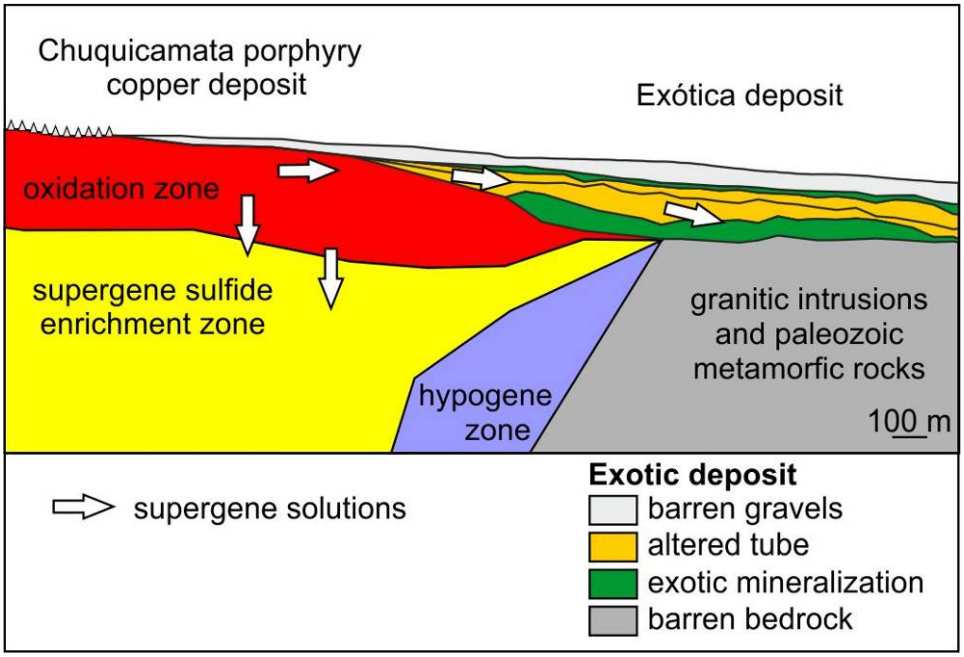

Figure 2: Schematic north(left)-south(rignt) section of the relation between the Chuquicamata porphyry copper deposit and the Exótica exotic deposit.

Clasts from oxidized granodiorite porphyry from Chuquicamata near the base of the gravel units (Newberg, 1967) indicate that gravel deposition started, when the porphyry was already exposed to oxidation and to erosion. Reworking of already mineralized clasts with broken rims of exotic mineralization suggests that the exotic mineralization process was contemporaneous to the gravel deposition, at least in the northern part of the Exótica deposit (Newberg, 1967).

Supergene alunite at Chuquicamata was dated by Sillitoe and McKee (1996, K/Ar) at 19.0±0.7 Ma and 15.2±0.7 Ma. These ages are concordant with those obtained on other supergene alunite occurring in other localities in northern Chile, including Collahuasi (15.2 ± 0.5 Ma, K-

Ar on alunite, Sillitoe and McKee, 1996), Centinela (Telégrafo 21.49± 0.36, Polo Sur 21.2± 0.2 and 19.2± 0.2, $^{40}Ar/^{39}Ar$ on alunite, Perelló et al., 2010), La Escondida (18 ± 0.7 to 14.7 ± 0.5 Ma, K-Ar on alunite, Alpers and Brimhall, 1989). Ages obtained at the close-by El Tesoro exotic deposit are in the same range (K-Ar and ^{40}Ar-^{39}Ar dating of supergene alunite between 22.9 ± 0.4 and 19.2 ± 0.4 Ma, and between 14.8 ± 0.4 and 12.6 ± 2.0 Ma; K-Ar age on cryptomelane of 21.9 ± 1.2 Ma, Tapia et al. 2012).

As discussed in Chapter 1, the main stage of mineralization at the Exótica deposit is likely related to the Late Oligocene - Upper Miocene Andean uplift, i.e., contemporaneous to the main stage of supergene processes in Northern Chile. Alternatively, it could be younger, and have been formed, , at least partly, during the Middle - Late Miocene Andean uplift. A key factor to precise the emplacement of the Exótica deposit is the availability of water during the period between the end of the main supergene processes affecting the porphyry deposits of northern Chile (around 15 Ma, e.g., Sillitoe and McKee, 1996) and present day. Several authors (e.g. Sillitoe et al., 1996; Rech et al., 2006; Dunai et al., 2005; Bissig and Riquelme, 2010) propose onset of hyperarid climate around 15 Ma and even before. However, it is known from recent paleoclimatic records, that even under hyperarid climate, wetter periods may occur (e.g. Latorre et al., 2002 and 2006). Several studies have shown that short wetter periods have existed during the last 15 Ma in Nortehrn Chile (e.g. Hartley and May, 1998; Hartley and Chong, 2002; Saez et al., 2012) opening, tehrefore, the possibility for supergene processes after 15 Ma. Reich et al. (2008, 2009) propose a later stage in the formation of exotic deposit in the Atacama desert starting at ~2–1.5 Ma and continuing until at least the late Pleistocene, during which most of the atacamite could have precipitated.

2.1.3. Mineralogical characterization of the exotic mineralization at the Exótica deposit

According Münchmeyer (1996), who described the principal exotic deposits of northern Chile, the mineralization consists mainly of turquoise, chrysocolla, copper wad and atacamite. Exotic mineralization is frequently associated with the argillic alteration in the host gravels and rocks (Münchmeyer, 1996).

At the Exótica deposit, the alteration of the mineralized bedrock and sediments varies from intense argillic to unaltered (Mortimer et al., 1978). The principal copper bearing exotic minerals are chrysocolla, copper pitch and wad, and atacamite. While atacamite ($Cu_2(OH)_3Cl$) is a well defined crystalline mineral, chrysocolla ($(Cu_{2-x}Al_x(H_{2-x}Si_2O_5)(OH)_4 \bullet nH_2O$, $x < 1$) and copper wad and pitch are better characterized as mineraloïds. The following section gives an overview on the state-of–the–art on chrysocolla, copper wad and copper pitch. The three mineraloïds have similar characteristics, including an important silica content, and a pseudo amorphous component in the structure.

Chrysocolla

No consensus has been reached yet about the chrysocolla structure, despite numerous studies based on X-ray diffraction (XRD), infrared spectroscopy, extended X-ray absorption fine structure (XAFS), X-ray photoelectron spectrometry (XPS), thermogravimetry, differential thermal analysis (Prosser et al., 1965), energy-dispersive X-ray spectroscopy (EDS) and electron paramagnetic resonance (Selvin et al., 2001). Several structures have been proposed to explain the observations made on chrysocolla (Van Oosterwyck-Gastuche, 1970; Schwartz, 1934; Sun, 1963; Newberg, 1967; Farges et al., 2006; Frost et al., 2012; Frost and Xi, 2013; Prosser et al., 1965). Chukhrov et al. (1969) defined chrysocolla as an official mineral phase with an orthorhombic lattice and unknown spatial group. Van Oosterwyck-Gastuche (1970) based on infrared observations proposes "an intermediate structure between sheets and mono-chains". Others authors consider chrysocolla to be a mixture of an amorphous material with an unknown cryptocrystalline phase (Schwartz, 1934; Sun, 1963; Newberg, 1967). An attempt to characterize chrysocolla using XAFS was made by Farges et al. (2006), concluding to the presence of spertiniite ($Cu(OH)_2$). In contrast Frost et al. (2012) and Frost and Xi (2013) exclude the presence of spertiniite in their samples by using thermogravimetric, XPS, and Ramman analysis.

The XRD diffractograms on chrysocolla are characterized by the absence of distinct diffraction peaks (Prosser et al., 1965; Frost et al., 2012) and by the appearance of a general pattern with humps at characteristic positions, similarly to other so called “X-ray amorphous” minerals like ferrihydrite and schwertmannite (Dold, 2003a) or silicates like opal (Lynne, 2005).

As a logical consequence of the lack of defined structure, the chemical composition of chrysocolla, including its water content, is variable too. This was already pointed out by Foote and Bradley (1913, p. 184), who wrote that observations made on chrysocolla are “not in accord with the view that every mineral is a definite chemical compound, but it accounts far the fact regarding composition, in a way that no definite formula can do”. Chemical analysis shows that in addition to the main elements Cu and Si, up to 7.3 wt.% of Al_2O_3 is found in chrysocolla, but generally around 1wt.% (Sun et al., 1963; Prosser et al., 1985; Newberg, 1967; Van Oosterwyck-Gastuche, 1970; Campos et al., 2015). Traces of Ca, Co, Fe, K, Mg, Mn, Na, Pb, among other elements are frequent and reflect the chemical environment in which it precipitates. Color of chrysocolla changes from cream white to deep blue or green. Data from

Campos et al. (2015) by quantitative automated mineral analysis by scanning electron microscopy (QEMSCAN®) show that the chemical composition of chrysocolla varies even at a small scale.

Newberg (1967) suggested that the precursor of the chrysocolla is a gelatinous silica polymer issued from the saturation of silica in solution (>100-140 ppm Si), based on data obtained from laboratory experiments. The results suggest that silica content cannot be too high, to avoid precipitation of amorphous silica. Other important parameters are: the copper content, the presence of ions able to form copper salts, and the pH. Gelatinous copper-rich material was described from several mines (e.g. Moreton, 2007) and was also studied in detail in Exótica (Lambiel, 2014).

Copper wad and copper pitch

Used as a descriptive term by miners (similarly as limonite for the iron oxide family), copper wad designates a dark brown to black earthy material forming patina and cements, and contains mainly copper and manganese with variable amounts of silica. This term is complementary with the term copper pitch, which describes a similar but massive material that shows conchoidal fracture (Guild, 1929).

Copper pitch is described by Schwartz (1934) as a frequent but "impossible to define" material consisting of a mixture of copper oxides, manganese oxides, silicate and water forming banded structures with chrysocolla, concentric shells, and nodules. X-ray diffraction, scanning electron microscopy, and electron probe microanalysis performed by Mote et al. (2001) show that the copper wad from exotic mineralization at El Salvador (Chile) contains a significant proportion of cryptomelane and birnessite. X-ray diffraction on copper pitch from Inspiration Mine (Arizona) yield patterns indistinguishable from the pattern of chrysocolla, what led Throop and Buseck (1971) to define copper pitch as a normal chrysocolla colored by the presence of Mn or Fe. QEMSCAN® studies of Menzies et al. (2015) illustrate the important chemical variability of copper wad and copper pitch, with principally Mn, and the presence of Mg, Al, Fe, Si, P, Ca, Cl, and S. Pincheira et al. (2003) define copper wad and copper pitch as "black copper silicates", both without defined structure and with a similar chemical composition.

2.2. Methodology

2.2.1 Sampling

Copper wad and copper pitch were identified in 40 of the 74 samples taken in the Chuquicamata and Mina Sur open pits (Table 2, Fig. 3). Access was limited by the development of the mine exploitation during the sampling campaigns (2010-2011). The two clusters of samples in the northern part of the mine correspond to areas operated during sampling, and the cluster in the southern sector of the mine corresponds to external parts remaining after exploitation. Therefore, the samples from the southern cluster of the Mina Sur Mine represent marginal mineralization, as the richest central parts had been already mined or covered by waste rock dumps. In addition, samples from 11 drill cores on two east-west sections complete the sampling were the operation did not allow to take a sample (Fig. 4). Moreover, typical samples of chrysocolla and copper pitch from the Chuquicamata district but of unknown exact location were collected.

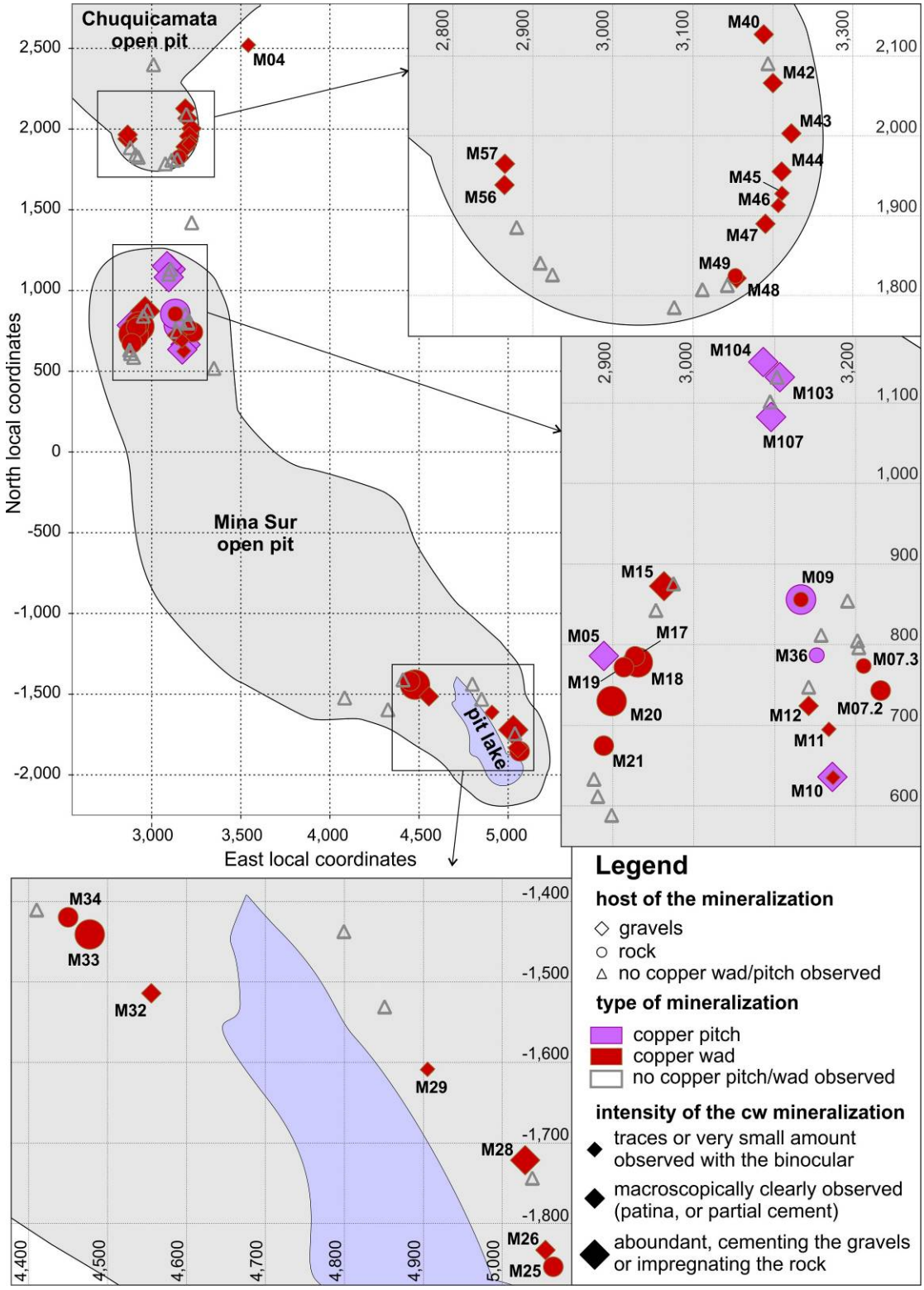

Figure 3: Location of the samples collected in the Chuquicamata and Mina Sur mines.

Table 2: List of the samples used for the copper wad and copper pitch description.

ID	Chuquicamata local coordinates		GWS84 coordinates		altitude	type of mineralization	host of the mineralization	Analyses
	East	North	East	North				
M04	3538	2525	510217	7533932	2624	copper wad	rock	XRD, UNIQUANT
M05	2889	785	509279	7532329	2503	copper pitch	rock	
M07.1	3231	742	509603	7532222	2537	copper wad	gravels	XRD, UNIQUANT
M07.2	3210	773	509593	7532262	2658	copper wad	gravels	
M09.1	3133	855	509531	7532357	2503	copper wad	gravels	XRD, UNIQUANT
M09.3	3133	855	509531	7532357	2503	copper pitch	gravels	
M10.2	3171	635	509532	7532133	2505	copper pitch	rock	XRD, UNIQUANT
M10.3	3171	635	509532	7532133	2505	copper pitch	rock	
M11	3166	695	509537	7532193	2506	copper wad	rock	
M12	3142	723	509518	7532225	2506	copper wad	rock	Thin section, XRD, UNIQUANT
M15	2963	872	509367	7532402	2495	copper wad	rock	Thin section, XRD, UNIQUANT; SEM
M17	2927	785	509317	7532322	2499	copper wad	gravels	XRD, UNIQUANT; SEM
M18	2931	777	509319	7532314	2499	copper wad	gravels	Thin section, XRD, UNIQUANT; SEM
M19	2913	771	509301	7532311	2500	copper wad	gravels	XRD, UNIQUANT
M20	2898	729	509279	7532272	2523	copper wad	gravels	Thin section (M20.2 and M20.3)
M21	2889	673	509260	7532219	2523	copper wad	gravels	Thin section
M25	5064	-1854	510976	7529363	2373	copper wad	gravels	
M26	5055	-1833	510970	7529385	2373	copper wad	rock	
M28	5029	-1721	510963	7529499	2382	copper wad	rock-gravels	
M29	4904	-1608	510860	7529632	2372	copper wad	rock	XRD, UNIQUANT; SEM
M32	4555	-1514	510532	7529783	2387	copper wad	rock	XRD, UNIQUANT; SEM
M33	4477	-1441	510468	7529869	2385	copper wad	gravels	Thin section, SEM
M34	4450	-1420	510444	7529894	2388	copper wad	gravels	Thin section
M36	3152	786	509538	7532285	2604	copper pitch	gravels	XRD, UNIQUANT
M40.1	3189	2127	509801	7533600	2572	copper wad	rock	XRD, UNIQUANT
M40.2	3189	2127	509801	7533600	2572	copper wad	rock	XRD, UNIQUANT; SEM

ID	Chuquicamata local coordinates		GWS84 coordinates		altitude	type of mineralization	host of the mineralization	Analyses
	East	North	East	North				
M42	3200	2066	509802	7533538	2570	copper wad	rock	XRD, UNIQUANT
M43	3223	2003	509814	7533472	2568	copper wad	rock	Thin section
M44	3211	1955	509794	7533427	2557	copper wad	rock	Thin section, XRD, UNIQUANT
M45	3210	1929	509789	7533401	2557	copper wad	rock	
M46	3206	1914	509782	7533387	2558	copper wad	rock	
M47	3191	1890	509763	7533366	2558	copper wad	rock-gravels	SEM
M48	3155	1822	509716	7533305	2560	copper wad	rock	SEM
M49	3153	1825	509715	7533308	2562	copper wad	gravels	
M56	2865	1939	509450	7533469	2564	copper pitch	rock	XRD, UNIQUANT
M57	2865	1965	509455	7533495	2564	copper wad	rock	XRD, UNIQUANT; SEM
M103	3106	1132	509552	7532634	2624	copper pitch	rock	
M104	3086	1151	509535	7532656	2620	copper pitch	rock	SEM on thin section
M107 (MC26)	3096	1083	509533	7532587	2620	copper pitch	rock	XRD, UNIQUANT; SEM on thin section; sequential extraction
M120	4265	6565	511610	7537788	2890	copper wad	rock	
MC25	unknown coordinates					copper pitch	?	XRD, UNIQUANT; SEM on thin section
MC27	unknown coordinates					copper pitch	?	XRD, UNIQUANT; SEM on thin section
MC24	unknown coordinates					copper pitch	?	SEM on thin section; sequential extraction
MC41	unknown coordinates					copper pitch	?	SEM on thin section

Nine samples were selected for thin sections (Table 2). In order to avoid any dissolution by water, the samples were dry sawn and impregnated under vacuum with an epoxy resin (Epoxy Technology 301-1) before proceeding to a standard thin section fabrication procedure. Polishing was obtained in four steps with diamond powder of 6, 3, 1 and 0.5 µm.

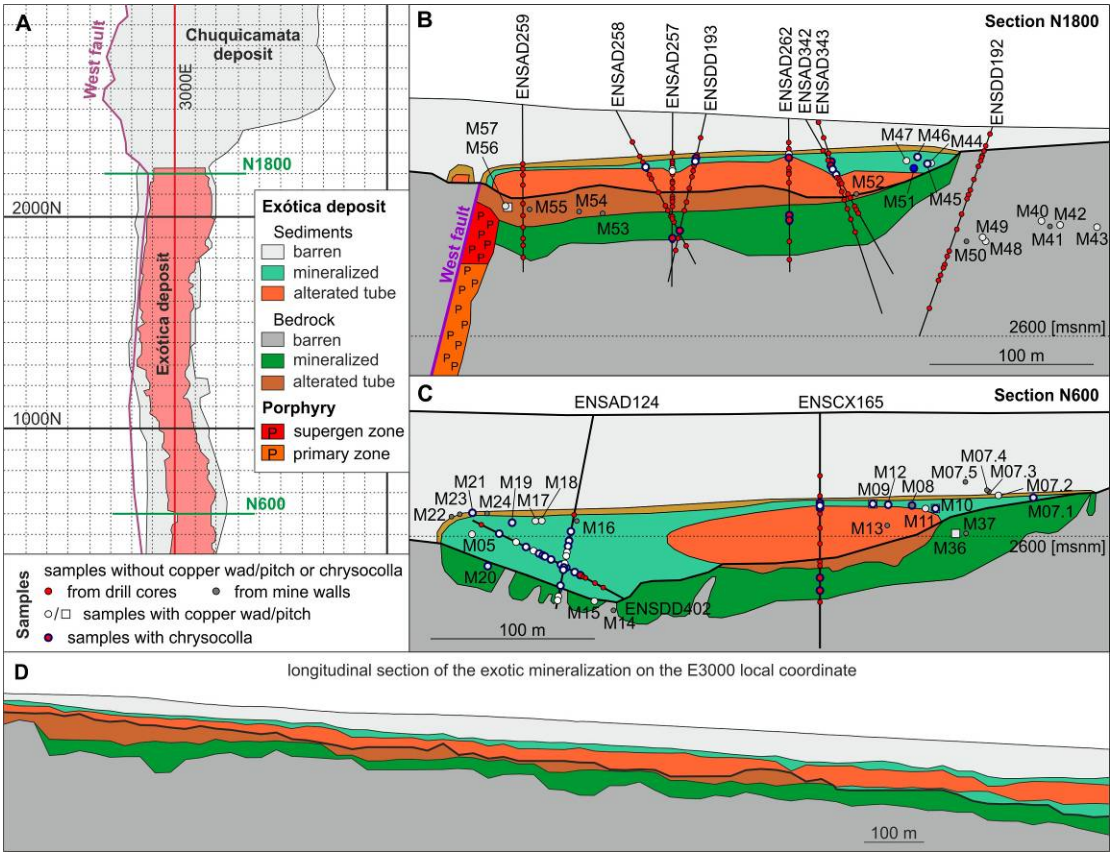

Figure 4: (A) Outer limits of the Chuquicamata and Exótica deposits, and position of the altered tube (in reddish orange). Location of the samples in sections N1800 (B) and N600 (C) in the (modified) CODELCO model. Altitude of the mine samples is estimated after the field observations (altitude obtained with the GPS in the open pits are not reliable). (D) Longitudinal section on the E3000 local coordinate showing the central position of the altered tube in the exotic mineralization.

2.2.2 Semi-quantitative chemical analyzes and X-ray diffraction

Copper wad and copper pitch patina and massive mineralization were separated manually under the binocular microscope to carry out chemical and mineralogical characterization. Problems were experienced to separate copper wad, as it is frequently present as a very thin patina on small grains or in fractures. It was possible to separate reasonable pure copper wad in 17 samples (Table 2). Separation is easier for copper pitch, which presents a more massive texture. Five samples of copper pitch were analyzed as well (Table 2).

Semi-quantitative chemical analyzes

UniQuant® X-ray fluorescence methodology was used to obtain a semi-quantitative chemical characterization of the separated material, on the Philips PW2400 vacuum X-ray fluorescence spectrometer of the Department of Earth and Environmental Sciences, University of Lausanne.

Precision and accuracy of the method was assured using the manufacturer recommended standards and calibration procedures ustilized at the laboratory at University of Lausanne.

X-ray diffraction (XRD)

Powder samples were prepared for the X-ray diffraction. When the quantity of separated material was not sufficient to fill the normal sample holder (around 0.6 cm^3 of pressed powder), the sample was spread on a glass pellet. The diffractometer used was a Bruker D8 Advanced theta/2theta machine with a 2D detector (wave length 1.5406 Å Cu Kα 1, step size 0.00787 °theta, step time 185 s., rotation of the sample handler 15 turns/s.; Crystallography Laboratory, Science Faculty, University of Geneva). Around 50 samples were analyzed, principally to study chrysocolla and copper wad, and to identify the minerals assemblage in the Exótica Deposit.

2.2.3 In situ microfluorescence (μ-XRF)

Thirty samples from the mine and from drill cores were analyzed by in situ microfluorescence (μ-XRF) with an Eagle III μ-XRF instrument (Section of Earth and Environmental Sciences, University of Geneva). The qualitative element distributions and variations in cements, impregnations, and patinas of copper wad, and in the copper pitch veins (Table 2), were studied. The reliability of the method for the most important chemical elements in this study was verified comparing the obtained results in a representative sample with those obtained with microprobe element maps. It confirmed that the μ-XRF is less precise but equally reliable to detect variations in element distributions.

2.2.4 SEM backscattered electrons and secondary electrons imaging

Semi-quantitative chemical data and mineral textures were obtained by SEM-EDS on thin sections and on copper wad patinas (Jeol JSM 7001F at 15 kV; Section of Earth and Environmental Sciences, University of Geneva).

2.2.5 Sequential extractions

All the previously presented methods have the limitation of providing bulk data on copper pitch and copper wad. However, both materials are a mixture of a probably pseudo amorphous and chemically variable material with crystalline phases. The sequential extraction method allows to dissolve different mineral phases and mineral groups present in a mixture using specifically designed dissolution steps. To apply this method to the copper pitch and copper wad mineralization, the seven steps sequential extraction protocol of Dold (2003c) was modified adding a supplementary step targeting specifically the manganese oxides-hydroxides ($HONH_2$-HCl 0.25M, pH2, for two hours, modified after Sondag, 1981 and Hall et al., 1996). This modified sequential extraction protocol (See Table 3) was applied to crushed powder samples to study the dissolving mineralogy and to patina samples to study the surface textural and geochemical effect of each leach solution.

Table 3: Steps of the sequential extraction protocol (after Dold, 2003, Sondag, 1981, and Hall et al., 1996)

Step	Solvent	Targeted phases
1	deionized water, 1 hour	water-soluble fraction
2	NH_4-acetate, pH 4.5, 2 hours	carbonates and exchangeable ions
3a	hydroxylamine hydrochloride, pH 2, 2 hours	amorphous manganese oxy-hydroxydes
3b	NH_4-oxalate, pH 3, 1 hour in the darkness	reactive Fe(III) hydroxides
4	NH_4-oxalate 80°C, pH 3, 2 hours	Fe(III) oxides
5	H_2O_2 35%, 1 hour	organic matter and supergene sulfides
6	$KClO_4$ and HCl	primary sulfides
7	HNO3, HF and $HClO_4$	residual fraction (principally silicates)

Sequential extraction on powder samples

The sequential extraction applied to powder samples provides information on the chemical composition of the mineral phases or mineral groups dissolved. The leach solution of each extraction step were analyzed with Inductively Coupled Plasma – Mass Spectrometry (ICP-MS) for Ag, As, Ba, Bi, Cd, Co, Cr, Na, Fe, La, Mg, Mn, Mo, Ni, Pb, Sb, Se, Sn, Sr, Ti, V, W, Y, Zn, and with ICP – Optical Emission Spectrometry (ICP-OES) for Al, Ca, Cu, Fe, K, Li, Mn, P, Pb and Si, to study the chemical composition of the dissolved phases. Solutions were filtered (0.2 µm?) and acidified with suprapure HNO_3 (1%). Between two steps of extraction, the sample was dried and analyzed by XRD to identify the dissolved phases by Sequential X-ray Diffraction (SXRD) (Dold, 2003a). Two pure samples were selected for this study (binocular observation and XRD verification after the selection). The first sample is a chrysocolla sample from Exótica deposit (MC24, Fig. 5), selected to observe the behavior of this mineral during the sequential extraction protocol. The second sample is a copper pitch sample, from the northern part of the Exótica deposit (MC26, Fig. 6 B). Figure 7 shows the XRD pattern of each powder sample before the application of the sequential extraction process. The experience was run in triplicates.

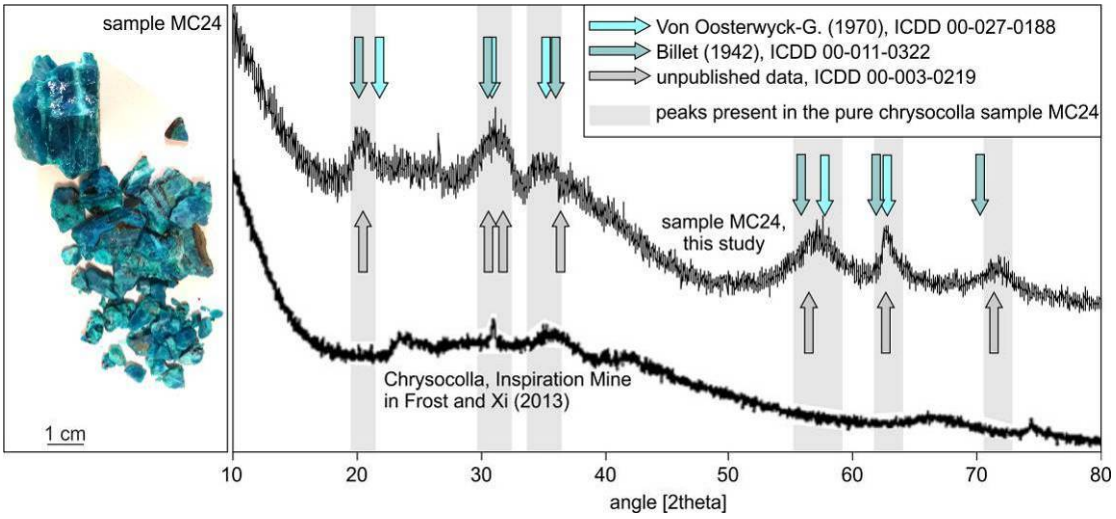

Figure 5: Result of the XRD analysis of the pure chrysocolla sample MC24.

Sequential extraction on patina samples

Since copper wad forms only thin patina and not enough powder can be obtained for conclusive XRD analysis, an alternative method to observe changes after applying the same sequential extraction protocol than for powder chrysocolla and copper pitch samples was developed.

After detailed SEM observation, 6 samples with copper wad patina including the main morphological types were selected. The entire (not crushed) samples of copper wad and copper pitch, were exposed to the different solvents and their effects were studied by SEM backscattered electrons imaging (BEI). Explain, give full name!. Seven samples of copper wad patina and one sample of copper pitch were selected for this purpose (Table 1).

Samples of less than 1 centimeter diameter were mounted with glue on the aluminum conductive supports for the SEM before the dissolution sequence was applied. The step 6 and 7 were not possible to apply because of the disintegration of the samples. After each dissolution step, samples were washed with deionized water to avoid the re-precipitation of new minerals from solvent trapped in the porosity, dried, and an ultra-thin coating (ca 10 nm) of gold was deposited on the samples by low vacuum sputter coating before imaging with the SEM. Seven aliquots of each sample were prepared, to apply one dissolution step to each aliquot. The advantage of this method is to observe the effect of each dissolution step without interferences of different steps.

2.2.6 QEMSCAN®

Automated mineral analysis and textural imaging of the studied samples were performed using an FEI QEMSCAN® Quanta 650F facility at the Department of Earth Sciences, University of Geneva, Switzerland. The system is equipped with two Bruker QUANTAX light-element energy dispersive X-ray spectrometer (EDS) detectors. Analyses were conducted at high vacuum, accelerating voltage of 25 kV, and a beam current of 10 nA on carbon-coated polished thin sections. FieldImage operating mode (Pirrie et al., 2004) was used for analyses. Between 99 and 169 individual fields were measured per sample, with 1500 pixels per field, and point spacing of 5 μm. The standard 1000 counts per point were acquired, thus yielding a limit of detection of approximately 2wt% per element for mineral classifications. Measurements were performed using iMeasure v5.3.2 software and data processing using iDiscover® v5.3.2 software package. Final results consist of: i) high-quality spatially resolved and fully quantified mineralogical maps; ii) BSE images with identical resolution as the mineralogical maps; iii) X-ray element distribution maps.

2.2.7 Geochemical Modeling

To model the interaction between the solutions and the host rock during the formation of the mineralization at Exótica, the geochemical modeling program *PHREEQC* (Parkhurst and Appelo, 1999) was used. The llnl database was complemented with data for additional minerals including rhomboclase (Majzlan et al., 2006), libethenite (Majzlan et al., 2014) and montmorillonite (Vieillard, 2000).

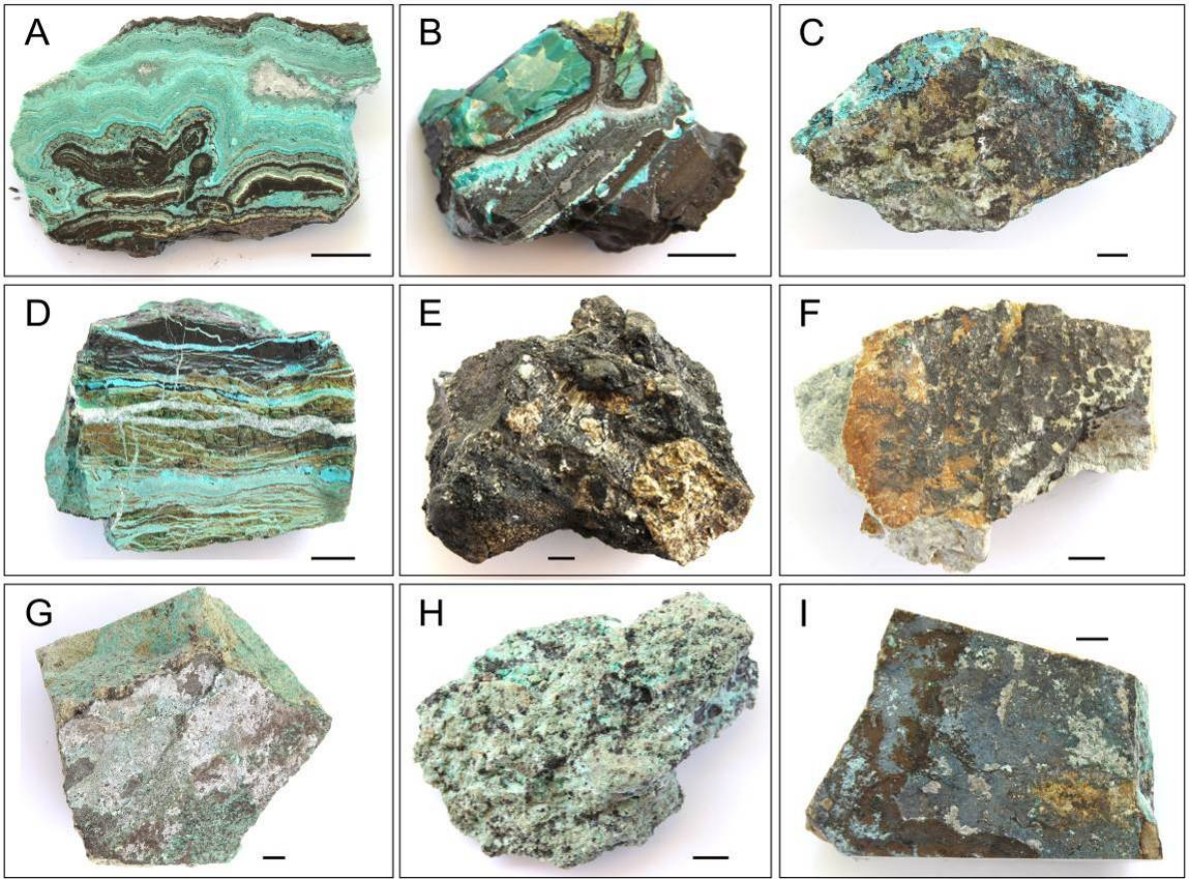

Figure 6: Representative chrysocolla, copper pitch, and copper wad, samples (locations indicated in Fig. 3) . (A) M10.2, massive sample of chrysocolla, copper pitch and gypsum vein, contact between bedrock and sediments, east of N600 section. The copper pitch on the top of the sample presents a copper wad-like powdery patina; (B) M107, massive sample of copper pitch, chrysocolla and gypsum; (C) M44.2, rock with important patina made of copper wad, chrysocolla and gypsum, from the north of Exótica mine; (D) MC27; massive sample with copper pitch, chrysocolla, gypsum and atacamite, unknown location in Exótica deposit; (E) M33, sediments cemented with copper wad from the south-west of Exótica; (F) M40.1, rock with copper wad and iron oxides patina, from the north of Exótica deposit; (G) M17.2, angular clast with copper wad, atacamite and gypsum patina, from the west of section N600; H. M07.1, sediments cemented with chrysocolla and small copper wad, from the north of Exótia deposit; I. M48, rock with a patina of copper wad, chrysocolla and gypsum, from the north of the Exótica deposit.

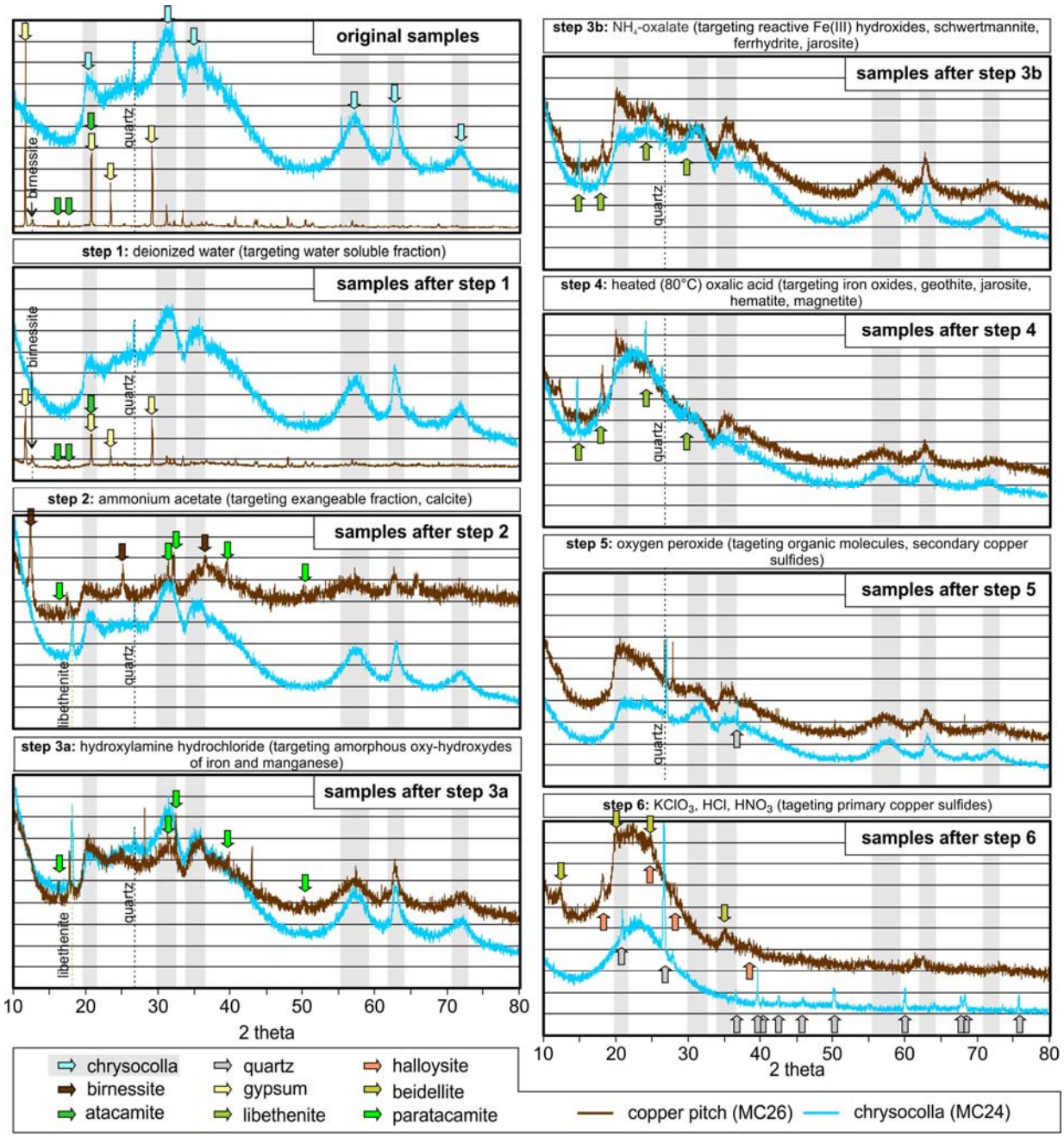

Figure 7: Results of the XRD analyses on the chrysocolla and copper pitch samples before the sequential extraction and after each step of dissolution. Arrows indicate the principal peaks of the identified mineral phases.

2.3. Results and Discussion

2.3.1 Mineral Distribution

In the northern part of the Exótica deposit, i.e., the area more proximal to the source of supergene solutions, the central axis of the mineralization is constituted by a strongly altered zone, forming an "altered tube" or conduit, hereforth referred to as “the tube”. In a transversal section, from the center to the border, the following zones described below have been distinguished on the basis of the mineralogical observations and of the copper content (Fig. 4).

(a) The center of the "tube" shows strong kaolinization, alteration that affects sediments and underlying bedrock. Traces of alunite are also identified. Strongly altered samples present copper content lower than the mean value of the deposit (CuO between 0.1 to 0.6 wt.%, with some values up to 1.0 wt.%), and iron contents reaching up to 52 wt.% of Fe_2O_3. Manganese content is generally below the detection limit, with values reaching up to 0.3 wt.% in the iron richest samples.

(b) In the outer part of the central tube, copper content of the less altered samples increases to generally between 0.4 and 0.7, with values up to 1.1 wt.% and manganese up to 0.5 wt.%. Mean iron content slightly increases, from 20 wt.% in the central zone to 22 wt.% in this zone, but punctual high values due to hematitization are no more observed. Main alteration minerals are kaolinite and sericite. Element mapping, executed with a QEMSCAN® show that copper can occur as rims in iron rich material (sample 258@45m) such as impregnating the altered material (samples 342@80m and 343@80m). It has not been possible to attribute the copper contents to specific mineral phases; possibly it is adsorbed clay minerals, due to their low point of zero charge (PZC) or coprecipitated with Fe(III) oxyhydroxides.

(c) Adjacent to the altered tube occurs the richest mineralization (in places > 30 wt.% Cu). Copper occurs mainly as chrysocolla, copper pitch, copper wad, and atacamite. Atacamite, frequently together with gypsum, is mainly present in fractures crosscutting the previous mineralization.

This zoning indicates a pH gradient from strongly acidic conditions in the center of the tube (kaolinite, alunite; pH 2-3) to almost neutral conditions in the outer zone where atacamite (pH 4.5) and chrysocolla (pH 7) dominate (Dold, 2006b). South of N-1200 the altered tube gradually disappears.

Copper wad and chrysocolla occur mainly as open space filling, particularly as intergranular cement and as patina covering clasts and bedrock fissures. In places, copper wad and chrysocolla impregnate sediments and rocks, but generally it is found as fine open space filling. Massive veins of chrysocolla and copper pitch are mainly observed in the northern part of the Exótica Deposit (including the zone "c" adjacent to the altered tube) where they frequently form alternating massive bands.

2.3.2 Mineralogical and geochemical bulk characterization of chrysocolla, copper pitch, and copper wad

Chrysocolla ($Cu_{2-x}Al_x(H_{2-x}Si_2O_5)(OH)_4 \bullet nH_2O$, $x < 1$) occurs at Exótica as massive light blue to turquoise-blue aggregates (Fig. 5), partly in veins, and as patinas on clasts and fissures of the bedrock. XRD shows the typical signature for pseudo amorphous material with "humps" instead of definite peaks as it has been described for opal-A by Nicolau et al. (2014) and for

opal-CT by Hatipoğlu, 2010. Figure 5 shows the XRD obtained from the purest chrysocolla sample from Exótica. The principal hump at around 21.5° [2θ] (Billiet, 1942; Von Oosterwyck-Gastuche, 1970) is also characteristic for opal-A (Nicolau et al., 2014). Other humps already described as characteristic for chrysocolla by Billiet (1942), Von Oosterwyck-Gastuche (1970) or Frost and Xi (2013) are also present in the diffractrogram of Fig. 5. XRD carried out by Frost and Xi (2013) indicates that chrysocolla may show patterns with less marked humps (Fig. 5).

The chemical composition of chrysocolla from Exótica (Table 4) is in agreement with other published analyses of this mineral, with CuO between 36 and 47 wt.%, SiO_2 between 37 and 43 wt.% and Al_2O_3 up to 3.3 wt.% (Fig. 8). Other trace elements were detected, Mn (from 0.3 to 0.7%), Fe (from 6.19 to 0.22 wt.%), Ca (from 1.08 to 0.74 wt.%), S (from 0.32 to 1.1 wt.%), K (from 0.09 to 0.41 wt.%), Cl (from 0.06 to 5.18 wt.%), Zn (from 0.05 to 0.34 wt.%), P (from 0.07 to 0.31 wt.%).

Copper pitch at Exótica occurs mainly as black to dark brown glassy to dusty massive aggregates (Fig. 6). Copper pitch frequently occurs together with chrysocolla as alternating bands (Fig. 6 D) or in more complex textures (Fig. 6 A and B). XRD on copper pitch samples show similar patterns to those obtained for chrysocolla, except for the presence of peaks attributed to birnessite ($(Na,Ca)_{0.5}(Mn^{4+},Mn^{3+})_2O_4 \bullet 1.5H_2O$) (Fig. 9). Taking in account the experimental results of Yu et al. (2012), the obtained peaks would correspond to birnessite precipitated under acidic rather than alkaline conditions (Fig. 9).

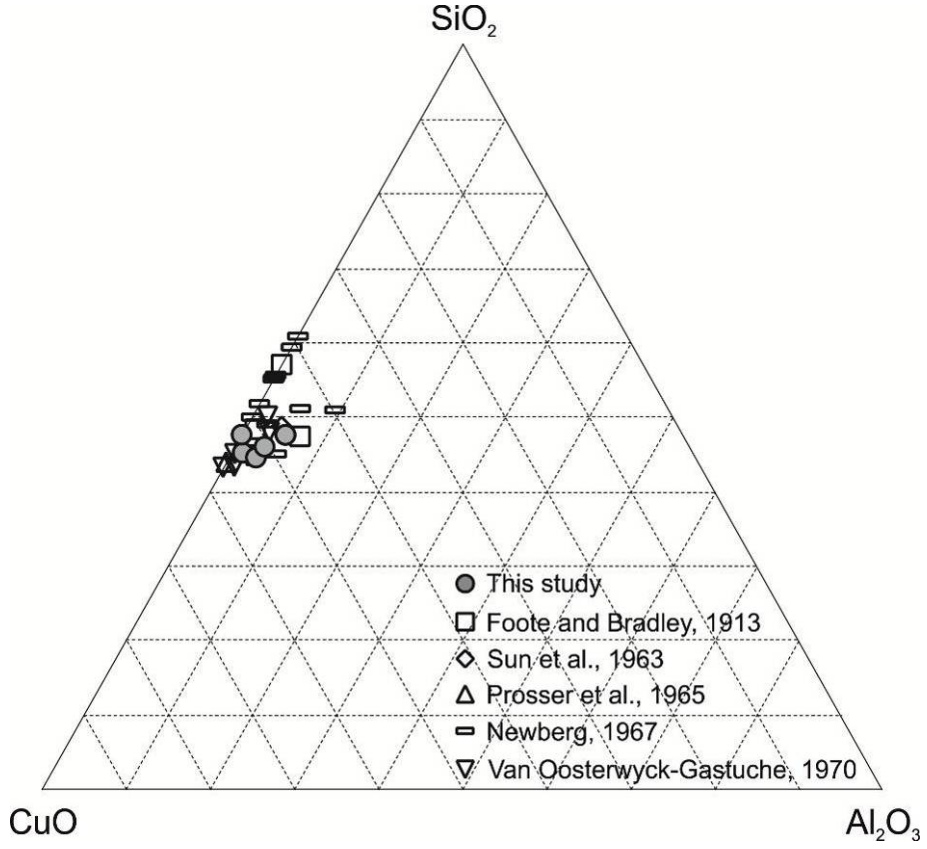

Figure 8: CuO-SiO_2-Al_2O_3 plot of chrysocolla (data in Table 4).

Table 4: Semi-quantitative Uniquant® results [wt%] on copper pitch, copper wad and chrysocolla samples. (n.d. = not detected)

ID	Type of mineralization	Cu	Si	Mn	Fe	Al	Ca	S	K	Cl	Mg	Zn	P	Mo	Na	Co	Ti	Pb	Sr	Ba	V
M04.2	copper wad	35.70	14.43	4.23	1.54	2.65	0.57	1.08	0.90	2.17	0.59	0.41	1.35	0.10	1.24	n.d.	0.07	0.06	n.d.	n.d.	n.d.
M07.1	copper wad	23.76	20.21	8.95	0.76	2.83	1.16	0.91	1.86	0.49	0.37	0.74	0.06	0.37	n.d.	n.d.	0.04	n.d.	0.11	n.d.	n.d.
M07.1	copper wad	25.25	18.67	9.66	1.23	2.97	1.36	0.55	1.01	0.62	0.50	0.63	0.35	0.25	n.d.	n.d.	0.15	n.d.	0.09	n.d.	0.03
M09.1	copper wad	12.97	14.00	15.35	6.45	7.91	0.76	2.00	0.75	0.64	0.30	0.25	0.14	0.24	n.d.	0.23	0.14	n.d.	0.11	n.d.	0.01
M10.2a	copper pitch	35.60	13.06	14.42	0.40	2.68	0.58	1.18	0.23	0.14	n.d.	0.14	0.06	0.14	n.d.	0.19	n.d.	0.07	n.d.	n.d.	0.01
M10.2b	copper pitch	38.51	10.03	14.58	0.68	2.79	1.07	2.01	0.22	0.53	n.d.	0.19	0.11	0.05	n.d.	0.30	n.d.	n.d.	n.d.	n.d.	n.d.
M15.2	copper wad	7.40	10.94	37.26	1.13	3.08	2.84	3.92	1.73	n.d.	n.d.	0.18	0.06	0.30	n.d.	0.20	0.02	n.d.	0.09	0.42	0.04
M17	copper wad	47.41	7.04	7.41	0.23	0.16	3.42	3.41	0.16	5.03	0.36	0.24	0.28	n.d.	n.d.	0.06	0.05	0.17	0.04	n.d.	0.03
M18.2	copper wad	3.06	22.85	10.80	3.72	9.09	1.68	0.67	2.34	n.d.	0.79	0.07	0.13	0.07	1.56	0.17	0.36	n.d.	0.11	0.02	0.05
M19.1	copper wad	2.99	24.68	10.95	3.46	9.44	0.92	0.14	2.07	n.d.	0.28	0.17	0.15	0.21	n.d.	n.d.	0.32	n.d.	0.37	0.07	n.d.
M29.1	copper wad	24.27	18.21	7.05	2.50	3.62	0.91	1.35	n.d.	0.81	2.26	0.79	n.d.	n.d.	n.d.	n.d.	0.05	0.49	n.d.	n.d.	n.d.
M32	copper wad	5.74	21.95	5.32	6.15	10.96	2.39	0.84	0.47	n.d.	1.56	0.59	0.07	n.d.	n.d.	n.d.	0.36	0.09	n.d.	n.d.	n.d.
M36	copper wad	37.01	15.55	6.71	0.68	1.90	1.31	0.82	0.19	1.95	n.d.	0.16	0.13	0.24	n.d.	n.d.	0.04	n.d.	n.d.	n.d.	0.02
M40.1	copper wad	6.96	16.04	14.48	10.42	6.79	0.81	0.44	2.82	0.41	0.61	0.19	0.65	0.24	n.d.	n.d.	0.15	0.23	0.04	n.d.	0.01
M40.2	copper wad	23.51	12.58	28.30	1.40	0.25	0.40	0.26	0.55	0.15	n.d.	0.08	0.57	0.45	n.d.	0.23	n.d.	0.18	0.05	n.d.	n.d.
M42	copper wad	9.65	15.57	1.42	28.37	3.25	1.05	0.77	0.22	0.21	0.67	0.06	0.33	0.06	n.d.	n.d.	n.d.	0.12	0.02	n.d.	n.d.
M44.2	copper wad	36.33	12.66	8.07	4.74	2.68	0.93	0.52	0.48	0.52	n.d.	0.18	0.24	0.06	n.d.	n.d.	0.23	0.09	n.d.	n.d.	n.d.
M56	copper wad	36.99	16.44	7.12	1.39	1.83	1.09	0.40	0.14	n.d.	0.40	0.21	0.09	0.14	n.d.	0.14	0.04	0.04	0.06	n.d.	0.01
M57	copper wad	17.49	14.80	13.25	5.43	3.43	4.11	1.57	0.77	0.24	0.72	0.51	0.59	0.23	n.d.	0.15	0.09	0.08	0.09	0.08	0.02
MC25	copper pitch	41.76	8.96	18.80	n.d.	0.45	0.23	0.16	0.14	1.39	n.d.	0.19	0.08	0.20	n.d.	0.37	n.d.	n.d.	n.d.	0.06	n.d.
MC26	copper pitch	28.12	14.54	14.34	3.45	2.19	1.93	1.76	0.34	n.d.	n.d.	0.16	0.05	0.02	n.d.	0.32	n.d.	n.d.	0.03	0.04	n.d.
MC27	copper pitch	43.30	13.11	10.84	0.06	0.33	0.41	0.18	0.06	1.30	n.d.	0.18	0.05	0.03	n.d.	0.13	n.d.	n.d.	0.03	0.29	n.d.
M45	chrysocolla	33.32	12.1	0.67	6.19	6.28	1.08	0.41	0.39	5.18	n.d.	0.09	0.31	n.d.	n.d.	n.d.	0.05	0.02	n.d.	n.d.	n.d.
M47.2	chrysocolla	44.73	17.78	0.36	0.22	1.47	0.74	0.32	0.43	0.19	n.d.	0.05	0.07	n.d.	n.d.	n.d.	0.01	0.04	0.02	n.d.	n.d.
MC24	chrysocolla	37.75	20.01	0.29	0.27	1.75	0.84	1.1	0.09	0.06	n.d.	0.34	0.20	n.d.	n.d.	n.d.	n.d.	n.d.	n.d.	n.d.	n.d.

Copper pitch at Exótica is composed mainly of Cu (values between 3 and 47 wt.%), Si (values between 7 and 25 wt.%), Mn (values between 1.5 and 37 wt.%), Al (values between 0.2 and 11 wt.%) and Fe (values between 0.2 and 28 wt.%) (Fig. 10). Other elements are present as traces (Table 4).

Copper wad is present as patina in fractures of the mineralized bedrock (Fig. 6 F, G and I) as well as cement in the mineralized gravels (Fig. 6 C, E and H). The intensity of copper wad mineralization varies from small patches to intense cementation. In all its appearances, copper wad is frequently in assemblage with gypsum, iron oxides, chrysocolla, atacamite ($Cu_2(OH)_3Cl$), libethenite ($Cu_2(PO_4)(OH)$). The textural relationships between these minerals were investigated with SEM secondary electron imaging. The signature of the pseudo amorphous copper wad is covered by the presence of small amount of well crystallized minerals and makes it characterization by XRD not possible. In addition to the gangue minerals (principally quartz and feldspars), gypsum, atacamite, paratacamite and birnessite were identified.

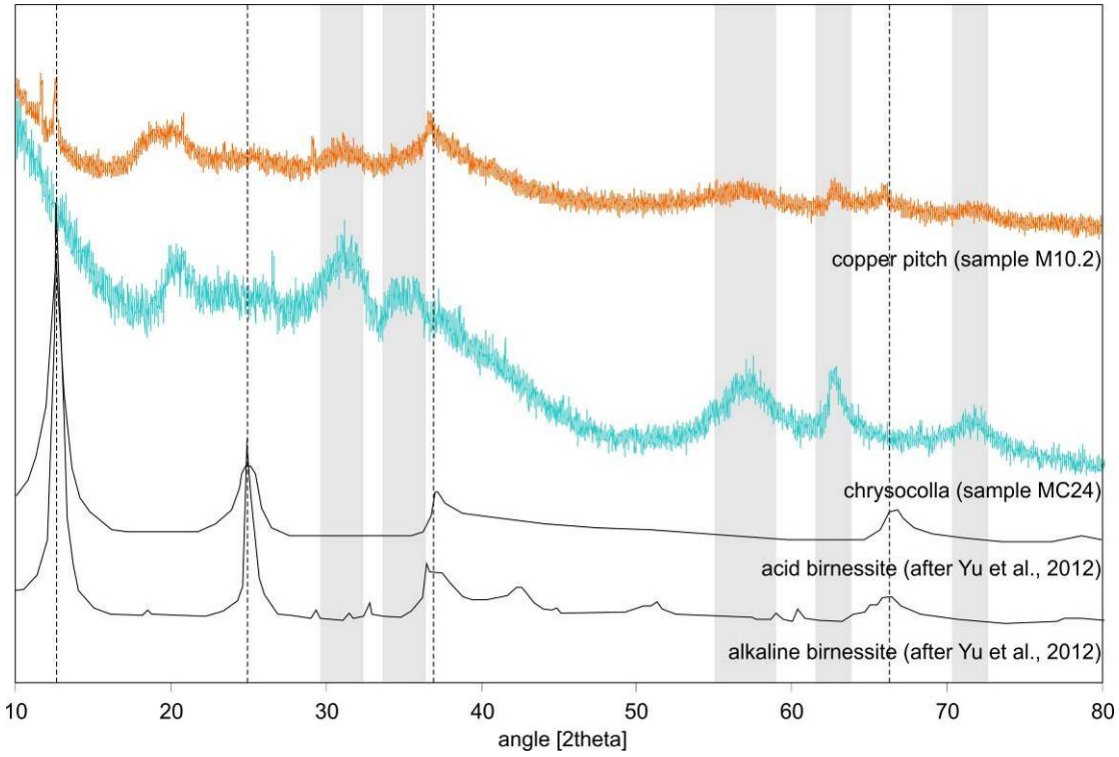

Figure 9: XRD patterns obtained on samples M10.2 (pure copper pitch) and MC24 (pure chrysocolla) compared with the pattern obtained on acid and alkaline birnessite samples by Yu et al. (2012). The comparison indicates more similarities between the birnessite contained in the copper pitch with the acid birnessite than with the alkaline birnessite, which gives indications about the conditions of precipitation of the copper pitch.

The results of the microfluorescence on copper pitch - chrysocolla illustrate the distribution of Mn, Fe and Cu, and how the variations of chemical composition affect the color of the sample. Manganese gives a black color to the material, and iron, probably as Fe^{2+}, a more greenish tint. Iron seems to substitute manganese. In absence of manganese and iron, the color is the typical light blue color of chrysocolla (Fig. 11 A).

Microfluorescence also allows to observe the textural relationship between the clasts/bedrock and the copper wad mineralization. Copper wad cements fractures or fills open space in most samples (Fig. 11 D), and only rarely impregnates the sediments or the bedrock (Fig. 11 C), sometimes along fractures (Fig. 11 B).

2.3.3 Textural considerations for the ore formation

The study of thin sections by optical microscopy and SEM backscattered electrons imaging show that atacamite – gypsum veins cut always the previous mineralization (Fig. 12). Thus, the atacamite mineralization is therefore seen as the latest event in the ore formation process.

Chrysocolla shows small inclusions in sample MC27. Heating and cooling of the samples indicated that these inclusions are empty (or filled with air), but it gives the indication that the material was sufficiently viscous to trap gas during the precipitation.

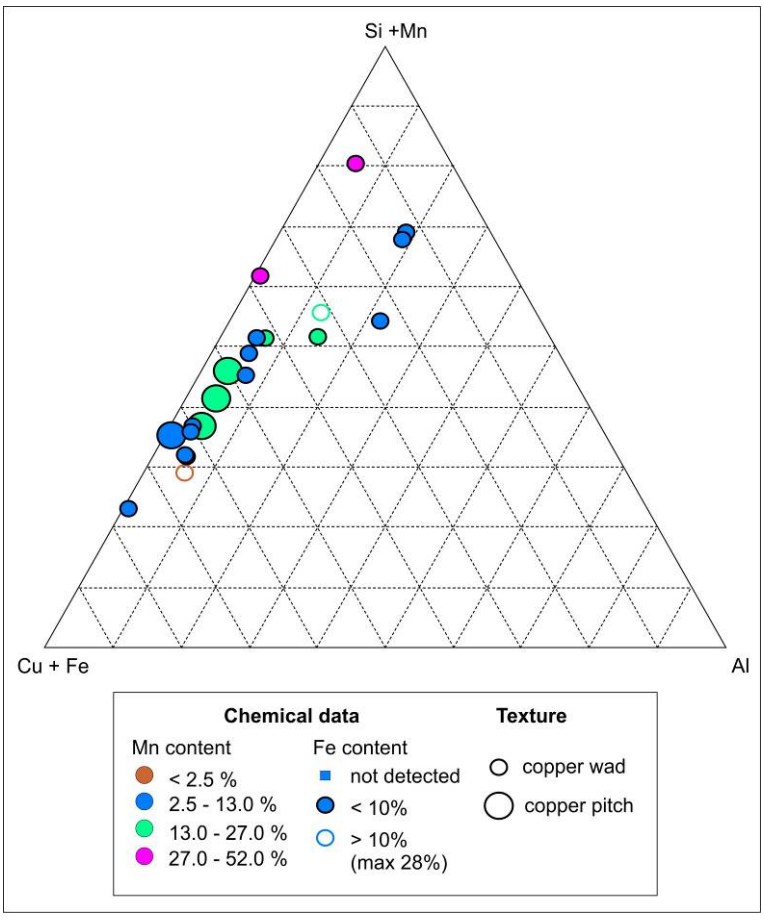

Figure 10: Results of the Uniquant® semi-quantitative analyses for copper wad and copper pitch, presented in a Cu+Fe - Si+Mn - Al triangular diagram [wt%]. Si and Mn are roughly linearly related, as illustrated with the symbol colors. The iron content is generally not relevant in comparison to the copper content, apart for the two samples signalized with empty symbols. The size of the symbols makes the difference between copper pitch and copper wad.

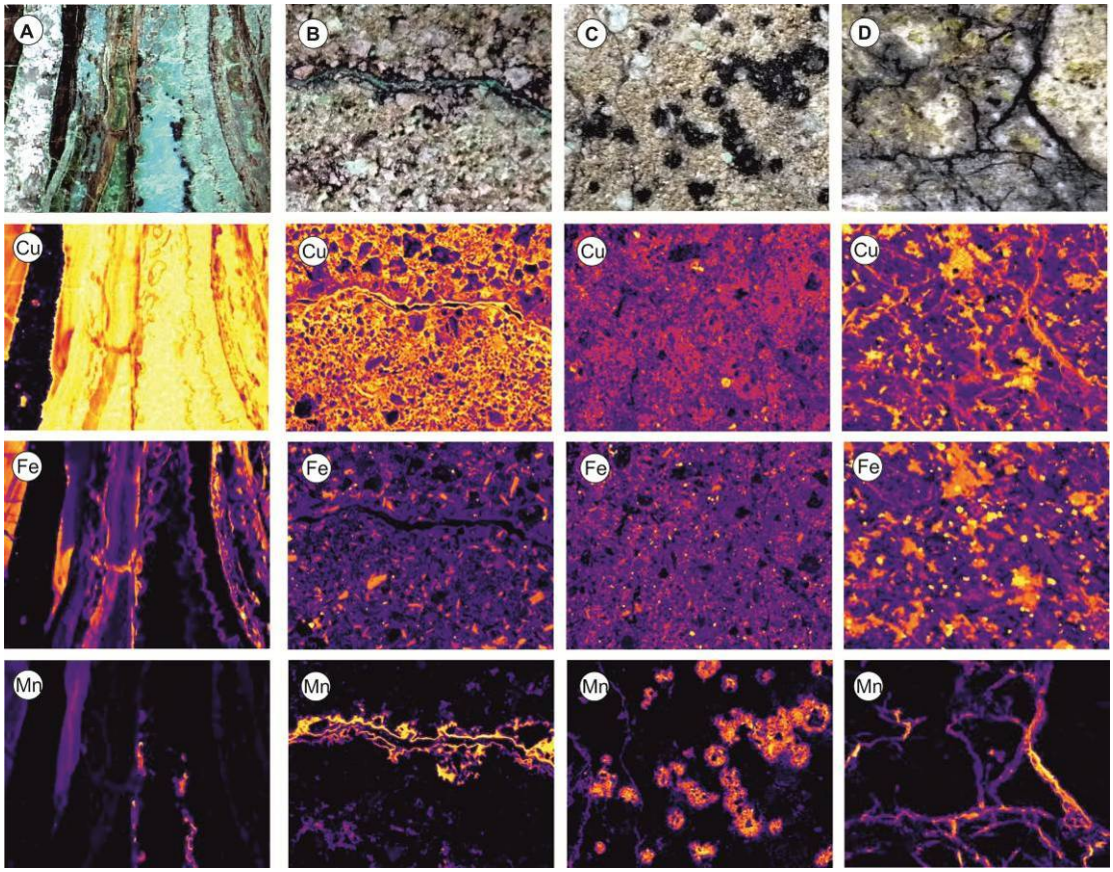

Figure 11: Microfluorescence results on some samples from Exótica Deposit (qualitative scale, black being the absence of the element, and yellow the highest intensity). A. Sample MC27, chrysocolla and copper pitch; B. M17, fine sandstone with copper wad in fractures; C. M21.2, fine earthy sandstone with copper wad patches; D. M18.2, sandstone partly cemented with copper wad (field of analysis is 3.5 cm wide).

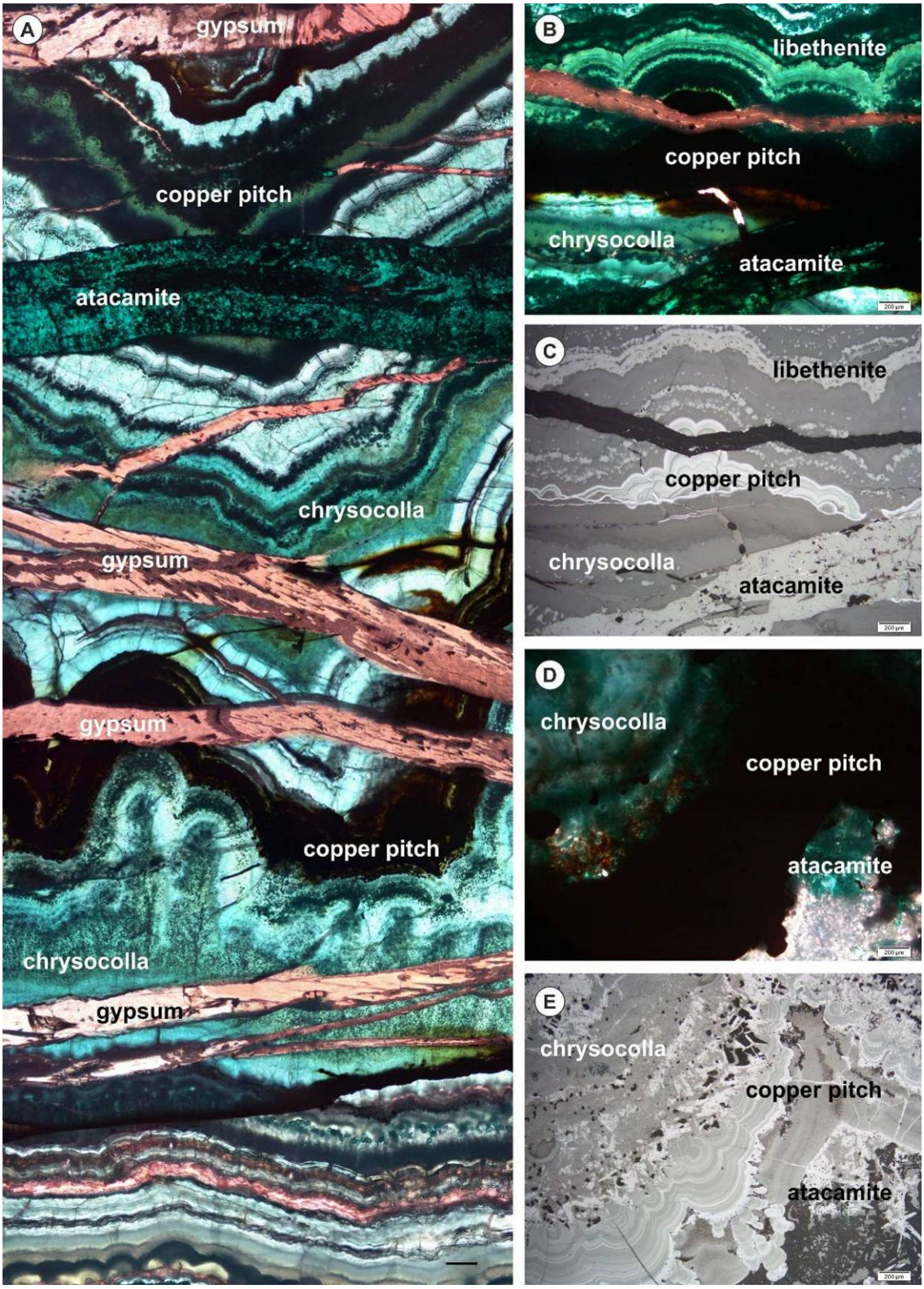

Figure 12: A. Transmitted light, plane-polarized, sample MC41, massive chrysocolla-copper pitch mineralization crosscut by gypsum-atacamite veins; B Transmitted light, plane-polarized, sample MC41, chrysocolla-copper pitch massive mineralization, with libethenite in the chrysocolla, crosscut by gypsum and atacamite veins; C. same area as (B) in reflected light, plane-polarized ; D. Transmitted light, plane-polarized, sample MC25, copper pitch-

chrysocolla massive mineralization with atacamite and gypsum; E. same area as (D), reflected light, plane-polarized.
Samples M104, M107, MC25, MC27 and MC41 are constituted only by chrysocolla-copper pitch veins, and MC24 shows the contact of a chrysocolla – copper pitch vein with the gangue. All the samples show that the veins are always constituted by various generations of precipitates. For both, chrysocolla and copper pitch, similar textures are observed, and they are frequently alternated into the same sequence. The veins are basically made of sub-parallel generations of chrysocolla and copper pitch, differentiated by the color and the chemical composition (Fig. 13), with generally botryoidal patterns. The veins frequently cut other prior veins with a sharp contacts, indicating that the material was at least partially consolidated when the later generation of mineralization occurred (Fig. 13 N). In the case of gels, an important viscosity could be sufficient to obtain this type of contact. This structure could be the filling of desiccation cracks. All generations of veins frequently contain clasts of gangue or of previously consolidated chysocolla or copper pitch (Figs. 13 B, D, G, I). The sharp angles of the chrysocolla and copper pitch clasts suggest that they were totally consolidated when reworked. No sign of dissolution associated with the reworking was observed, suggesting fast consolidation (e.g. dehydration).

In some cases, small crystals of libethenite are observed at the contact of two generations of chrysocolla or in the chrysocolla mass (Figs. 13 F, N and O). The co-precipitation of chrysocolla and libethenite is described by Crane et al. (2001) when silica exceeds saturation. A manganese oxide (possibly Romanèchite, $(Ba,H_2O)_2Mn_5O_{10}$) is observed more rarely in the same context but mainly in copper pitch (Fig. 13 H).

The EDS chemical data shows that the material contains principally Si, Cu and Mn. Pure copper silicates with a crystalline shape are rarely observed (Fig. 13 A). Some concretions of pure SiO_2 are observed but rare (Fig. 13 G). While in chrysocolla silica is always an important chemical component, some zones of copper pitch are almost silica-free, showing the typical botryoidal texture (Fig. 13 C).

The textural observation of the chrysocolla – copper pitch veins suggest that a possible gel precursor for the chrysocolla, which was described by various authors (Newberg, 1967; Moreton, 2007; Faimon and Blecha, 2008) and also studied in Exótica (Lambiel et al. 2014), might be the precursor in pond-like precipitation environments for the chrysocolla-copper pitch formation.

It is difficult to confirm the gel precursor of the chrysocolla and the copper pitch only based on the texture. However, some textures seem to indicate the presence of gel during the precipitation, and no one excludes it. The presence of libethenite crystals in the chrysocolla, which are not the product of a replacement of chrysocolla by libethenite (Crane et al., 2001) indicates that the material was not totally consolidated. Moreover, the same libethenite is observed crystallizing in two crossed veins, indicating that the first and the second veins could have been both present as gel when it precipitated (Fig. 13 N). In samples MC24 and MC25, the clasts in chrysocolla veins are showing an arrangement, which could be due to a decantation into a gel (Fig. 13 I).

As it is assumed that the supergene mineralization took place in a semi-arid to arid climate conditions (Houston and Hartley, 2003), periodic strong storm events occur in these environments (e.g. ENSO cycles). The textural observations on chrysocolla and copper pitch suggest that this mineral assemblage might be formed in horizontal to sub-horizontal low

energy ponds, were the Cu-Si-Mn-rich gel-precursor precipitated. Aging or dehydration consolidates to form the chrysocolla-copper pitch mineralization. Dehydrations cracks will be filled by the next solutions and storm events may induce through high energy flow, reworking of the precipitates and posterior consolidation by the precipitation of the next generation of Cu-Mn-Si rich gels.

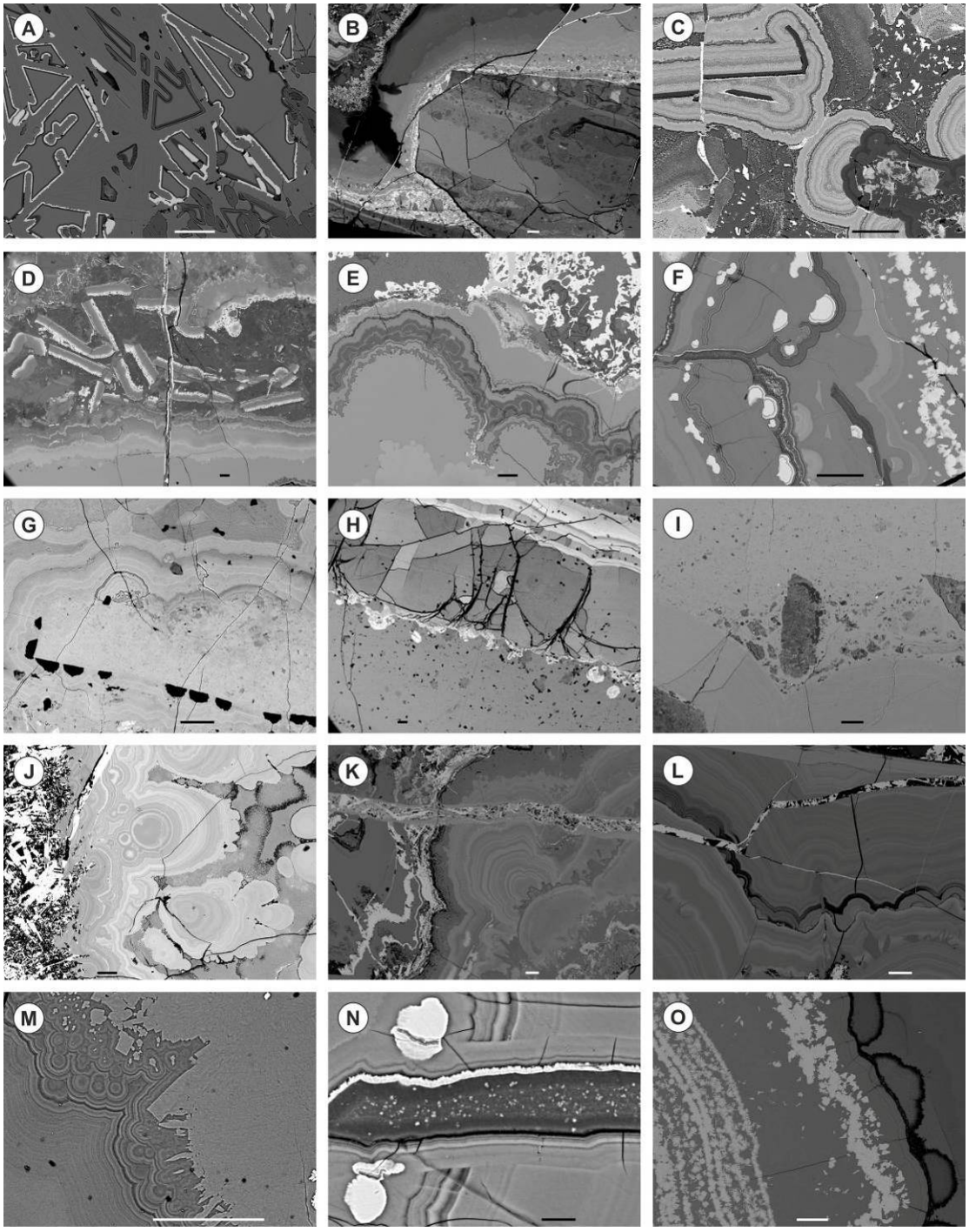

Figure 13: SEM backscattered electrons imaging on copper pitch and chrysocolla massive samples. A. M107, chrysocolla (dark grey) and atacamite (light grey); B. M107, angular clast of chrysocolla containing minimum tree generations of mineralization (large uniforme vein in the center, darker chrysocolla containg clasts of gangue, and light grex vein containing clasts of chrysocolla and gangue in the upper part), in a matrix of chrysocolla with botryoidal texture;

C. M107, chrysocolla (dark grey) and copper pitch (light grey) concretions; D. M104, partly reworked concretions of copper pitch (light grey) and aluminium-rich chrysocolla (light grey), crosscut by an atacamite-gypsum vein (in the center); E. M104, copper pitch - chrysocolla concretion with varying contents of Al, Si, Mn, and Cu, and Cu-Mn oxides (with) containing atacamite (light grey); F. MC41, chrysocolla concretions encompassing libethenite crystals (white), and borders of copper pitch (dark grey); G. MC24, angular clast of chrysocolla encompassed in a concretion of chrysocolla, and presence of pure SiO_2 (black); H. MC24, copper pitch vein with varying contents of Mn and Cu, in a matrix of chrysocolla - gypsum. White material at the contact of both materials is copper pitch; I. MC24, clasts in a matrix of chrysocolla indicating a possible sedimentation in a gel-like material; J. MC25, copper pitch concretion, atacamite - gypsum mineralization (on the left); K-L. MC25, copper pitch concretion, crosscut by an atacamite-bearing vein; M. MC41, chrysocolla (on the right) and copper pitch (concretion on the left); N. MC41, chrysocolla vein crosscutting a chrysocolla concrection, with libethenite at their contact (white); O. MC41, libethenite crystals in a chrysocolla mineralization. Bars represent 100 μm.

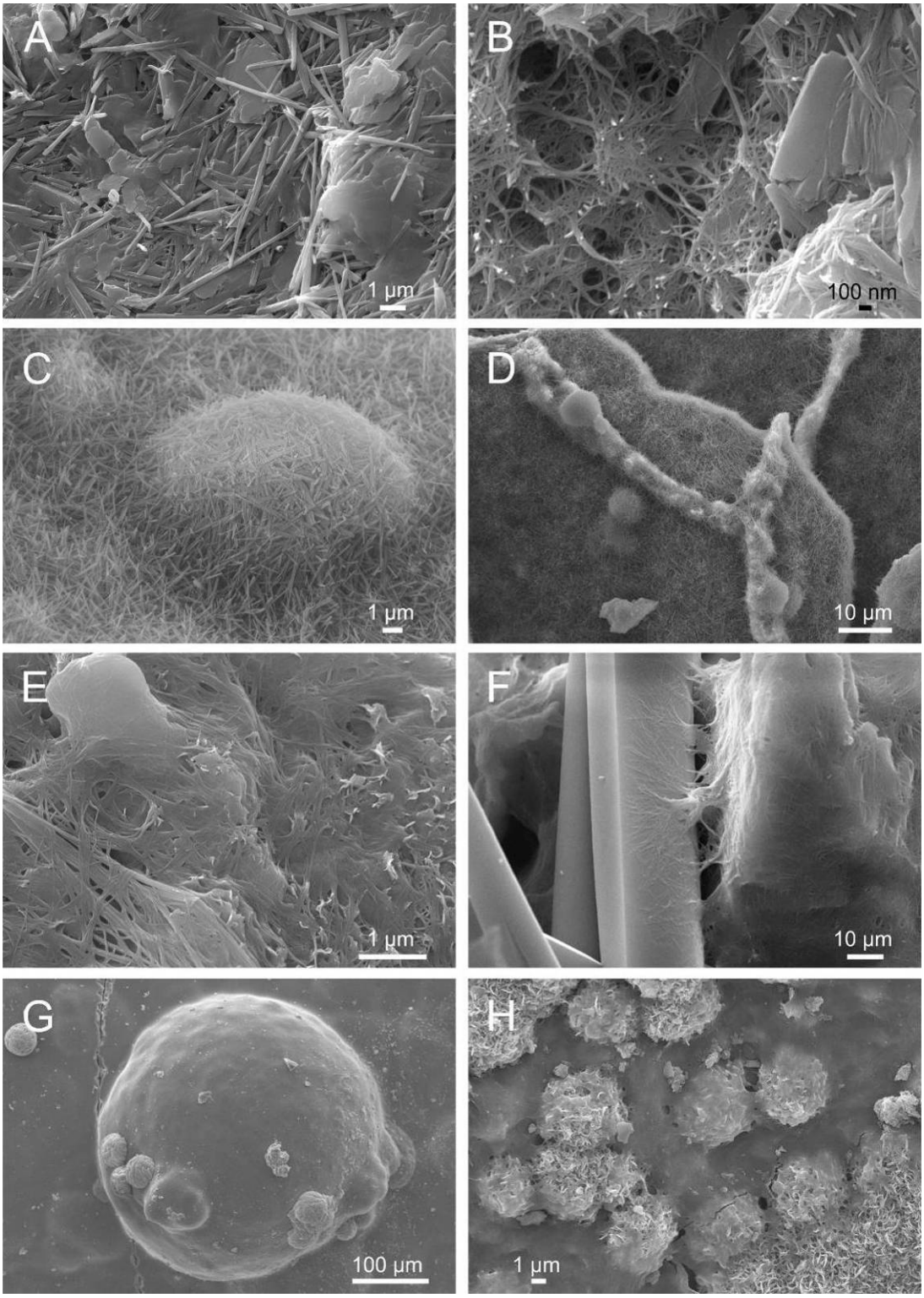

Figure 14: Examples of morphologies recognized with SEM secondary electron imaging on copper wad patina. The morphological terms (e.g., "rod-shaped fibers") refer to the classification detailed in the text. Chemical composition according morphology is indicated in Fig. CP_EDS and on Table 5, main elements being Cu, Si, Al, and Mn (except in the cases where otherwise indicated). A-B M15.2, rod-shaped fibers; C-D M18.2, rod-shaped fibers; E-F M33, dense mesh of fibers covering the topography of the sample; G M47.2, topography of the sample covered by fine serpentine fibers; H M48, dense mesh of fibers covering grains of manganese oxides in rosette (birnessite?).

Textures on copper wad patina

Although macroscopically no clear differences in the copper wad samples are recognized, the use of secondary electron imaging reveals a wast variety of morphologies. They have been grouped into the following four main forms: rods (e.g., Figs. 14 A, B, C and D), dense mesh of fibers (e.g., Figs. 14 E, F, G and H), small grains aggregates (e.g., Figs. 15 A, B and C), and bundles of fibers (e.g., Figs. 15 E, F, G and H).

Qualitative element analyses by SEM-EDS on representative spots containing the different morphologies are presented in Table 5 and in Fig. 16. Close examination of the analytical data suggests that small variations of the chemical composition can partly explain the large morphological range but, in general, no direct attribution between chemistry and morphology can be made at this stage.

However, the different micro textures of copper wad suggest that the formation of these nano-minerals took place in an open space environment. Therefore, copper wad might be the result of capillary driven surface migration process of Mn-Cu-rich solutions, in contrast to the precipitation of copper pitch in a more saturated environment.

Rod-shaped fibers

The rod-shaped texture is observed in samples M15.2 (Fig. 14 A) and M18.2 (Figs. 14 C-D). The patina surfaces show an interlaced of fine (<0.2 μm diameter) and straight needles, giving a lawn-like aspect to the sample. It is associated with high contents in Al (between 9.7 and 22.7%) and Si (between 9.5 and 24.5%), and generally moderate in Mn (between 1.2 and 11%, in places up to 28.7%) and Cu (between 0.5 and 5.5%).

Table 5: EDS analyses on copper wad patinas [wt%]. (n.d. = not detected)

sample	analyse	texture	C	O	Al	Si	K	Mn	Fe	Cu	Cl	Mg	Ca	Zn	Co	Ti	Ba	Au (coating)
M32a	2a	honeycomb-like cells	3.0	31.2	10.3	13.9	n.d.	7.9	7.8	7.7	0.2	0.5	0.7	n.d.	n.d.	0.6	n.d.	16.4
M32a	2b	honeycomb-like cells	3.7	35.7	9.2	12.7	0.2	8.9	7.5	7.8	0.2	0.5	0.7	n.d.	n.d.	0.5	n.d.	12.3
M32a	3	honeycomb-like cells	2.3	31.0	5.6	10.5	0.2	12.7	8.3	11.5	n.d.	1.0	0.7	n.d.	n.d.	0.5	n.d.	15.8
M32b	1c	honeycomb-like cells	4.4	29.0	2.9	9.3	n.d.	16.0	7.5	19.4	0.2	0.7	0.8	n.d.	n.d.	0.5	n.d.	9.4
M32b	3c	honeycomb-like cells	3.4	32.1	4.0	6.9	n.d.	14.0	12.2	11.3	0.3	0.6	0.9	n.d.	n.d.	1.0	n.d.	13.3
M32a	1	bundles	2.9	14.3	1.7	13.9	n.d.	7.6	2.7	38.9	n.d.	0.2	1.1	n.d.	n.d.	n.d.	n.d.	16.8
M32b	1a	bundles	2.8	30.6	5.2	15.0	0.2	8.9	11.5	13.2	0.2	0.9	1.0	n.d.	n.d.	0.3	n.d.	10.5
M32b	2	bundles	4.5	40.0	8.9	10.1	0.6	17.0	n.d.	5.9	0.1	0.2	0.4	n.d.	n.d.	n.d.	n.d.	12.3
M32b	3a	bundles	4.7	27.8	3.7	14.4	n.d.	9.4	7.9	21.9	0.2	0.4	0.9	n.d.	n.d.	0.8	n.d.	8.0
M15.5	4	dense mesh	2.4	30.2	1.3	8.8	1.9	34.2	n.d.	7.4	n.d.	n.d.	n.d.	n.d.	n.d.	n.d.	n.d.	13.9
M33	1	dense mesh	3.4	31.3	3.1	7.5	0.6	23.9	2.9	15.6	n.d.	0.3	0.2	n.d.	n.d.	n.d.	1.0	10.2
M33	2a	dense mesh	2.8	12.6	1.7	8.2	0.5	34.7	3.1	22.0	n.d.	0.2	0.4	n.d.	n.d.	0.2	1.6	12.0
M33	2b	dense mesh	3.3	27.7	2.3	5.8	0.4	30.3	n.d.	18.2	0.2	0.2	0.3	n.d.	n.d.	n.d.	1.2	10.0
M47.2	3a	dense mesh	4.4	15.6	1.9	20.9	0.2	0.0	n.d.	42.7	0.3	0.3	0.6	n.d.	n.d.	n.d.	n.d.	13.2
M47.2	3b	dense mesh	2.5	7.6	1.4	19.2	n.d.	0.4	n.d.	52.8	n.d.	0.1	0.8	n.d.	n.d.	n.d.	n.d.	15.2
M47.2	5	dense mesh	2.5	7.4	1.4	18.6	n.d.	0.0	n.d.	56.6	n.d.	0.2	0.7	n.d.	n.d.	n.d.	n.d.	12.6
M48	1a	dense mesh	4.9	26.3	1.9	21.5	n.d.	0.3	0.9	34.1	n.d.	0.2	1.0	n.d.	n.d.	n.d.	n.d.	9.0
M48	2a	dense mesh	3.5	24.0	1.3	14.1	0.3	17.5	n.d.	28.2	n.d.	0.1	0.6	n.d.	0.3	n.d.	n.d.	10.1
M57	2	dense mesh	2.0	25.5	3.3	10.1	n.d.	22.6	n.d.	20.0	0.3	0.5	3.2	n.d.	n.d.	n.d.	n.d.	12.6
M32b	1b	fibres	0.8	7.0	1.8	6.3	n.d.	28.8	11.9	28.2	0.3	0.3	1.3	1.6	n.d.	0.6	1.0	10.3
M32b	3b	fibres	n.d.	11.2	4.4	12.0	0.2	19.8	22.7	19.4	0.2	0.4	1.2	n.d.	n.d.	2.1	n.d.	6.4
M17	1	grains	4.4	25.5	1.8	16.5	n.d.	6.7	n.d.	29.2	0.2	0.2	0.6	n.d.	n.d.	n.d.	n.d.	14.8
M17	2	grains	8.1	27.1	1.5	9.8	0.2	9.6	n.d.	22.6	0.4	0.2	0.4	n.d.	n.d.	n.d.	n.d.	20.3
M17	3a	grains	3.7	26.4	1.8	21.2	n.d.	1.7	n.d.	30.9	0.3	0.1	0.7	n.d.	n.d.	n.d.	n.d.	13.3
M17	3b	grains	3.3	27.8	1.8	11.1	0.6	15.7	n.d.	25.4	0.6	0.7	0.5	n.d.	n.d.	n.d.	n.d.	12.7
M29.1	1	grains	1.5	6.3	1.5	8.4	n.d.	0.0	n.d.	74.0	n.d.	0.3	0.2	n.d.	n.d.	n.d.	n.d.	7.7
M29.1	2	grains	n.d.	0.3	0.6	3.6	n.d.	0.0	n.d.	91.1	n.d.	n.d.	n.d.	n.d.	n.d.	n.d.	n.d.	4.4
M29.1	4	grains	1.1	3.4	2.1	8.0	0.6	0.0	43.1	33.7	n.d.	0.3	n.d.	n.d.	n.d.	n.d.	n.d.	7.7

sample	analyse	texture	C	O	Al	Si	K	Mn	Fe	Cu	Cl	Mg	Ca	Zn	Co	Ti	Ba	Au (coating)
M40.2	1	grains	0.7	8.1	0.4	7.9	0.4	49.7	n.d.	28.3	n.d.	n.d.	n.d.	n.d.	0.6	n.d.	n.d.	4.0
M40.2	4	grains	0.7	7.0	0.2	3.4	0.5	45.4	n.d.	28.5	n.d.	n.d.	n.d.	n.d.	0.2	n.d.	0.8	13.4
M48	1b	grains	2.2	22.9	0.3	1.0	0.7	37.0	n.d.	22.6	n.d.	n.d.	n.d.	n.d.	0.5	n.d.	n.d.	12.7
M48	2b	grains	1.5	22.6	0.3	0.4	0.8	39.4	n.d.	23.9	n.d.	n.d.	n.d.	n.d.	0.7	n.d.	n.d.	10.5
M57	1c	grains	2.7	17.3	0.8	0.7	0.4	32.6	n.d.	19.5	n.d.	n.d.	0.6	n.d.	n.d.	n.d.	1.0	24.5
M15.5	5	rod-shaped	2.3	42.2	12.3	16.7	0.9	11.0	n.d.	1.9	n.d.	n.d.	n.d.	n.d.	n.d.	n.d.	n.d.	12.8
M15.5	2	rod-shaped	1.9	44.6	19.6	22.0	0.2	2.3	n.d.	0.8	n.d.	n.d.	n.d.	n.d.	n.d.	n.d.	n.d.	8.6
M15.5	1	rod-shaped	2.2	43.2	17.5	22.0	0.4	3.8	n.d.	2.0	n.d.	n.d.	n.d.	n.d.	n.d.	n.d.	n.d.	9.0
M18.2	1	rod-shaped	0.8	46.2	22.7	24.5	0.3	4.1	n.d.	n.d.	n.d.	n.d.	n.d.	n.d.	n.d.	n.d.	n.d.	1.4
M18.2	3a	rod-shaped	1.6	29.1	9.7	9.5	1.6	28.7	2.9	4.5	n.d.	n.d.	n.d.	n.d.	n.d.	n.d.	n.d.	12.5
M18.2	3b	rod-shaped	1.3	36.5	11.6	11.2	1.1	24.7	n.d.	5.5	n.d.	n.d.	n.d.	n.d.	n.d.	n.d.	n.d.	8.0
M18.2	3c	rod-shaped	2.3	41.9	15.3	15.5	0.6	10.1	n.d.	1.6	n.d.	n.d.	n.d.	n.d.	n.d.	n.d.	n.d.	12.8
M18.2	5	rod-shaped	1.6	46.3	21.2	22.5	n.d.	1.2	n.d.	0.5	n.d.	n.d.	n.d.	n.d.	n.d.	n.d.	n.d.	6.7

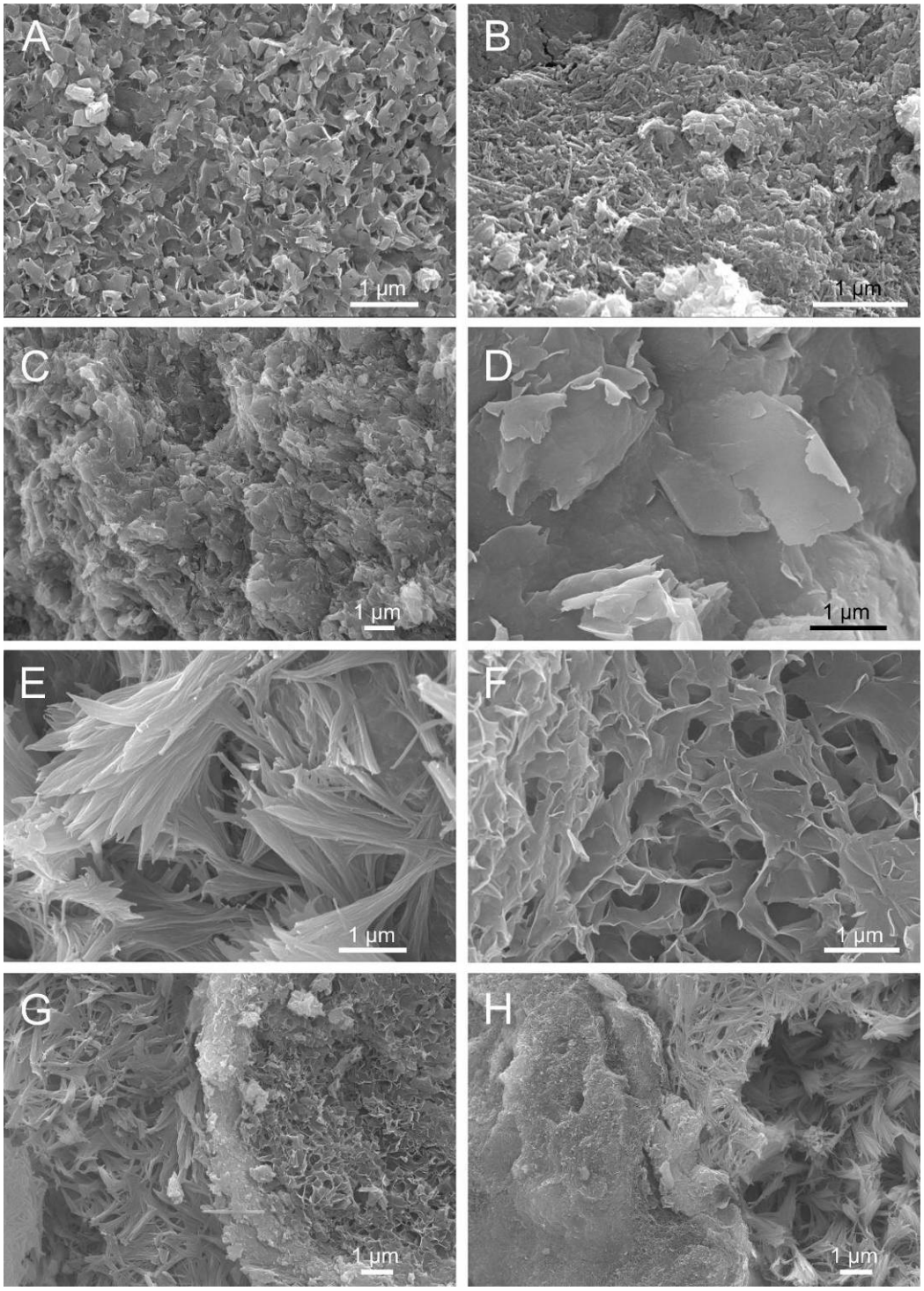

Figure 15: Examples of morphologies recognized with SEM secondary electron imaging on copper wad patina. The morphological terms (e.g., "rod-shaped fibers") refer to the classification detailed in the text. Chemical composition according morphology is indicated in Fig. 7B and on Table 5, main elements being Cu, Si, Al, and Mn (except in the cases where otherwise indicated). A M57, small plates of copper wad; B M17, malformed needles of copper wad; C M40.2, small grains of copper wad; D M29.1, small grains of copper wad; E.M32a, bunches of fibres; F. M32a, honneycomb-like cells; G. M32b, bunches of fibres (on the left) below honneycomb-like cells (on the right); H. M32b, bunches of fibres (on the right), and mesh of fibres (on the top).

Fibers covering the topography of the sample in a dense mesh
In samples M15.2 (Fig. 14 B), M33 (Fig. 14 E-F), M47.2 (Fig. 14 G), M48 (Fig. 14 H) and M57, copper wad patina is made by serpentine-shaped fibers forming a dense cobweb-like mesh. Copper wad with this texture shows, compared rod-shaped textures, similar Si content (between 5.8 and 21.5%), more Cu (between 7.4 and 56.6%) and Mn (less than 0.5% in several spots, chrysocolla?, up to 34.7% in others), and less Al (between 1.3 and 3.3%),

The rod-shaped fibers and the serpentine-shaped fiber textures are similar to those observed by García-Romero and Suárez (2013) in the fibrous phyllosilicates sepiolite-palygorskite.

Bundles of fibers and honeycomb-like cells
The variety of morphologies of copper wad observed in samples M32a and M32b (Figs. 15 E-H) are interpreted as different cuts of a framework consisting mainly of fiber bundles (e.g., corollas, Fig. 15 E, serpentine-shape fibers, Fig. 15 H). The honeycomb-like cells, Fig. 15 F could represent a dissolution of a mass of fibers (Fig. 15 G). A similar texture is described by Nelson (2007), and is interpreted as a dissolution texture of the chrysocolla surface. Representative analyses of these textures are given in Table 5, all analyzed points contain principally Cu, Mn Si, Al, and Fe.

Other small grain aggregates
Various samples show a copper wad patina made of small grains aggregates, with varying shapes between small plates (sample M57, Fig. 15 A) and malformed needles (sample M17, Fig. 15 B). In samples M40.2 and M29.1 (Figs. 15 C-D), grains have no particular shape. Important variations of chemical composition are observed (Table 5).

In sample M57 copper wad patina contain small plates (Fig. 15 A) with high Mn and Cu amounts and no Si (Table 5). Malformed needles in sample M17 (Fig. 15 B) consist of Si (9.8% - 21.2%), Cu (22.6 - 30.9%), and less Mn (1.7 - 15.7%). The granular texture of Sample M40.2 (Fig. 15 C) consists of Mn (45.4 - 49.7%), Cu (28.3 - 28.5%), and less Si (7.9 - 3.4%). The sheets shown in Fig. 15 B (Sample M29.1) contain Cu (74.0 wt%) and Si (8.4 wt%) and no Mn is detected.

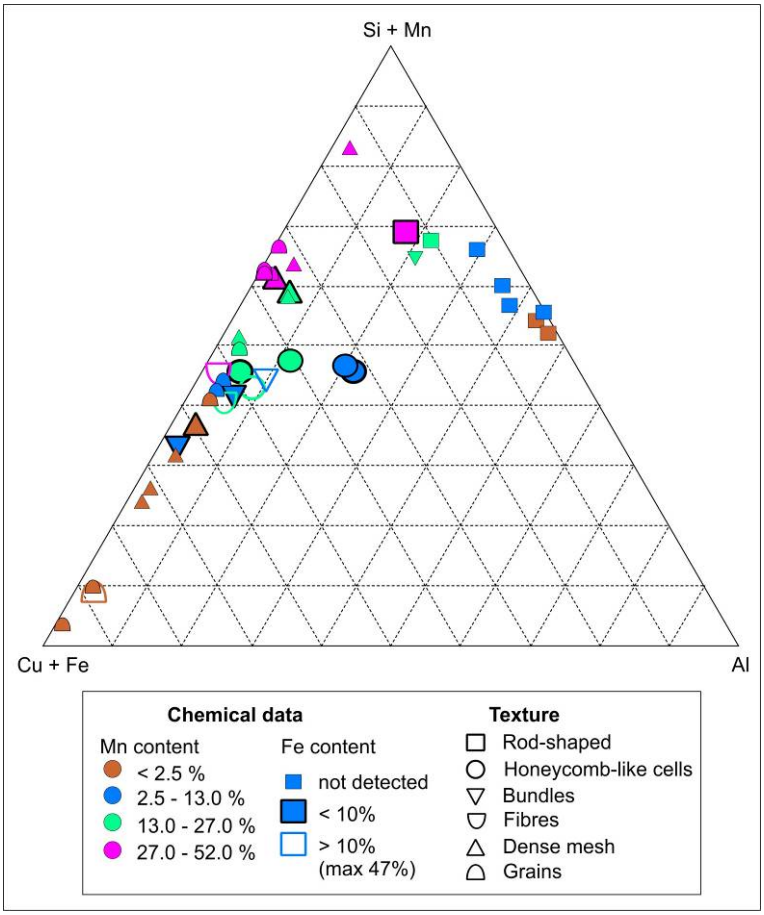

Figure 16: Results of the EDS semi-quantitative chemical analyses on copper wad patina presented in a Cu+Fe - Si+Mn - Al triangle [wt%]. Si and Mn are linearly related, as illustrated with the symbols colors. Contrariwise, copper and iron are rather negatively related, as illustrated with the size and filling of the symbols. The shape of the symbol indicate the texture of the copper wad patina.

In sample M48, spherical aggregates of copper wad grains are observed (Fig. 14 H) They are partly covered by cobweb-like fibers (Si 21.5%, Cu 34.1%, Al 1.9%). The spherical aggregates contain principally manganese (37-39.4%) and copper (22.6 - 23.9%), and almost no silica. It could be pure birnessite plus a copper oxide covered by chrysocolla (?) fibers. Mn-oxide rosettes are commonly described in the literature and interpreted as birnessite (e.g. Sun et al., 2012; Halbach et al., 2002).

2.3.5 High resolution mineralogical and geochemical characterization by sequential extractions combined with senquential XRD (SXRD), and SEM-EDS.

Sequential extractions and SXRD on copper pitch and chrysocolla

The XRD results on a chrysocolla sample (1 g) and a copper pitch sample (1 g) after each sequential dissolution step are presented in Fig. 7. The chemical composition (ICP) of the leach solutions of each dissolution step are illustrated in Fig. 17. The XRD patterns of the original samples. i.e., the powder used for the sequential extraction before the first step, are also shown. The pattern of the chrysocolla sample corresponds to almost pure chrysocolla; only a small peak located at 26.7° 2theta shows the presence of quartz. The XRD pattern of the copper pitch

sample is in a first approximation very different, with several definite peaks pointing to the presence of gypsum and atacamite.

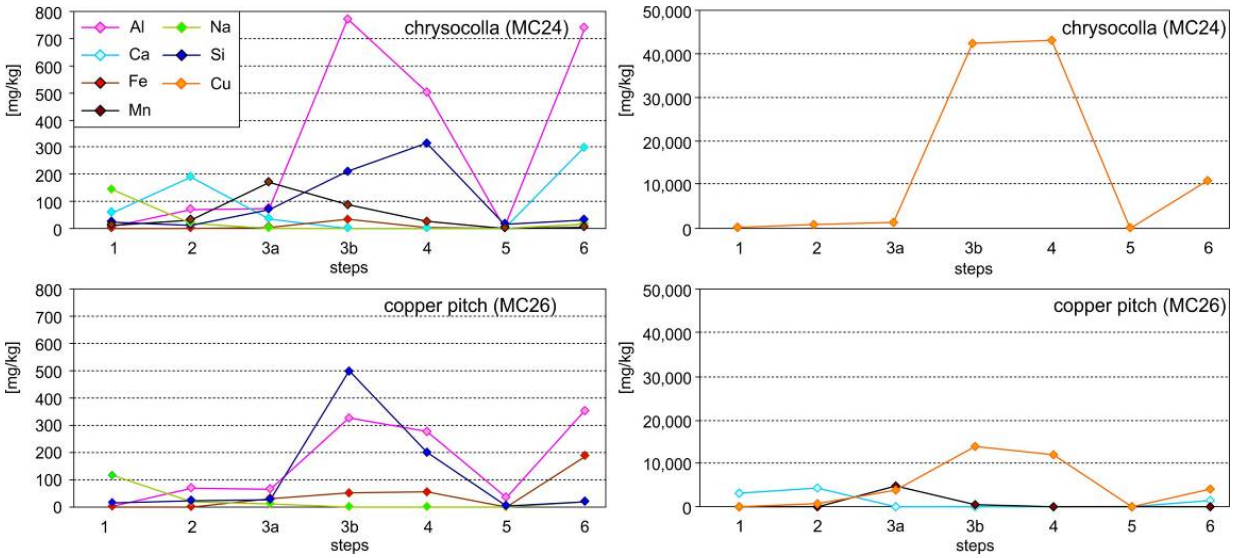

Figure 17: Results of the ICP analyses made on the solutions resulting of each extraction step for Al, Ca, Cu, Fe, Mn, Na and Si. Results corresponding to the sequential extraction on sample MC24 (chrysocolla) are presented in the upper part, and on sample MC26 (copper pitch) in the lower part. The results obtained after steps 3b and 4 are corrected taking in account the formation of a precipitate in the solutions during acidification.

Step 1 (deionized water). This first step of the sequential extraction sequence applied does not affect the mineralogy of the chrysocolla sample and drastically reduces the gypsum present in the copper pitch sample (Fig. 7). The liberation of between 3200 and 4100 [mg/kg] of Ca in the solution during step 1 confirm the dissolution of gypsum in the copper pitch (Fig. 17, Table 6). The liberated amount of Cu is negligible compared with the following steps (31.4 [mg/kg]).

Step 2 (NH_4-acetate designed to target the exchangeable fraction and also dissolves calcite; Dold, 2003). In the chrysocolla sample, a new peak appears at 18.2° 2θ during the leach. It corresponds to the main libethenite ($Cu_2(PO_4)(OH)$), a common Cu-phosphate in oxidation zones of Cu ore deposits due to apatite weathering. The newly observed peaks are interpreted as peaks that were not possible to observe before the dissolution of gypsum and atacamite, as detection limit of XRD is between 2 and 5 %, depending on the crystalinity of the trace minerals. The new peak could be also be due to neo-formation during the extraction, however, due to the fact that NH_4-acetate is a very weak leach, it is unlikely that it dissolves a present phosphate mineral to form then libethenite during this leach. In the copper pitch sample, gypsum and also atacamite appear to have fully dissolved and peaks of birnessite and paratacamite ($Cu_3(Cu,Zn)(OH)_6Cl_2$) appear. The ICP analyses on the solution resulting from the dissolution step 2 (Fig. 17) are consistent with these observations.

Table 6: Results obtained by ICP-OES and/or MS on solutions resulting from each sequential extraction step, for the main chemical elements. All the results are presented in Annex 3.1. Samples 3.1, 3.2 and 3.3 are three aliquots of MC24 pure chrysocolla sample, and sample 4.1, 4.2 and 4.3 from MC26 copper pitch sample.

	sample	step	Al	Ca	Cu	Fe	K	Mn	Na	P	Si
			[mg/kg]	[mg/kg]	[mg/kg]	[mg/kg]	[mg/kg]	[mg/kg]	[mg/kg]	[mg/kg]	[mg/kg]
			ICP-OES	*ICP optic*	*ICP optic*	*mix*	*ICP optic*	*mix*	*ICP-MS*	*ICP optic*	*ICP optic*
Sample 3.1 step 1	3.1	1	5.786E+00	5.596E+01	8.379E+01	1.702E-02	3.040E+01	1.274E+01	1.528E+02	4.926E+00	2.394E+01
Sample 3.2 step 1	3.2	1	5.984E+00	5.670E+01	8.601E+01	1.400E-02	3.161E+01	1.182E+01	1.433E+02	5.134E+00	2.455E+01
Sample 3.3 step 1	3.3	1	5.785E+00	5.872E+01	8.649E+01	1.909E-02	3.155E+01	1.209E+01	1.475E+02	4.976E+00	2.431E+01
Sample 4.1 step 1	4.1	1	5.231E+00	4.147E+03	4.140E+01	4.587E-01	1.934E+01	1.769E+00	1.087E+02	4.817E+00	2.023E+01
Sample 4.2 step 1	4.2	1	4.371E+00	3.159E+03	3.143E+01	4.695E-01	1.543E+01	1.822E+00	1.142E+02	4.815E+00	1.538E+01
Sample 4.3 step 1	4.3	1	4.445E+00	4.031E+03	3.942E+01	4.941E-01	1.854E+01	1.845E+00	1.160E+02	4.811E+00	1.991E+01
Sample 3.1 step 2	3.1	2	7.744E+01	1.922E+02	6.157E+02	9.969E-02	5.612E+01	2.706E+01	1.944E+01	3.431E+02	1.316E+01
Sample 3.2 step 2	3.2	2	6.940E+01	1.892E+02	6.110E+02	2.654E-02	4.976E+01	2.922E+01	1.921E+01	3.418E+02	1.138E+01
Sample 3.3 step 2	3.3	2	4.771E+01	1.851E+02	6.017E+02	3.513E-02	5.204E+01	2.905E+01	2.145E+01	3.424E+02	1.252E+01
Sample 4.1 step 2	4.1	2	6.980E+01	3.559E+03	5.407E+02	5.262E-01	5.184E+01	2.434E+00	2.000E+01	3.415E+02	1.668E+01
Sample 4.2 step 2	4.2	2	7.064E+01	4.294E+03	6.576E+02	5.882E-01	4.720E+01	2.467E+00	2.027E+01	3.419E+02	2.166E+01
Sample 4.3 step 2	4.3	2	6.464E+01	4.057E+03	6.500E+02	7.108E-01	4.264E+01	2.646E+00	1.938E+01	3.412E+02	2.302E+01
Sample 3.1 step 3a	3.1	3a	6.871E+01	2.357E+01	8.660E+02	2.092E+00	8.785E+00	1.211E+02	4.666E-01	3.006E+02	5.136E+01
Sample 3.2 step 3a	3.2	3a	7.282E+01	3.479E+01	1.203E+03	2.736E+00	1.855E+01	1.697E+02	6.749E-01	3.003E+02	6.916E+01
Sample 3.3 step 3a	3.3	3a	7.726E+01	3.668E+01	1.238E+03	2.754E+00	1.932E+01	1.617E+02	7.274E-01	3.007E+02	7.019E+01
Sample 4.1 step 3a	4.1	3a	5.940E+01	6.860E+01	3.573E+03	2.627E+01	4.660E+01	4.287E+03	9.556E+00	2.993E+02	2.483E+01
Sample 4.2 step 3a	4.2	3a	6.361E+01	5.747E+01	3.769E+03	2.982E+01	7.284E+01	4.765E+03	1.046E+01	2.987E+02	2.697E+01
Sample 4.3 step 3a	4.3	3a	6.612E+01	5.933E+01	4.038E+03	2.962E+01	7.525E+01	4.700E+03	1.059E+01	2.989E+02	2.916E+01
Sample 3.1 step 3b	3.1	3b	7.925E+02	N.D.	2.538E+02	5.077E+00	2.745E+01	1.200E+01	3.438E-01	3.525E+02	1.858E+02
Sample 3.2 step 3b	3.2	3b	7.104E+02	N.D.	3.318E+02	5.399E+00	2.601E+01	1.115E+01	1.473E+00	3.432E+02	1.430E+02
Sample 3.3 step 3b	3.3	3b	8.051E+02	7.470E+00	3.887E+02	8.942E+00	3.012E+01	1.222E+01	1.460E+00	3.657E+02	1.796E+02
Sample 4.1 step 3b	4.1	3b	2.613E+02	N.D.	6.111E+02	2.141E+01	3.381E+01	2.017E+02	2.860E-01	2.767E+02	2.745E+01
Sample 4.2 step 3b	4.2	3b	2.749E+02	N.D.	7.281E+02	2.376E+01	3.042E+01	1.903E+02	1.056E-01	2.779E+02	2.685E+01
Sample 4.3 step 3b	4.3	3b	2.733E+02	2.985E+00	4.419E+02	2.334E+01	3.078E+01	1.958E+02	6.144E-01	2.771E+02	2.678E+01

	sample	step	Al	Ca	Cu	Fe	K	Mn	Na	P	Si
			[mg/kg]	[mg/kg]	[mg/kg]	[mg/kg]	[mg/kg]	[mg/kg]	[mg/kg]	[mg/kg]	[mg/kg]
			ICP-OES	*ICP optic*	*ICP optic*	*mix*	*ICP optic*	*mix*	*ICP-MS*	*ICP optic*	*ICP optic*
Sample 3.1 step 4	3.1	4	4.468E+02	N.D.	8.944E+02	2.378E+00	2.503E+01	1.621E+00	0.000E+00	3.408E+02	2.775E+02
Sample 3.2 step 4	3.2	4	4.820E+02	N.D.	1.242E+03	2.765E+00	3.780E+01	2.168E+00	0.000E+00	3.602E+02	2.588E+02
Sample 3.3 step 4	3.3	4	4.474E+02	N.D.	8.776E+02	2.529E+00	2.573E+01	1.288E+00	3.668E-03	3.447E+02	2.882E+02
Sample 4.1 step 4	4.1	4	2.537E+02	N.D.	1.353E+03	3.396E+01	3.857E+01	1.333E+01	0.000E+00	3.015E+02	1.653E+02
Sample 4.2 step 4	4.2	4	2.605E+02	N.D.	2.003E+03	3.568E+01	3.252E+01	1.016E+01	0.000E+00	3.014E+02	1.637E+02
Sample 4.3 step 4	4.3	4	2.530E+02	N.D.	6.644E+02	3.715E+01	3.283E+01	1.146E+01	0.000E+00	3.003E+02	1.516E+02
Sample 3.1 step 5	3.1	5	3.837E+00	3.731E-01	9.419E+00	5.430E-02	N.D.	6.860E-02	N.A.	4.252E+01	1.249E+01
Sample 3.2 step 5	3.2	5	3.035E+00	3.275E-01	7.221E+00	4.780E-02	N.D.	1.000E-01	N.A.	4.982E+01	1.640E+01
Sample 3.3 step 5	3.3	5	2.666E+00	1.509E-01	4.430E+00	2.428E+00	N.D.	8.920E-02	N.A.	4.606E+01	7.299E+00
Sample 4.1 step 5	4.1	5	3.604E+01	N.D.	1.456E+01	6.133E-01	1.810E+01	5.900E+00	N.A.	2.082E+02	3.380E+00
Sample 4.2 step 5	4.2	5	3.630E+01	N.D.	1.944E+01	7.900E-01	1.924E+01	4.280E+00	N.A.	2.142E+02	4.960E+00
Sample 4.3 step 5	4.3	5	3.588E+01	N.D.	1.755E+01	7.200E-01	2.128E+01	6.300E+00	N.A.	2.118E+02	5.020E+00
Sample 3.1 step 6	3.1	6	3.298E+02	1.526E+02	4.700E+03	9.956E+00	1.908E+04	1.820E+00	1.012E+01	4.727E+02	1.253E+01
Sample 3.2 step 6	3.2	6	7.402E+02	2.956E+02	1.079E+04	1.584E+01	2.304E+04	4.713E+00	1.569E+01	4.841E+02	3.065E+01
Sample 3.3 step 6	3.3	6	5.725E+02	2.046E+02	8.524E+03	1.595E+01	2.015E+04	3.444E+00	1.388E+01	4.762E+02	2.310E+01
Sample 4.1 step 6	4.1	6	2.772E+02	2.155E+01	2.944E+03	9.473E+01	2.169E+04	6.020E+00	1.113E+01	4.323E+02	1.998E+01
Sample 4.2 step 6	4.2	6	3.522E+02	1.494E+03	4.047E+03	1.862E+02	2.252E+04	9.048E+00	1.830E+01	4.321E+02	1.993E+01
Sample 4.3 step 6	4.3	6	3.671E+02	8.625E+00	4.168E+03	1.350E+02	2.159E+04	8.510E+00	1.311E+01	4.329E+02	1.903E+01

During **step 3a** (hydroxylamine hydrochloride, designed to target the amorphous oxi-hydroxides of manganese), does not affect the XRD pattern obtained on the chrysocolla sample, and libethenite peaks remain. In the copper pitch sample, XRD evidences the dissolution of birnessite, but paratacamite remains stable. The color change of the copper pitch sample from dark brown to green illustrates the loss of manganese. This color change evidences that the dark brown color of copper pitch is due to its presence of birnessite. The geochecmial data from the sequential extractions confirms these findings (Table 6, about 1000 [mg/kg] Cu and 150 [mg/kg] Mn in the chrysocolla sample, and about 3700 [mg/kg] of Cu and 4500 [mg/kg] of Mn in the copper pitch sample) (Fig. 17), and suggest that an important amount of Cu is co-precipitated with the birnessite. .

During the acidification of the solutions issued from the sequential extraction steps 3b and 4 on samples of chrysocolla and copper pitch, a blue precipitate formed in the tubes, most likely as Cu-oxalate complexes. Semi-quantitative XRF analyses (Table 7) indicate that the precipitates consist mainly of copper (over 98% for the chrysocolla and over 97 wt.% for the copper pitch sample, both in steps 3b and 4).

Table 7: Results of XRF analyses on the precipitates formed in the solutions after the acidification of the samples for the ICP analyses.

		Precipitate in the solution resulting from step 3b of extraction	Precipitate in the solution resulting from step 4 of extraction
chrysocolla sample	Al_2O_3	0.256	0.082
	Cu	98.21	98.792
	Fe_2O_3	0.079	0.07
	MnO	0.224	0.063
	MgO	-	0.11
	P_2O_5	0.107	0.091
	SiO_2	0.326	0.258
	Zn	0.643	0.525
copper pitch sample	Al_2O_3	0.7	0.316
	Cu	95.792	97.785
	Fe_2O_3	0.289	0.246
	MnO	1.795	0.313
	MgO	0.052	0.134
	P_2O_5	0.12	0.104
	SiO_2	0.719	0.756
	Zn	0.178	0.14

Step **3b** (NH_4-oxalate in the darkness, designed to target the iron(III) hydroxides) does not dissolve any crystalline phase in the chrysocolla sample. The results of ICP were corrected taking in account the precipitate which formed after acidification of the sample. The dissolution of amorphous material is suggested by the liberation of important amounts of Cu (up to 42,000 [mg/kg] in chrysocolla and 13,000 [mg/kg] in copper pitch), Al (around 860 [mg/kg] in chrysocolla and 320 [mg/kg] in copper pitch) and Si (around 240 [mg/kg] in chrysocolla and around 500 in copper pitch), resulting in stronger libethenite peaks. In the copper pitch sample, paratacamite disappears, and the peaks of libethenite continue to be present.

Step 4 (NH_4-oxalate at 80°C, designed to target the iron oxides) modifies the shape of the background pattern by an increase of the main hump of chrysocolla, suggesting the dissolution of amorphous phases. A similar but less pronounced change is also observed in the copper pitch sample. Libethenite is not dissolved. The main released chemical elements during this step are Si, Cu and Al in both samples (Table 6).

Step 5 (H_2O_2, designed to target the organic matter and the secondary Cu-sulfides), dissolved libethenite present in both samples. The first hump of the chrysocolla pattern keeps collapsing. Chemical data of the solutions resulting from this step show that the released amount of copper is very low (between 4 and 20 [mg/kg], Table 6). The tiny libethenite needles recognized under thin section (Fig 12 C) and SEM (Fig 13 O) appear to produce clear peaks in the XRD analyses, even if this mineral is present in low amounts.

Step 6: $KClO_3$, HCl, HNO_3, is a mixed acid leach, designed originally to target the primary sulfides. The results show that it also leads to the destruction of the chrysocolla XRD pattern in both samples. In the chrysocolla sample, the peaks of quartz continue to be clear. In the copper pitch sample, no quartz is observed, but other peaks appear, which are difficult to interpret. The pattern could indicate a clay mineral. But without a detailed analysis of the clay fraction (< 2 μm), which was not possible due to the small amount of available material, it is nearly impossible to say which clay minerals are present. In the context of the Exótica deposit, it could be kaolinite, halloysite ($Al_2Si_2O_5(OH)_4 \bullet nH_2O$) and/or beideite ($(Na,Ca_{0.5})_{0.3}Al_2((Si,Al)_4O_{10})(OH)_2 \bullet nH_2O$). During step 6, the main liberated elements are K (around 2000 [mg/kg] in both samples), Cu (between 5000 and 10,000 [mg/kg] in the chrysocolla sample and between 3,000 and 4,200 [mg/kg] in the copper pitch sample), and smaller amount of Al, Ca, Fe and others (see Table 6).

As shown, the sequential extraction combined with the XRD analyses indicates that the chrysocolla sample shows typical XRD patterns, and that the structure starts to collapse with the use of NH_4-oxalate. The sample contains also small amounts of libethenite and quartz, appearing when chrysocolla starts to dissolve. In the copper pitch sample, the presence of crystalline phases mixed with the copper pitch mask the typical XRD pattern of chrysocolla. After the dissolution of gypsum and atacamite, the chrysocolla XRD pattern and the libethenite peak appear, the birnessite peaks become clearer and the similitude of the XRD patterns of chrysocolla and the copper pitch is evident.

Thus, this analytical approach has shown that copper pitch is in essence chrysocolla with co-precipitated birnessite. Additionally, by the use of sequential dissolution of a sample, additional trace minerals can be identified, which were usually camouflaged by the high detection limit of XRD.

Textural observation on copper wad patinas and copper pitch surfaces after sequential extraction

The textural relation between the copper pitch and wad and the crystalline phases cannot be established with the sequential extraction on powder, but were studied in details with the sequential extraction on entire samples.

Since copper wad forms only thin superficial patinas, not enough powder could be obtained for conclusive XRD analysis. Therefore, a sequential extraction was applied to seven samples with copper wad patina surfaces (M10.2, M15.2, M18.2, M32, M33, M48 and M57) to observe textural and chemical changes after each dissolution step. The samples were selected to include

the main morphological types of copper wad described above. The same method was applied to a conchoidal surface of copper pitch sample (sample M107). The textural changes by the different dissolution steps were generally comparable in the seven samples of copper wad. Since copper pitch is massive and vitreous, changes after applying the sequential extraction protocol were not conclusive.

Steps 1 and 2 have no effect on the texture, apart the disappearance of gypsum. Only in sample M18.2, which had a lawn like patina made of very fine needles, the textures, were largely dissolved after the first 2 steps (Fig. 18 A). After step 3a, dissolution is widespread and cracks are observed is some samples (M18.2, M48, M57, Figs. 18 B, C and D). EDS qualitative chemical analysis shows that Mn is depleted after step 3a. The effects of Step 3b in samples M15.2, M18.2, M32 and M33 are relatively low or even not detectable (Fig. 18 E). In contrast, in samples M10.2, M48 and M57 (composed of mainly small grained aggregates and dense mesh of fibers), dissolution and cracking is more prominent, suggesting that chrysocolla is and important component (Fig. 18 F). In all samples, step 4 produces intensive dissolution (Fig. 18 G) and Cu depletion. By applying step 5 the texture is totally destroyed and cracked in all samples (Figs. 18 H and I). EDS analysis reveals a relative Si enrichment after step 5 (Fig. 19) due to more stable silicates like quartz.

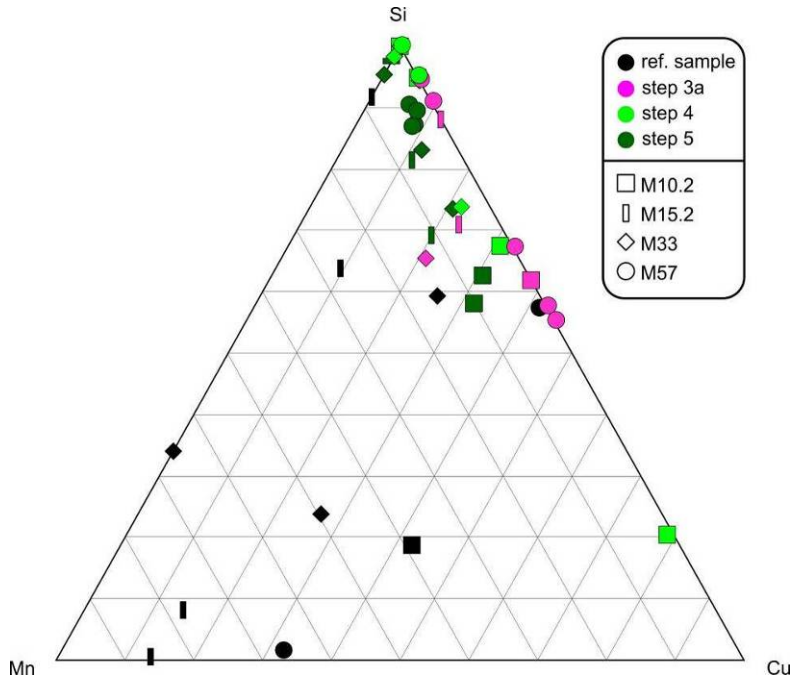

Figure 19: Results of the EDS analyses on copper wad patinas to illustrate the manganese depletion after step 3a, the copper depletion after step 4 and the silicate relative increase after step 5.

The SEM observation on copper wad patina across the different dissolution steps has allowed to evidence changes that were not recognized in the sequential extractions applied to powder copper pitch samples. Specifically, after step 3a, in addition of the disappearance of birnessite crystals (easily identified with the EDS analyses, as it is a pure Mn oxide, without Si, Cu or Al), the copper wad patina samples show generalized dissolution pattern on the Si-Cu-Mn bearing pseudo-amorphous material that mainly forms the patina (Fig. 18 B-D). With these results, it is reasonable to propose that also the pseudo-amorphous material mainly forming copper pitch partly dissolves in this stage even if not clearly evidenced by XRD, that, at first

glance, only shows disappearance of birnessite peaks. The high Cu (between 3473 and 4038 [mg/kg]) and Mn (between 4287 and 4765 [mg/kg]) amounts dissolved in this stage (Table 6) as well as the slight changes in the background morphology between steps 2 and 3a of the copper pitch XRD patterns (Fig. 7) support this hypothesis.

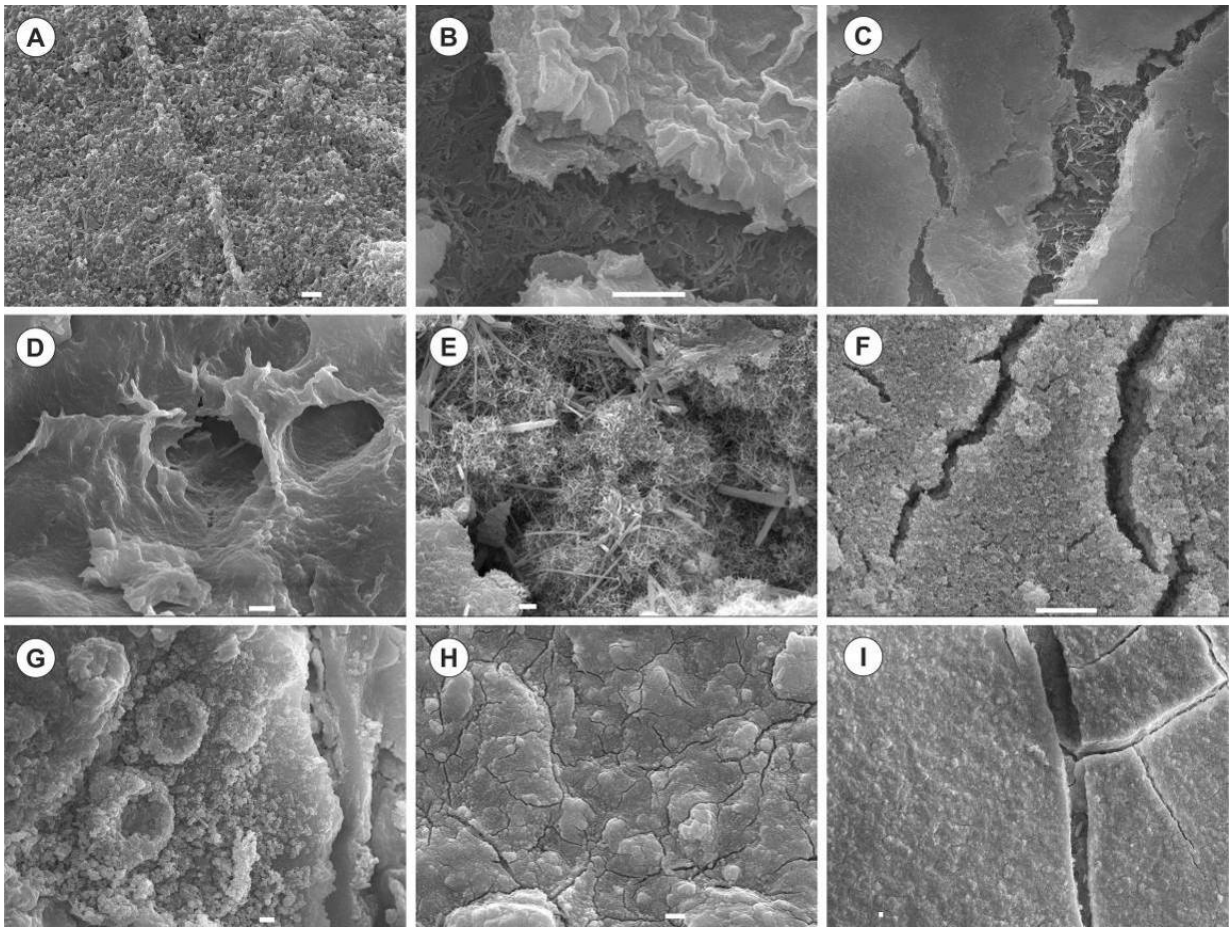

Figure 18: SEM secondary electrons imaging at various steps of the sequential extraction on copper wad patina. A. M18.2, step 1; B. M48, step 3a; C. M57, step 3a; D. M33, step3a; E. M15.2, step 3b; F. M10.2, step 3b; G. M48, step 4; H. M15.2, step 5; I. M10.2, step 5. Bars represent 1 µm.

2.4. Geological context and genetic model for Exótica

2.4.1 Characterization

The mineralogical and geochemical observations made in this study show an important similarity in the mineralogical structure of copper wad, copper pitch, and chrysocolla. A main difference is the chemical composition, with high manganese contents in copper pitch and in copper wad (from 1.42 to 37.26 wt.%, generally around 10 wt.%), and low contents in chrysocolla (lower than 0.7 wt.%). In copper pitch, manganese is mainly contained in birnessite and pseudo-amorphous Mn-oxides, which implies that the geochemical conditions for the precipitation of birnessite have to be fulfilled for precipitation of copper pitch. The morphology of the XRD pattern indicates that birnessite at Exótica precipitated under acidic conditions rather than alkaline. This is consistent with the prevailing acidic rock drainage environment at the Exótica deposit.

In the analyzed copper wad patina, only small amount of crystalline birnessite were observed. In the majority of the samples, manganese seems to be directly associated with the pseudo-amorphous fraction, just like copper, as evidenced with the sequential extractions.

The present study confirms that the difference between copper pitch and copper wad is mainly textural (Pincheira et al., 2003), and interpreted, based on the results of our study, to be controlled by the precipitation mode. Copper pitch and copper wad are frequently observed in the same sample, with a transition from massive copper pitch to copper wad on the external part. Copper pitch, similarly to massive chrysocolla, precipitates in open spaces, mainly along fractures (Fig. 6 A-B-D). Certain copper pitch and chrysocolla accumulations could represent precipitations in surface ponds, in a similar way to what today is observed in the pit and described by Lambiel (2014). In turn, copper wad, such as chrysocolla patina, precipitates in smaller interstices by fluids migrating mainly by capillarity, and its formation is favored by local evaporation and interaction solution-rock (neutralization, liberation of silica). In the northern part of the deposit, proximal to the source, the mineralization processes took place near the surface (Fig. 4; Münchmeyer, 1996), what allowed the precipitation of chysocolla and copper pitch in desiccation cracks or even in temporary water ponds, and the formation of large veins of massive material. This configuration was not possible in the southern deeper mineralization, where copper wad and chrysocolla occur principally as cement or patina in the open space of the gravels.

Even if iron is known to be potentially part of copper wad/copper pitch, the low Fe amounts measured in most copper pitch and copper wad samples (Table 4) suggests that the iron present in the Exótica deposit mineralization is preferentially fixed in iron oxides and hydroxides. Under intermediate oxidation conditions, the mobilization of Fe^{2+} by aqueous solutions is easy at low and neutral pH. In more oxidizing conditions, Fe^{2+} is oxidized to Fe^{3+}. Ferric iron has a low solubility and hydrolyses starting from pH around 2, depending on pH, Eh and element concentrations in solution to jarosite ($KFe_3(OH)_6(SO_4)_2$) and schwertmannite ($Fe_8O_8(OH)_6(SO_4)\cdot nH_2O$), ferrihydrite ($5Fe_2O_3\bullet 9H_2O$), goethite ($\alpha$-FeOOH). At near neutral pH, but mainly due to dehydration also hematite (α-Fe_2O_3) can be formed. Thus, iron precipitates before Mn in Exótica at lower pH, resulting in a iron poor Cu pitch and wad. On the other hand, the formed Fe(III)hydroxides are Cu poor in Exótica, as at lower pH Cu will not adsorb and/or co-precipitate with the Fe(III) hydroxides, while with higher pH, Eh Cu will adsorb and/or co-precipitated with Cu pitch and wad.

2.4.2 Spatial distribution

Münchmeyer (1996) reports that copper wad is mainly associated to the argillic altered host rocks and sediments, such as atacamite, while chrysocolla is mainly associated with unaltered rock and sediments, and frequently intercalated with copper pitch in the northern part of the deposit. The strongly kaolinized central tube does not contain any noteworthy copper mineralization. The results of the present study (including chemical bulk analyses and QEMSCAN®) confirm the absence of copper mineralization in the altered central zone of the deposit. Copper wad was observed in cemented levels of great extent in the southern part of the Mina Sur open pit, and was also present, in less important amount, in most of the samples of the northern part of the deposit used in this study (Fig. 4). Chrysocolla is frequently present in the northern part of the deposit, as cement or patina, in banded veins, or as impregnation in the altered host sediments. As banded veins, it is frequently associated with copper pitch. Copper pitch also rarely occurs without chrysocolla. Atacamite was observed principally in veins together with gypsum, crosscutting the main exotic mineralization made principally of

chrysocolla and copper wad / copper pitch, even if atacamite is also observed, in smaller amounts, as part of this main exotic mineralization. No particular spatial repartition was observed at the deposit scale in this study, apart the absence of copper mineralization in the central altered tube.

2.4.3 Geochemical modeling

Dold (2006b) made a first attempt to model the chemical processes at the origin of the exotic mineralization at Exótica, using a titration with $CaCO_3$ to simulate the neutralization of acidic supergene solutions. He obtained a precipitation sequence in agreement with the one described in the Exótica deposit, i.e., kaolinite, atacamite, and chrysocolla with increasing pH. However the formation of copper-pitch-wad was not discussed in this study. Therefore, in the present study, the complex interaction of Cu-Mn-Si was modeled with PHREEQC® (Parkhurst and Appelo, 1999) and Medusa in order to decipher the observed associations and textures of chrysocolla, copper pitch, and copper wad and understand the geochemical conditions, which allow the formation of this mineral assemblage.

The detailed mineralogical and textural relationships discussed above suggest that copper pitch is essentially chrysocolla with more or less crystalline Mn-oxide (birnessite) co-precipitated most likely in pond-like, desiccation cracks, or any saturated empty spaces, in a stagnant or low flow regime. Copper wad presents a large range of textures and precipitates mainly as surface patinas on the gangue mineralogy with lesser amount of crystalline Mn-oxides (birnessite), suggesting a faster precipitation kinetic than in case of copper-pitch. The texture of copper wad suggests a precipitation mode strongly related to capillary transport due to evaporation under a hot and dry climate (leading to an increase of ions in solution), and pH-Eh and chemical composition of the solution mainly controlled by water-rock interaction at local scale. This also explains the higher heterogeneity of copper wad compared to copper-pitch.

Copper pitch or copper wad are complex and variable mixtures of precipitates, and no thermodynamic data exists for this assemblages. In order to simplify the conditions for geochemical modeling, copper pitch and copper wad were considered to be a mixture of chrysocolla and birnessite, and when in the model both minerals reach saturation, it is considered that copper pitch/wad may form. However, it has to be stated clearly that this approach gives only indicative geochemical conditions in which the copper pitch/wad may form. The complex texture of copper wad suggests that the precipitation is mainly driven due to geochemical microenvironments at the water-rock interface.

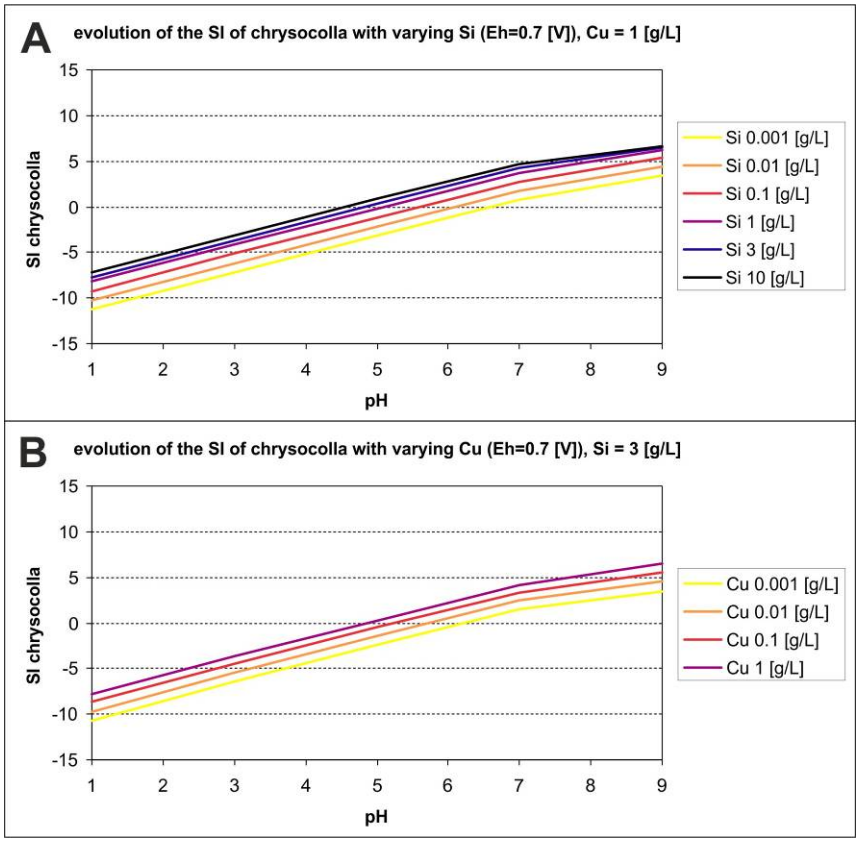

Figure 20: Saturation indices of chrysocolla calculated with PHREEQC, considering Eh of 0.7 [V]. A. Mn and Cu contents of 1 [g/L], and Si contents of 0.001, 0.01, 0.1, 1, 3, and 10 [g/L]. The increase of Si in solution diminish the pH at which chrysocolla becomes over-saturated (SI>0). B. Si content of 3 [g/L], Mn and Cu contents of 0.001, 0.01, 0.1 and 1 [g/L]. The increase of Cu diminishes the pH at which chrysocolla becomes over-saturated (SI<0).

To approach the geochemical border conditions, in which the mineral assemblage chrysocolla-birnessite could form, a simulation series was performed to study the precipitation of these minerals with varying pH and Eh and concentrations (Fig. 21). The results of the modeling indicate that chrysocolla precipitation strongly depends on the silica concentrations in solution (Fig. 20 A), as already observed by Newberg (1967). Copper and manganese concentrations also have important influence on saturation indices of chrysocolla and birnessite (Fig. 20 B).

The co-precipitation of chrysocolla and birnessite, interpreted as condition for precipitation of copper pitch/wad, was studied at different, pH, Eh and Cu, Mn and Si concentrations (Fig. CHRYSO_BIRNESSTE1). Hydrogeochemical conditions observed in Exótica, where bluish-gel type Cu-rich precipitates formed recently in the open pit (Lambiel, 2014) were pH 5.8-6.8, Eh = 0.55 V with Cu around 0.1 g/L and Mn around 0.01 g/L (Si was not analyzed). The gel mineralization precipitating from these solutions did not contain relevant contents of silicates, suggesting a too low silica content for crysocolla formation. Acid mine drainage (AMD), forming in similar conditions than supergene solutions, frequently present higher copper contents, up to 1 [g/L] (Dold, 2006a; Dold, 2014). The Si concentrations in a oxidation zone of a porphyry copper tailings impoundment (Piuquenes/La Andina) were around 50 mg/l, and no chrysocolla precipitation was observed (Dold, 2006a), so that it can be assumed that Si concentrations should be clearly above 0.1 g/L. Calculations with MEDUSA indicate that the stability field of chryscolla take an actual importance with silica concentration in solution over

2 [g/L] (as $Si(OH)_4$). Nevertheless, PHREEQC calculation show that even at low concentration, chrysocolla is able to saturate under Eh-pH conditions in agreement with the Exótica deposit environment (Fig. 20). For this study, copper and manganese concentrations of 0.001, 0.1 and 1 [g/L] were considered (Fig 21).

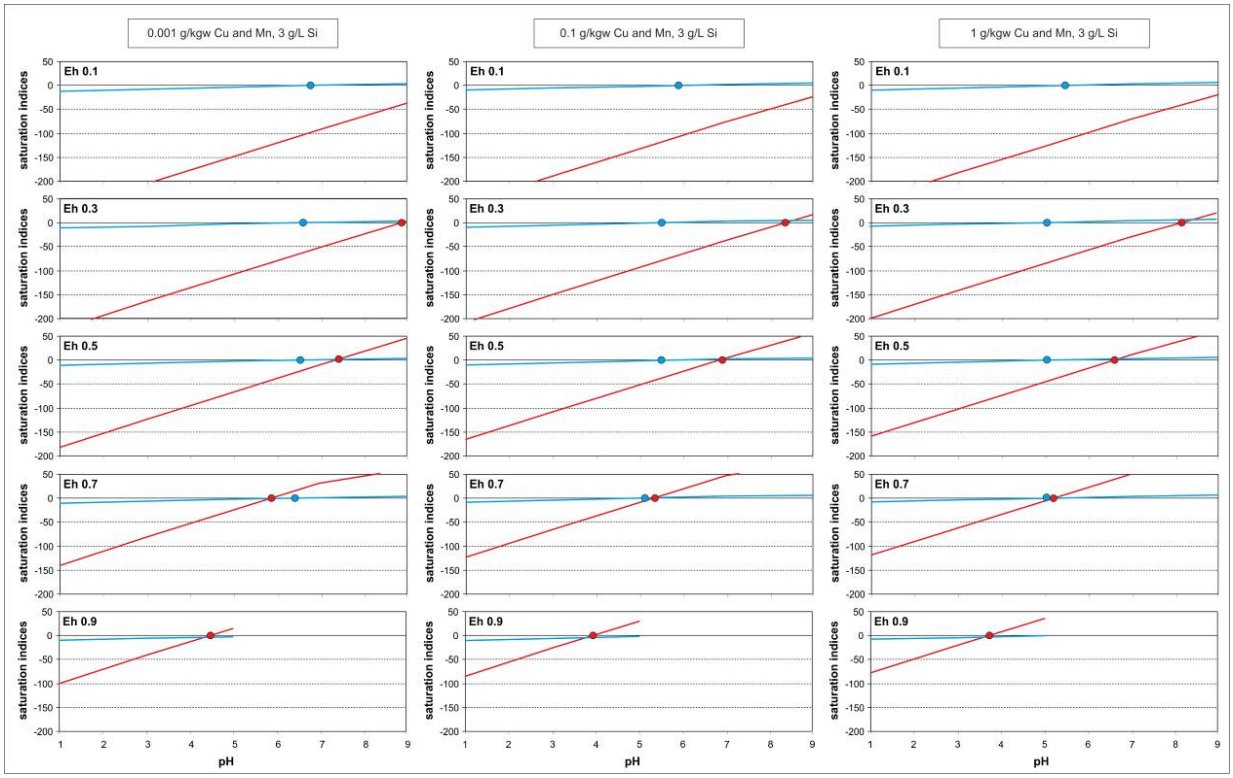

Figure 21: Saturation indices for birnessite and chrysocolla calculated with PHREEQC for Si 3 [g/L], Mn and Cu 0.001, 0.01 and 1 [g/L] and Eh of 0.1, 0.3, 0.5 0.7 and 0.9 [V]. As general trend, chrysocolla reaches oversaturation at lower pH than birnessite. However, with increasing redox potential, birnessite becomes oversaturated at lower pH than chrysocolla.

Eh variations only have a small impact on the chrysocolla precipitation, precipitating at pH values above ~5 (Fig. 21). In contrast, birnessite has a linearly decreasing pH of the solubility boundary with the increase of the Eh (Fig. 21). With a Si concentration of 3 [g/L], increasing Cu and Mn concentrations expands the stability field of both minerals towards lower pH (Fig. 20). Thus, the window in which copper pitch/wad can precipitate (chrysocolla and birnessite over-saturated) range from Eh between 0.6 [V] and 0.9 [V] and pH between 4.5 and 9. With lower Eh, only chrysocolla is able to precipitate, and with higher Eh, only birnessite (Fig. 21). Increase of the Si concentration in solution implies a pH decreasefor the precipitation of chysocolla, but does not affect importantly the conditions of precipitation of birnessite. Consequently, this increase slighly enlarges the favorable window for the precipitation of chrysocolla without birnessite at Eh lower than 0.7 [V], and allows the precipitation of copper pitch under more oxidant and acidic conditions (Fig. 22).

2.4.4 Conceptual model of the genesis of the Exótica Deposit

In order to visualize and interpret this geochemical behavior of copper pitch/wad formation in the context of Chuquicamata Exótica ore formation, the following conceptual model is proposed.

The Exótica deposit is considered to be the product of the downstream water circulation of supergene solutions (acid rock drainage) coming from the sulfide oxidation at the Chuquicamata porphyry copper ore body and entering in contact with sediments and underlying bedrocks located to the south of the main porphyry deposit (e.g. Newberg, 1967; Mortimer et al., 1978; Münchmeyer, 1996). In the central axis of the exotic deposit, sediments and bedrock are strongly altered (kaolinitisized) and form an altered tube with low Cu mineralization (in Fig. 4). The main exotic mineralization formed roughly concentric around the altered tube and south of the end of the altered tube. The altered tube is recognized as such in the CODELCO geological model until around 3 km South from the Chuquicamata deposit (until the local coordinates N-1200 CODELCO). However, the mineralization continues at least for 4 km to the south (Ossandón et al., 2001).

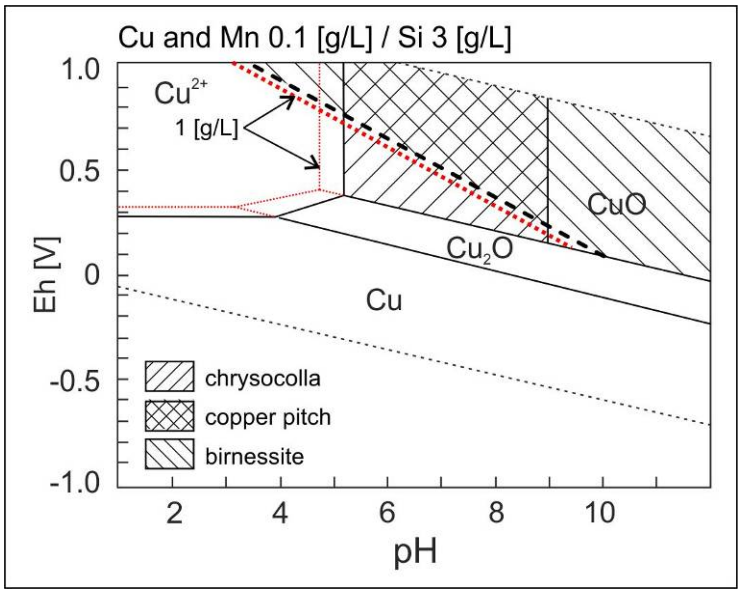

Figure 22: Eh-pH diagram for Cu-Si-Mn system at 25°C showing the stability fields of chrysocolla and birnessite. Were both stability field overlap, the conditions for copper pitch/wad formation are given. Increasing concentrations result in expansion of the stability field toward acidic pH.

A four steps water-rock interaction scenario is proposed to produce the observed alteration and mineralization assemblage in the Exótica deposit, (Fig. 23). The considered stages are (1) interaction of rainwater with acid-bearing soluble salts formed by evaporation on the top of the oxidation zone of the Chuquicamata porphyry; (2) interaction of the resulting solution with the mineralogy observed in the oxidation zone of the Chuquicamata porphyry; (3) interaction of the resulting solution with the altered sediments of the central altered tube; (4) interaction of the resulting solution with unaltered sediments that host the main part of the exotic mineralization (Fig. 23), inducing the mineralization

Stage 1: Rainwater interacting with soluble sulfates and chlorite formed by evaporation on the top of the oxidation zone of the porphyry system.

In the dry and warm climatic conditions of northern Chile, the evaporation of very acid waters commonly forms efflorescences and crusts of copper and iron sulfates and salts which store the free sulfuric acid (e.g. Rhomboclase, $[(H_3O)Fe(SO_4)_2 \cdot 3H_2O]$, Nordstrom and Alpers, 1999; Schwertmannite, $Fe^{3+}{}_{16}O_{16}(SO_4)_2(OH)_{12} \bullet nH_2O$, Alarcon et al. 2014) resulting from the

oxidation processes (Bandy, 1938; Nordstrom and Alpers, 1999; Dold, 2006; Smuda et al. 2014). Surface water, mainly from occasional precipitations, interacts with these soluble minerals in the crusts and is rapidly acidified and charged in ions. At Chuquicamata, those salts are known to be an important source of acidity for the rainwater entering in the system. These acidic waters may react with the copper minerals typical of the oxidation zone of the Chuquicamata deposit such as chalcantite and anlterite (Bandy, 1938), as well as with manganese oxides (e.g birnessite). After this stage, solutions would present highly oxidative (Eh >1.0 [V]) and acid (pH 1-3) conditions.

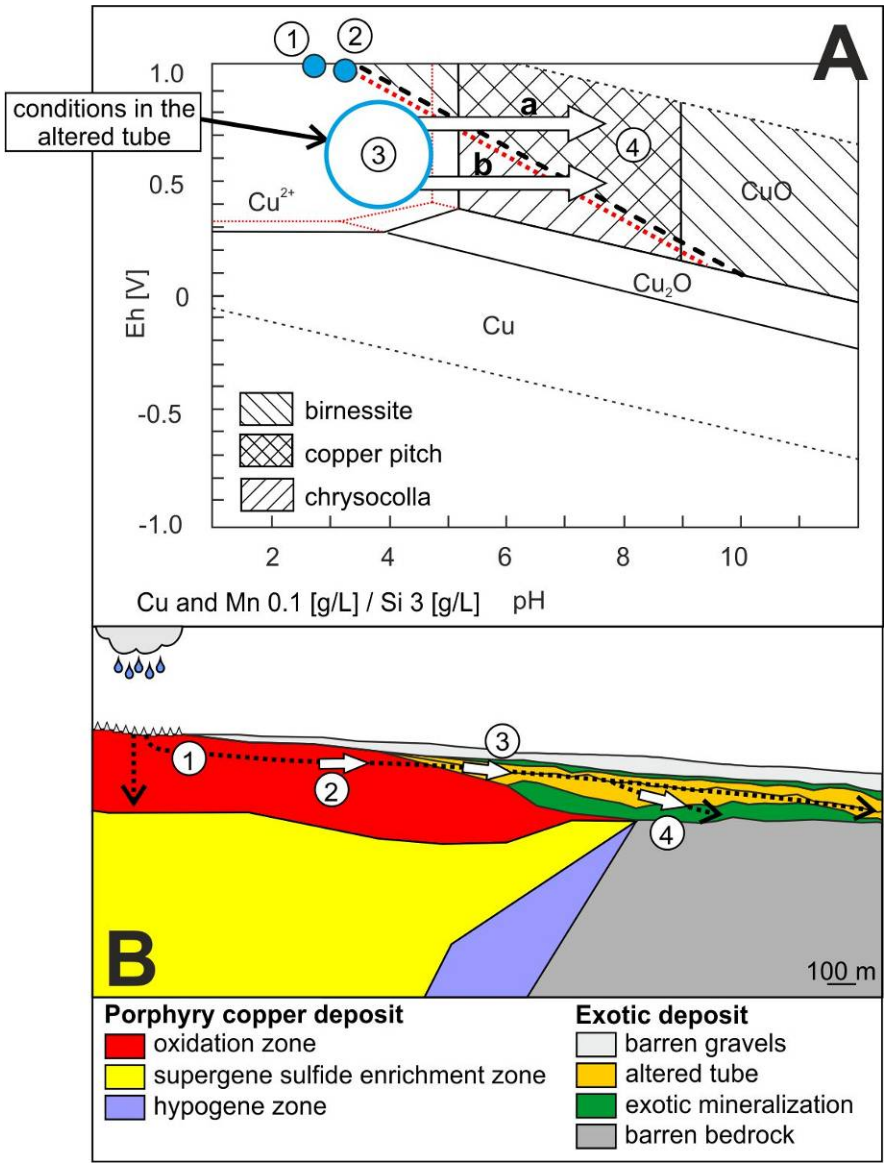

Figure 23: A. Eh-pH diagram with the stability field of chrysocolla, birnessite, and copper pitch/wad and the evolution of the solution along the flow-path in the Chuquicamata-Exótica system. B. Situation of the stages on a N-S schematic vertical section. Proposed sequence for the Exótica deposit mineralization. (1) Rainwater interacting with soluble sulfates and chlorite formed by evaporation on the top of the oxidation zone of the porphyry system; (2) interaction with the oxidation of the Chuquicamata porphyry copper deposit; (3) interaction with the central altered tube of the Exótica deposit; (4) interaction with unaltered sediments and bedrock.

Stage 2: Interaction of the resulting solution with the mineralogy observed in the oxidation zone of the Chuquicamata porphyry copper deposit.

The Chuquicamata oxidation zone presents a high copper content (up to several percents copper in the oxidation zone in the central part of the deposit, Chapter 1), mainly as chalcanthite and antlerite in the central part of the deposit, and in other less common phases in its external parts, such as cuprite, native copper, and mineraloïds including copper wad (Bandy, 1938; Chapter 1). A perched chalcocite blanket is also described in the oxidation zone (Ossandón et al., 2001). Gangue minerals are principally quartz and K-feldspars, but, as the porphyry was previously leached and altered, the neutralization potential is low. For this reason, copper and manganese concentrations are expected to increase during this stage, and pH should remain low (around 2-3), and Eh high (around 1 [V]).

Stage 3: Interaction with the central altered tube of the Exótica deposit.

X-ray diffraction shows that the mineralogy of the central altered tube of the the Exótica deposit in mainly constituted by quartz and feldspar (sericitizied) remaining from the original assemblage, and montmorillonite, kaolinite, iron oxides (goethite), and some Fe-Al oxyhydroxy sulfates (jarosite, alunite) produced by the interaction with acid solutions, as well as gypsum.

The mineral assemblage produced by acid alteration has expected to have a low neutralization potential. Neither relevant copper nor manganese mineralization are observed in this zone, which implies an environment with still low pH (2-4) but slightly lower Eh (around 0.7 [V], Fig. 23). Nevertheless, it cannot be excluded that some copper and/or manganese mineralization could have occur and been posteriorly remobilized by a subsequent event. As virtually no copper and manganese oxides precipitate, Mn and Cu in solution stay high. This stage could be important to provide the Si in solution necessary to precipitate copper silicate as chrysocolla.

Stage 4: interaction with unaltered sediments and bedrock.

The sediments hosting the exotic mineralization are principally constituted by clasts with a quartz-feldspar-mica mineralogical assemblage derived from the unaltered Fortuna granodiorite. The neutralization potential of this zone is higher than in the central parts of the tube, and therefore the solution-rock interaction leads to an increase of the pH (without significant Eh change), resulting in the precipitation of copper pitch and/or copper wad if conditions are oxidizing (Eh >0.7 [V], Fig. 23 A.a) and of chrysocolla in less oxidative conditions (Fig. 23 A.b). In the latter case, the pH increases to near neutral values due to the neutralization potential of the fresh host sediments and basement rock would allow the precipitation of copper pitch and copper wad.

Figure 23 A illustrates that small pH and Eh changes, as well as changes in concentration, can induce changes in the precipitating mineral assemblage. The particular hydrogeological settings due to semi-arid to arid climate, and particularly the existence of solution stagnation periods between two precipitation events and the alternation between evaporation and infiltration episodes lead to alternating regime of mobilization and precipitation. During dry periods, sulfide oxidation occurs in the oxidation zone. During these periods, high evaporation mobilizes elements in the pore water towards the surface through capillary transport and precipitates the metals as efflorescent salts, mainly as water soluble sulfate minerals, as it can

be observed nowadays in waste-rock dumps and sulfidic mine tailings (e.g. Dold, 2006; Smuda et al., 2007; Smuda et al., 2014). During rain events, the flushing of the system results in the dissolution of the efflorescent salts and in a subsequent increase of the concentrations of the metals and protons in solution, as well as in more oxidizing conditions. If iron is mobilized during this event, it oxidizes and precipitates fast as secondary Fe(III) hydroxides and/or sulfates (e.g. jarosite-alunite, schwertmannite, goethite) due to the low solubility of ferric iron. Elements stable as oxyanions in oxidizing conditions (e.g. As, Mo) will be adsorbed to these Fe(III) hydroxides at low pH and enriched close to the source. Interaction of the acid solution with the minerals in the oxidation zone put metals like Cu and Mn in solution. If these solutions percolate laterally towards Exótica, where neutralization reactions with the unaltered sediments increase pH up to 4.5-6 and decrease Eh to 0.7-0.5 [V] (Fig. 23), chrysocolla may start to precipitate. In the northern part of the Exótica deposit, close to the ARD source, chrysocolla – copper wad assemblages belonging to the exotic mineralization are observed near the surface in desiccation crakes, or even in surface ponds. Therefore, chrysocolla is considered as a result of the outcrop of the Cu-Mn rich solutions described above. The alternated banded texture of chrysocolla and copper pitch can be explained by a succession of flushing events, mainly superficial run-off from solution of type 1 entering in the stability field of birnessite, triggering the formation of copper pitch. Once most of Mn precipitated as birnessite, chrysocolla precipitation takes over until the next flushing event. The complex textures observed in this banded material suggests that chrysocolla precipitated as highly hydrated gels that progressively solidified. This is shown by chrysocolla bands/aggregates that appear to have incorporated partially or totally solidified material. Presence of chrysocolla clasts with brittle fracture indicates reworking of solidified material.

In contrast, the mainly under-surface percolation of Cu and Mn rich solutions in the gravels results in a diminution of Eh and an increase of pH with increasing distance from the solution source, due to the neutralization potential of the host-rock (Fig. 23 A). These changes of the Eh-pH conditions favor the precipitation of chrysocolla as cement in the gravels of the central to southern part of Exótica, and also explain why chrysocolla clearly dominates the mineral paragenesis at depth. At a certain distance of the ARD source, solutions reach neutral pH conditions and relatively low Eh (around 0.5 [V]), and birnessite becomes oversaturated (Fig. 23 A). It explains the presence of important copper wad mineralization at the far south of Exótica (Münchmeyer, 1996).

The presence of the altered tube in the central axis of the Exótica deposit indicates that the constant production of acidic metal rich solutions in the oxidation zone consumed successively the neutralization potential along the flow-path, resulting in a constant re-dissolution and re-precipitation of the metals downstream, i.e, to the South, in a process comparable to roll-front deposits.

The conceptual model presented in Fig. 23 does not consider the presence of chloride in the mineralizing solution. Textural relationships of atacamite and gypsum mineralization in the Exótica deposits observed in this study, show that atacamite is mainly part of a late mineralization stage, with atacamite-gypsum veins cross cutting the principal chrysocolla - copper wad/pitch mineralization. The presence of atacamite in the Chuquicamata deposit oxidation zone (only observed in the upper 30 meters below surface, Bandy, 1938; Jarrell, 1944), and in the central part of the exotic deposit (Münchmeyer, 1996), likely results from the late interaction of chloride rich water with the soluble copper salts present in the oxidation zone (Bandy, 1938). Reich et al. (2008) and Tapia et al. (2012), also propose a recent episode of mineralization including the precipitation of atacamite in other deposits of northern Chile. It

can be concluded that at certain periods, flux of chloride-rich solutions triggered atacamite formation. Nowadays, atacamite precipitation is observed at an outcrop of the lower saline aquifer of the Calama basin, in the southern-eastern end of the Exótica pit (Lambiel, 2014). After 3 Ma, the Calama basin region was characterized by the appearance of salars (e.g. Salar de Talabre; May et al., 1999; Hartley and Chong, 2002). Nevertheless, no hydrogeological connection has been established between the Calama basin and the upper oxidation zone of Chuquicamata, that could suggest that these salars are the source for chlorine necessary for the formation of atacamite. May et al. (2005) suggest that at about 3 Ma, the Calama Basin was subject to gentle folding, followed by entrenchment of the Río Loa and Río San Salvador through Miocene to Pliocene strata to reach a new higher base-level. Additionally, occasional fluctuations in climate suggesting increased runoff are indicated by the development of diatomites together with lacustrine and palustrine limestones in the Calama Desert (May et al., 2005). It can be hypothesized that these changes in the tectonic and climatic settings could have resulted in the rise of a deep saline aquifer water table, which might have been temporarily hydrogeologically connected with the Exótica system. The input of external chlorine-rich solution in the Exótica system could have taken place in on the eastern flank of the exotic mineralization, around 3 km away from the ARD source, where nowadays the out-crop a carbonate-rich aquifer is observed in the pit wall (Lambiel, 2014). The late Miocene-Pliocene uplift reported by Reich et al. (2006) may have also played a role making available chloride rich solutions to Chuquicamata and Exótica.

The formation of an exotic deposit ofsuch a great extent as Exótica deposit require important amounts of water. In this context, climate is a key parameter to understand the chronology of the mineralization. The climate of the Calama basin was extensively studied, but its evolution is not fully understood yet (Chapter 1). Several authors propose an onset of the hyperarid conditions after the main supergene event, dated with supergene alunite until around 15 Ma (Sillitoe et al., 1996; Bissig and Riquelme, 2010). Others, such as Hartley and May (1998), Hartley and Chong (2002) or Saez et al. (2012) propose a latter onset for the hyperarid conditions, including a period of semi-aridity between 8 and 3 Ma for Hartley and Chong (2002). Moreover, it is also known from present observations, that even under hyperarid climates, wetter periods may occur. For instance, Latorre et al. (2002 and 2006) describe a wetter phase at 11.8 and 10.5 ka in the Salar de Atacama region. Even if short, these wetter periods would be able to reactivate the supergene processes in the Chuquicamata area thanks to the highly soluble character of the previously discussed mineralogy at the top of the oxidation zone.

The presence of pebbles of exotic mineralization in gravels in the northern part of the Exótica deposit, indicate that the exotic mineralization process took place during the sedimentationof these gravels (Mortimer et al.,1978). These local gravel units were tentatively correlated with the Jalquinche Formation at the base El Loa Group in the Calama area (Chapter 1), what signify a maximum age of around 22 Ma for the exotic mineralization (Chapter 1; May et al. 1999, 2005; Blanco, 2008; Rech et al., 2010).

The Exótica deposit rests on the southern end of the supergene profile of the Chuquicamata deposit suggesting that if the Exótica deposit was formed during the main Late Oligocene - Early Miocene supergene stage, it should have been at the end of the event. Alternatively, the Exótica deposit could result from leaching of exposed immature supergene profile because of a subsequent Middle - Late Miocene Andean uplift. Copper contained in the oxidation zone (including as soluble salts) and in a chalcocite blanket "perched" in the oxidation zone (Ossandón et al., 2001), indicating a rapid drop of the oxidation front and supporting therefore

an exhumation event, could be leached. The soluble salts, mainly acid-bearing sulfates, could trigger the acidity necessary to explain strong acidic alteration observed in parts of Exótica deposit. In both alternatives, i.e., formation at the end of the 19-15 Ma main supergene enrichment event at Chuquicamata, or during the subsequent Middle - Late Miocene Andean uplift, the Exótica deposit the water amount necessary to its formation has to be taken in account. A latter formation of the Exótica deposit would imply either a delayed onset of hyperarid conditions, or an important wet episode during a general hyperarid climate.

2.5. Conclusions

This study provides new data to understand the nature of copper pitch, copper wad and chrysocolla in the Exotica deposit downstream of the Chuquicamata porphyry copper deposit, Chile. On the textural point of view, copper pitch shows the same general texture as chrysocolla, but includes variable proportions of other minerals, principally birnessite, atacamite, paratacamite, libethenite, and gypsum (Fig. 7). Samples of copper pitch with a dusty copper wad-like aspect were analyzed with XRD and give the same results than those obtained on the more typical glassy copper pitch. Chemical analyses on copper pitch and chrysocolla support the hypothesis of Throop and Buseck (1971) that copper pitch is a manganese rich chrysocolla and not a mineral in itself (Table 4). Chemical compositions obtained by XRF (Uniquant®) and in situ chemical analyses (SEM EDS) on the copper wad samples illustrate a more inhomogeneous but similar composition (Table 4 and 5) than copper pitch, probably due to an important fraction of other minerals finely mixed with it (Table 4). Cu, Si, Mn, Al, and Fe are the main chemical elements in copper pitch and copper wad, but the proportions are much more variable in copper wad. The presence of potassium, magnesium, calcium, chloride, and titanium is frequent, and cobalt and barium are present in some samples. Sequential extraction indicates that manganese is mostly associated with birnessite in copper pitch. The data suggests that copper is mainly associated with the chrysocolla-like pseudo-amorphous material.

A four stages conceptual model is proposed to explain the morphology and the mineralogical assemblage described in the Exótica deposit. The Exótica deposit overlaps the southern extent of the Chuquicamata supergene profile, including the oxidized zone, and do not represent a lateral extention of the oxidation zone. Stage 1: interaction of rainwater with soluble salts at the surface of the Chuquicamata oxidation zone, pH decreases until 1-2 and Eh increases up to >1.0 [V]; stage 2: interaction of the resulting solution with the low neutralization ppotential oxidation zone of the Chuquicamata deposit, pH remains low (2-3) and Eh high (~1.0 [V]; stage 3: interaction of the resulting solution with the low neutralization potential altered zone present in the center of the Exótica deposit, pH remains low (2-4) and Eh slighly decreases (~0.7 [V]); stage 4, propagation of the exotic altered zone in the fresh sediments, presenting an higher neutralization potential, inducing a gradual increase of the pH and a decrease of the Eh. In oxidizing conditions (Eh > 0.7 [V]), copper pitch precipitates, and under Eh conditions <0.7 [V], chryscolla precipitates first, followed by copper pitch under circum neutral pH values The evolution of the physico-chemical conditions in the mineralizing solutions and the mineralogy are illustrated in Fig. 23.

2.6. Acknowledgements

The constructive collaboration with the geologic team of the Chuquicamata mine (CODELCO) made this work possible. We specially thank Manuel Vergara, Fernanado Ramirez, Victorino Moyano, and their collaborators, and Carlos Barrios for his inestimable help. We thank A. Martigner for the SEM analyses, K. Kouzmanov for the QEMSCAN® analyses, R.Spikings for the $^{39}Ar/^{40}Ar$ datations, F. Capponi for the XRF analyses and J.-M. Boccard for the technical support, University of Geneva, Switzerland. The project was financed by the Swiss National Science Foundation Project FN129988.

References Chapters 1 and 2

Ague, J.J., Brimhall, G., 1989, Geochemical modeling of steady state fluid flow and chemical reaction during supergene enrichment of porphyry copper deposits: Economic Geology, v.84, pp. 506-528.

Alpers, C.N., and Brimhall, G.H, 1989, Paleohydrologic evolution and geochemical dynamics of cumulative supergene metal enrichment at La Escondida, Atacama Desert, Northern Chile: Economic Geology, v. 84, pp. 229-255.

Anderson, J.A., 1982, Characteristics of leached capping and techniques of appraisal: in S.R. Titley, ed., Advances in geology of the porphyry copper deposits, southern North America: Tucson, University Arisona Press, pp. 275-295.

Aracena, I., Ossandón, G., and Zentilli, M., 1997, Mineralogía y distribución del zinc en Chuquicamata: Enriquecimiento supérgeno de zinc?: Congreso Geológico Chileno, VIII, Antofagasta, p. 1908−1912.

Arcuri, T, and Brimhall, G., 2003, The Chloride Source for Atacamite Mineralization at the Radomiro Tomic Porphyry Copper Deposit, Northern Chile: Economic Geology, v. 98, pp. 1667-1681.

Ballard, J.R., Palin, J.M., Williams, I.S., and Campbell, I.H., 2001, Two ages of porphyry intrusion resolved for the super-giant Chuquicamata copper deposit of northern Chile by ELA-ICP-MS and SHRIMP: Geology, v. 29, pp. 383-386.

Bandy, M.C., 1938, Mineralogy of three sulphate deposits of northern Chile: The American Mineralogist, v. 23 (11), pp. 669-760.

Barra, F., Alcota, H., Rivera, S., Valencia, V., Munizaga, F., and Maksaev, V., 2013, Timing and formation of porphyry Cu–Mo mineralization in the Chuquicamata district, northern Chile: new constraints from the Toki cluster: Mineralium Deposita, v. 48, pp. 629-651.

Bennett, P.C., El Shishtawy, A.M., Sharp Jr., J.M., and Atwia M.G., 2014, Source and migration of dissolved manganese in the Central Nile Delta Aquifer, Egypt: Journal of African Earth Sciences, v. 96, pp. 8-20.

Billiet, V., 1942, The relations of chrysocolla, katangite, plancheite, bisbeeite, shattuckite and dioptase,Verh. Kon. Vlaamsche Acad. Wetensch., Letteren schoone Kunsten Belgie, Klasse Wetensch. 4, 58 pp.

Bladh, K.W., 1982, The formation of goethite, jarosite and alunite during the weathering od sulfide-bearing felsic rocks: Economic Geology, v. 77, pp. 176-184.

Blanco, N., 2008. Estratigrafía y evolución tectono-sedimentaria de la cuenca cenozoica de Calama (Chile, 22°S). M.S. Thesis. University of Barcelona. 68 p. (Spanish).

Boni, M., and Mondillo, N., 2015, The "Calamines" and the "Others": the great family of supergene nonsulfide zinc ores: Ore Geology Reviews, v. 67, pp. 208-233.

Braxton, D., and Mathur, R., 2001, Exploration applications of copper isotopes in the supergene environment: a case study of the Bayugo Porphyry Copper-Gold Deposit, Southern Philippines: Economic Geology, v. 106, pp. 1447-1463.

Brimhall, G.H., Alpers, C.N., and Cunningham, A.B., 1985, Analysis of supergene ore-forming processes and ground-water solute transport using mass balance principles: Economic Geology, v. 80, pp. 1227-1256.

Bissig, T., and Riquelme, R., 2010, Andean uplift and climate evolution in the southern Atacama desert deduced from geomorphology and supergene alunite-group minerals: Earth and Planetary Letters, v. 299, pp. 447-457.

Campbell, I.H, Ballard, J.R., Palin, J.M., Allen, C., and Faunes, A., 2006, U-Pb Zircon Geochronology of Granitic Rocks from the Chuquicamata-El Abra Porphyry Copper Belt of Northern Chile: Excimer Laser Ablation ICP-MS Analysis: v.101, pp. 1327-1344.

Campos, E., Menzies, A., Sola, S., Hernández, V., and Riquelme, R., 2015, Understanding exotic-Cu mineralisation: Part I - Characterization of Chrysocolla: 13th SGA meeting, Nancy, v. 3, pp. 1153-1155.

Chukhrov, F.V., Zvyagin, B.B., Gorshkov, A.I., Ermilova, L.P., and Rundnits-Kaya, E.S., 1969, Chrysocolla: New minerals, American Mineralogist, p.993.

Crane, M.J., Sharpe, J.L., and Williams P.A., 2001, Formation of chrysocolla ad secondary copper phosphates in the highly weathered supergen zones of some Australian deposits; Records of the Australian Museum, v. 53, pp. 49-56.

Cuadra, P., Zentilli, M., Puig, A., and Tidy, E., 1997, Dataciones radiométricas recientes en Radomiro Tomic: Congreso Geológico Chileno, VIII, Antofagasta, v. II, pp. 916-919.

Dill, H.G., Hansen, B., Keck, E. and Weber, B., 2010, Cryptomelane: A tool to determine the age and the physical–chemical regime of a Plio-Pleistocene weathering zone in a granitic terrain (Hagendorf, SE Germany): Geomorphology, v. 121, pp. 370-377.

Dilles, J., Tomlinson, A., Martin, M., and Blanco, N., 1997, El Abra and Fortuna complexes: A porphyry copper batholith sinistrally displaced by the Falla Oeste: Congreso Geológico Chileno, VIII, Antofagasta, v. III, p. 1883–1887.

Dold, B., and Fontboté, L., 2001, Element cycling and secondary mineralogy in porphyry copper tailings as a function of climate, primary mineralogy, and mineral processing: Journal of Geochemical Exploration, v. 74, pp. 3-55.

Dold, B., 2003a, Dissolution kinetics of schwertmannite and ferrihydrite in oxidized mine samples and their detection by differential X-ray diffraction (DXRD): Applied Geochemistry, v. 18, pp. 1531-1540.

Dold, B., 2003b, Enrichment processes in oxidizing sulfide mine tailings: lessons for supergene ore formation: SGA Newslettre, v. 16, pp. 1 and 10-15.

Dold, B., 2003c, Speciation of the most soluble phases in a sequential extraction procedure adapted for geochemical studies of copper sulfide mine waste: Journal of Geochemical Exploration, v. 80, pp. 55-68.

Dold, B., Blowes, D.W., Dickhout, R., Spangenberg, J.E., and Pfeifer, R., 2005, Low molecular weight carboxylic acids in oxidizing porphyry copper tailings: Environmental Sciences and Technologies, v. 39, pp. 2515-2521.

Dold, B., 2006a, Element flows associated with marine shore mine tailings deposits: Environmental Science and Technology, v. 40, pp. 752-758.

Dold, B., 2006b, Geochemical modeling of the exotic mineralization of the Exótica Deposit at Chuquicamata, Chile: Congreso Geológico Chileno, XI, Antofagasta, v. II, pp. 247-250.

Dold, B., Gonzales-Toril, E., Aguiler, A., Lopez-Pamo, E., Cisternas, M.E., Bucchi, F., and Amils R., 2013, Acid rock drainage and rock weathering in Antarctica: important sources for iron cycling in the southern ocean: Environmental Science and Technology, v. 47(12), pp. 6129-6136.

Dold, B., 2014, Evolution of Acid Mine Drainage formation in sulphidic mine tailings: Minerals, v.4, pp. 621-641.

Dunai, T.J., González López, G.A., Juez-Larré, J., 2005, Oligocene-Miocene age of aridity in the Atacama Desert revealed by exposure dating of erosion-sensitive landforms: Geology, v. 33, pp. 321-324.

Enders, M.S., 2000, The evolution of supergene enrichment in the Morenci Porphyry Copper Deposit, Greenlee County, Arizona: PhD thesis, University of Arizona, p. 252.

Evans, H.T., 1981, Copper coordination in low chalcocite and djurleite and other copper-rich sulfides: American Mineralogist, v. 66, pp.807-818.

Faimon, J., and Blecha, M., 2008, Interaction of freshly precipitated silica gel with aqueous silicic acid solutions under ambient and near neutral pH-conditions: a detailed analysis of linear rate law: Aquatic Geochemistry, v. 14, pp. 1-40.

Farges, F., Benzerara, K., and Brown, Jr., G.E., 2006, Chrysocolla redefined as spertiniite: SLAC-PUB-12232; 13th International Conference on X-ray absorption fine structure (XAFS13), Stanford, California.

Fam R., R., and Rojas O., 1997, Eventos de mineralización de Cu en el distrito Chuquicamata, II region - Chile: Congreso Geológico Chileno, VIII, Antofagasta, v. III, pp. 1923-1927.

Field C.W., and Gustafson L.B., 1976, Sulfur isotopes in the porphyry copper deposit at El Salvador, Chile: Economic Geology, v. 71, p. 1533-1548.

Foote, H.W., and Bradley, W.M., 1913, On solid solution in minerals. IV. The composition of amorphous minerals as illustrated by Chrysocolla: American Journal of Science, v. 36, pp. 180-184.

Frost, R.L., and Xi, Y., 2013, Is chrysocolla (Cu, Al)$_2$H$_2$Si$_2$O$_5$(OH)$_4$·nH$_2$O related to spertiniite Cu(OH)$_2$? - A vibrational spectroscopic study: Vibrational Spectroscopy, v. 64, pp. 33-38.

Frost, R.L., Xi, Y., and Wood, B.J., 2012, Thermogravimetric analysis, PXRD, EDX and XPS study of chrysocolla (Cu, Al)$_2$H$_2$Si$_2$O$_5$(OH)$_4$·nH$_2$O - structural implications: Thermochimica Acta, v. 545, pp. 157-162.

Gammons, C.H., and Seward, T.M., 1996, Stability of manganese (II) chloride complexes from 25 to 300°C: Geochimica et Cosmochimica Acta, v. 60 (22), pp. 4295-4311.

García-Romero, E., and Suárez, M., 2013, Sepiolite-palygorskite: textural study and genetic considerations: Applied Clay Science, v. 86, pp. 129-144.

Gottschalk, V.H., and Buehler H.A., 1912, Oxidation of sulphides (second paper): Economic Geology, v. 7, pp. 15-34.

Gustafson, LB., and Hunt, J.P., 1975, The porphyry copper deposit at EI Salvador, Chile, Economic Geology, v. 70, p. 875-912. Guild, F.N., 1929, Copper pitch ore: The American Mineralogist, v. 14 (9), pp. 313-318.

Halbach, M., Halbach, P., and Lüders, V., 2002, Sulfide-impregnated and pure silica precipitates of hydrotherma origin from the Central Indian Ocean: Chemical Geology, v. 182, pp. 357-375.

Hall, G.E.M., Vaive, J.E., Beer, R., and Hoashi, M., 1996, Selective leaches revisited, with emphasis on the amorphous Fe oxyhydroxide phase extraction: Journal of Geochemical Exploration, v. 56, pp. 59-78.

Hartley, J.H., and May, G., 1998, Miocene gypscretes from the Calama Basin, northern Chile: Sedimentology, v. 45, pp. 351-364.

Hartley, J.H., and Chong, G., 2002, Late Pliocene age for the Atacama Desert: Implications for the desertification of western South America: Geology, v. 30, pp. 43-46.

Hartley, J.H., and Rice, C.M., 2005, Controls on supergene enrichment of porphyry copper deposits in the Central Andes: a review and discussion: Mineralium Deposita, v. 40, pp. 515-525.

Hatipoğlu, M., 2010, The nano-grain sizes of the opaline matrix components in Anatolian fire opals: Journal of Non-Crystalline Solids, v. 356, pp. 1408-1415.

Houston, J., and Hartley, A.J., 2003, The central andean west-slope rainshadow and its potential contribution to the origin of hyper-aridity in the Atacama desert: International Journal of Climatology, v. 23, pp. 1453-1464.

Jarrell, W., 1944, Oxidation at Chuquicamata, Chile: Economic geology, v. 39, pp. 251-286.

Koski, R.A., 2012, Supergene ore and gangue characteristics in volcanogenic massive sulfide occurrence model: U.S. Geological Survey Scientific Investigations Report 2010–5070–C, chap. 12, 6 p.

Lambiel, F., 2014, New insights into the ore genesis of the Exotica deposit at Chuquicamata (Northern Chile) through the neoformation of Cu-oxide minerals from gel-like precursors: master thesis, University of Geneva, 96 p.

Latorre, C., Betancourt, J.L., Rylander, K.A., and Quade, J., 2002, Vegetation invasions into absolute desert: A 45 000 yr rodent midden record from the Calama-Salar de Atacama basins, northern Chile (lat 22°-24°): Geological Society of America Bulletin, v. 114 (3), pp. 349-366.

Latorre, C., Betancourt, J.L., and Arroyo, M.T.K., 2006, Late Quaternary vegetation and climate history of a perennial river canyon in the Río Salado basin (22°S) of Northern Chile: Quaternary Research, v. 65, pp. 450-466.

Lindsay, D.D., 1998, Structural control and anisotropy of mineralization in the Chuquicamata porphyry deposit, Chile: Unpublished Ph.D. thesis, Halifax, NS, Dalhousie University, 381 p.

López, V.M., 1939, The primary mineralization at Chuquicamata, Chile, S.A.: Economic Geology, v. 34, p. 674–711.

Lynne, B.Y., Campbell, K.A., Moore, J.N., and Brown, P.R.L., 2005, Diagenesis of a 1900-year-old siliceous sinter (opal-A to quartz) at Opal Mound, Roosevelt Hot Springs, Utah, U.S.A.: Sedimentary Geology, v. 179, pp. 249-278.

Majzlan, J., Navrotsky, A., McCleskey, R.B., and Alpers, C.N., 2006, Thermodynamic properties and crystal structure refinement of ferricopiapite, coquimbite, rhomboclase and $Fe_2(SO_4)_3(H_2O)_5$: European Journal of Mineralogy, v. 18, pp. 175-186.

Majzlan, J., Zittlau, A., and Števko, M., 2014, Thermodynamic properties of secondary copper minerals: 4th Central European Mineralogical Conference, Skalský Dvůr, Czech Geological Society.

Mathur, R., Ruiz, J, and Munizaga, F., 2000, Relationship between copper tonnage of Chilean base-metal porphyry deposits and Os isotope ratios: Geology, v. 28, pp. 555-558.

May, G., Hartley, A.J., and Stuart F.M., 1996, Oligocene-recent sedimentary and tectonic evolution of the Calama Basin, N. Chilean forearc: third ISAG, St Malo (France), pp. 435-437.

May, G., Hartley, A.J., Stuart F.M., and Chong G., 1999, Tectonic signatures in arid continental basins: an example from the Upper Miocene-Pleistocene, Calama Basin, andean forearc, northern Chile: Palaeogeography, Palaeoclimatology, Palaeoecology, v. 151, pp. 55-77

May, G., Hartley, A.J., Chong, G., Stuart, F., Turner, P. and Kape, S.J., 2005, Eocene to Pleistocene lithostratigraphy, chronostratigraphy and tectono-sedimentary evolution of the Calama Basin, northern Chile: Revista Geológica de Chile, v. 32 (1), pp. 33-58.

McInnes, B.I.A, Farley, K.A., Sillitoe, R.H., and Kohn, B.P., 1999, Application of apatite (U/Th)/He thermochronometry to the determination of the sense and amount of vertical fault displacement at the Chuquicamata porphyry copper deposit, Chile: Economic Geology, v.94, pp. 937-948.

Menzies, A., Campos, E., Hernández, V., Sola, S., and Riquelme, R., 2015, Understanding Exotic-Cu mineralisation: Part II - characterisation of black copper (cobre negro) ore: 13th SGA meeting, Nancy, v. 3, pp. 1177-1180.

Moncur, M.C.; Ptacek, C.J.; Blowes, D.W., and Jambor, J.L., 2005, Release, transport and attenuation of metal from an old tailing impoundment: Applied Geochemistry, v. 20, pp. 639-659.

Moreton, S., 2007, Copper-bearing silica gel from the walls of Tankardstown Mine, Co. Waterford, Ireland: Journal af the Russell Society, v. 10, pp. 10-17.

Mortimer B., C., Münchmeyer F., C., and Urqueta D., I., 1978, Emplazamiento del yacimiento Exótica, Chile: Revista Geológica de Chile, v. 6, pp. 41-51.

Mote, T.I., Becker, T.A., Renne, P., and Brimhall, G.H., 2001, Chronology of exotic mineralization at El Salvador, Chile, by 40Ar/ 39Ar dating of copper wad and supergene alunite: Economic Geology, v. 96, p. 351-366.

Müller G., Quiroga J. (2003) Geology of the MM Copper Deposit, Chuquicamata District – An Update. (Abstract)Actas, X Congreso Geológico Chileno, Concepción. Münchmeyer, C., 1996, Exotic Deposits - Products of lateral migration of supergene solutions from porphyry copper deposits: in Camus, F., Sillitoe, R.H., and Petersen, R. (eds), Andean copper deposits: new discoveries, mineralization, styles and metallogeny, Society of Economic Geologists, special publication 5, pp. 43-58.

Münchmeyer, C., 1996, Exotic Deposits - Products of lateral migration of supergene solutions from porphyry copper deposits: in Camus, F., Sillitoe, R.H., and Petersen, R. (eds), Andean copper deposits: new discoveries, mineralization, styles and metallogeny, Society of Economic Geologists, Special Publication 5, pp. 43-58.

Newberg, D.W., 1967, Geochemical implications of chrysocolla-bearing alluvial gravels: Economic Geology, v. 62, pp. 932-956.

Nicolau, C., Reich, M., and Lynne, B., 2014, Physico-chemical and environmental controls on siliceous sinter formation at the high-altitude El Tatio geothermal field, Chile: Journal of Volcanology and Geothermal Research, v. 282, pp. 60-75.

Nordstrom, D.K., and Alpers, C.N., 1999, Geochemistry of acid mine waters: in Plumlee G.S., and Logsdon M.J. (eds), The Environmental geochemistry of mineral deposits, Part A. Processes, techniques, and health issues: Reviews in Economic Geology, v. 6A, pp. 133-156.

Nordstrom, D.K., Blowes, D.W., and Ptacek, C.J., 2015, Hydrogeochemistry and microbiology of mine drainage: An update: Applied GEochemistry, v. 57, pp. 3-16.

Oerter, E., Amundson, R., Heimsath, A., Jungers, M., Chong, G., and Renne, P., 2016, Early to Middle Miocene climate in the Atacama desert of northern Chile: Palaeogeography, Palaeoclimatology, Palaeoecology, v. 441, pp. 890-900.

Ossandón, G., and Zentilli, M., 1997, El distrito de Chuquicamata: una concentración de cobre de clase mundial: Congreso Geológico Chileno, VIII, Antofagasta, v. II, pp. 1888-1892.

Ossandón C., G, Fréraut C., R., Gustafson, L.B., Lindsay, D.D, and Zentilli, M., 2001, Geology of the Chuquicamata mine: a progress report: Economic Geology, v. 96, pp. 249-270.

Padilla Garza, R.A., Titley, S.R., and Pimentel B., F., 2001, Geology of the Escondida porphyry copper deposit, Antofagasta Region, Chile: Economic Geology, v. 96, pp. 307-324.

Pananont, P., Mpodozis, C., Blanco, N, Jordan, T.E., and Brown, L.D., 2004, Cenozoic evolution of the northwestern Salar de Atacama Basin, northern Chile: Tectonics, v. 23, TC6007.

Parc, S., Nahon, D., Tardy, Y, and Vieillard P., 1989, Estimated solubility products and fields of stability for cryptomelane, nsutite, birnessite, and lithiophorite based on natural lateritic weathering sequences: The American Mineralogist, v. 74, pp. 466-475.

Parkhurst D. L. and Appelo C. A. J., 1999, User's guide to PHREEQC (Version 2) - a computer program for speciation, batchreaction, one-dimensional transport, and inverse geochemical calculations. U.S. Geological Survey.

Perelló, J., Cox, D., Garamjav, D., Sanjdorj, S., Diakov, S., Schissel, D., Munkhbat, T-O., and Oyun G., 2001, Oyu Tolgoi, Mongolia: Siluro-Devonian porphyry Cu-Au-(Mo) and high-sulfidation Cu mineralization with a Cretaceous chalcocite blanket: Economic Geology, v. 96, pp. 1407-1428.

Perelló, J., Razique, A., Schloderer, J., and Asad-Ur-Rehman, 2008, The Chagai Porphyry Copper Belt, Baluchistan Province, Pakistan: Economic Geology, v- 103, pp. 1583-1612.

Perelló, J., Muhr, R., Mora, R., Martínez, E., Brockway, H., Swaneck, T., Artai, J., Mpodozis, C., Münschmeyer, C., Clifford, J., Acuña, E., Valenzuela, D., and Argandoña, R., 2010, Wealth Creation through Exploration in a Mature Terrain: The Case History of the Centinela District, Northern Chile Porphyry Copper Belt: Society of Economic Geologists, Inc. Special Publication 15, chapter 13, pp. 229–252

Pincheira, M., Dagnino, A., Kelm, U., and Helle, S., 2003, "Copper pitch y copper wad": contraste entre las fases presentes en las cabezas y en los ripios en pruebas de lixiviación de materiales de Mina Sur, Chuquicamata: Congreso Geológico Chileno, X, Concepción.

Pinget M., M-C., 2016, pHD thesis, Section of Earth and Evironmental Sciences, University of Geneva.

Pinget M., M.C., Dold, B., Zentilli, M. and Fontboté, L., 2015, Reported supergene sphalerite rims at the Chuquicamata porphyry deposit (northern Chile) revisited: evidence for a hypogene origin: Economic Geology, v. 110, pp. 253–262.

Pirrie, D., Butcher, A.R., Power, M.R., Gottlieb, P., and Miller, G.L., 2004, Rapid quantitative mineral and phase analysis using automated scanning electron microscopy (QEMSCAN); potential applications in forensic geoscience: Geological Society, London, Special Publications 2004, v. 232, p. 123-136

Plumlee, G.S., 1999, The environmental geology of mineral deposits: Reviews in Economic Geology, v. 6, part A, pp. 71-116.

Pósfai, M., and Buseck, P., 1994, Djurleite, digenite, and chalcocite: Intergrowths and transformations: American Mineralogist, v. 79, pp. 308-315.

Pronk, J.T., and Johnson, D.B., 1992, Oxidation and reduction of iron by acidophilic bacteria: Geomicrobiology Journal, v. 10, p. 153-171.

Prosser, A.P., Wright, A.J., and Stephens, J.D., 1965, Physical and chemical properties of natural copper silicates which resemble chrysocolla: Transactions of the Institution of Mining and Metallurgy, v. 74, pp. 233-258.

Ramdohr, P., 1980, The minerals and their intergrowths, Pergamon press, 1207 pages.

Rech, J.A., Currie, B.S., Michalski, G., and Cowan, A.M., 2006, Neogene climate change and uplift in the Atacama Desert, Chile: v. 34, pp. 761-764.

Rech, J.A., Currie, B.S., Shullenberger, E.D., Dunagan, S.P., Jordan, T.E., Blanco, N., Tomlison, A.J., Rowe, H.D., and Houston, J., 2010, Evidence for the development of the Andean rain shadow from a Neogene isotopic record in the Atacama Desert, Chile: Earth and Planetary Science Letters, v. 292, pp. 371-382.

Rech, J.A., Curries, B.S., Michalski, G. and Cowan, A.M., 2014, Neogene climate change and uplift in the Atacama Desert, Chile: Geology, v. 34, pp. 761-764.

Reich, M., Palacios, C., Vargas, G., Luo, Shangde, Cameron, E.M., Leybourn, M.I., Parada, M.A., Zúñiga, A., and You, C.-F., 2009, Supergene enrichment of copper deposits since the onset of modern hyperaridity in the Atacama Desert, Chile: Mineralium Deposita, v. 44, pp. 497–504

Reich, M., Snyder, G.T., Álvarez, F, Pérez, A., Palacios, C., vargas, G., Cameron, E.M., Muramatzu, Y., and Fehn, U., 2013, Using iodine isotopes to constrain supergene fluid sources in arid regions: insights from the Chuquicamata oxide blanket: Economic Geology, v. 108, pp. 163–171.

Reynolds, P., Ravenhurst, C., Zentilli, M., and Lindsay, D., 1998, High-precision 40Ar/39Ar dating of two consecutive hydrothermal events in the Chuquicamata porphyry copper system, Chile: Chemical Geology, v. 148, p. 50−60.

Riquelme, R., Hérail, G., R., Martinod, J., Charrier, R., Darrozes, J., 2007. Late Cenozoic geomorphologic signal of Andean forearc deformation and tilting associated with the uplift and climate changes of the Southern Atacama Desert (26°S–28°S): Geomorphology 86, 283-306.

Rivera, S.L., Alcota, H., Proffett, J., Díaz, J., Leiva, G., and Vergara, M., 2013, Update of the geologic setting and pporphyry Cu-Mo deposits of the Chuquicamata District, Northern Chile: Society of Economic Geology Special Publication 16, pp. 19-54.

Saéz, A., Cabrera, L., Garcés, M., van den Bogaard, P. Jensen, A., and Gimeno, D., 2012, The stratigrafic record of changing hyperaridity in the Atacama Desert over the last 10 Ma: Earth and Planetary Science Letters, v. 355-356, pp. 32-38.

Sato, M., 1992, Persistency-field Eh-pH diagrams for sulfides and their application to supergene oxidation and enrichment of sulfide ore bodies: Geochimica et Cosmochimica Acta, v. 56, pp. 3133-3156.

Schürmann, E., 1888, Uber die Verwandtschaft der Schwermetalle zum Schwefel: Justis Liebig's Annalen der Chemie, v. 249, p. 326–350.

Schwartz, G.M., 1934, Paragenesis of the oxidized ores of copper: Economic Geology: v. 29, pp. 55-75.

Schwertmann, U., 1965, Zur Goethite und Hämatitbildung amorpher Eisen (III), hydroxyde: Zeitschr. Pflanzenernährung, Dunung Bodenkunde, v. 108, pp. 37-45.

Selvin, P.C., Watanabe, S., Ayala-Arenas, J.S., 2001, Thermoluminescence and electron paramagnetic resonance (EPR) studies of mineral chrysocolla (dioptase): Radiation Physics and Chemistry, v. 61., pp. 531-533.

Sikka, D.B., Petruk, W., Nehru, C.E., and Zhang, Z., 1991, Ore Geology Reviews, v. 6. pp. 257-290.

Sillitoe, R.H., Mortimer, C., and Clark, A.H., 1968, A chronology of landform evolution and supergene mineral alteration, southern Atacama Desert, Chile: Transactions of the Institution of Mining and Metallurgy (section B: Applied Earth Sciences), v. 77, pp. B166-169.

Sillitoe, R.H., and Clark, A.H., 1969, Copper and copper-iron sulfides as the initial products of supergen oxidation, Copiapó mining district, northern Chile: The American Mineralogist, v. 54, pp. 1684-1710.

Sillitoe, R.H., Folk, R.L., and Saric N., 1996, Bacteria as mediators of copper sulfide enrichment during weathering: Science, News series, v. 272 (5265), pp. 1153-1155.

Sillitoe, R.H., and McKee, E.H., 1996, Age of supergene oxidation and enrichment in the Chilean Porphyry Copper Province: Economic Geology, v. 91, pp. 164-179.

Sillitoe, R.H., 2005, Supergene oxidized and enriched porphyry copper and related deposits: Economic Geology 100th Anniversary Volume, pp. 723-768.

Sillitoe, R.H., 2010, Porphyry copper systems: Economic Geology, v. 105, pp. 3-41.

Singer, P.C., and Stumm, W., 1970, Acid mine drainage: the rate-determining step: Science, v. 167, p. 1121-1123.

Smuda, J., Dold, B., Friese, K., Morgenstern, P., Glaesser, W., 2007. Mineralogical and geochemical study of element mobility at the sulfide-rich Excelsior waste rock dump from the polymetallic Zn-Pb-(Ag-Bi-Cu) deposit, Cerro de Pasco, Peru. Journal of Geochemical Exploration 92, 97-110.

Smuda J., Dold B., Spangenberg J.E., Friese K., Kobek M.R., Bustos C.A., Pfeifer H.-R., 2014. Element cycling during the transition from alkaline to acidic environment in an active porphyry copper tailings impoundment, Chuquicamata, Chile. Journal of Geochemical Exploration v. 140, pp. 23-40.

Sondag, F., 1981, Selective extraction procedures applied to geochemical prospecting in an area contaminated by old mine workings: Journal of Geochemical Exploration, v. 15, pp. 645-652.

Sun, M-S., 1963, The nature of chrysocolla from Inspiration Mine, Arizona: The american Mineralogist, v. 48, pp. 649-658.

Sun, M-S., Zhou, H., Glasby, G.P., Yang, Q., Yin, X., Li, J., and Chen, Z., 2012, Formation of Fe-Mn-Si oxide and nontronite deposits in hydrothermal fields on the Valu Fa Ridge, Lau Basin: Journal of Asian Earth Sciences, v. 43, pp. 64-76.

Tapia, M., Riquelme, R., Campos, E., Marquardt, C., Mpodozis, C., Mora, R., and Münschmeyer, C., 2015, Exotic Cu mineralization in the Centinela District: evolution and climatic change during the Neogene in the Atacama Desert (Northern Chile)

Throop, A.H., and Buseck, P.R., 1971, Nature and origin of black chrysocolla in the Inspiration MIne, Arizona: Economic Geology, v. 66, pp. 1168-1175.

Tomlinson, A., and Blanco, N.,1997, Structural evolution and displacement history of the West fault system, Precordillera, Chile: Part 1. Premineral, history. Part 2. Synmineral, history: Congreso Geológico Chileno, VIII, Antofagasta, v. III, p. 1873–1882.

Van Oosterwyck-Gastuche, M-C., 1970, La structure de la chrysocolle: Comptes rendus de l'académie des sciences, Paris, Série D, v. 271, pp. 1837-1840.

Vaughan,D.J. and Craig, J.R., 1997 Sulfide ore mineral stabilities, morphologies, and intergrowth textures. In: Barnes, H.L. Geochemistry of hydrothermal ore deposits (3rd ed.), Wiley, New York, p. 367-434.

Vieillard, P., 2000, A new method for the prediction of Gibbs free energy of formation of hydrated clay minerals based on the electronegativity scale: Clays and Clay Minerals, v.48(4), pp. 459-473.

Whiteside, L.S., and Goble, R.J., 1986, Structural and compositional changes in copper sulphides during leaching and dissolution: Canadian Mineralogist, v. 24, pp. 247-258.

Xiao, W., Gammons, C.H., and Williams-Jones, A.E., 1998, Experimental study of copper(I) chloride complexing in hydrothermal solutions at 40 to 300°C and saturated water vapor pressure: Geochimica and Cosmochimica Acta, v. 62(17), pp. 2949-2964.

Yu, Q., Sasaki, K., Tanaka, K., Ohnuki, T., and Hirajima, T., 2012, Structural factors of biogenic birnessite produced by fungus *Paraconiothyrium* sp. WL-2 stran affecting sorption of Co^{2+}: Chemical Geology, v. 310-311, pp. 106-113.

Zentilli, M., Krogh, T., Maksaev, V., and Alpers, C., 1994, Uranium-lead dating of zircons from the Chuquicamata and La Escondida porphyry copper deposits, Chile: inherited zircon cores of Paleozoic age with Tertiary overgrowths. Comunicaciones, U.de Chile, (ISSN -0069-357X), v. 45, pp. 101-110.

Zentilli, M. and Maksaev, V., 1995, Metallogenetic model for the late Eocene - early Oligocene supergiant porphyry event, northern Chile (Invited paper): Proceedings of the Second Giant Ore Deposits Workshop, Queen's University, Kingston, Ontario, April 22-27, 1995, 2nd Printing, 152-165.

Zentilli, M., Boric, R., Heaman, L., Mathur, R., and Hanley, J., 2015, New developments on the geology of MMH: is it the "missing half" of Chuquicamata?: Extended abstract, SIM2 Exploración andina: nuevos hallazgos y actualizaciones, 14th Chilean Congress, La Serena, Chile.

Chapter 3

Reported "supergene" sphalerite rims at the Chuquicamata porphyry deposit (northern Chile) revisited: evidence for a hypogene origin

Marie-Caroline Pinget M.[1]

Department of Earth Sciences, University of Geneva, rue de Maraîchers 13, Geneva, Switzerland

Bernhard Dold

SUMIRCO (Bernhard Dold Sustainable Mining Research & Consult .EIRL), Casilla 28, San Pedro de la Paz, Chile

Marcos Zentilli

Department of Earth Sciences, Dalhousie University, 1355 Oxford Street Halifax, NS, Canada

Lluís Fontboté

Department of Earth Sciences, University of Geneva, rue de Maraîchers 13, Geneva, Switzerland

[1] Corresponding author: marie-caroline.pinget@unige.ch

Chapter pubished as:

Pinget M., M.-C., Dold, B., Zentilli, M., and Fontboté, L., 2015, Reported "supergene" sphalerite rims at the Chuquicamata porphyry deposit (northern Chile) revisited: evidence for a hypogene origin: Economic Geology, v. 110, pp. 253–262

Economic Geology, v. 110, pp. 253–262

REPORTED SUPERGENE SPHALERITE RIMS AT THE CHUQUICAMATA PORPHYRY DEPOSIT (NORTHERN CHILE) REVISITED: EVIDENCE FOR A HYPOGENE ORIGIN

Marie-Caroline Pinget M.,[1,†] Bernhard Dold,[2] Marcos Zentilli,[3] and Lluís Fontboté[1]

[1] *Department of Earth Sciences, University of Geneva, rue de Maraîchers 13, Geneva CH 1205, Switzerland*

[2] *SUMIRCO (Bernhard Dold Sustainable Mining Research and Consulting.EIRL), Casilla 28, San Pedro de la Paz 413000, Biobio, Chile*

[3] *Department of Earth Sciences, Dalhousie University, 1355 Oxford Street Halifax, Nova Scotia B3P 2G2, Canada*

Abstract

Previous studies attributed a supergene origin to sphalerite rimming copper minerals occurring in Chuquicamata in a mineral assemblage including typically chalcocite-digenite ($Cu_{1.85}S_{1.12}$ and $Cu_{1.99}S_{1.01}$), covellite (CuS and $Cu_{1.08}S_{0.92}$), and sphalerite (up to 1.2 wt % Fe). Microscopic observations on samples from a central and a southern section, completed by scanning electronic microscope (SEM) backscattering electron imaging and electron microprobe analyses, suggest that all sphalerite in Chuquicamata is hypogene. A scenario, backed by observations in each step, that explains the formation of the peculiar "sphalerite rims" is the following: (1) precipitation of chalcopyrite, typical of the early and main hydrothermal stages; (2) precipitation of sphalerite rimming chalcopyrite and in voids and in weakness sites during the late hydrothermal stage; (3) partial or total replacement of chalcopyrite by chalcocite-digenite during the late hydrothermal stage; and (4) formation of lamellar covellite, principally at the expense of chalcopyrite, suggesting increasingly oxidizing and/or acidic conditions. This covellite may be linked to supergene processes and/or to the late hydrothermal stage. The findings of the present work have implications for the position of the lower limit of the supergene enrichment in the eastern-southern part of the deposit, as the sphalerite rims, now interpreted as hypogene, were the only potential supergene sulfide in the eastern vertical section of the southern section.

Introduction

Moderate amounts of zinc ranging from a background value of 0.010 wt % to an average value in the northern Zn-rich area of 0.17 wt % (Aracena et al., 1997) occur mainly as sphalerite in the Chuquicamata porphyry deposit. The complex intergrowth textures between copper sulfides and sphalerite have occasionally reduced the efficiency of sulfide separation by flotation, and in addition, the presence of zinc caused serious problems during flash smelting as volatized zinc might condensate in the furnace duct walls (Aracena et al., 1997). Previous workers (Aracena et al., 1997; Ossandón et al., 2001) interpreted part of the sphalerite to be clearly hypogene and part as tentatively supergene. An unpublished report to CODELCO (M.C. Graves and M. Zentilli, writ. commun., 1995), however, expressed reservations about the supergene origin of sphalerite.

Within the framework of supergene and exotic mineralization at Chuquicamata (Pinget et al., 2011, 2012), this question has been reexamined and certain sphalerite rims previously used as the main argument for a supergene origin have been studied in detail. The aim was to elucidate whether part of the sphalerite at Chuquicamata could be added to the very short list of sphalerite global occurrences interpreted to be supergene or if it was rather part of a high sulfidation mineral assemblage produced during a late hydrothermal stage (Ossandón et al., 2001, Fig. 1). For this purpose, 93 samples located in three east-west sections in the northern, central, and southern parts of the deposit were microscopically described. These textural observations were completed with scanning electron microscope (SEM) backscattered electron imaging, and electron microprobe analyses.

† Corresponding author: e-mail, marie-caroline.pinget@unige.ch

Geologic Setting

The Chuquicamata porphyry copper deposit is part of the Eocene metallogenic belt located in the southern Peru and northern Chile. The Cu-Mo mineralization occurs mainly in the Chuquicamata Intrusive Complex, which extends from south of the Chuquicamata deposit to north of the Radomiro Tomic deposit (~14 km) with a north-northeast orientation (Ossandón et al., 2001; Rivera et al., 2012). The granodioritic East porphyry (35.2 ± 0.4 Ma SHRIMP zircon U-Pb, Campbell et al., 2006; 34.6 ± 0.2 Ma LA-ICP-MS U/Pb zircon, Ballard et al., 2001) is the largest and is cut by small bodies of the West, Banco, and Fino porphyries (ages from 33.1–34.1 Ma, SHRIMP and LA-ICP-MS U/Pb ziron, Campbell et al., 2006; Ballard et al., 2001). Most of the Cu has been introduced during potassic alteration (~35–34 Ma, $^{40}Ar/^{39}Ar$, Rivera et al., 2012), after the East porphyry emplacement and after the emplacement of most of the smaller porphyries of the complex. Ossandón et al. (2001) referred to this mineralization event as the early hydrothermal stage, characterized by chalcopyrite-bornite with little pyrite in rocks affected by potassic alteration. The early hydrothermal stage of Ossandón et al. (2001) also includes minor chalcopyrite-pyrite mineralization in the outer chloritic alteration zone. Locally, higher Cu grades are associated with intense potassic alteration (Rivera et al., 2012). Molybdenite with an Re/Os age of 32 ± 0.2 Ma (Mathur et al., 2001) occurs in quartz-molybdenite veins that were defined as the quartz-molybdenite stage by Ossandón et al. (2001).

Quartz-sericite-pyrite hydrothermal alteration halos along D veins containing pyrite and chalcopyrite form the main copper sulfide that overprints potassic alteration in the central part of the deposit. Mainly within a zone immediately east

Submitted: September 5, 2013
Accepted: April 2, 2014

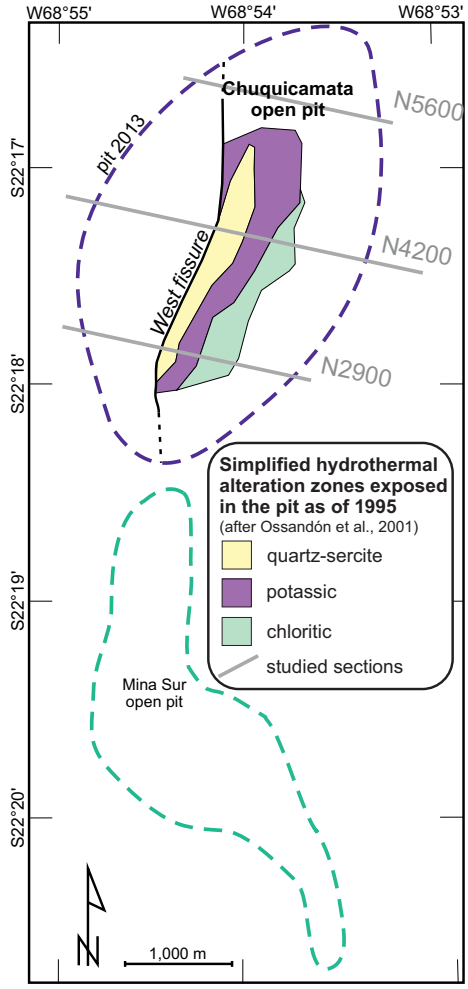

FIG. 1. Location of the sections used to describe the sphalerite in the Chuquicamata porphyry deposit.

of the West Fissure (Fig. 2), advanced argillic alteration is developed as inner halos in pyritic veins with quartz-sericite-pyrite selvages, and in part it is pervasive (Rivera et al., 2012). Coarse-grained alunite is reported by Ossandón et al. (2001), however, only traces of pyrophyllite are reported. The sulfide assemblages noted above are overprinted by high sulfidation mineral assemblages including pyrite-bornite ± enargite, chalcocite-pyrite ± enargite, and covellite-pyrite ± enargite. Sphalerite commonly occurs together with enargite or covellite-digenite-pyrite (Ossandón et al., 2001; Rivera et al., 2012).

A distinct late hydrothermal stage containing relatively high amounts of sphalerite is characterized by Cu-bearing sulfides veinlets containing red hematite, anhydrite, and very little or no pyrite (Ossandón et al., 2001; Rivera et al., 2012). The typical mineral assemblages attributed to this stage include covellite-digenite (Ossandón et al., 2001) in combination with chalcopyrite, bornite, digenite and/or covellite (Rivera et al., 2012). Low Fe sphalerite (up to 1.2 wt %, Aracena et al., 1997; Ossandón et al., 2001; this work) is commonly included in these assemblages.

Descriptions of supergene alteration and enrichment at the porphyry copper deposit of Chuquicamata were provided by Bandy (1938), López (1939), and Jarrell (1944). Ossandón et al. (2001), in their general description of the deposit, summarized also the main available data on supergene processes. According to Ossandón et al. (2001), the principal supergene sulfides are chalcocite and covellite.

Sampling and Methodology

A significant part of the supergene alteration profile of the Chuquicamata deposit has been removed during its long exploitation. The present study could be undertaken thanks to a complete and well-documented collection of samples taken in the period from 1970 to 1990 that is preserved at the mine site.

Three vertical sections oriented approximately east-west were chosen in the north, central, and south part of the Chuquicamata open pit (Fig. 1). In each section, polished samples were described (30 from section N5600, 38 from section N4200, and 25 from section N2900). Only one sample containing sphalerite was observed among the samples from the northern section and, therefore, the present study focuses on the two other sections (N2900 and N4200). In each one a western and an eastern vertical sequence have been sampled (Table 1). The samples cover a wide range of supergene leaching and enrichment stages as well as hydrothermal alteration. Figure 2A shows the locations of the samples containing sphalerite of these two sections.

The western depth sequence in both sections is mostly located in the quartz-sericite-pyrite alteration zone, and the

TABLE 1. Location of the Samples Described in This Study

Drill hole	Depth (m)	Hydrothermal alteration	Section	Vertical sequence	Sphalerite texture
CHDD2779	135	PIR	N2900	West	Sl as grains with cp
CHDD1539	208	CMH	N2900	East	Sl as rims
CHDD2249	168	CMH	N2900	East	Sl as rims
CHDD2249	190	CMH	N2900	East	Sl as rims
CHDD2249	216	CMH	N2900	East	Sl as rims
CHDD1652	454	PI	N4200	West	Sl as grains into dg
CHDD2319	338	PI	N4200	West	Sl as grains into dg
CHDD2319	393	PI	N4200	West	Sl as grains into dg
CHDD1247	10	PF	N4200	East	Sl as rims
CHDD1226	120.1	PF	N4200	East	Sl as rims
CHDD2313	122	PF	N4200	East	Sl as rims

Notes: Abbreviations: CMH = chloritic alteration, cp = chalcopyrite, dg = digenite, PF = background of potassic alteration, PI = intense potassic alteration, PIR = intense residual potassic ateration, Sl = sphalerite

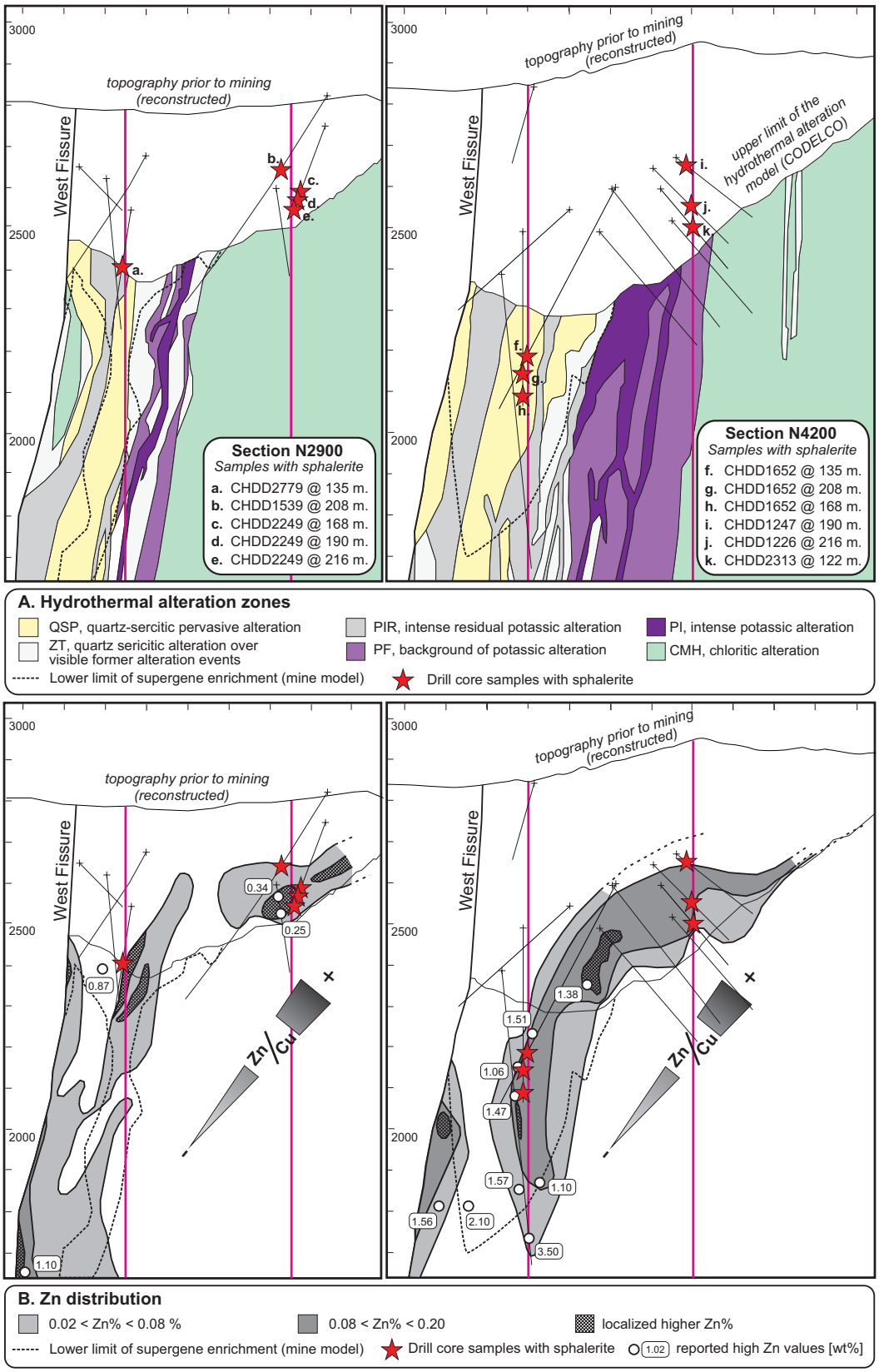

FIG. 2. Studied sections and location of the samples containing sphalerite. A. Hydrothermal alteration from mine model. B. Zn abundance data (in wt %) from CODELCO, Division Norte. The arrow Zn illustrates an estimation based on petrographic observations showing that Zn/Cu ratios in the late hydrothermal stage are clearly higher in the eastern than in the western part (° for the estimation, only Cu-bearing minerals formed in the late hydrothermal stage have been considered).

eastern depth sequence in the chloritic alteration zone. Sphalerite is more abundant near the surface and in the eastern part of the deposit compared to deeper areas and the western part (Fig. 2A).

The samples with presence of sphalerite were described in polished section and SEM backscattered electron imaging (BSE). Electron microprobe analyses were undertaken to complete the textural observations (analytical parameters and results in Table 2). These analyses were supplemented by electron microprobe unpublished data presented in a written report to CODELCO (M.C. Graves and M. Zentilli, writ. commun., 1995). The microprobe analyses were used to quantify amounts of trace elements that are potentially characteristic of the various types of sphalerite. The following elements were analyzed: S, Mn, Fe, Cu, Zn, Se, Ag, Cd. Figure 3 shows the analyzed samples and the location of the analyses. The grains analyzed have been selected to be representative of all the observed textures of the sphalerite, and in the case of the rims, to be from the widest rims.

Results

In the studied sections and vertical sequences, sphalerite occurs together with chalcocite-digenite (electron microprobe gives compositions between $Cu_{1.85}S_{1.12}$ and $Cu_{1.99}S_{1.01}$) and covellite (composition between CuS and $Cu_{1.08}S_{0.92}$) of the late hydrothermal stage (Ossandón et al., 2001). In places these copper minerals replace chalcopyrite and pyrite of the previous stages.

The occurrence of relatively high zinc values in the porphyry copper deposit of Chuquicamata is well known (Aracena et

Table 2. Compositions of Sulfides by Electron Microprobe

Sample	Mineral	Texture	No.	S (wt %)	Fe (wt %)	Cu (wt %)	Zn (wt %)	Ag (wt %)	Cd (wt %)	As (wt %)	Te (wt %)	Total
1226@120m	sl	2	10	31.1	0.23	11.3	56.5	0.112	0.089	--	--	99.0
1226@120m	sl	2	11	31.4	0.260	12.2	55.7	0.100	<	--	--	99.6
1226@120m	sl	2	12	31.9	0.528	10.1	57.3	0.103	<	--	--	99.9
1226@120m	sl	2	13	31.8	0.275	9.2	57.7	0.122	<	--	--	99.1
1226@120m	cc-dg	-	37	22.6	0.718	76.4	--	<	--	<	<	99.7
1226@120m	cc-dg	-	38	22.5	0.545	76.6	--	<	--	<	<	99.6
1226@120m	cv	-	39	30.3	0.756	68.8	--	0.063	--	<	<	99.8
1247@9.9m	sl	2	2	32.1	0.490	7.28	59.4	<	<	--	--	99.3
1247@9.9m	sl	2	3	32.1	n.d	7.97	60.1	<	0.104	--	--	100.3
1247@9.9m	sl	2	4	31.9	0.140	11.3	56.1	0.069	0.185	--	--	99.8
1247@9.9m	sl	2	5	31.3	<	12.9	54.3	0.084	0.159	--	--	98.7
1247@9.9m	cv	-	31	33.2	<	66.4	--	<	--	<	<	99.6
1247@9.9m	cc-dg	-	32	23.1	<	77.3	--	0.062	--	<	<	100.4
2249@168m	sl	3	14	32.5	1.263	2.83	62.7	<	<	--	--	99.3
2249@168m	cc-dg	-	41	22.8	1.045	75.4	--	<	--	<	<	99.2
2319@338m	sl	1	6	32.8	0.111	1.39	66.2	<	0.086	--	--	100.6
2319@338m	sl	1	7	33.0	0.392	2.55	65.2	<	<	--	--	101.1
2319@338m	sl	1	8	32.9	0.074	1.73	66.3	<	<	--	--	101.0
2319@338m	sl	1	9	32.9	<	2.30	65.3	<	0.214	--	--	100.7
2319@338m	cc-dg	-	33	22.1	0.073	77.9	--	<	--	<	0.077	100.1
2319@338m	cv	-	34	33.3	0.135	67.0	--	<	--	<	<	100.5
2779@135m	sl	1	16	32.9	<	0.358	66.4	<	0.257	--	--	99.9
2779@135m	sl	1	17	32.5	0.150	0.128	67.5	<	0.282	--	--	100.5
2779@135m	sl	1	18	32.7	1.007	0.717	65.8	<	0.280	--	--	100.6
2779@135m	cv	-	44	32.9	0.206	65.7	--	<	--	<	<	98.8
1447@327.4 m	sl	2	*	30.1	0.12	11.7	54.0	--	--	0.25	--	96.6
1447@327.4 m	sl	2	*	31.3	0.22	8.10	60.1	--	--	<	--	99.7
1447@327.4 m	sl	2	*	31.4	0.55	7.02	61.2	--	--	0.15	--	100.3
1447@327.4 m	sl	2	*	32.7	0.15	2.56	65.2	--	--	0.28	--	101.3
1448@194.9 m	sl	3	*	31.9	1.27	2.69	62.9	--	--	0.18	--	99.0
1448@194.9 m	sl	3	*	32.9	0.22	1.28	67.0	--	--	0.27	--	100.6
1448@309.5 m	sl	1	*	32.5	1.02	<	67.6	--	--	<	--	101.1
1448@200.5 m	sl	3	*	32.6	1.41	2.15	67.1	--	--	0.19	--	103.4
1907@303.5m	sl	1	*	32.8	<	0.44	68.7	--	--	0.33	--	102.2
1946@234.6m	sl	1	*	32.6	<	<	67.4	--	--	0.19	--	100.2
1946@12.0m	sl	2	*	31.5	0.23	7.89	60.5	--	--	<	--	100.1
1946@12.0m	sl	2	*	31.8	<	6.88	62.7	--	--	<	--	101.5
2230@65.5m	sl	2	*	31.3	0.23	5.26	0.86	--	--	<	--	99.47
2230@65. m	sl	2	*	31.7	0.13	4.88	64.6	--	--	<	--	101.3
2230@65.5m	sl	2	*	31.5	0.15	8.8	60.4	--	--	<	--	100.8
2290@316.5m	sl	1	*	32.5	0.31	<	67.6	--	--	<	--	100.4

Notes: Results of the microprobe analyses (-- = not analyzed, < = below the determination limit, * = M.C. Graves and M. Zentilli, unpub. report for CODELCO); abbreviations: cc-dg = chalcocite-digenite, cv = covellite, sl = sphalerite; sphalerite: texture 1 = anhedral grains, texture 2 = rims on cc-dg, texture 3 = rims on cc-dg and cp; determination limits (this study) are: in sphalerite 0.065 wt % for Fe, 0.3 wt % for Se, 0.063 wt % for Ag, and 0.066 wt % for Cd; in Cu sulfides 0.063 wt % for Te and 0.45 wt % for As; Mn was analyzed in sphalerite, but was less than the determination limit (<DL), similarly, Se was <DL in all analyzed minerals; for this study: JEOL 8200 electron microprobe, beam current 20 nA, acceleration voltage 40 kV; for Graves and Zentilli: JEOL 733 electron microprobe, beam current 15 nA, acceleration voltage 15 kV

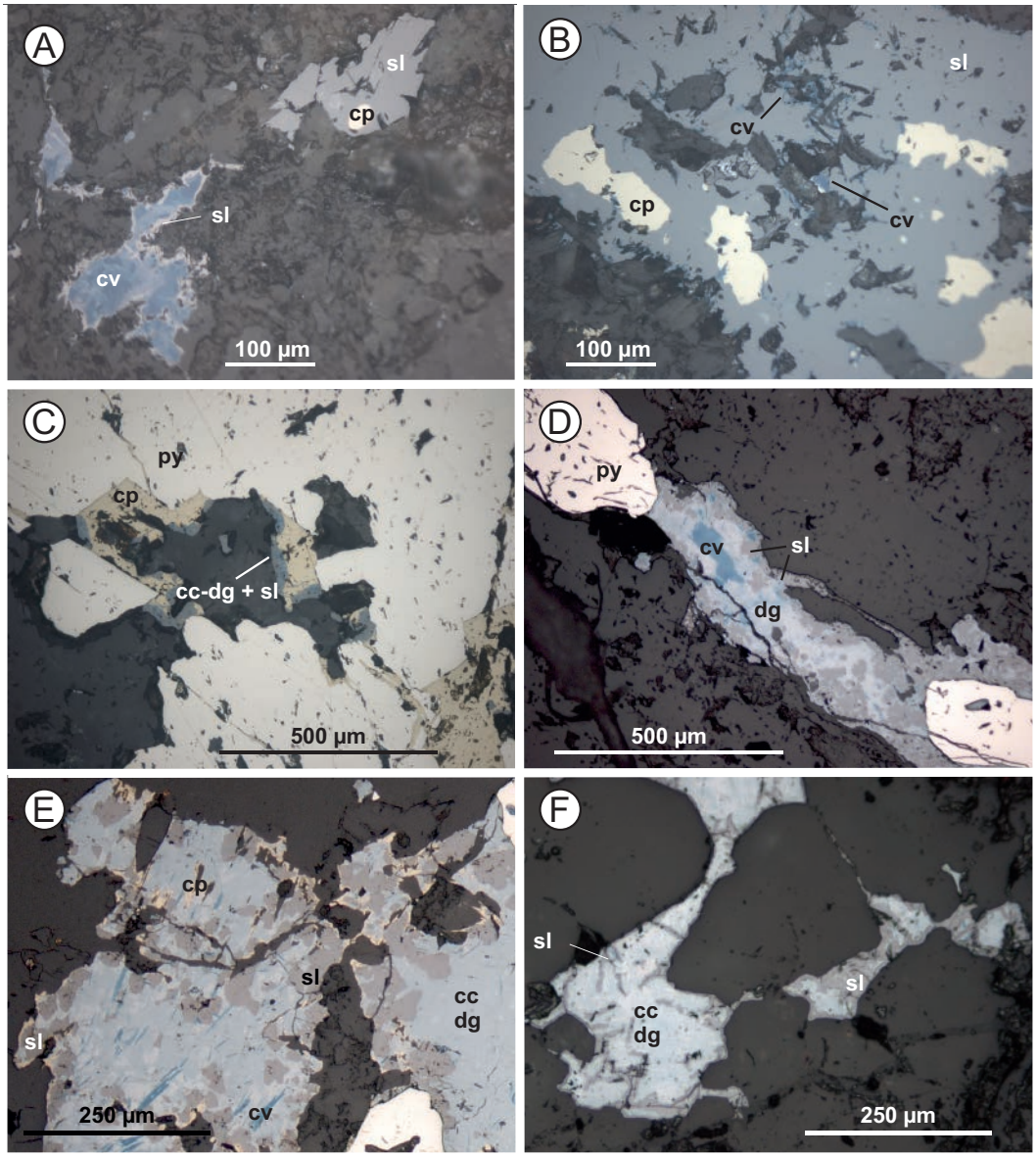

FIG. 3. Samples with microprobe analyses. A to E: Reflected light, plane-polarized. F: SEM backscattered electron imaging. EMPA spot analyses as numbered in Table 2. A. CHDD1226@12.0m. B. CHDD1247@9.9m. C. CHDD2319@338m. D. CHDD2249@168m. E. CHDD2779@135m. F. CHDD2779@135m, BSE view. Abbreviations: cp = chalcopyrite, cv = covellite, dg = digenite, py = pyrite, sl = sphalerite.

al., 1997; Ossandón et al., 2001). Figure 2B illustrates Zn values in sections N2900 and N4200, with isovalues at 0.08 and 0.20 wt %. In addition to areas with relatively high average zinc contents, drilling intervals have reported high zinc values up to several weight percent (Fig. 2B). In addition to the main Zn carrier sphalerite, microprobe analyses yield tennantite containing between 6.9 and 9.6% Zn in weight (Zentilli, unpub. data, 1994).

In the western part of the deposit (Fig. 2B), sphalerite is located deeper (below 2,300 m in section N4200 and below 2,400 m in section N2900) than in the eastern part, and the zinc isovalues delineate vertical shapes roughly parallel to the West Fissure. Sphalerite occurs mainly as anhedral grains (Figs. 3C, E-F, 4A-B, D-E), together with chalcocite-digenite, covellite, chalcopyrite, and pyrite.

In the eastern part of the deposit, zinc isovalues define horizontal shapes (above 2,500 m in section N2900 and above 2350 m in section N4200). Sphalerite is present at mineral boundaries, in fractures and/or in weakness sites mainly along crystallographic planes of chalcopyrite (with or without the presence of a blue copper sulfide at the contact between sphalerite and chalcopyrite, Figs. 3D, 4C) and as rims on and in fractures within chalcocite-digenite (Figs. 3A-B, 4F).

Sphalerite in the western vertical sequences

In the western vertical sequences of both N4200 and N2900 sections, sphalerite is principally present as anhedral grains. In section N4200, it occurs as complex intergrowths with digenite, chalcopyrite and covellite, disseminated or

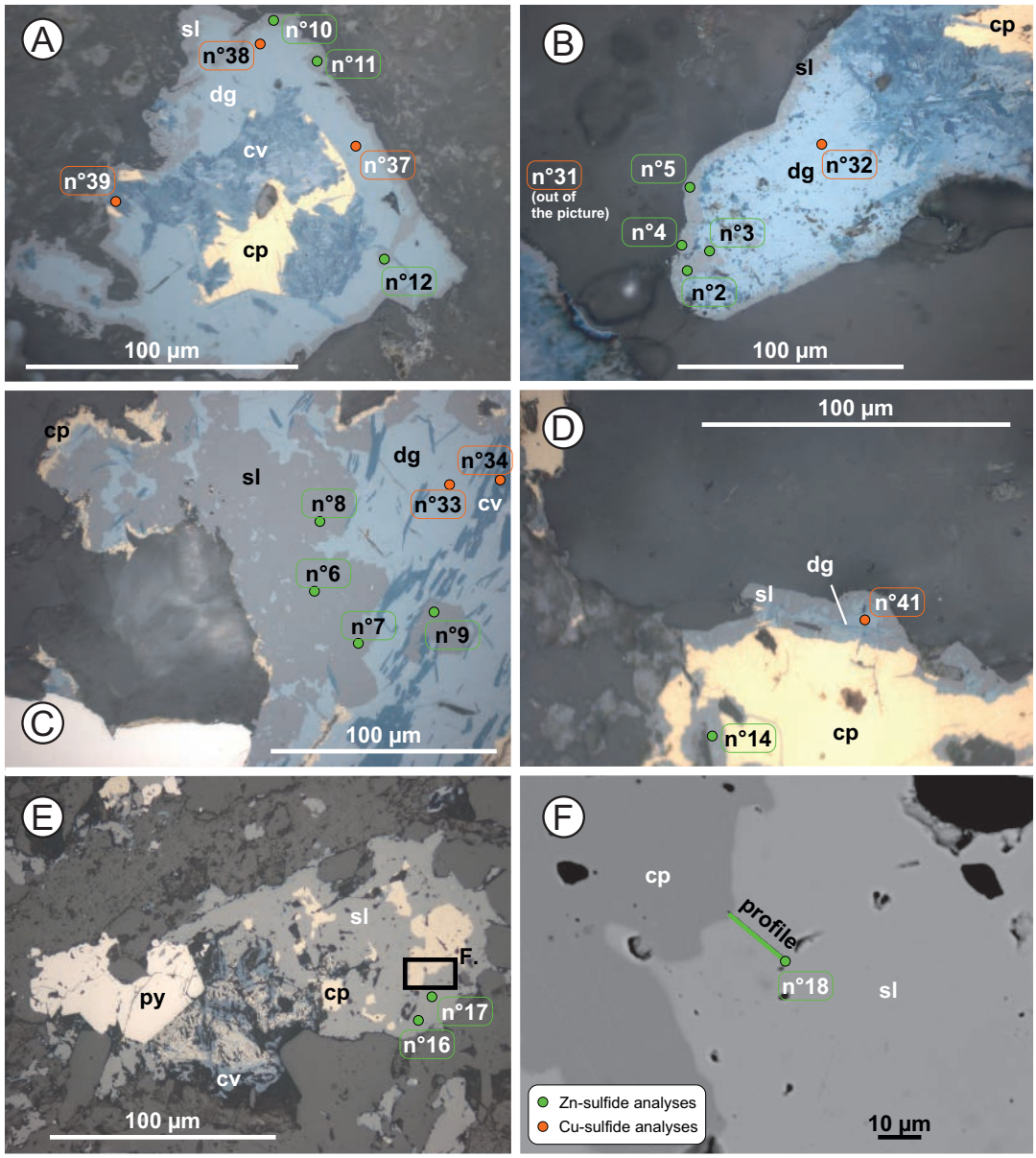

FIG. 4. Photomicrographs of sphalerite from sections N2900 and N4200, reflected light, plane-polarized. Abbreviations: cc = chalcocite, cp = chalcopyrite, cv = covellite, dg = digenite, py = pyrite, sl =sphalerite. A. CHDD2779@135.4m, sphalerite grain with relict chalcopyrite inclusion, covellite grain with sphalerite rim. B. CHDD2779@135.4m, sphalerite grain containing relict chalcopyrite inclusions. C. CHDD2249@190m, pyrite and chalcopyrite grains, chalcocite-digenite-covellite (inner part) and sphalerite (outer part) rimming the chalcopyrite. D. CHDD1652@454m, vein with relict rounded pyrite grains rimmed by covellite, chalcocite, and sphalerite. E. CHDD2319@338m, hypogene intergrowth of digenite, chalcocite, covellite, with sphalerite and chalcopyrite. F. CHDD1226@120m, chalcocite-digenite grains with rims of sphalerite.

in veinlets (Figs. 3C, 4D-E). In places, SEM-BSE imaging reveals fine inclusions of digenite in sphalerite (Fig. 5E-F). In section N2900, sphalerite occurs principally as large anhedral grains containing rounded chalcopyrite grains (Fig. 4A-B). Scanning electron microscope BSE imaging shows a sharp contact between chalcopyrite and sphalerite (Fig. 5D). In a few cases, sphalerite occurs as rims around covellite (Fig. 4A).

The microprobe analyses of anhedral grains of sphalerite (intergrown with digenite or in large grains containing chalcopyrite) reveal copper values from 0.15 to 2.55 wt %, iron values up to 0.39 wt % in the grains without associated chalcopyrite, and up to 1.50 wt % in grains intergrown with chalcopyrite (increasing iron approaching the chalcopyrite), and cadmium contents up to 0.28 wt % (not detected in all analyses). The variations of the chemical composition of sphalerite are principally the consequence of analytical limits (the ~2–5-μm-diam size of the electron beam does not allow avoiding inclusions of neighbor minerals or small inclusions of other minerals in the analysis). Local diffusion gradients between sphalerite and neighbors minerals (pyrite, chalcopyrite, digenite) could have an effect too, but cannot be assessed due to the grain-size issues.

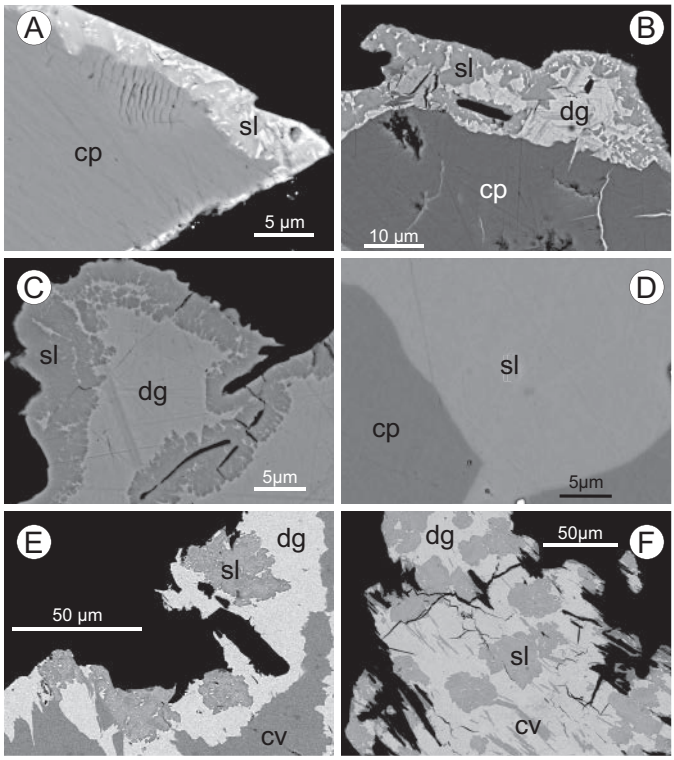

FIG. 5. SEM backscattered electron imaging. Thin sections (coated with an ultra-thin coating (ca. 10 nm) of carbon) were mounted on a conductive support (i.e., aluminum stub), prior to imaging with a Jeol JSM 7001F scanning electron microscope (15.0 kV, Department of Earth Sciences, University of Geneva, Switzerland). A. CHDD1539@208m, chalcopyrite with sphalerite rims. B. CHDD2249@168m, chalcopyrite with digenite-sphalertie rim. C. CHDD1226@120m, digenite with sphalerite rim. D. CHDD2119@135m, detail of the sphalerite-chalcopyrite contact. E. CHDD2319@393m, sphalerite and covellite grains into digenite. F. CHDD2319@338m, sphalerite and covellite grains into digenite. See Figure 4 caption for abbreviations.

Sphalerite in the eastern vertical sequences

In the eastern vertical sequences of both sections, the above-described textures were not observed. In the samples from section N2900, sphalerite is present at mineral boundaries, fractures and/or in weakness sites mainly along crystallographic planes in chalcopyrite, and a blue copper sulfide with $Cu_{1.89}S_{1.11}$ composition (presumably digenite) is almost always present between the sphalerite and chalcopyrite (Figs. 3D, 4C). In section N4200, sphalerite is present at mineral boundaries and other weakness sites of chalcocite-digenite (Figs. 3A-B, 4F). In some of these samples, chalcopyrite is present together with the chalcocite-digenite (Fig. 3A-B). In both sequences, digenite, chalcocite-digenite, and the presumed digenite ($Cu_{1.89}S_{1.11}$) are finely intergrown with covellite, in more or less significant proportions. In polished sections, sphalerite is observed as rims on anhedral grains of chalcopyrite or chalcocite-digenite.

The SEM-BSE imaging highlights different textures. The contact between digenite and the rimming sphalerite is complex (Fig. 5C): fingers of digenite penetrate sphalerite and relicts of sphalerite are present within the digenite near the principal contact. In the case of sphalerite rimming chalcopyrite, the contact is sharp (Fig. 5A). Finally, where there is digenite between the chalcopyrite grain and the sphalerite rim, the contact between sphalerite and digenite is complex, but the contact between chalcopyrite and digenite is sharp (Fig. 5B).

The microprobe analyses on sphalerite as rims on digenite (Table 2) yield higher copper values than those on sphalerite rims on chalcopyrite (from 1.95–10.09 wt %), lesser iron (from 0.55 wt % down to the determination limit), and frequently traces of silver (from 0.069–0.185 wt %). These analyses do not necessarily indicate the presence of these elements within the mineral structure of the sphalerite because the digenite and sphalerite present a complex contact with a fine mixture of both minerals and therefore the microprobe beam most likely included small grains of digenite as part of the sphalerite. In sample CHDD1226@120m, microprobe analyses on digenite do not report any silver, whereas on covellite they yield values up to 0.063 wt % silver. In sample CHDD1247@10m, microprobe analyses have a determined value of 0.062 wt % silver in digenite. It appears that the highest silver values are found in sphalerite analyses and probably are due to optically invisible inclusions of silver-rich minerals (Fig. 6), although they have not been described before for the late hydrotehrmal stage. Ossandón et al. (2001) reported only some tennantite attributed to the main hydrothermal stage.

Discussion and Conclusion

Anhedral grains of low iron sphalerite, occurring together with digenite and covellite in the western part of the studied sections, were attributed to the late hydrothermal stage (Ossandón et al., 2001). It is a plausible interpretation as several porphyry systems include late stages of intermediate to high sulfidation that contain chalcocite-digenite, covellite, and low iron sphalerite (e.g., Sillitoe, 2010, see also recompilation by Baumgartner et al., 2008, table 1). Sphalerite in the eastern part of the studied sections has similar low iron contents. In general, in the eastern part of the studied sections, there is a higher ratio of Zn over Cu in the late hydrothermal stage than in the western part (Fig. 2B), supporting the hypothesis that eastern sphalerite, essentially rims, belongs to a distal zone of the late hydrothermal stage. The high silver values found in microprobe analyses in the sphalerite rims from the western part of the studied sections suggest the presence of microinclusions of sulfosalts (presumably falhore) in the sphalerite, which is also consistent with interpretation as a distal zone of the late hydrothermal stage (Bendezú and Fontboté, 2009).

Nevertheless, owing to textural resemblance of the sphalerite rims with textures observed in copper minerals in the supergene enrichment environment, Aracena et al. (1997) proposed that these sphalerite "rings" around copper sulfides were supergene. Only in a few deposits supergene sphalerite has been mentioned. Lawrence and Rafter (1962, p. 219) reported "cryptocrystalline supergene sphalerite" that in part forms "stalagmitic concretions" and "cream colored masses" on "free surfaces" in the Broken Hill Ag-Pb-Zn deposit. Belogub et al. (2008), in VHMS-type deposits of South Urals, reported botryoidal supergene sphalerite, mostly at the borders of primary pyrite grains. Bawden et al. (2003, p. 914) reported in samples from the Mike Carlin-type gold deposit (Nevada) a "pale colored, micrograin (<1 μm), framboidal sphalerite," interpreted to have a biogenic origin. The

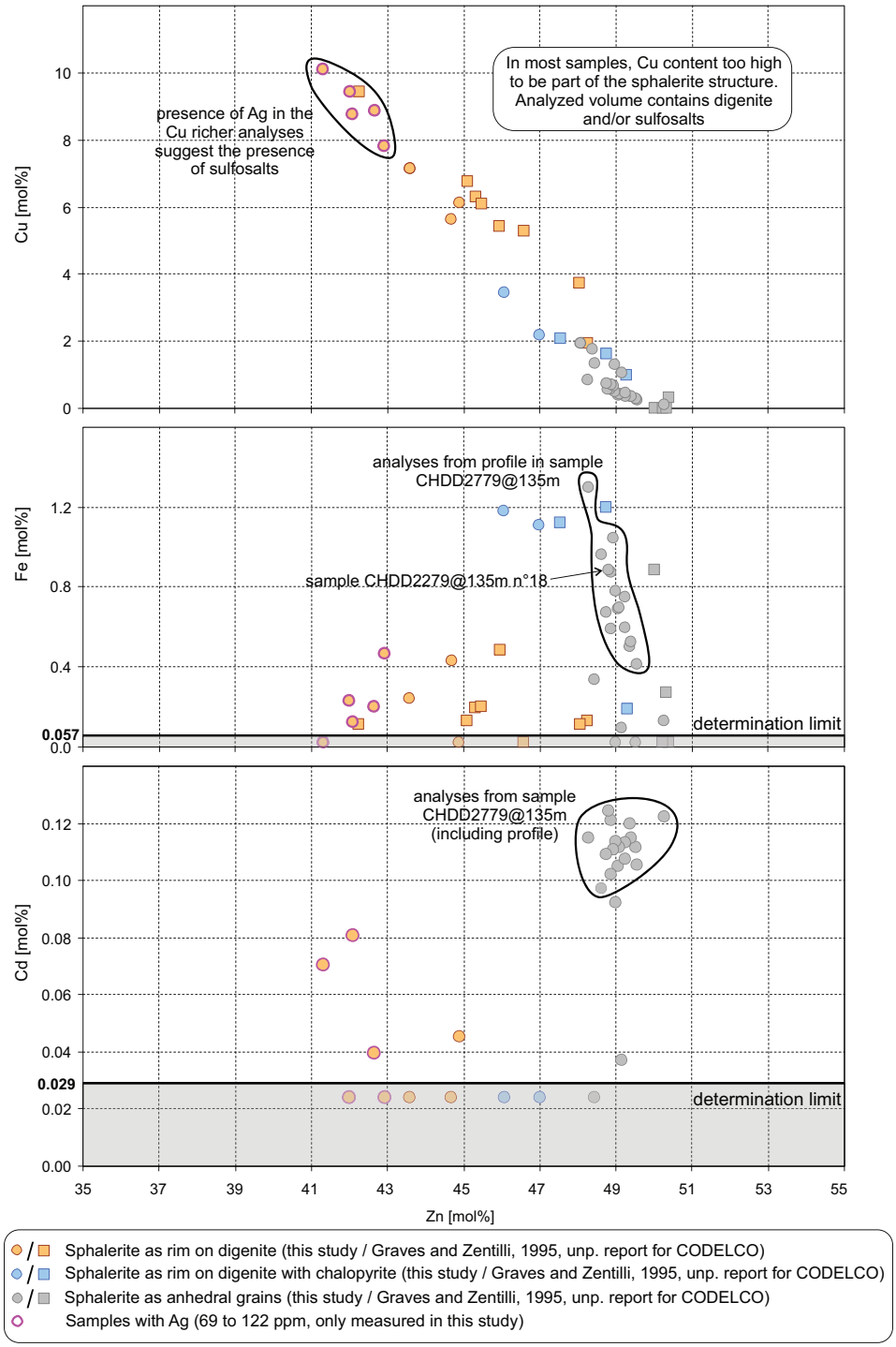

FIG. 6. Results of microprobe analyses on sphalerite. The circles are for the results of this study and the squares for the results of the study of Graves and Zentilli (writ. commun., 1995)

reported iron values for this framboidal sphalerite are low (0.35 to <0.1 mol %). Sillitoe (2005) mentioned "supergene sphalerite" at Chuquicamata on the basis of Aracena et al. (1997) and Ossandón et al. (2001) publications.

As illustrated by the figures presented in this work (e.g., Figs. 3A-B, 4C-F), the studied rims of sphalerite with all its typical optical properties do not correspond with the descriptions of the cryptocrystalline masses of sphalerite in Broken Hill interpreted to be supergene by Lawrence and Rafter (1962). In addition, comparison with the botryoidal sphalerite crusts of the Urals, at Chuquicamata sphalerite does not rim pyrite but chalcocite-digenite and chalcopyrite.

The fact that at Chuquicamata, sphalerite rims copper minerals is a key observation that makes unlikely the supergene

interpretation proposed previously (Aracena et al., 1997). Copper has a higher position into the electromotive Schürmann's series than zinc (Schürmann, 1888; Sillitoe, 2005) and under no circumstances, in the supergene environment, Zn would replace Cu into the sulfide structure.

In fact, the contrary process should be expected: that copper minerals replace the sphalerite. And this very process is the one that is compatible with the textures described in the present work.

A possible scenario to explain the sphalerite rims on chalcocite-digenite is presented in Figure 7A-D, all the steps of the sequence having been observed in the described samples.

The first step (Fig. 7A, step a) is the precipitation of chalcopyrite, typical of the early and main hydrothermal stages (Ossandón et al, 2001).

The second step (Fig. 7B, step b) corresponds to the late hydrothermal stage of Ossandón et al. (2001); sphalerite precipitates as rims on chalcopyrite and in voids, and also partly replaces chalcopyrite, mainly along fractures and crystallographic planes. This step is visible for instance in Figure 5A.

During the third step (Fig. 7C, step c) chalcopyrite is replaced by digenite, or by a chalcocite-digenite mixture with a fabric typical of hexagonal chalcocite (Fig. 8). Hexagonal chalcocite is stable at temperatures above 103°C and the digenite stability field disappears below 70°C (Vaughan and Craig, 1997), i.e., these findings are not consistent with supergene processes. In contrast, these minerals are typical for the late hydrothermal stage of Ossandón et al. (2001). The replacement of chalcopyrite by digenite may be total (Fig. 5C) or principally concentrated at the contact between chalcopyrite and sphalerite (Fig. 5B). This observation suggests that the contact between both minerals provides favorable sites to initiate the replacement process. Digenite and chalcocite-digenite not only replace chalcopyrite but also the sphalerite rims (Fig. 5B-C).

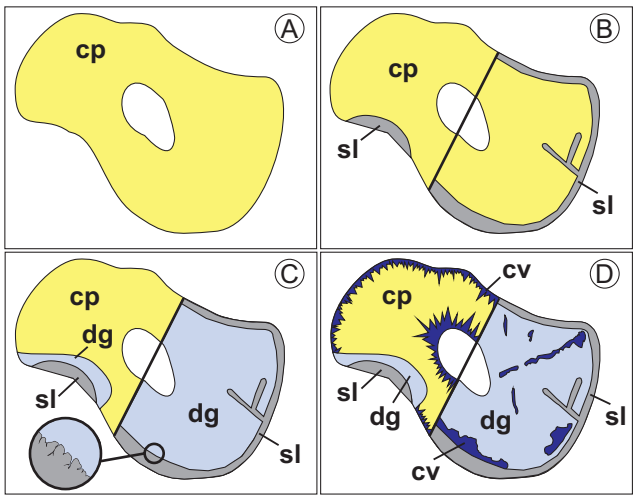

FIG. 7. Possible sequence of events to obtain textures similar to those observed in the sphalerite rims on digenite or chalcopyrite-digenite grains. A. Hypogene grain of chalcopyrite. B. Precipitaton of late hydrothermal sphalerite on the borders, in cracks, and replacing weakness sites mainly along crystallographic planes. C. Partial (left) or complete (right) (late hydrothermal?) replacement of chalcopyrite by digenite ± chalcocite. In places, digenite may also replace sphalerite. D. Supergene replacement of chalcopyrite by lamellar covellite. See Figure 4 caption for abbreviations.

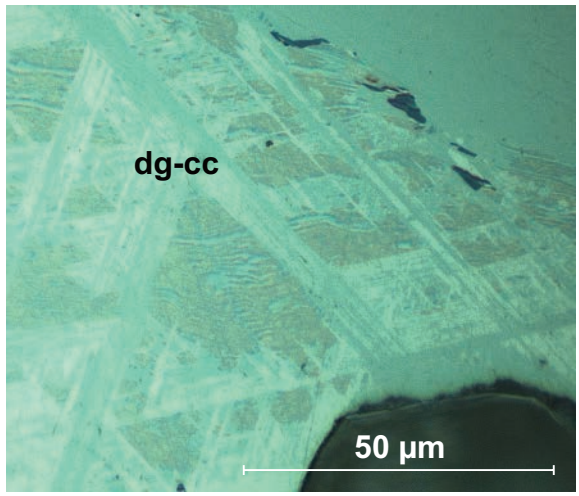

FIG. 8. Photomicrograph of digenite (dg)-chalcocite (cc) intergrowth, reflected light, plane-polarized (CHDD1226@120.1m).

Finally, during a fourth step (Fig. 7D step d) lamellar covellite is formed, principally at the expense of chalcopyrite, in places replacing digenite and suggesting increasingly oxidizing and/or acidic conditions (Sato, 1992). This covellite may be linked to supergene processes although a hypogene process during the late hydrothermal stage cannot be excluded, at least in certain cases.

In summary, the sequence step a to step b to step c explains the formation of sphalerite rims previously interpreted as formed by the supergene replacement of digenite and chalcocite-digenite. Rather, the observations presented here indicate that these copper minerals replace sphalerite. Moreover, the observations made in the present work suggest that the rims record a complex process, i.e., initial sphalerite precipitaton (and maybe partially replacing) atop the chalcopyrite during the early hydrothermal stage, and subsequently during the late hydrothermal stage digenite-chalcocite as replacements of both remaining chalcopyrite and sphalerite rims, preferentially along the contact between both minerals.

The new interpretation that the sphalerite rims are hypogene has implications for the position of the lower limit of the supergene enrichment in the southeastern part of the deposit because previously the sphalerite rims were the only potential supergene sulfide in the eastern vertical section of section N2900." It appears that no supergene sulfide enrichment was developed in this area, which is consistent with the flux direction of supergene waters forming the exotic deposit (e.g, Münchmeyer, 1996; Rivera et al., 2012) and the fact that hypogene mineralization was weaker in the southeastern part than in the western and northern parts. For the eastern part of the deposit 1,300 m more to the north (section N4200) and the western part of both sections, where abundant evidence of supergene enrichment exist, the results of the present work do not change the position of the lower limit of the supergene sulfide enrichment.

Acknowledgments

The careful review by John Dilles has improved this manuscript. The constructive collaboration with the geologic team of the Chuquicamata mine made this work possible. We thank

A. Martigner for the SEM analyses, K. Kouzmanov for the microprobe analyses, and J.-M. Boccard for the technical support, University of Geneva, Switzerland. The project was financed by the Swiss National Science Foundation Project FN129988.

REFERENCES

Aracena, I., Ossandón, G., and Zentilli, M., 1997, Mineralogía y distribución del zinc en Chuquicamata: Enriquecimiento supérgeno de zinc?: Congreso Geológico Chileno, VIII, Antofagasta, p. 1908–1912.

Ballard, J.R, Palin, J.M, Williams, I.S., Campbell, I.H., and Faunes A., 2001, Two ages of porphyry intrusion resolved for super-giant Chuquicamata copper deposit of northern Chile by ELA-ICP-MS: Geology, v. 29, p. 383–386.

Bandy, M.C., 1938, Mineralogy of three sulphate deposits of northern Chile: Journal of the Mineralogical Society of America, v. 3, p. 669–760.

Baumgartner, R., Fontboté, L., and Vennemann, T., 2008, Mineral zoning and geochemistry of epithermal polymetallic Zn-Pb-Ag-Cu-Bi mineralization at Cerro de Pasco, Peru: Economic Geology, v. 103, p. 493–537.

Bawden, T.M., Einaudi, M.T., Bostick, B.C., Meibom, A., Wooden, J., Norby, J.W., Orobona, M.J.T., and Chamberlain, C.P., 2003, Extreme ^{34}S depletions in ZnS at the Mike gold deposit, Carlin Trend, Nevada: Evidence for bacteriogenic supergene sphalerite: Geology, v. 31, p. 913–916.

Belogub, E.V., Novoselov, K.A., Yakovleva, V.A., and Spiro, B., 2008, Supergene sulphides and related minerals in the supergene profiles of VHMS deposits from the South Urals: Ore Geology Review, v. 33, p. 239–254.

Bendezu, R., and Fontboté, L., 2009, Cordilleran epithermal Cu-Zn-Pb-(Au-Ag) mineralization in the Colquijirca district, Central Peru: Deposit-scale mineralogical patterns: Economic Geology, v. 104, p. 905–944.

Campbell, I.H., Ballard, J.R., Palin, J.M., Allen, C., and Faunes, A., 2006, U-Pb zircon geochronology of granitic rocks from the Chuquicamata-El Abra porphyry copper belt of northern Chile: Excimer laser ablation ICP-MS analysis: Economic Geology, v. 101, p. 1327–1344.

Jarrell, O.W., 1944, Oxidation at Chuquicamata, Chile: Economic Geology, v. 39, p. 251–286.

Lawrence, L.J., and Rafter, T.A., 1962, Sulfur isotope distribution in sulfides and sulfates from Broken Hill South, New South Wales: Economic Geology, v. 57, p. 217–225.

López, V.M., 1939, The primary mineralization at Chuquicamata, Chile, S.A.: Economic Geology, v. 34, p. 674–711.

Mathur, R., Ruiz, J., and Munizaga, F., 2000, Relationship between copper tonnage of Chilean base metal porphyry deposits and Os isotope ratios: Geology, v. 28, p. 555–558.

Münchmeyer, C., 1996, Exotic deposits—products of lateral migration of supergene solutions from porphyry copper deposits: Society of Economic Geologists Special Publication 5, p. 43–58.

Ossandón, G., Fréraut, R., Gustafson, L.B., Lindsay, D.D., and Zentilli, M., 2001, Geology of the Chuquicamata mine: A progress report: Economic Geology, v. 96, p. 351–366.

Pinget, M.C., Fontboté, L., Dold, B., Ramirez, F., and Vergara, M., 2011, The supergene enrichment at Chuquicamata revisited: SGA Biennal Meeting, 11th, Antofagasta, Proceedings, p. 823–825.

Pinget, M.C., Dold, B., Fontboté, L., Vergara, M., and Rojas de la Rivera, J., 2012, Mineralogía de la mineralización exótica en Chuquicamata: nuevos avances: Congreso Geológico Chileno, 13th, Antofagasta, Proceedings, p. 37–39.

Rivera, S.L., Alcota, H., Proffett, J., Díaz, J., Leiva, G., and Vergara, M., 2012, Update of the geologic setting and porphyry Cu-Mo deposits of the Chuquicamata district, northern Chile: Society of Economic Geologists Special Publication 16, p. 19–54.

Sato, M., 1992, Persistency-field Eh-pH diagrams for sulfides and their application to supergene oxidation and enrichment of sulfide ore bodies: Geochimica et Cosmochimica Acta, v. 56, p. 3133–3156.

Schürmann, E., 1888, Uber die Verwandtschaft der Schwermetalle zum Schwefel: Justis Liebig's Annalen der Chemie, v. 249, p. 326–350.

Sillitoe, R.H., 2005, Supergene oxidized and enriched porphyry copper related deposits: Economic Geology 100th Anniversary Volume, p. 723–768.

——2010, Porphyry copper systems: Economic Geology, v. 105, p. 3–41.

Vaughan, D., and Craig, J., 1997, Sulfide ore mineral stabilities, morphologies and intergrowth textures, *in* Barnes, H.L., ed., Geochemistry of hydrothermal ore deposits, 3rd ed.: New York, Wiley, p. 367–434.

Annex 2.1

Mine wall samples (CODELCO collection)	East	North	altitude
	(local coordinates)		[m]
CH2833	4265	5561	2914
CH3848	3870	4400	2842
CH3852	3870	4340	2842
CH3869	3833	4078	2842
CH3870	3835	4085	2842
CH3910	3194	4467	2842
CH3923	3156	4353	2842
CH3934	3458	4005	2758
CH3936	3459	4033	2758
CH3937	3460	4075	2758
CH3939	3459	4140	2758
CH3949	3459	4234	2758
CH3951	3459	4316	2758
CH3952	3460	4344	2758
CH3954	3460	4398	2758
CH3956	3294	2817	2758
CH3978	3317	2920	2758
CH3984	3280	4243	2842
CH4004	3360	2878	2758
CH4007	3355	2860	2758
CH4035	3582	3069	2758
CH5737	3672	5548	2842
CH5785	3615	4473	2658
CH5786	3600	4468	2658
CH5787	3592	4468	2658
CH5795	3312	4492	2746
CH5805	3468	4388	2684
CH5849	3673	4370	2684
CH5857	4074	5580	2842
CH5866	3776	4250	2746
CH5867	3773	4226	2746
CH5929	3433	4490	2697
CH5985	3691	4414	2684
CH5986	3686	4404	2684
CH6178	3960	5400	2794
CH6231	3192	4445	2794
CH6232	3210	4458	2794
CH6233	3213	4488	2794
CH6248	3624	4188	2697
CH6285	3377	4315	2710
CH6293	3330	4058	2710
CH6295	3330	4065	2710
CH6301	3612	4166	2697
CH6317	3599	4248	2684
CH6318	3593	4240	2684

Mine wall samples (CODELCO collection)	East	North	altitude
	(local coordinates)		[m]
CH6335	3545	4092	2684
CH6336	3540	4083	2684
CH6341	3535	4065	2684
CH6343	3516	4012	2684
CH6360	3600	4090	2697
CH6362	4145	4270	2794
CH6364	3147	4275	2794
CH6388	3743	4220	2722
CH6389	3743	4218	2722
CH6400	3725	4141	2722
CH6411	3722	4124	2722
CH6470	3594	4440	2658
CH6471	3566	4475	2658
CH6532	3588	4155	2684
CH6553	3175	4475	2794
CH6572	3695	4229	2710
CH6573	3695	4228	2710
CH6574	3695	4227	2710
CH6575	3695	4227	2710
CH6576	3695	4226	2710
CH6577	3695	4225	2710
CH6578	3695	4224	2710
CH6579	3695	4224	2710
CH6580	3694	4222	2710
CH6581	3694	4220	2710
CH6582	3694	4220	2710
CH6583	3694	4220	2710
CH6584	3694	4219	2710
CH6585	3694	4218	2710
CH6586	3694	4218	2710
CH6589	3695	4230	2710
CH6590	3695	4229	2710
CH6591	3695	4229	2710
CH6592	3695	4228	2710
CH6593	3695	4225	2710
CH6594	3694	4220	2710
CH6936	3297	4378	2746
CH6951	3262	4320	2710
CH6981	3727	4378	2697
CH6983	3720	4348	2697
CH6986	3707	4292	2697
CH6987	3688	4267	2697
CH6997	3660	4150	2697
CH7013	3735	4240	2710
CH7015	3727	4209	2710
CH7022	3723	4177	2710
CH7024	3720	4153	2710

Mine wall samples (CODELCO collection)	East	North	altitude
	(local coordinates)		[m]
CH7026	3724	4095	2710
CH7035	3698	4038	2710
CH7037	3698	4036	2710
CH7040	3694	4005	2710
CH7163	3556	4495	2645
CH7300	3415	4365	2684
CH7359	3650	4198	2684
CH7382	3415	4338	2684
CH7383	3415	4310	2684
CH7385	3414	4278	2684
CH7386	3414	4248	2684
CH7393	3413	4218	2684
CH7418	3423	3106	2710
CH7446	3530	4500	2645
CH7447	3528	4470	2645
CH7460	3366	4066	2697
CH7461	3364	4054	2697
CH7462	3360	4036	2697
CH7470	3350	4010	2697
CH7471	3368	4107	2697
CH7472	3367	4155	2697
CH7488	3492	4304	2658
CH7489	3488	4329	2658
CH7518	3274	4453	2746
CH7620	3577	4414	2645
CH7622	3610	4433	2645
CH7623	3615	4455	2645
CH7624	3624	4473	2645
CH7625	3626	4485	2645
CH8032	3515	4447	2645
CH8033	3515	4480	2645
CH8136	3405	4308	2684
CH8137	3400	4444	2684
CH8159	3352	3084	2710
CH8162	3305	3092	2710
CH8260	3533	4210	2658
CH8263	3532	4251	2658
CH8372	3383	4025	2684
CH8373	3388	4046	2684
CH8374	3392	4063	2684
CH8375	3395	4074	2684
CH8473	3403	4265	2684
CH8474	3403	4250	2684
CH8498	3367	4323	2697
CH8573	3349	4412	2697
CH8697	3505	4394	2645
CH8698	3505	4380	2645

Mine wall samples (CODELCO collection)	East	North	altitude
	(local coordinates)		[m]
CH8699	3506	4370	2645
CH8722	3368	4414	2697
CH8733	3368	4453	2697
CH8734	3369	4487	2697
CH8779	3554	4310	2645
CH8782	3570	4310	2645
CH8783	3600	4380	2645
CH8784	3600	4380	2645
CH8785	3600	4380	2645
CH8786	3600	4380	2645
CH8803	3350	4334	2697
CH8804	3350	4372	2697
CH8855	3546	4317	2697
CH8950	3510	4363	2645
CH8952	3350	4484	2697
CH8970	3387	4246	2684
CH8975	3307	3044	2710
CH9001	3511	4350	2645
CH9022	3444	4382	2658
CH9122	3524	4309	2645
CH9163	3358	4133	2684
CH9252	3490	4463	2645
CH9254	3491	4491	2645
CH9563	3459	4151	2619
CH9564	3456	4147	2619
CH9565	3455	4135	2619
CH9570	3371	4262	2658
CH9571	3370	4180	2658
CH9572	3371	4242	2658
CH9573	3371	4229	2658
CH9582	3356	4068	2658
CH9583	3350	4041	2658
CH9584	3345	4024	2658
CH9607	3343	4000	2645

Drill cores with polished sections (CODELCO collection)	East	North
	(local coordinates)	
135	3190	5000
143	3314	4200
148	3547	5600
226	3870	5597
249	3442	5600
301	3044	2900
305	3440	4196

Drill cores with polished sections (CODELCO collection)	East	North
	(local coordinates)	
438	3950	5570
446	3760	5607
753	3667	5590
975	3624	2938
1051	2816	6325
1064	3450	5550
1067	3450	5610
1068	3691	5650
1069	3450	5590
1070	3860	5675
1226	3603	4200
1234	3526	4200
1244	3543	4150
1247	3660	4200
1414	3721	5567
1539	3538	2850
1541	3314	2851
1582	3239	2960
1598	3742	4150
1599	3340	5650
1604	3504	4152
1652	3511	4250
1698	3399	4250
1721	3601	5598
1727	3699	5647
1775	3439	5530
1823	3799	5591
1828	3846	4199
1829	3915	5526
1833	3837	4200
1885	3647	5550
1889	3100	2871
1910	3520	5600
1919	3559	4200
1951	3858	5670
1985	4096	5600
1992	3969	5550
2011	2937	2952
2213	3280	4200
2249	3533	2952
2300	4008	5663
2313	3624	4149
2319	3287	4199
2329	3698	5557
2330	4073	5650
2369	3474	4201
2504	3524	4200

Drill cores with polished sections (CODELCO collection)	East	North
	(local coordinates)	
2594	3004	2904
2638	3284	5649
2695	3078	2940
2696	3034	2942
2709	3374	4253
2778	3011	2942
2779	3065	2950
2813	3503	4250
2912	3273	4200
2925	3368	4200
2999	3329	4200
3446	3236	4200
3813	3415	2890
3906	3650	4200
4222	3336	4150
4346	3236	4150

Annex 2.2

Heating Step	40Ar/39Ar	±1σ	37Ar/39Ar	±1σ	36Ar/39Ar	±1σ	$40Ar^*/39Ar_k$	±1σ	40Ar(mol)	40Ar* (%)	$39Ar_k$ (%)	Age (Ma)	±2σ (Ma)
1 alunite, J=0.001108±0.0000125													
1	26.74943	0.07806	0.00000	0.01260	0.08962	0.00112	0.264496	0.32156	1.891E-15	0.99	2.16	0.53	1.29
2	5.18533	0.01106	0.00427	0.00463	0.00533	0.00022	3.609420	0.06432	1.095E-15	69.61	6.44	7.20	0.26
3	5.20960	0.01059	0.00072	0.00213	0.00250	0.00011	4.471127	0.03294	2.041E-15	85.82	11.96	8.92	0.13
4	5.41425	0.01095	0.00000	0.00168	0.00179	0.00010	4.885582	0.03105	2.798E-15	90.24	15.77	9.74	0.12
5	5.91985	0.01188	0.00000	0.00110	0.00147	0.00006	5.484358	0.02176	4.771E-15	92.64	24.59	10.93	0.09
6	6.40104	0.01285	0.00000	0.00093	0.00209	0.00009	5.783211	0.02850	4.974E-15	90.35	23.71	11.52	0.11
7	10.14083	0.02039	0.00000	0.00123	0.01410	0.00016	5.972643	0.04763	5.108E-15	58.90	15.37	11.90	0.19
Age gradient between 0.5 and 11.9 Ma													
Total Fusion Age 297.9±123.0 Ka													
2 alunite, J=0.001111±0.0000125													
1	36.52357	0.07647	0.00000	0.00738	0.10056	0.00102	6.807904	0.29558	5.073E-15	18.64	7.47	13.59	1.18
2	27.69527	0.06191	0.00000	0.00924	0.06878	0.00075	7.368842	0.21795	3.225E-15	26.61	6.26	14.71	0.87
3	25.28007	0.05435	0.00143	0.00636	0.05957	0.00060	7.677026	0.17395	3.756E-15	30.37	7.99	15.32	0.69
4	23.35874	0.05216	0.00000	0.00760	0.05053	0.00059	8.425987	0.17192	3.072E-15	36.07	7.07	16.81	0.68
5	27.15945	0.06058	0.00000	0.00888	0.06179	0.00075	8.899001	0.21738	3.441E-15	32.77	6.81	17.75	0.86
6	21.52303	0.05210	0.00000	0.01140	0.04344	0.00084	8.686915	0.24788	1.786E-15	40.36	4.46	17.33	0.98
7	28.17674	0.06868	0.00000	0.01297	0.06466	0.00090	9.068795	0.26353	2.033E-15	32.19	3.88	18.09	1.05
8	20.99134	0.05045	0.00000	0.00959	0.03967	0.00069	9.266780	0.20360	2.060E-15	44.15	5.28	18.48	0.81
9	17.29370	0.03527	0.00000	0.00496	0.02632	0.00037	9.513684	0.10906	3.291E-15	55.01	10.23	18.97	0.43
10	22.07642	0.04695	0.00000	0.00540	0.04308	0.00050	9.346154	0.14514	3.685E-15	42.34	8.98	18.64	0.58
11	36.98459	0.11094	0.02750	0.01713	0.09290	0.00121	9.533287	0.34897	2.348E-15	25.78	3.41	19.01	1.38
12	18.67137	0.03880	0.00000	0.00625	0.03029	0.00045	9.718542	0.13385	3.178E-15	52.05	9.15	19.37	0.53
13	19.20626	0.03991	0.00000	0.00401	0.03256	0.00037	9.583636	0.10966	4.760E-15	49.90	13.33	19.11	0.43
14	24.54491	0.05313	0.00000	0.00778	0.05295	0.00068	8.897552	0.19880	2.589E-15	36.25	5.67	17.75	0.79
Plateau Age 18.95±0.27 Ma													

Heating	40Ar/39Ar	±1σ	37Ar/39Ar	±1σ	36Ar/39Ar	±1σ	$40Ar^*/39Ar_k$	±1σ	40Ar(mol)	40Ar* (%)	$39Ar_k$ (%)	Age	±2σ
Step												**(Ma)**	**(Ma)**
3 alunite, J=0.001118±0.0000125													
1	22.31187	0.05196	0.00000	0.01432	0.04996	0.00084	7.547517	0.24506	1.615E-15	33.83	4.51	15.16	0.98
2	15.23660	0.03225	0.00000	0.00569	0.01950	0.00030	9.472286	0.09017	2.749E-15	62.17	11.23	19.00	0.36
3	11.57915	0.02393	0.00000	0.00353	0.00804	0.00021	9.201775	0.06331	3.204E-15	79.47	17.23	18.46	0.25
4	12.79533	0.02645	0.00000	0.00478	0.01182	0.00020	9.302373	0.06224	3.205E-15	72.70	15.59	18.67	0.25
5	13.88751	0.03020	0.00000	0.00382	0.01540	0.00034	9.334399	0.10301	2.199E-15	67.21	9.86	18.73	0.41
6	20.09188	0.04700	0.00000	0.00650	0.03399	0.00047	10.046539	0.13854	2.715E-15	50.00	8.41	20.15	0.55
7	22.15061	0.05253	0.00000	0.00847	0.04204	0.00067	9.727881	0.19743	1.999E-15	43.92	5.62	19.51	0.79
8	16.04236	0.03493	0.00000	0.00494	0.02090	0.00038	9.865918	0.11411	2.662E-15	61.50	10.33	19.79	0.46
9	14.89373	0.03097	0.00000	0.00528	0.01724	0.00033	9.796879	0.09935	2.776E-15	65.78	11.60	19.65	0.40
10	20.88675	0.04836	0.00482	0.00960	0.03094	0.00057	11.742532	0.16799	1.886E-15	56.22	5.62	23.53	0.67
Plateau Age 18.66±0.22 Ma													
4 alunite, J=0.001122±0.0000125													
1	141.22665	0.39903	0.00000	0.01627	0.46885	0.00432	2.679832	1.21480	1.025E-14	1.90	4.34	5.42	4.90
2	146.71996	0.34402	0.00000	0.01184	0.48739	0.00436	2.694494	1.24345	1.418E-14	1.84	5.79	5.45	5.02
3	166.82999	0.37392	0.00000	0.01110	0.55626	0.00499	2.454595	1.42684	1.331E-14	1.47	4.78	4.96	5.76
4	107.88979	0.24683	0.00000	0.00818	0.35086	0.00316	4.210823	0.90347	1.005E-14	3.90	5.58	8.50	3.64
5	84.92850	0.19040	0.00000	0.00738	0.26540	0.00240	6.501754	0.68738	9.187E-15	7.66	6.47	13.11	2.76
6	63.83920	0.13767	0.00000	0.00726	0.19274	0.00174	6.884877	0.49907	9.135E-15	10.78	8.57	13.88	2.00
7	121.24513	0.27875	0.00000	0.01094	0.40164	0.00362	2.558595	1.03432	1.117E-14	2.11	5.51	5.17	4.18
8	131.19345	0.28593	0.00000	0.01358	0.43154	0.00387	3.671030	1.11068	1.124E-14	2.80	5.13	7.42	4.48
9	165.96795	0.46796	0.00000	0.01575	0.55707	0.00511	1.352465	1.43804	9.338E-15	0.81	3.37	2.74	5.81
10	207.64610	0.69510	0.00000	0.02354	0.69453	0.00649	2.410261	1.79017	8.380E-15	1.16	2.42	4.87	7.23
11	171.03611	0.52668	0.00000	0.02191	0.55783	0.00524	6.195879	1.46328	6.085E-15	3.62	2.13	12.50	5.88
12	131.74005	0.44069	0.00000	0.02568	0.42247	0.00401	6.899215	1.10952	4.974E-15	5.24	2.26	13.91	4.46
13	61.85679	0.18438	0.00000	0.01527	0.16466	0.00167	13.198149	0.47488	3.330E-15	21.34	3.22	26.52	1.89
14	38.58673	0.10080	0.00000	0.01472	0.08101	0.00097	14.647047	0.28193	2.418E-15	37.96	3.75	29.41	1.12

Heating Step	40Ar/39Ar	±1σ	37Ar/39Ar	±1σ	36Ar/39Ar	±1σ	$40Ar^*/39Ar_k$	±1σ	40Ar(mol)	40Ar* (%)	$39Ar_k$ (%)	Age (Ma)	±2σ (Ma)
15	27.30718	0.06195	0.00000	0.01216	0.04735	0.00059	13.315043	0.17290	2.939E-15	48.76	6.44	26.75	0.69
16	19.93378	0.08196	0.00152	0.02917	0.01551	0.00164	15.350138	0.48875	6.201E-16	77.01	1.86	30.81	1.95
17	23.39443	0.05584	0.00000	0.01174	0.02561	0.00056	15.827145	0.16852	1.989E-15	67.65	5.09	31.76	0.67

Annex 2.3

			drill core	7196	7196	7196	7569	7569	7569	7569	7569	7830	7830	7987	7987	7987	7987	MC24	MC25	MC26
			depth	11m	28.5m	44.5m	33.5m	43.2m	54.5m	72m	92m	14.5m	28.7m	27m	31.5m	49m	64.5m			
step	element	det.lim	units																	
1	Ag	2	ppm	<2	<2	<2	<2	<2	<2	<2	<2	<2	<2	<2	<2	<2	<2	<2	<2	<2
2	Ag	2	ppm	<2	<2	<2	<2	<2	<2	<2	<2	<2	<2	<2	<2	<2	<2	<2	3	<2
3	Ag	2	ppm	<2	<2	<2	<2	<2	<2	<2	<2	<2	<2	<2	<2	<2	<2	3	3	2
4	Ag	2	ppm	<2	<2	<2	<2	<2	<2	<2	<2	<2	<2	<2	<2	<2	<2	<2	<2	<2
5	Ag	2	ppm	<2	<2	<2	<2	<2	<2	<2	<2	<2	<2	<2	<2	<2	<2	<2	<2	<2
6	Ag	2	ppm	<2	<2	<2	<2	<2	<2	<2	<2	<2	<2	<2	<2	<2	<2	<2	3	2
7	Ag	2	ppm	<2	<2	<2	<2	<2	<2	<2	<2	<2	<2	<2	<2	<2	<2	<2	<2	<2
1	Al	0.01	%	<0.01	<0.01	<0.01	<0.01	<0.01	<0.01	<0.01	<0.01	<0.01	<0.01	<0.01	<0.01	<0.01	<0.01	<0.01	<0.01	<0.01
2	Al	0.01	%	0.05	0.03	0.01	0.04	0.03	0.03	0.02	0.02	0.05	0.06	0.01	0.01	0.02	0.02	0.12	<0.01	<0.01
3	Al	0.01	%	0.9	0.03	0.02	0.04	0.03	0.04	0.03	0.02	0.06	0.05	0.04	0.03	0.05	0.05	0.92	0.27	0.16
4	Al	0.01	%	0.3	0.05	0.05	0.09	0.06	0.06	0.04	0.04	0.16	0.13	0.09	0.1	0.11	0.12	0.29	0.18	0.2
5	Al	0.01	%	0.11	0.03	0.01	<0.01	<0.01	<0.01	<0.01	<0.01	0.04	<0.01	0.04	0.02	0.02	0.02	<0.01	<0.01	0.02
6	Al	0.01	%	0.28	0.06	0.11	0.11	0.07	0.05	0.05	0.05	0.13	0.1	0.07	0.12	0.16	0.16	0.26	0.26	0.36
7	Al	0.01	%	7.36	7.66	6.11	7.61	6.54	7.88	7.65	8.07	8.98	8.57	8.33	7.73	7.99	7.92	0.1	0.04	0.61
1	As	3	ppm	<3	<3	<3	<3	<3	<3	<3	<3	<3	<3	<3	<3	<3	<3	<3	<3	<3
2	As	3	ppm	<3	<3	<3	<3	<3	<3	<3	<3	<3	<3	<3	<3	<3	<3	<3	26	<3
3	As	3	ppm	<3	<3	<3	<3	<3	<3	<3	<3	<3	<3	<3	<3	<3	<3	6	207	4
4	As	3	ppm	4	<3	<3	<3	<3	<3	<3	<3	9	<3	<3	<3	<3	<3	<3	13	<3
5	As	3	ppm	4	<3	<3	<3	<3	<3	<3	<3	<3	<3	<3	<3	<3	<3	<3	<3	<3
6	As	3	ppm	46	<3	17	<3	<3	<3	<3	<3	14	<3	<3	<3	<3	<3	<3	18	<3
7	As	3	ppm	<3	<3	9	4	7	<3	<3	<3	10	<3	<3	<3	<3	<3	<3	<3	<3
1	Ba	1	ppm	<1	<1	<1	<1	<1	<1	3	<1	<1	<1	<1	<1	<1	<1	<1	<1	<1
2	Ba	1	ppm	2	13	2	4	4	3	120	26	3	2	4	3	4	5	3	25	3
3	Ba	1	ppm	<1	2	<1	<1	<1	<1	4	1	<1	<1	<1	<1	<1	4	10	115	163
4	Ba	1	ppm	<1	8	2	1	1	2	3	2	9	<1	1	3	1	2	2	68	27
5	Ba	1	ppm	<1	<1	1	<1	<1	<1	<1	<1	<1	<1	<1	<1	<1	<1	<1	<1	<1
6	Ba	1	ppm	3	10	12	12	5	5	2	4	21	4	4	2	3	5	5	95	27
7	Ba	1	ppm	486	899	105	268	653	783	658	1130	288	62	543	840	853	909	3	14	8

			drill core	7196	7196	7196	7569	7569	7569	7569	7569	7830	7830	7987	7987	7987	7987	MC24	MC25	MC26
			depth	11m	28.5m	44.5m	33.5m	43.2m	54.5m	72m	92m	14.5m	28.7m	27m	31.5m	49m	64.5m			
step	element	det.lim	units																	
1	Be	0.5	ppm	<0.5	<0.5	<0.5	<0.5	<0.5	<0.5	<0.5	<0.5	<0.5	<0.5	<0.5	<0.5	<0.5	<0.5	<0.5	<0.5	<0.5
2	Be	0.5	ppm	<0.5	<0.6	<0.7	<0.8	<0.9	<0.10	<0.11	<0.12	<0.13	<0.14	<0.15	<0.16	<0.17	<0.18	9.3	0.7	0.7
3	Be	0.5	ppm	<0.5	<0.5	<0.5	<0.5	<0.5	<0.5	<0.5	<0.5	<0.5	<0.5	<0.5	<0.5	<0.5	<0.5	2.3	1.7	1.1
4	Be	0.5	ppm	<0.5	<0.5	<0.5	<0.5	<0.5	<0.5	<0.5	<0.5	<0.5	<0.5	<0.5	<0.5	<0.5	<0.5	6.6	1.3	0.6
5	Be	0.5	ppm	<0.5	<0.5	<0.5	<0.5	<0.5	<0.5	<0.5	<0.5	<0.5	<0.5	<0.5	<0.5	<0.5	<0.5	<0.5	<0.5	<0.5
6	Be	0.5	ppm	<0.5	<0.5	1.2	<0.5	<0.5	<0.5	<0.5	<0.5	<0.5	<0.5	<0.5	<0.5	<0.5	<0.5	3.6	1.2	0.6
7	Be	0.5	ppm	0.6	1.4	2.1	1.2	1.2	1.3	1.7	1.7	2.3	2.8	1.3	1.3	1.4	1.4	<0.5	<0.5	<0.5
1	Bi	5	ppm	<5	<5	<5	<5	<5	<5	<5	<5	<5	<5	<5	<5	<5	<5	<5	<5	<5
2	Bi	5	ppm	<5	<5	<5	<5	<5	<5	<5	<5	<5	<5	<5	<5	<5	<5	<5	<5	<5
3	Bi	5	ppm	<5	<5	<5	<5	<5	<5	<5	<5	<5	<5	<5	<5	<5	<5	<5	<5	<5
4	Bi	5	ppm	<5	<5	<5	<5	<5	<5	<5	<5	<5	<5	<5	<5	<5	<5	<5	<5	<5
5	Bi	5	ppm	<5	<5	<5	<5	<5	<5	<5	<5	<5	<5	<5	<5	<5	<5	<5	<5	<5
6	Bi	5	ppm	<5	<5	<5	<5	<5	<5	<5	<5	<5	<5	<5	<5	<5	<5	<5	<5	<5
7	Bi	5	ppm	<5	<5	<5	<5	<5	<5	<5	<5	<5	<5	<5	<5	<5	<5	<5	<5	<5
1	Ca	0.01	%	<0.01	0.1	0.14	<0.01	0.05	<0.01	<0.01	<0.01	0.02	<0.01	0.28	<0.01	<0.01	<0.01	0.06	1.72	2.86
2	Ca	0.01	%	0.03	0.03	0.02	<0.01	0.02	0.01	0.01	<0.01	0.02	<0.01	0.07	0.04	0.02	0.01	0.22	0.38	4.4
3	Ca	0.01	%	<0.01	<0.01	<0.01	<0.01	<0.01	<0.01	<0.01	<0.01	<0.01	<0.01	<0.01	<0.01	<0.01	<0.01	<0.01	<0.01	<0.01
4	Ca	0.01	%	<0.01	<0.01	<0.01	<0.01	<0.01	<0.01	<0.01	<0.01	<0.01	<0.01	<0.01	<0.01	<0.01	<0.01	<0.01	<0.01	<0.01
5	Ca	0.01	%	<0.01	<0.01	<0.01	<0.01	<0.01	<0.01	<0.01	<0.01	<0.01	<0.01	<0.01	<0.01	<0.01	<0.01	<0.01	<0.01	<0.01
6	Ca	0.01	%	<0.01	<0.01	<0.01	<0.01	<0.01	<0.01	<0.01	<0.01	<0.01	<0.01	<0.01	<0.01	0.09	0.09	0.28	0.01	0.32
7	Ca	0.01	%	0.02	0.07	0.11	0.04	0.04	0.04	0.11	0.03	0.11	0.1	0.05	0.14	0.49	0.28	<0.01	<0.01	0.02
1	Cd	1	ppm	<1	<1	<1	<1	<1	<1	<1	<1	<1	<1	<1	<1	<1	<1	<1	<1	<1
2	Cd	1	ppm	<1	<1	<1	<1	<1	1	<1	<1	<1	<1	<1	<1	<1	1	3	5	<1
3	Cd	1	ppm	<1	<1	<1	<1	<1	<1	<1	<1	<1	<1	<1	<1	<1	<1	3	3	<1
4	Cd	1	ppm	<1	<1	<1	<1	<1	<1	<1	<1	<1	<1	<1	<1	<1	<1	1	2	<1
5	Cd	1	ppm	<1	<1	<1	<1	<1	2	1	<1	<1	<1	<1	<1	<1	<1	<1	<1	<1
6	Cd	1	ppm	<1	<1	<1	<1	<1	<1	<1	<1	<1	<1	<1	<1	<1	<1	5	3	1
7	Cd	1	ppm	<1	<1	<1	<1	<1	<1	<1	<1	<1	<1	<1	<1	<1	<1	<1	<1	<1
1	Co	1	ppm	<1	<1	<1	<1	<1	<1	<1	<1	<1	<1	<1	<1	<1	<1	2	<1	<1
2	Co	1	ppm	<1	<1	<1	<1	<1	<1	<1	<1	<1	<1	<1	<1	<1	<1	3	2	2
3	Co	1	ppm	<1	<1	1	1	1	1	1	1	<1	1	<1	<1	1	2	20	486	723

			drill core	7196	7196	7196	7569	7569	7569	7569	7569	7830	7830	7987	7987	7987	7987	MC24	MC25	MC26
			depth	11m	28.5m	44.5m	33.5m	43.2m	54.5m	72m	92m	14.5m	28.7m	27m	31.5m	49m	64.5m			
step	element	det.lim	units																	
4	Co	1	ppm	<1	<1	<1	<1	<1	<1	<1	<1	<1	<1	<1	<1	<1	<1	1	75	123
5	Co	1	ppm	<1	<1	<1	<1	<1	<1	<1	3	<1	<1	<1	<1	<1	<1	<1	<1	26
6	Co	1	ppm	<1	<1	4	<1	1	<1	<1	8	<1	2	<1	<1	<1	<1	<1	123	108
7	Co	1	ppm	<1	<1	2	<1	<1	<1	<1	<1	<1	<1	<1	<1	<1	<1	<1	<1	<1
1	Cr	1	ppm	<1	<1	<1	<1	<1	<1	<1	<1	<1	<1	<1	<1	<1	<1	<1	<1	<1
2	Cr	1	ppm	<1	<1	<1	<1	<1	<1	<1	<1	<1	<1	<1	<1	<1	<1	<1	<1	<1
3	Cr	1	ppm	<1	<1	<1	<1	<1	<1	<1	<1	<1	<1	<1	<1	<1	<1	<1	2	<1
4	Cr	1	ppm	1	<1	<1	<1	<1	<1	<1	<1	<1	<1	<1	<1	<1	<1	1	2	<1
5	Cr	1	ppm	<1	<1	<1	<1	<1	<1	<1	<1	<1	<1	<1	<1	<1	<1	<1	<1	<1
6	Cr	1	ppm	5	4	3	3	5	3	3	2	3	4	2	2	7	4	1	2	2
7	Cr	1	ppm	2	3	3	1	2	1	1	1	2	1	2	<1	<1	<1	<1	<1	<1
1	Cu	0.5	ppm	41.9	0.7	9.3	2.3	6.3	1.6	4.9	0.7	9	15.7	8.5	8.4	19.3	6.7	963	534	346
2	Cu	0.5	ppm	967	41.6	70.1	89.5	2560	91.5	154	71.3	265	>10000	522	109	448	78.8	>10000	>10000	>10000
3	Cu	0.5	ppm	567	15.2	48.9	19.6	1370	37.3	56.9	12.1	65.8	725	431	105	1010	123	>10000	>10000	>10000
4	Cu	0.5	ppm	1560	90.1	242	49.9	1040	36.5	54.3	7.5	202	416	378	283	101	19.9	>10000	>10000	>10000
5	Cu	0.5	ppm	149	13.1	10	1.3	4060	5200	3070	129	2.4	3050	26.4	19.3	6.6	2.9	317	13.4	350
6	Cu	0.5	ppm	1620	52.8	677	87.2	7360	386	200	7.8	153	916	96.8	245	59.3	12.8	>10000	>10000	>10000
7	Cu	0.5	ppm	616	77.8	543	934	159	6.4	3.6	0.8	157	336	78.2	94.8	103	9.3	188	74.3	769
1	Fe	0.01	%	<0.01	<0.01	<0.01	<0.01	<0.01	<0.01	<0.01	<0.01	<0.01	<0.01	<0.01	<0.01	<0.01	<0.01	<0.01	<0.01	<0.01
2	Fe	0.01	%	<0.01	0.01	<0.01	<0.01	<0.01	0.01	0.01	<0.01	0.01	<0.01	<0.01	<0.01	<0.01	0.01	<0.01	<0.01	<0.01
3	Fe	0.01	%	0.23	0.05	0.26	0.06	0.02	<0.01	<0.01	0.01	0.04	<0.01	0.44	0.06	0.07	0.34	<0.01	<0.01	0.05
4	Fe	0.01	%	3.7	0.54	2.14	0.42	0.1	<0.01	<0.01	0.04	0.71	0.04	0.69	0.22	0.3	0.44	<0.01	<0.01	0.1
5	Fe	0.01	%	0.28	0.01	0.02	<0.01	<0.01	0.02	<0.01	0.34	<0.01	<0.01	0.01	<0.01	<0.01	<0.01	<0.01	<0.01	0.02
6	Fe	0.01	%	4.07	0.41	5.33	0.34	0.44	0.42	0.28	1.62	0.66	0.77	0.07	0.18	0.21	0.22	0.01	<0.01	0.3
7	Fe	0.01	%	1.4	5.24	7.54	0.7	0.73	0.25	0.22	1.27	1.01	0.41	1.04	0.24	0.4	0.32	0.01	<0.1	0.18
1	K	0.01	%	0.01	0.03	<0.01	0.02	0.02	0.02	0.02	0.02	0.03	0.02	0.04	0.02	<0.01	<0.01	0.03	0.03	0.02
2	K	0.01	%	<0.01	0.02	<0.01	0.02	0.02	0.02	0.02	0.02	0.03	0.02	0.01	0.02	0.02	0.03	0.03	0.03	0.03
3	K	0.01	%	<0.01	<0.01	<0.01	<0.01	<0.01	<0.01	<0.01	<0.01	<0.01	<0.01	<0.01	<0.01	<0.01	<0.01	<0.01	0.02	0.05
4	K	0.01	%	<0.01	0.02	<0.01	0.02	0.01	0.01	0.01	0.01	0.07	0.01	<0.01	0.01	<0.01	<0.01	<0.01	<0.01	<0.01
5	K	0.01	%	<0.01	<0.01	<0.01	<0.01	<0.01	<0.01	<0.01	<0.01	0.02	<0.01	0.01	<0.01	<0.01	<0.01	<0.01	<0.01	<0.01
6	K	0.01	%	N.A.	N.A.	N.A.	N.A.	N.A.	N.A.	N.A.	N.A.	N.A.	N.A.	N.A.	N.A.	N.A.	N.A.	N.A.	N.A.	N.A.

			drill core	7196	7196	7196	7569	7569	7569	7569	7569	7830	7830	7987	7987	7987	7987	MC24	MC25	MC26
			depth	11m	28.5m	44.5m	33.5m	43.2m	54.5m	72m	92m	14.5m	28.7m	27m	31.5m	49m	64.5m			
step	**element**	**det.lim**	**units**																	
7	K	0.01	%	2	4.08	0.42	4.33	4.37	6.15	4.36	5.54	3.36	1.86	3.3	3.9	3.32	3.33	0.08	0.03	0.07
1	La	0.5	ppm	<0.5	<0.5	<0.5	<0.5	<0.5	<0.5	<0.5	<0.5	<0.5	<0.5	<0.5	<0.5	<0.5	<0.5	<0.5	<0.5	<0.5
2	La	0.5	ppm	<0.5	<0.5	<0.5	<0.5	<0.5	<0.5	<0.5	<0.5	<0.5	<0.5	<0.5	<0.5	0.7	0.6	1.1	<0.5	<0.5
3	La	0.5	ppm	<0.5	<0.5	<0.5	<0.5	<0.5	<0.5	<0.5	<0.5	<0.5	<0.5	1.3	1.1	4.2	2.3	<0.5	<0.5	<0.5
4	La	0.5	ppm	<0.5	0.9	0.8	1.6	3.5	1.3	2.5	1.4	<0.5	<0.5	2.3	2.2	0.6	1	<0.5	<0.5	<0.5
5	La	0.5	ppm	<0.5	<0.5	<0.5	<0.5	<0.5	<0.5	<0.5	<0.5	<0.5	<0.5	<0.5	<0.5	<0.5	<0.5	<0.5	<0.5	<0.5
6	La	0.5	ppm	3.3	4.1	3.7	3.7	6.8	4.4	7.3	2.6	1.4	0.6	6.5	4.4	5.8	3.5	3.4	<0.5	0.7
7	La	0.5	ppm	6	10.9	19.1	9.5	13.3	8.8	5.2	10.3	5	1.9	2.2	2.5	14.1	2.4	<0.5	<0.5	<0.5
1	Li	1	ppm	<1	<1	<1	<1	<1	<1	<1	<1	<1	<1	<1	<1	<1	<1	4	1	<1
2	Li	1	ppm	<1	<1	<1	<1	<1	<1	<1	<1	<1	<1	<1	<1	<1	<1	<1	<1	<1
3	Li	1	ppm	<1	<1	<1	<1	<1	<1	<1	<1	<1	<1	<1	<1	<1	<1	<1	<1	<1
4	Li	1	ppm	2	<1	<1	<1	<1	<1	<1	<1	<1	<1	<1	<1	<1	2	<1	<1	<1
5	Li	1	ppm	<1	<1	<1	<1	<1	<1	<1	<1	<1	<1	<1	<1	<1	<1	<1	<1	<1
6	Li	1	ppm	<1	<1	<1	<1	<1	<1	<1	<1	<1	<1	<1	<1	2	1	<1	<1	<1
7	Li	1	ppm	9	3	2	9	8	9	7	5	7	3	4	5	3	3	<1	<1	<1
1	Mg	0.01	%	<0.01	<0.01	<0.01	<0.01	<0.01	<0.01	<0.01	<0.01	<0.01	<0.01	<0.01	<0.01	<0.01	<0.01	0.08	0.04	0.05
2	Mg	0.01	%	0.02	<0.01	<0.01	<0.01	<0.01	<0.01	0.01	<0.01	<0.01	<0.01	<0.01	<0.01	<0.01	0.01	0.16	0.02	0.01
3	Mg	0.01	%	<0.01	<0.01	<0.01	<0.01	<0.01	<0.01	<0.01	<0.01	<0.01	<0.01	<0.01	<0.01	0.01	0.02	0.02	<0.01	<0.01
4	Mg	0.01	%	<0.01	<0.01	<0.01	<0.01	<0.01	<0.01	<0.01	<0.01	<0.01	<0.01	0.03	0.05	0.06	0.08	<0.01	<0.01	<0.01
5	Mg	0.01	%	<0.01	<0.01	<0.01	<0.01	<0.01	<0.01	<0.01	<0.01	<0.01	<0.01	<0.01	<0.01	<0.01	<0.01	<0.01	<0.01	<0.01
6	Mg	0.01	%	0.02	<0.01	<0.01	<0.01	<0.01	<0.01	<0.01	<0.01	<0.01	<0.01	0.03	0.06	0.1	0.12	<0.01	<0.01	<0.01
7	Mg	0.01	%	0.09	0.18	0.03	0.16	0.18	0.18	0.13	0.19	0.35	0.24	0.26	0.11	0.09	0.1	<0.01	<0.01	<0.01
1	Mn	2	ppm	<2	2	6	<2	2	<2	<2	<2	<2	<2	4	<2	<2	13	132	30	20
2	Mn	2	ppm	10	5	3	3	4	6	13	9	<2	2	9	9	36	90	272	181	119
3	Mn	2	ppm	11	<2	<2	<2	<2	<2	<2	<2	<2	<2	39	6	14	520	1480	>10000	>10000
4	Mn	2	ppm	99	4	8	<2	<2	<2	<2	<2	<2	<2	79	82	77	62	172	6420	7140
5	Mn	2	ppm	9	<2	<2	<2	<2	<2	<2	<2	<2	<2	<2	<2	<2	3	3	12	1010
6	Mn	2	ppm	89	4	29	2	<2	<2	<2	<2	3	<2	37	62	111	107	155	6710	6450
7	Mn	2	ppm	54	51	39	45	41	31	33	34	103	31	136	35	79	42	3	60	64
1	Mo	1	ppm	<1	1	<1	<1	<1	8	5	6	<1	<1	8	3	1	2	<1	<1	<1
2	Mo	1	ppm	<1	<1	<1	<1	<1	3	<1	1	<1	<1	<1	<1	<1	<1	<1	<1	<1

			drill core	7196	7196	7196	7569	7569	7569	7569	7569	7830	7830	7987	7987	7987	7987	MC24	MC25	MC26
			depth	11m	28.5m	44.5m	33.5m	43.2m	54.5m	72m	92m	14.5m	28.7m	27m	31.5m	49m	64.5m			
step	element	det.lim	units																	
3	Mo	1	ppm	43	14	68	10	<1	3	2	6	<1	<1	150	22	2	8	9	331	68
4	Mo	1	ppm	362	87	243	17	2	1	2	2	1	<1	72	9	<1	<1	1	29	6
5	Mo	1	ppm	155	2	45	1	<1	<1	<1	<1	<1	<1	<1	1	<1	<1	<1	17	2
6	Mo	1	ppm	418	20	603	12	6	16	33	3	2	<1	<1	<1	<1	<1	<1	33	4
7	Mo	1	ppm	14	10	412	53	13	3	<1	<1	<1	<1	<1	1	<1	<1	<1	<1	<1
1	Na	0.01	%	0.04	0.01	0.03	0.01	0.01	0.01	0.02	0.01	0.03	0.02	0.03	0.04	0.02	0.01	0.21	0.16	0.15
2	Na	0.01	%	<0.01	<0.01	<0.01	<0.01	<0.01	<0.01	<0.01	<0.01	<0.01	<0.01	<0.01	<0.01	<0.01	<0.01	<0.01	<0.01	<0.01
3	Na	0.01	%	<0.01	<0.01	<0.01	<0.01	<0.01	<0.01	<0.01	<0.01	<0.01	<0.01	<0.01	<0.01	<0.01	<0.01	<0.01	<0.01	<0.01
4	Na	0.01	%	<0.01	<0.01	<0.01	<0.01	<0.01	<0.01	<0.01	<0.01	0.01	0.02	<0.01	<0.01	<0.01	<0.01	<0.01	<0.01	<0.01
5	Na	0.01	%	<0.01	<0.01	<0.01	<0.01	<0.01	<0.01	<0.01	<0.01	<0.01	<0.01	<0.01	<0.01	<0.01	<0.01	<0.01	<0.01	<0.01
6	Na	0.01	%	<0.01	0.01	0.02	0.01	<0.01	<0.01	0.01	<0.01	0.02	0.02	0.01	<0.01	<0.01	0.01	<0.01	<0.01	<0.01
7	Na	0.01	%	0.55	2.28	4.37	1.1	1.04	1.35	2.77	1.98	2.25	3.63	1.9	3.35	3.68	3.83	<0.01	<0.01	0.03
1	Ni	1	ppm	<1	<1	<1	<1	<1	<1	<1	<1	<1	<1	<1	<1	<1	<1	1	<1	<1
2	Ni	1	ppm	<1	<1	<1	<1	<1	<1	<1	<1	<1	<1	<1	<1	<1	<1	3	<1	<1
3	Ni	1	ppm	<1	1	1	<1	1	1	1	1	1	<1	1	1	1	1	2	3	<1
4	Ni	1	ppm	<1	<1	<1	<1	<1	<1	<1	<1	<1	<1	<1	<1	<1	<1	<1	<1	<1
5	Ni	1	ppm	<1	<1	<1	<1	<1	<1	<1	<1	<1	<1	<1	<1	<1	<1	<1	<1	<1
6	Ni	1	ppm	<1	1	2	1	2	<1	<1	1	<1	2	<1	<1	3	1	<1	<1	<1
7	Ni	1	ppm	<1	<1	<1	<1	<1	<1	<1	<1	<1	<1	<1	<1	<1	<1	<1	<1	<1
1	P	0.01	%	<0.01	<0.01	<0.01	<0.01	<0.01	<0.01	<0.01	<0.01	<0.01	<0.01	<0.01	<0.01	<0.01	<0.01	<0.01	<0.01	<0.01
2	P	0.01	%	<0.01	<0.01	<0.01	<0.01	<0.01	<0.01	<0.01	<0.01	<0.01	<0.01	<0.01	<0.01	<0.01	<0.01	0.01	<0.01	<0.01
3	P	0.01	%	<0.01	<0.01	<0.01	<0.01	<0.01	<0.01	<0.01	<0.01	<0.01	<0.01	0.02	<0.01	0.01	0.02	0.1	0.1	0.02
4	P	0.01	%	<0.01	<0.01	<0.01	<0.01	<0.01	<0.01	<0.01	<0.01	<0.01	<0.01	0.01	<0.01	<0.01	<0.01	0.03	<0.01	<0.01
5	P	0.01	%	<0.01	<0.01	<0.01	<0.01	<0.01	<0.01	<0.01	<0.01	<0.01	<0.01	<0.01	<0.01	<0.01	<0.01	<0.01	<0.01	<0.01
6	P	0.01	%	0.03	<0.01	0.03	<0.01	<0.01	<0.01	<0.01	<0.01	<0.01	<0.01	<0.01	<0.01	0.03	0.02	0.04	<0.01	<0.01
7	P	0.01	%	<0.01	<0.01	0.03	0.03	<0.01	0.03	<0.01	0.02	0.01	<0.01	<0.01	<0.01	<0.01	<0.01	<0.01	<0.01	<0.01
1	Pb	2	ppm	<2	<2	<2	<2	<2	<2	<2	<2	<2	<2	<2	<2	<2	<2	<2	<2	<2
2	Pb	2	ppm	<2	<2	<2	<2	<2	<2	<2	<2	<2	2	<2	<2	<2	<2	4	16	4
3	Pb	2	ppm	<2	<2	<2	<2	<2	<2	<2	<2	<2	<2	<2	<2	<2	<2	16	13	12
4	Pb	2	ppm	<2	<2	<2	<2	<2	<2	<2	<2	<2	<2	<2	3	<2	<2	10	8	8
5	Pb	2	ppm	<2	<2	<2	<2	<2	<2	<2	<2	<2	<2	<2	<2	<2	<2	<2	<2	<2

			drill core	7196	7196	7196	7569	7569	7569	7569	7569	7830	7830	7987	7987	7987	7987	MC24	MC25	MC26
			depth	11m	28.5m	44.5m	33.5m	43.2m	54.5m	72m	92m	14.5m	28.7m	27m	31.5m	49m	64.5m			
step	element	det.lim	units																	
6	Pb	2	ppm	<2	<2	4	<2	4	<2	<2	3	4	<2	<2	<2	<2	2	8	8	7
7	Pb	2	ppm	9	<2	13	6	19	3	2	3	4	<2	<2	5	7	4	<2	<2	<2
1	S	0.01	%	0.04	0.11	0.15	0.03	0.07	0.02	0.02	0.02	0.06	0.03	0.29	0.04	0.01	<0.01	0.37	1.7	2.7
2	S	0.01	%	0.05	<0.01	0.01	<0.01	<0.01	<0.01	<0.01	<0.01	<0.01	0.15	<0.01	<0.01	<0.01	<0.01	0.03	0.07	3.38
3	S	0.01	%	<0.01	<0.01	<0.01	<0.01	<0.01	<0.01	<0.01	<0.01	<0.01	<0.01	<0.01	<0.01	<0.01	<0.01	<0.01	0.01	0.08
4	S	0.01	%		0.01	0.02	0.02	0.02	<0.01	<0.01	<0.01	<0.01	0.13	0.05	<0.01	<0.01	<0.01	<0.01	<0.01	0.01
5	S	0.01	%	<0.01	<0.01	<0.01	<0.01	0.19	0.33	0.24	0.46	<0.01	0.19	<0.01	<0.01	<0.01	<0.01	<0.01	<0.01	0.01
6	S	0.01	%	<0.01	0.02	0.04	0.06	0.68	0.18	0.13	1.78	0.15	0.9	<0.01	<0.01	<0.01	<0.01	<0.01	<0.01	0.06
7	S	0.01	%	0.03	0.03	0.21	1.25	0.65	0.01	<0.01	0.07	0.26	0.44	<0.01	<0.01	<0.01	<0.01	<0.01	<0.01	<0.01
1	Sb	5	ppm	<5	<5	<5	<5	<5	<5	<5	<5	<5	<5	<5	<5	<5	<5	<5	<5	<5
2	Sb	5	ppm	<5	<5	<5	<5	<5	<5	<5	<5	<5	<5	<5	<5	<5	<5	<5	<5	<5
3	Sb	5	ppm	<5	<5	<5	<5	<5	<5	<5	<5	<5	<5	<5	<5	<5	<5	<5	<5	<5
4	Sb	5	ppm	<5	<5	<5	<5	<5	<5	<5	<5	<5	<5	<5	<5	<5	<5	<5	<5	<5
5	Sb	5	ppm	<5	<5	<5	<5	<5	<5	<5	<5	<5	<5	<5	<5	<5	<5	<5	<5	<5
6	Sb	5	ppm	<5	<5	<5	<5	<5	<5	<5	<5	<5	<5	<5	<5	<5	<5	<5	<5	<5
7	Sb	5	ppm	<5	<5	<5	<5	<5	<5	<5	<5	<5	<5	<5	<5	<5	<5	<5	<5	<5
1	Sc	0.5	ppm	<0.5	<0.5	<0.5	<0.5	<0.5	<0.5	<0.5	<0.5	<0.5	<0.5	<0.5	<0.5	<0.5	<0.5	<0.5	<0.5	<0.5
2	Sc	0.5	ppm	<0.5	<0.5	<0.5	<0.5	<0.5	<0.5	<0.5	<0.5	<0.5	<0.5	<0.5	<0.5	<0.5	<0.5	0.7	1.4	1.6
3	Sc	0.5	ppm	<0.5	<0.5	<0.5	<0.5	<0.5	<0.5	<0.5	<0.5	<0.5	<0.5	<0.5	<0.5	<0.5	<0.5	3.2	1.7	3.6
4	Sc	0.5	ppm	<0.5	<0.5	<0.5	<0.5	<0.5	<0.5	<0.5	<0.5	<0.5	<0.5	<0.5	<0.5	<0.5	<0.5	1.3	1.1	2.9
5	Sc	0.5	ppm	<0.5	<0.5	<0.5	<0.5	<0.5	<0.5	<0.5	<0.5	<0.5	<0.5	<0.5	<0.5	<0.5	<0.5	<0.5	<0.5	<0.5
6	Sc	0.5	ppm	<0.5	<0.6	<0.7	<0.8	<0.9	<0.10	<0.11	<0.12	<0.13	<0.14	<0.15	<0.16	<0.17	<0.18	0.6	0.6	2.7
7	Sc	0.5	ppm	1.8	1.4	<0.5	2	2.9	2.7	2.1	2.2	3.8	2.4	2.5	2.5	2	2.1	<0.5	<0.5	<0.5
1	Sn	10	ppm	<10	<10	<10	<10	<10	<10	<10	<10	<10	<10	<10	<10	<10	<10	<10	<10	<10
2	Sn	10	ppm	<10	<10	<10	<10	<10	<10	<10	<10	<10	<10	<10	<10	<10	<10	<10	<10	<10
3	Sn	10	ppm	<10	<10	<10	<10	<10	<10	<10	<10	<10	<10	<10	<10	<10	<10	<10	<10	<10
4	Sn	10	ppm	<10	<10	<10	<10	<10	<10	<10	<10	<10	<10	<10	<10	<10	<10	<10	<10	<10
5	Sn	10	ppm	<10	<10	<10	<10	<10	<10	<10	<10	<10	<10	<10	<10	<10	<10	<10	<10	<10
6	Sn	10	ppm	20	20	20	20	20	20	20	20	20	20	20	20	20	20	20	20	20
7	Sn	10	ppm	<10	<10	<10	<10	<10	<10	<10	<10	<10	<10	<10	<10	<10	<10	<10	<10	<10
1	Sr	0.5	ppm	0.7	1	3.8	1	0.5	1.2	<0.5	0.5	<0.5	<0.5	4.8	<0.5	<0.5	<0.5	11.6	26.2	42.4

			drill core	7196	7196	7196	7569	7569	7569	7569	7569	7830	7830	7987	7987	7987	7987	MC24	MC25	MC26
			depth	11m	28.5m	44.5m	33.5m	43.2m	54.5m	72m	92m	14.5m	28.7m	27m	31.5m	49m	64.5m			
step	**element**	**det.lim**	**units**																	
2	Sr	0.5	ppm	3.8	1.2	1.7	3.5	1.2	6.6	3.8	5.2	0.8	1.5	2	3	2.6	2.7	41.1	12.6	39.8
3	Sr	0.5	ppm	<0.5	<0.5	0.6	0.6	<0.5	1.4	<0.5	0.8	<0.5	<0.5	<0.5	0.6	<0.5	<0.5	1.9	11.9	11.4
4	Sr	0.5	ppm	1.7	5.5	4.9	5.8	0.7	12.5	1.9	11.7	4.5	1.1	2.3	2.6	1.8	1.3	1.4	5.2	4.7
5	Sr	0.5	ppm	1	<0.5	3.6	<0.5	<0.5	0.7	<0.5	1.1	<0.5	<0.5	<0.5	<0.5	<0.5	<0.5	<0.5	<0.5	0.6
6	Sr	0.5	ppm	6.1	5.9	18.2	12.7	1.7	21.2	2.9	13.9	7.6	1.1	2	1.1	4.1	2.7	12.3	7.2	26.8
7	Sr	0.5	ppm	169	192	338	379	158	384	228	246	159	79.1	158	224	289	329	0.8	0.6	5.6
1	Ti	0.01	%	<0.01	<0.01	<0.01	<0.01	<0.01	<0.01	<0.01	<0.01	<0.01	<0.01	<0.01	<0.01	<0.01	<0.01	<0.01	<0.01	<0.01
2	Ti	0.01	%	<0.01	<0.01	<0.01	<0.01	<0.01	<0.01	<0.01	<0.01	<0.01	<0.01	<0.01	<0.01	<0.01	<0.01	<0.01	<0.01	<0.01
3	Ti	0.01	%	<0.01	<0.01	<0.01	<0.01	<0.01	<0.01	<0.01	<0.01	<0.01	<0.01	<0.01	<0.01	<0.01	<0.01	<0.01	<0.01	<0.01
4	Ti	0.01	%	<0.01	<0.01	<0.01	<0.01	<0.01	<0.01	<0.01	<0.01	<0.01	<0.01	<0.01	<0.01	<0.01	<0.01	<0.01	<0.01	<0.01
5	Ti	0.01	%	<0.01	<0.01	<0.01	<0.01	<0.01	<0.01	<0.01	<0.01	<0.01	<0.01	<0.01	<0.01	<0.01	<0.01	<0.01	<0.01	<0.01
6	Ti	0.01	%	0.02	<0.01	<0.01	<0.01	<0.01	<0.01	<0.01	<0.01	<0.01	<0.01	<0.01	<0.01	<0.01	<0.01	<0.01	<0.01	<0.01
7	Ti	0.01	%	0.11	0.09	0.05	0.17	0.18	0.12	0.1	0.11	0.14	0.1	0.14	0.11	0.08	0.08	<0.01	<0.01	<0.01
1	V	2	ppm	<2	<2	<2	<2	<2	<2	<2	<2	<2	<2	<2	<2	<2	<2	<2	<2	<2
2	V	2	ppm	<2	<2	<2	<2	<2	<2	<2	<2	<2	<2	<2	<2	<2	<2	<2	<2	<2
3	V	2	ppm	<2	<2	<2	<2	<2	<2	<2	<2	<2	<2	5	<2	<2	5	22	62	4
4	V	2	ppm	4	<2	<2	<2	<2	<2	<2	<2	3	<2	4	<2	4	6	9	7	<2
5	V	2	ppm	<2	<2	<2	<2	<2	<2	<2	<2	<2	<2	<2	<2	<2	<2	<2	<2	<2
6	V	2	ppm	4	<2	<2	<2	<2	<2	<2	<2	<2	<2	<2	<2	3	2	7	8	<2
7	V	2	ppm	25	18	13	20	31	27	21	25	47	24	27	18	13	9	<2	<2	<2
1	W	10	ppm	<10	<10	<10	<10	<10	<10	<10	<10	<10	<10	<10	<10	<10	<10	<10	<10	<10
2	W	10	ppm	<10	<10	<10	<10	<10	<10	<10	<10	<10	<10	<10	<10	<10	<10	<10	<10	<10
3	W	10	ppm	<10	<10	<10	<10	<10	<10	<10	<10	<10	<10	<10	<10	<10	<10	<10	<10	<10
4	W	10	ppm	<10	<10	<10	<10	<10	<10	<10	<10	<10	<10	<10	<10	<10	<10	<10	<10	<10
5	W	10	ppm	<10	<10	<10	<10	<10	<10	<10	<10	<10	<10	<10	<10	<10	<10	<10	<10	<10
6	W	10	ppm	<10	<10	<10	<10	<10	<10	<10	<10	<10	<10	<10	<10	<10	<10	<10	<10	<10
7	W	10	ppm	<10	30	40	30	40	20	<10	40	20	10	<10	<10	<10	<10	<10	<10	<10
1	Y	0.5	ppm	<0.5	<0.5	<0.5	<0.5	<0.5	<0.5	<0.5	<0.5	<0.5	<0.5	<0.5	<0.5	<0.5	<0.5	<0.5	<0.5	<0.5
2	Y	0.5	ppm	<0.5	<0.5	<0.5	<0.5	<0.5	<0.5	<0.5	<0.5	<0.5	<0.5	<0.5	<0.5	<0.5	<0.5	3.6	0.6	1.1
3	Y	0.5	ppm	<0.5	<0.5	<0.5	<0.5	<0.5	<0.5	<0.5	<0.5	<0.5	<0.5	0.9	<0.5	1.2	0.9	3.6	2.2	2.9
4	Y	0.5	ppm	<0.5	<0.5	<0.5	<0.5	<0.5	<0.5	0.7	<0.5	0.5	<0.5	2.7	<0.5	<0.5	<0.5	0.7	<0.5	1.6

			drill core	7196	7196	7196	7569	7569	7569	7569	7569	7830	7830	7987	7987	7987	7987	MC24	MC25	MC26
			depth	11m	28.5m	44.5m	33.5m	43.2m	54.5m	72m	92m	14.5m	28.7m	27m	31.5m	49m	64.5m			
step	**element**	**det.lim**	**units**																	
5	Y	0.5	ppm	<0.5	<0.5	<0.5	<0.5	<0.5	<0.5	<0.5	<0.5	<0.5	<0.5	<0.5	<0.5	<0.5	<0.5	<0.5	<0.5	<0.5
6	Y	0.5	ppm	<0.5	<0.5	0.6	<0.5	<0.5	<0.5	<0.5	<0.5	0.5	<0.5	<0.6	<0.5	1.7	1.1	6.7	1.2	12.8
7	Y	0.5	ppm	0.8	0.9	1.7	1.7	1.9	2	1.2	1.7	1.6	0.9	0.8	0.8	1.6	1.1	<0.5	<0.5	1.6
1	Zn	0.5	ppm	2.5	0.6	7.6	3.3	1.9	3.3	6.6	0.8	1.9	0.8	28.6	5.7	2.1	19.4	163	21.2	26
2	Zn	0.5	ppm	17	18.9	7	14.6	22.2	79.3	167	28.7	7.2	11.2	130	53.6	51.4	166	676	263	52.9
3	Zn	0.5	ppm	6.2	2	7.3	1.1	0.9	9.6	37	4.9	0.8	0.6	98.2	26.2	27.3	276	813	222	160
4	Zn	0.5	ppm	14.5	3.8	63.9	1.5	1.7	14.7	83.1	8.8	4	1.6	132	125	60.2	132	367	79.8	81.2
5	Zn	0.5	ppm	3.2	2.1	4.1	<0.5	1.3	78.6	522	26.3	1.4	<0.5	16.6	19.4	6.1	20.5	<0.5	<0.5	4.9
6	Zn	0.5	ppm	24.5	3.3	396	2.4	6.1	12.6	97.9	3.6	9.7	2.4	69.5	197	68.6	123	271	91.5	139
7	Zn	0.5	ppm	26.3	17	259	14.9	30.6	33	68.5	47.4	41.1	15	97.3	83.6	59.9	91	6.2	2.5	26.4
1	Zr	0.5	ppm	<0.5	<0.5	<0.5	<0.5	<0.5	<0.5	<0.5	<0.5	<0.5	<0.5	<0.5	<0.5	<0.5	<0.5	<0.5	<0.5	<0.5
2	Zr	0.5	ppm	<0.5	<0.5	<0.5	<0.5	<0.5	<0.5	<0.5	<0.5	<0.5	<0.5	<0.5	<0.5	<0.5	<0.5	<0.5	<0.5	<0.5
3	Zr	0.5	ppm	1	0.8	0.9	0.8	0.8	1	1	1	0.8	0.8	0.9	0.9	0.8	0.8	0.6	0.9	0.9
4	Zr	0.5	ppm	1.3	<0.5	<0.5	<0.5	<0.5	<0.5	<0.5	<0.5	<0.5	<0.5	<0.5	<0.5	<0.5	<0.5	<0.5	<0.5	<0.5
5	Zr	0.5	ppm	<0.5	<0.5	<0.5	<0.5	<0.5	<0.5	<0.5	<0.5	<0.5	<0.5	<0.5	<0.5	<0.5	<0.5	<0.5	<0.5	<0.5
6	Zr	0.5	ppm	3.5	<0.5	3.8	<0.5	<0.5	<0.5	<0.5	1.2	0.5	0.6	<0.5	<0.5	<0.5	<0.5	<0.5	<0.5	<0.5
7	Zr	0.5	ppm	5.4	2.8	4.7	2.9	6.1	4.8	4.3	7.4	8.9	5	3.3	11.1	1.8	3.2	<0.5	<0.5	<0.5

Annex 2.4

	supergene zones	hydro-thermal alteration	area [m2]	volume [m3]	masse volumique [kg/m3]	Cu [%]	enrichment	removed/added Cu		Cu in supergene zone	total removed/ added Cu of supergene zone	total Cu in supergene zone	largeur de la zone d'alteration	hypothetic high of the porphyry
N2200	prim	chl	1.47E+04	1.47E+06	2650	**0.0028**	0							
N2200	sup-	chl	2.00E+04	2.00E+06	2650	0.0013	-0.0015	-7.95E+06	0.00E+00	6.89E+06				
N2200	sup+	chl	1.09E+03	1.09E+05	2650	0.0125	0.0097	2.79E+06	2.79E+06	3.60E+06				
N2200	zo	chl	1.25E+04	1.25E+06	2650	0.0048	0.002	6.62E+06	6.62E+06	1.59E+07	1.46E+06	2.64E+07	1.23E+02	16
N2200	sup-	qs	5.73E+03	5.73E+05	2650	**0.0035**	-0.0004	-6.07E+05	0.00E+00	5.31E+06				
N2200	sup+	qs	3.20E+03	3.20E+05	2650	**0.0244**	0.0205	1.74E+07	1.74E+07	2.07E+07				
N2200	zo	qs	5.89E+03	5.89E+05	2650	0.0003	-0.0036	-5.62E+06	0.00E+00	4.68E+05	1.12E+07	2.65E+07	6.00E+01	180
N2300	prim	chl	5.11E+04	5.11E+06	2650	0.0028	0		0.00E+00					
N2300	sup-	chl	8.59E+03	8.59E+05	2650	0.0027	-0.0001	-2.28E+05	0.00E+00	6.14E+06				
N2300	sup+	chl			2650	0	0	0.00E+00	0.00E+00	0.00E+00				
N2300	zo	chl	1.04E+04	1.04E+06	2650	0.0012	-0.0016	-4.41E+06	0.00E+00	3.31E+06	**-4.64E+06**	9.45E+06	1.11E+02	-56
N2300	prim	qs	8.55E+03	8.55E+05	2650	**0.0039**	0		0.00E+00					
N2300	sup-	qs	1.79E+04	1.79E+06	2650	**0.0035**	-0.0004	-1.90E+06	0.00E+00	1.66E+07				
N2300	sup+	qs	5.98E+03	5.98E+05	2650	0.0224	0.0196	3.11E+07	3.11E+07	3.55E+07				
N2300	zo	qs	1.72E+04	1.72E+06	2650	0.0016	-0.0023	-1.05E+07	0.00E+00	7.29E+06	1.87E+07	5.94E+07	1.78E+02	102
N2300	prim	zt	7.53E+04	7.53E+06	2650	0.0022	0		0.00E+00					
N2300	sup-	zt	1.08E+04	1.08E+06	2650	0.0066	0.0044	1.26E+07	1.26E+07	1.90E+07				
N2300	sup+	zt	3.42E+03	3.42E+05	2650	0.0133	0.0111	1.01E+07	1.01E+07	1.21E+07				
N2300	zo	zt	4.96E+03	4.96E+05	2650	0.0016	-0.0006	-7.89E+05	0.00E+00	2.10E+06	2.19E+07	3.31E+07	5.00E+01	752
N2400	prim	chl	7.40E+04	7.40E+06	2650	0.0014	0		0.00E+00					
N2400	sup-	chl	1.31E+04	1.31E+06	2650	0.0016	0.0002	6.94E+05	6.94E+05	5.55E+06				
N2400	sup+	chl			2650	0	0	0.00E+00	0.00E+00	0.00E+00				
N2400	zo	chl	1.26E+04	1.26E+06	2650	0.0012	-0.0002	-6.66E+05	0.00E+00	3.99E+06	2.85E+04	9.55E+06	1.71E+02	0
N2400	prim	qs	3.62E+04	3.62E+06	2650	**0.0039**	0		0.00E+00					
N2400	sup-	qs	4.05E+04	4.05E+06	2650	0.0035	-0.0004	-4.29E+06	0.00E+00	3.75E+07				

	supergene zones	hydro-thermal alteration	area [m2]	volume [m3]	masse volumique [kg/m3]	Cu [%]	enrichment	removed/added Cu		Cu in supergene zone	total removed/ added Cu of supergene zone	total Cu in supergene zone	largeur de la zone d'alteration	hypothetic high of the porphyry
N2400	sup+	qs	6.46E+03	6.46E+05	2650	0.028	0.0241	4.13E+07	4.13E+07	4.80E+07				
N2400	zo	qs	4.65E+03	4.65E+05	2650	0.003	-0.0009	-1.11E+06	0.00E+00	3.69E+06	3.59E+07	8.92E+07	7.00E+01	496
N2400	prim	zt	4.64E+04	4.64E+06	2650	0.0056	0		0.00E+00					
N2400	sup-	zt	1.07E+04	1.07E+06	2650	0.007	0.0014	3.99E+06	3.99E+06	1.99E+07				
N2400	sup+	zt	1.79E+03	1.79E+05	2650	**0.0158**	0.0102	4.85E+06	4.85E+06	7.51E+06				
N2400	zo	zt	2.62E+04	2.62E+06	2650	0.0072	0.0016	1.11E+07	1.11E+07	5.00E+07	1.99E+07	7.75E+07	1.73E+02	78
N2500	prim	chl	2.06E+05	2.06E+07	2650	0.0017	0		0.00E+00					
N2500	sup-	chl	8.51E+04	8.51E+06	2650	0.003	0.0013	2.93E+07	2.93E+07	6.76E+07				
N2500	sup+	chl	1.48E+03	1.48E+05	2650	**0.007**	0.0053	2.08E+06	2.08E+06	2.75E+06				
N2500	zo	chl	3.26E+04	3.26E+06	2650	0.0018	1E-04	8.63E+05	8.63E+05	1.55E+07	3.22E+07	8.59E+07	4.83E+02	148
N2500	prim	qs	1.80E+04	1.80E+06	2650	**0.0039**	0		0.00E+00					
N2500	sup-	qs	8.10E+04	8.10E+06	2650	0.0096	0.0057	1.22E+08	1.22E+08	2.06E+08				
N2500	sup+	qs	7.74E+03	7.74E+05	2650	0.023	0.0191	3.92E+07	3.92E+07	4.72E+07				
N2500	zo	qs	1.82E+04	1.82E+06	2650	0.003	-0.0009	-4.33E+06	0.00E+00	1.44E+07	1.57E+08	2.68E+08	1.32E+02	1152
N2500	prim	zt	3.67E+04	3.67E+06	2650	**0.0065**	0		0.00E+00					
N2500	sup-	zt	7.03E+04	7.03E+06	2650	0.0071	0.0006	1.12E+07	1.12E+07	1.32E+08				
N2500	sup+	zt	1.02E+04	1.02E+06	2650	0.0183	0.0118	3.20E+07	3.20E+07	4.96E+07				
N2500	zo	zt	1.93E+04	1.93E+06	2650	0.0076	0.0011	5.61E+06	5.61E+06	3.88E+07	4.88E+07	2.21E+08	1.54E+02	184
N2600	prim	chl	1.55E+05	1.55E+07	2650	0.0014	0		0.00E+00					
N2600	sup-	chl	1.03E+05	1.03E+07	2650	0.0014	0	0.00E+00	0.00E+00	3.83E+07				
N2600	sup+	chl	1.24E+04	1.24E+06	2650	0.0183	0.0169	5.56E+07	5.56E+07	6.02E+07				
N2600	zo	chl	2.80E+04	2.80E+06	2650	**0.0026**	0.0012	8.90E+06	8.90E+06	1.93E+07	6.45E+07	1.18E+08	5.42E+02	321
N2600	prim	qs	6.40E+04	6.40E+06	2650	0.0039	0		0.00E+00					
N2600	sup-	qs	1.18E+05	1.18E+07	2650	0.0044	0.0005	1.56E+07	1.56E+07	1.37E+08				
N2600	sup+	qs	1.58E+04	1.58E+06	2650	0.0285	0.0246	1.03E+08	1.03E+08	1.19E+08				
N2600	zo	qs	1.80E+04	1.80E+06	2650	0.0011	-0.0028	-1.34E+07	0.00E+00	5.26E+06	1.05E+08	2.61E+08	1.63E+02	623
N2600	prim	zt	6.56E+04	6.56E+06	2650	0.0074	0		0.00E+00					

	supergene zones	hydro-thermal alteration	area [m2]	volume [m3]	masse volumique [kg/m3]	Cu [%]	enrichment	removed/added Cu		Cu in supergene zone	total removed/ added Cu of supergene zone	total Cu in supergene zone	largeur de la zone d'alteration	hypothetic high of the porphyry
N2600	sup-	zt	4.04E+04	4.04E+06	2650	0.0055	-0.0019	-2.03E+07	0.00E+00	5.89E+07				
N2600	sup+	zt	1.32E+04	1.32E+06	2650	**0.0226**	0.0152	5.32E+07	5.32E+07	7.91E+07				
N2600	zo	zt	1.45E+04	1.45E+06	2650	0.0099	0.0025	9.63E+06	9.63E+06	3.82E+07	4.25E+07	1.76E+08	1.00E+02	217
N2700	prim	chl	3.05E+05	3.05E+07	2650	**0.0018**	0		0.00E+00					
N2700	sup-	chl	1.03E+05	1.03E+07	2650	0.0028	0.001	2.74E+07	2.74E+07	7.66E+07				
N2700	sup+	chl	5.24E+03	5.24E+05	2650	0.007	0.0052	7.22E+06	7.22E+06	9.72E+06				
N2700	zo	chl	2.77E+04	2.77E+06	2650	0.0033	0.0015	1.10E+07	1.10E+07	2.42E+07	4.56E+07	1.11E+08	4.57E+02	209
N2700	prim	po	8.51E+04	8.51E+06	2650	0.0075	0		0.00E+00					
N2700	sup-	po	1.87E+04	1.87E+06	2650	**0.0081**	0.0006	2.98E+06	2.98E+06	4.02E+07				
N2700	sup+	po	6.47E+03	6.47E+05	2650	0.0134	0.0059	1.01E+07	1.01E+07	2.30E+07				
N2700	zo	po	5.79E+03	5.79E+05	2650	0.0027	-0.0048	-7.37E+06	0.00E+00	4.15E+06	5.73E+06	6.73E+07	6.10E+01	47
N2700	prim	qs	1.24E+05	1.24E+07	2650	0.0037	0		0.00E+00					
N2700	sup-	qs	1.48E+05	1.48E+07	2650	0.0067	0.003	1.17E+08	1.17E+08	2.62E+08				
N2700	sup+	qs	2.63E+04	2.63E+06	2650	0.0267	0.023	1.60E+08	1.60E+08	1.86E+08				
N2700	zo	qs	2.55E+04	2.55E+06	2650	0.0009	-0.0028	-1.89E+07	0.00E+00	6.08E+06	2.58E+08	4.54E+08	2.27E+02	1161
N2700	prim	zt	6.82E+02	6.82E+04	2650	**0.0074**	0		0.00E+00					
N2700	sup-	zt	2.22E+04	2.22E+06	2650	0.0079	0.0005	2.94E+06	2.94E+06	4.65E+07				
N2700	sup+	zt	1.05E+04	1.05E+06	2650	0.0268	0.0194	5.42E+07	5.42E+07	7.48E+07				
N2700	zo	zt	9.50E+03	9.50E+05	2650	0.0009	-0.0065	-1.64E+07	0.00E+00	2.27E+06	4.07E+07	1.24E+08	6.10E+01	341
N2800	prim	chl	4.02E+05	4.02E+07	2650	0.0021	0		0.00E+00					
N2800	sup-	chl	6.69E+04	6.69E+06	2650	0.0022	0.0001	1.77E+06	1.77E+06	3.90E+07				
N2800	sup+	chl	3.05E+02	3.05E+04	2650	**0.007**	0.0049	3.96E+05	3.96E+05	5.66E+05				
N2800	zo	chl	3.44E+04	3.44E+06	2650	0.0016	-0.0005	-4.56E+06	0.00E+00	1.46E+07	**-2.39E+06**	5.42E+07	3.71E+02	-12
N2800	prim	po	1.26E+05	1.26E+07	2650	0.0069	0		0.00E+00					
N2800	sup-	po	7.27E+04	7.27E+06	2650	0.0081	0.0012	2.31E+07	2.31E+07	1.56E+08				
N2800	sup+	po	2.93E+04	2.93E+06	2650	0.0127	0.0058	4.50E+07	4.50E+07	9.85E+07				
N2800	zo	po	2.82E+04	2.82E+06	2650	0.0042	-0.0027	-2.01E+07	0.00E+00	3.13E+07	4.80E+07	2.86E+08	2.66E+02	99

	supergene zones	hydro-thermal alteration	area [m2]	volume [m3]	masse volumique [kg/m3]	Cu [%]	enrichment	removed/added Cu		Cu in supergene zone	total removed/ added Cu of supergene zone	total Cu in supergene zone	largeur de la zone d'alteration	hypothetic high of the porphyry
N2800	prim	qs	1.02E+05	1.02E+07	2650	0.0086	0		0.00E+00					
N2800	sup-	qs	1.44E+05	1.44E+07	2650	0.0153	0.0153	5.86E+08	5.86E+08	5.86E+08				
N2800	sup+	qs	2.12E+04	2.12E+06	2650	0.0316	0.0316	1.77E+08	1.77E+08	1.77E+08				
N2800	zo	qs	1.49E+04	1.49E+06	2650	0.0062	0.0062	2.45E+07	2.45E+07	2.45E+07	7.88E+08	7.88E+08	1.15E+02	3005
N2900	prim	chl	5.89E+05	5.89E+07	2650	0.0022	0		0.00E+00					
N2900	sup-	chl	9.48E+03	9.48E+05	2650	0.0054	0.0032	8.04E+06	8.04E+06	1.36E+07				
N2900	sup+	chl	9.49E+03	9.49E+05	2650	**0.007**	0.0048	1.21E+07	1.21E+07	1.76E+07				
N2900	zo	chl	3.16E+04	3.16E+06	2650	0.0058	0.0036	3.02E+07	3.02E+07	4.86E+07	5.03E+07	7.98E+07	3.51E+02	246
N2900	prim	po	1.58E+05	1.58E+07	2650	0.0069	0		0.00E+00					
N2900	sup-	po	6.69E+04	6.69E+06	2650	0.0092	0.0023	4.08E+07	4.08E+07	1.63E+08				
N2900	sup+	po	1.54E+04	1.54E+06	2650	0.0264	0.0195	7.94E+07	7.94E+07	1.07E+08				
N2900	zo	po	2.26E+04	2.26E+06	2650	0.0103	0.0034	2.03E+07	2.03E+07	6.16E+07	1.41E+08	3.32E+08	2.38E+02	323
N2900	prim	qs	1.64E+05	1.64E+07	2650	0.005	0		0.00E+00					
N2900	sup-	qs	7.99E+04	7.99E+06	2650	0.0094	0.0069	1.46E+08	1.46E+08	1.99E+08				
N2900	sup+	qs	2.09E+04	2.09E+06	2650	0.037	0.0345	1.91E+08	1.91E+08	2.05E+08				
N2900	zo	qs	1.45E+04	1.45E+06	2650	0.0046	0.0021	8.06E+06	8.06E+06	1.77E+07	3.45E+08	4.21E+08	1.35E+02	1929
N3000	prim	chl	6.06E+05	6.06E+07	2650	0.0036	0		0.00E+00					
N3000	sup-	chl	1.15E+04	1.15E+06	2650	0.0056	0.002	6.12E+06	6.12E+06	1.71E+07				
N3000	sup+	chl	5.80E+02	5.80E+04	2650	**0.0099**	0.0063	9.68E+05	9.68E+05	1.52E+06				
N3000	zo	chl	4.70E+04	4.70E+06	2650	0.0072	0.0036	4.48E+07	4.48E+07	8.96E+07	5.19E+07	1.08E+08	3.48E+02	156
N3000	prim	po	1.47E+05	1.47E+07	2650	0.0053	0		0.00E+00					
N3000	sup-	po	4.19E+04	4.19E+06	2650	0.0069	0.0016	1.78E+07	1.78E+07	7.67E+07				
N3000	sup+	po	1.08E+04	1.08E+06	2650	0.008	0.0027	7.70E+06	7.70E+06	2.28E+07				
N3000	zo	po	1.98E+04	1.98E+06	2650	0.0062	0.0009	4.71E+06	4.71E+06	3.25E+07	3.02E+07	1.32E+08	1.95E+02	110
N3000	prim	qs	1.80E+05	1.80E+07	2650	0.0055	0		0.00E+00					
N3000	sup-	qs	1.21E+05	1.21E+07	2650	0.0096	0.0041	1.31E+08	1.31E+08	3.07E+08				
N3000	sup+	qs	4.37E+04	4.37E+06	2650	0.0247	0.0192	2.22E+08	2.22E+08	2.86E+08				

	supergene zones	hydro-thermal alteration	area [m2]	volume [m3]	masse volumique [kg/m3]	Cu [%]	enrichment	removed/added Cu		Cu in supergene zone	total removed/ added Cu of supergene zone	total Cu in supergene zone	largeur de la zone d'alteration	hypothetic high of the porphyry
N3000	zo	qs	1.70E+04	1.70E+06	2650	0.0018	-0.0037	-1.66E+07	0.00E+00	8.09E+06	3.37E+08	6.01E+08	1.72E+02	1343
N3100	prim	chl	5.87E+05	5.87E+07	2650	0.0015	0		0.00E+00					
N3100	sup-	chl	5.62E+03	5.62E+05	2650	0.0053	0.0038	5.66E+06	5.66E+06	7.89E+06				
N3100	sup+	chl	7.22E+03	7.22E+05	2650	0.0128	0.0113	2.16E+07	2.16E+07	2.45E+07				
N3100	zo	chl	4.48E+04	4.48E+06	2650	0.0057	0.0042	4.98E+07	4.98E+07	6.77E+07	7.71E+07	1.00E+08	4.01E+02	484
N3100	prim	po	1.46E+05	1.46E+07	2650	0.0089	0		0.00E+00					
N3100	sup-	po	2.98E+04	2.98E+06	2650	0.0117	0.0028	2.21E+07	2.21E+07	9.24E+07				
N3100	sup+	po	2.09E+04	2.09E+06	2650	0.0241	0.0152	8.43E+07	8.43E+07	1.34E+08				
N3100	zo	po	2.40E+04	2.40E+06	2650	0.0105	0.0016	1.02E+07	1.02E+07	6.68E+07	1.17E+08	2.93E+08	2.22E+02	223
N3100	prim	qs	1.41E+05	1.41E+07	2650	0.0049	0		0.00E+00					
N3100	sup-	qs	1.32E+05	1.32E+07	2650	0.0072	0.0023	8.05E+07	8.05E+07	2.52E+08				
N3100	sup+	qs	4.33E+04	4.33E+06	2650	0.0137	0.0088	1.01E+08	1.01E+08	1.57E+08				
N3100	zo	qs	7.15E+03	7.15E+05	2650	0.0026	-0.0023	-4.35E+06	0.00E+00	4.92E+06	1.77E+08	4.14E+08	1.14E+02	1197
N3200	prim	chl	5.86E+05	5.86E+07	2650	0.0025	0		0.00E+00					
N3200	sup-	chl	7.06E+03	7.06E+05	2650	0.015	0.0125	2.34E+07	2.34E+07	2.81E+07				
N3200	sup+	chl	4.09E+03	4.09E+05	2650	**0.0114**	0.0089	9.64E+06	9.64E+06	1.23E+07				
N3200	zo	chl	6.67E+04	6.67E+06	2650	0.0088	0.0063	1.11E+08	1.11E+08	1.55E+08	1.44E+08	1.96E+08	4.99E+02	436
N3200	prim	po	1.08E+05	1.08E+07	2650	0.0069	0		0.00E+00					
N3200	sup-	po	4.62E+04	4.62E+06	2650	0.0086	0.0017	2.08E+07	2.08E+07	1.05E+08				
N3200	sup+	po	2.15E+04	2.15E+06	2650	0.0166	0.0097	5.52E+07	5.52E+07	9.44E+07				
N3200	zo	po	1.61E+04	1.61E+06	2650	0.0032	-0.0037	-1.58E+07	0.00E+00	1.36E+07	6.02E+07	2.13E+08	1.54E+02	214
N3200	prim	qs	1.41E+05	1.41E+07	2650	0.006	0		0.00E+00					
N3200	sup-	qs	1.36E+05	1.36E+07	2650	0.0096	0.0036	1.30E+08	1.30E+08	3.46E+08				
N3200	sup+	qs	6.32E+04	6.32E+06	2650	0.0116	0.0056	9.37E+07	9.37E+07	1.94E+08				
N3200	zo	qs	6.56E+03	6.56E+05	2650	**0.0022**	-0.0038	-6.61E+06	0.00E+00	3.83E+06	2.17E+08	5.44E+08	1.48E+02	921
N3300	prim	chl	4.43E+05	4.43E+07	2650	0.0023	0		0.00E+00					
N3300	sup-	chl	1.33E+04	1.33E+06	2650	0.0044	0.0021	7.38E+06	7.38E+06	1.55E+07				

	supergene zones	hydro-thermal alteration	area [m2]	volume [m3]	masse volumique [kg/m3]	Cu [%]	enrichment	removed/added Cu		Cu in supergene zone	total removed/ added Cu of supergene zone	total Cu in supergene zone	largeur de la zone d'alteration	hypothetic high of the porphyry
N3300	sup+	chl	3.65E+03	3.65E+05	2650	0.01	0.0077	7.46E+06	7.46E+06	9.68E+06				
N3300	zo	chl	4.95E+04	4.95E+06	2650	0.0024	1E-04	1.31E+06	1.31E+06	3.15E+07	1.61E+07	5.66E+07	2.71E+02	98
N3300	prim	po	1.53E+05	1.53E+07	2650	0.0068	0		0.00E+00					
N3300	sup-	po	8.00E+04	8.00E+06	2650	0.008	0.0012	2.55E+07	2.55E+07	1.70E+08				
N3300	sup+	po	3.21E+04	3.21E+06	2650	0.0085	0.0017	1.45E+07	1.45E+07	7.23E+07				
N3300	zo	po	4.09E+04	4.09E+06	2650	0.0247	0.0179	1.94E+08	1.94E+08	2.68E+08	2.34E+08	5.10E+08	2.89E+02	449
N3300	prim	qs	9.81E+04	9.81E+06	2650	0.0052	0		0.00E+00					
N3300	sup-	qs	1.69E+05	1.69E+07	2650	0.0109	0.0057	2.55E+08	2.55E+08	4.88E+08				
N3300	sup+	qs	5.14E+04	5.14E+06	2650	0.0134	0.0082	1.12E+08	1.12E+08	1.82E+08				
N3300	zo	qs	1.30E+04	1.30E+06	2650	0.0018	-0.0034	-1.17E+07	0.00E+00	6.19E+06	3.55E+08	6.77E+08	1.34E+02	1924
N3400	prim	chl	4.65E+05	4.65E+07	2650	0.0015	0		0.00E+00					
N3400	sup-	chl	5.35E+03	5.35E+05	2650	0.0056	0.0044	6.24E+06	6.24E+06	7.94E+06				
N3400	sup+	chl	1.96E+03	1.96E+05	2650	0.0075	0.0063	3.27E+06	3.27E+06	3.89E+06				
N3400	zo	chl	5.85E+04	5.85E+06	2650	0.0175	0.0163	2.53E+08	2.53E+08	2.71E+08	2.62E+08	2.83E+08	3.86E+02	1709
N3400	prim	po	1.68E+05	1.68E+07	2650	0.0071	0		0.00E+00					
N3400	sup-	po	5.14E+04	5.14E+06	2650	0.0073	0.0002	2.72E+06	2.72E+06	9.94E+07				
N3400	sup+	po	2.05E+04	2.05E+06	2650	0.0181	0.011	5.97E+07	5.97E+07	9.82E+07				
N3400	zo	po	2.94E+04	2.94E+06	2650	0.0092	0.0021	1.64E+07	1.64E+07	7.18E+07	7.88E+07	2.69E+08	2.03E+02	206
N3400	prim	qs	5.90E+04	5.90E+06	2650	**0.00725**	0		0.00E+00					
N3400	sup-	qs	2.07E+05	2.07E+07	2650	0.0103	0.00305	1.68E+08	1.68E+08	5.66E+08				
N3400	sup+	qs	9.18E+04	9.18E+06	2650	0.027	0.01975	4.80E+08	4.80E+08	6.57E+08				
N3400	zo	qs	2.76E+04	2.76E+06	2650	0.0018	-0.00545	-3.99E+07	0.00E+00	1.32E+07	6.08E+08	1.24E+09	2.29E+02	1382
N3500	prim	chl	3.18E+05	3.18E+07	2650	0.002	0		0.00E+00					
N3500	sup-	chl	6.32E+03	6.32E+05	2650	0.0062	0.0042	7.03E+06	7.03E+06	1.04E+07				
N3500	sup+	chl			2650	0	0	0.00E+00	0.00E+00	0.00E+00				
N3500	zo	chl	5.02E+04	5.02E+06	2650	0.0033	0.0013	1.73E+07	1.73E+07	4.39E+07	2.43E+07	5.43E+07	2.41E+02	191
N3500	prim	po	2.06E+05	2.06E+07	2650	0.0098	0		0.00E+00					

	supergene zones	hydro-thermal alteration	area [m2]	volume [m3]	masse volumique [kg/m3]	Cu [%]	enrichment	removed/added Cu		Cu in supergene zone	total removed/ added Cu of supergene zone	total Cu in supergene zone	largeur de la zone d'alteration	hypothetic high of the porphyry
N3500	sup-	po	3.78E+04	3.78E+06	2650	0.0072	-0.0026	-2.60E+07	0.00E+00	7.20E+07				
N3500	sup+	po	2.62E+04	2.62E+06	2650	0.0199	0.0101	7.02E+07	7.02E+07	1.38E+08				
N3500	zo	po	4.78E+04	4.78E+06	2650	0.0069	-0.0029	-3.67E+07	0.00E+00	8.74E+07	7.42E+06	2.98E+08	2.76E+02	10
N3500	prim	qs	1.33E+05	1.33E+07	2650	**0.00725**	0		0.00E+00					
N3500	sup-	qs	1.82E+05	1.82E+07	2650	0.0084	0.00115	5.55E+07	5.55E+07	4.06E+08				
N3500	sup+	qs	8.70E+04	8.70E+06	2650	0.0132	0.00595	1.37E+08	1.37E+08	3.04E+08				
N3500	zo	qs	2.39E+04	2.39E+06	2650	0.0063	-0.00095	-6.01E+06	0.00E+00	3.98E+07	1.87E+08	7.50E+08	2.10E+02	463
N3600	prim	chl	3.04E+05	3.04E+07	2650	0.0009	0		0.00E+00					
N3600	sup-	chl			2650	0	0	0.00E+00	0.00E+00	0.00E+00				
N3600	sup+	chl			2650	0	0	0.00E+00	0.00E+00	0.00E+00				
N3600	zo	chl	5.06E+04	5.06E+06	2650	0.001	0.0001	1.34E+06	1.34E+06	1.34E+07	1.34E+06	1.34E+07	2.44E+02	23
N3600	prim	po	2.15E+05	2.15E+07	2650	0.0092	0		0.00E+00					
N3600	sup-	po	5.73E+04	5.73E+06	2650	0.0055	-0.0037	-5.61E+07	0.00E+00	8.34E+07				
N3600	sup+	po	2.46E+04	2.46E+06	2650	0.0082	-0.001	-6.52E+06	0.00E+00	5.34E+07				
N3600	zo	po	5.76E+04	5.76E+06	2650	0.0113	0.0021	3.21E+07	3.21E+07	1.73E+08	**-3.06E+07**	3.09E+08	3.13E+02	-40
N3600	prim	qs	1.43E+05	1.43E+07	2650	0.0093	0		0.00E+00					
N3600	sup-	qs	1.89E+05	1.89E+07	2650	0.0188	0.0095	4.76E+08	4.76E+08	9.43E+08				
N3600	sup+	qs	1.01E+05	1.01E+07	2650	0.0214	0.0121	3.23E+08	3.23E+08	5.71E+08				
N3600	zo	qs	2.56E+04	2.56E+06	2650	0.002	-0.0073	-4.95E+07	0.00E+00	1.36E+07	7.50E+08	1.53E+09	2.41E+02	1263
N3700	prim	chl	2.80E+05	2.80E+07	2650	0.0046	0		0.00E+00					
N3700	sup-	chl	2.17E+02	2.17E+04	2650	0.0083	0.0037	2.13E+05	2.13E+05	4.77E+05				
N3700	sup+	chl			2650	0	0	0.00E+00	0.00E+00	0.00E+00				
N3700	zo	chl	5.87E+04	5.87E+06	2650	0.0055	0.0009	1.40E+07	1.40E+07	8.55E+07	1.42E+07	8.60E+07	2.72E+02	43
N3700	prim	po	2.10E+05	2.10E+07	2650	0.0098	0		0.00E+00					
N3700	sup-	po	8.50E+04	8.50E+06	2650	0.0148	0.005	1.13E+08	1.13E+08	3.33E+08				
N3700	sup+	po	1.03E+04	1.03E+06	2650	0.0172	0.0074	2.02E+07	2.02E+07	4.70E+07				
N3700	zo	po	5.23E+04	5.23E+06	2650	0.0101	0.0003	4.16E+06	4.16E+06	1.40E+08	1.37E+08	5.20E+08	2.27E+02	232

	supergene zones	hydro-thermal alteration	area [m2]	volume [m3]	masse volumique [kg/m3]	Cu [%]	enrichment	removed/added Cu		Cu in supergene zone	total removed/ added Cu of supergene zone	total Cu in supergene zone	largeur de la zone d'alteration	hypothetic high of the porphyry
N3700	prim	qs	8.68E+04	8.68E+06	2650	0.0084	0		0.00E+00					
N3700	sup-	qs	2.21E+05	2.21E+07	2650	0.0092	0.0008	4.68E+07	4.68E+07	5.39E+08				
N3700	sup+	qs	1.05E+05	1.05E+07	2650	0.0218	0.0134	3.74E+08	3.74E+08	6.09E+08				
N3700	zo	qs	3.84E+04	3.84E+06	2650	0.0005	-0.0079	-8.03E+07	0.00E+00	5.09E+06	3.41E+08	1.15E+09	2.87E+02	533
N3800	prim	chl	2.75E+05	2.75E+07	2650	0.0021	0		0.00E+00					
N3800	sup-	chl	7.02E+03	7.02E+05	2650	**0.01145**	0.00935	1.74E+07	1.74E+07	2.13E+07				
N3800	sup+	chl			2650	0	0	0.00E+00	0.00E+00	0.00E+00				
N3800	zo	chl	4.59E+04	4.59E+06	2650	0.0042	0.0021	2.55E+07	2.55E+07	5.11E+07	4.29E+07	7.24E+07	2.61E+02	296
N3800	prim	po	3.02E+05	3.02E+07	2650	0.0045	0		0.00E+00					
N3800	sup-	po	5.24E+04	5.24E+06	2650	0.0077	0.0032	4.44E+07	4.44E+07	1.07E+08				
N3800	sup+	po	9.84E+03	9.84E+05	2650	0.0108	0.0063	1.64E+07	1.64E+07	2.82E+07				
N3800	zo	po	6.45E+04	6.45E+06	2650	0.0164	0.0119	2.03E+08	2.03E+08	2.80E+08	2.64E+08	4.15E+08	2.90E+02	764
N3800	prim	qs	1.12E+04	1.12E+06	2650	0.0161	0		0.00E+00					
N3800	prim	qs	1.41E+05	1.41E+07	2650	0.0161	0		0.00E+00					
N3800	sup-	qs	1.76E+05	1.76E+07	2650	0.012	-0.0041	-1.91E+08	0.00E+00	5.60E+08				
N3800	sup+	qs	9.01E+04	9.01E+06	2650	0.0285	0.0124	2.96E+08	2.96E+08	6.80E+08				
N3800	zo	qs	4.01E+04	4.01E+06	2650	0.0004	-0.0157	-1.67E+08	0.00E+00	4.25E+06	**-6.19E+07**	1.24E+09	2.66E+02	-55
N3900	prim	chl	3.03E+05	3.03E+07	2650	0.0033	0		0.00E+00					
N3900	sup+	chl			2650	0	0	0.00E+00	0.00E+00	0.00E+00				
N3900	zo	chl	4.09E+04	4.09E+06	2650	0.0011	-0.0022	-2.38E+07	0.00E+00	1.19E+07	**-2.38E+07**	1.19E+07	1.74E+02	-157
N3900	prim	po	3.47E+05	3.47E+07	2650	0.0094	0		0.00E+00					
N3900	sup-	po	5.92E+04	5.92E+06	2650	0.0084	-0.001	-1.57E+07	0.00E+00	1.32E+08				
N3900	sup+	po	1.57E+04	1.57E+06	2650	0.0183	0.0089	3.71E+07	3.71E+07	7.62E+07				
N3900	zo	po	8.23E+04	8.23E+06	2650	0.0211	0.0117	2.55E+08	2.55E+08	4.60E+08	2.76E+08	6.68E+08	3.35E+02	331
N3900	prim	qs	1.17E+05	1.17E+07	2650	0.0062	0		0.00E+00					
N3900	sup-	qs	1.91E+05	1.91E+07	2650	0.0126	0.0064	3.25E+08	3.25E+08	6.39E+08				
N3900	sup+	qs	8.57E+04	8.57E+06	2650	0.0233	0.0171	3.89E+08	3.89E+08	5.29E+08				

	supergene zones	hydro-thermal alteration	area [m2]	volume [m3]	masse volumique [kg/m3]	Cu [%]	enrichment	removed/added Cu		Cu in supergene zone	total removed/ added Cu of supergene zone	total Cu in supergene zone	largeur de la zone d'alteration	hypothetic high of the porphyry
N3900	zo	qs	4.16E+04	4.16E+06	2650	0.0073	0.0011	1.21E+07	1.21E+07	8.05E+07	7.25E+08	1.25E+09	2.69E+02	1641
N4000	prim	chl	5.52E+05	5.52E+07	2650	0.004	0		0.00E+00					
N4000	sup-	chl	1.20E+03	1.20E+05	2650	**0.01145**	0.00745	2.37E+06	2.37E+06	3.64E+06				
N4000	sup+	chl			2650	0	0	0.00E+00	0.00E+00	0.00E+00				
N4000	zo	chl	6.02E+04	6.02E+06	2650	0.0024	-0.0016	-2.55E+07	0.00E+00	3.83E+07	**-2.31E+07**	4.19E+07	3.18E+02	-69
N4000	prim	po	2.71E+05	2.71E+07	2650	0.0089	0		0.00E+00					
N4000	sup-	po	7.90E+04	7.90E+06	2650	0.011	0.0094	1.97E+08	1.97E+08	2.30E+08				
N4000	sup+	po	2.53E+04	2.53E+06	2650	0.0123	0.0034	2.28E+07	2.28E+07	8.25E+07				
N4000	zo	po	6.33E+04	6.33E+06	2650	0.021	-0.0068	-1.14E+08	0.00E+00	3.52E+08	1.06E+08	6.65E+08	3.08E+02	145
N4000	prim	qs	2.12E+05	2.12E+07	2650	0.012	0		0.00E+00					
N4000	sup-	qs	1.29E+05	1.29E+07	2650	0.0131	0.0011	3.76E+07	3.76E+07	4.47E+08				
N4000	sup+	qs	9.98E+04	9.98E+06	2650	0.0308	0.0188	4.97E+08	4.97E+08	8.15E+08				
N4000	zo	qs	4.33E+04	4.33E+06	2650	0.0046	-0.0074	-8.49E+07	0.00E+00	5.28E+07	4.50E+08	1.32E+09	2.40E+02	590
N4100	prim	chl	6.49E+05	6.49E+07	2650	0.0042	0		0.00E+00					
N4100	sup-	chl	8.14E+03	8.14E+05	2650	0.0146	0.0104	2.24E+07	2.24E+07	3.15E+07				
N4100	sup+	chl			2650	0	0	0.00E+00	0.00E+00	0.00E+00				
N4100	zo	chl	7.58E+04	7.58E+06	2650	0.0031	-0.0011	-2.21E+07	0.00E+00	6.23E+07	3.55E+05	9.38E+07	4.34E+02	1
N4100	prim	po	2.94E+05	2.94E+07	2650	0.0071	0		0.00E+00					
N4100	sup-	po	1.53E+05	1.53E+07	2650	0.0159	0.0088	3.56E+08	3.56E+08	6.43E+08				
N4100	sup+	po	1.18E+04	1.18E+06	2650	0.0105	0.0034	1.07E+07	1.07E+07	3.29E+07				
N4100	zo	po	6.73E+04	6.73E+06	2650	0.0125	0.0054	9.63E+07	9.63E+07	2.23E+08	4.63E+08	8.99E+08	3.08E+02	799
N4100	prim	qs	1.98E+05	1.98E+07	2650	0.0127	0		0.00E+00					
N4100	sup-	qs	1.78E+05	1.78E+07	2650	0.0166	0.0039	1.84E+08	1.84E+08	7.84E+08				
N4100	sup+	qs	6.80E+04	6.80E+06	2650	0.0302	0.0175	3.15E+08	3.15E+08	5.44E+08				
N4100	zo	qs	4.47E+04	4.47E+06	2650	0.0146	0.0019	2.25E+07	2.25E+07	1.73E+08	5.22E+08	1.50E+09	2.34E+02	663
N4200	prim	chl	6.52E+05	6.52E+07	2650	0.003	0		0.00E+00					
N4200	sup-	chl	5.44E+03	5.44E+05	2650	0.0064	0.0034	4.90E+06	4.90E+06	9.22E+06				

	supergene zones	hydro-thermal alteration	area [m2]	volume [m3]	masse volumique [kg/m3]	Cu [%]	enrichment	removed/added Cu		Cu in supergene zone	total removed/ added Cu of supergene zone	total Cu in supergene zone	largeur de la zone d'alteration	hypothetic high of the porphyry
N4200	sup+	chl			2650	0	0	0.00E+00	0.00E+00	0.00E+00				
N4200	zo	chl	6.90E+04	6.90E+06	2650	0.0078	0.0048	8.78E+07	8.78E+07	1.43E+08	9.27E+07	1.52E+08	4.04E+02	288
N4200	prim	po	4.24E+05	4.24E+07	2650	0.0074	0		0.00E+00					
N4200	sup-	po	1.02E+05	1.02E+07	2650	0.0114	0.004	1.08E+08	1.08E+08	3.08E+08				
N4200	sup+	po	6.83E+03	6.83E+05	2650	**0.021**	0.0136	2.46E+07	2.46E+07	3.80E+07				
N4200	zo	po	6.94E+04	6.94E+06	2650	0.022	0.0146	2.68E+08	2.68E+08	4.05E+08	4.01E+08	7.51E+08	2.90E+02	705
N4200	prim	qs	1.64E+05	1.64E+07	2650	0.0102	0		0.00E+00					
N4200	sup-	qs	1.87E+05	1.87E+07	2650	0.0112	0.001	4.97E+07	4.97E+07	5.56E+08				
N4200	sup+	qs	5.41E+04	5.41E+06	2650	0.028	0.0178	2.55E+08	2.55E+08	4.01E+08				
N4200	zo	qs	6.76E+04	6.76E+06	2650	0.0046	-0.0056	-1.00E+08	0.00E+00	8.24E+07	2.05E+08	1.04E+09	3.44E+02	220
N4300	prim	chl	6.68E+05	6.68E+07	2650	0.0023	0		0.00E+00					
N4300	sup-	chl	6.75E+03	6.75E+05	2650	0.0051	0.0028	5.01E+06	5.01E+06	9.12E+06				
N4300	sup+	chl			2650	0	0	0.00E+00	0.00E+00	0.00E+00				
N4300	zo	chl	6.36E+04	6.36E+06	2650	0.0061	0.0038	6.40E+07	6.40E+07	1.03E+08	6.90E+07	1.12E+08	3.00E+02	377
N4300	prim	po	3.37E+05	3.37E+07	2650	0.0077	0		0.00E+00					
N4300	sup-	po	1.10E+05	1.10E+07	2650	0.0143	0.0066	1.93E+08	1.93E+08	4.19E+08				
N4300	sup+	po	3.20E+03	3.20E+05	2650	0.0315	0.0238	2.02E+07	2.02E+07	2.67E+07				
N4300	zo	po	5.13E+04	5.13E+06	2650	0.0069	-0.0008	-1.09E+07	0.00E+00	9.38E+07	2.02E+08	5.39E+08	2.53E+02	392
N4300	prim	qs	1.81E+05	1.81E+07	2650	**0.0088**	0		0.00E+00					
N4300	sup-	qs	2.81E+05	2.81E+07	2650	0.0107	0.0019	1.42E+08	1.42E+08	7.98E+08				
N4300	sup+	qs	7.81E+04	7.81E+06	2650	0.031	0.0222	4.59E+08	4.59E+08	6.41E+08				
N4300	zo	qs	7.49E+04	7.49E+06	2650	0.0055	-0.0033	-6.55E+07	0.00E+00	1.09E+08	5.35E+08	1.55E+09	3.72E+02	617
N4400	prim	chl	7.59E+05	7.59E+07	2650	0.0016	0		0.00E+00					
N4400	sup-	chl	1.85E+03	1.85E+05	2650	**0.0051**	0.0035	1.72E+06	1.72E+06	2.50E+06				
N4400	sup+	chl			2650	0	0	0.00E+00	0.00E+00	0.00E+00				
N4400	zo	chl	6.20E+04	6.20E+06	2650	0.0095	0.0079	1.30E+08	1.30E+08	1.56E+08	1.32E+08	1.59E+08	2.62E+02	1184
N4400	prim	po	3.16E+05	3.16E+07	2650	0.0081	0		0.00E+00					

	supergene zones	hydro-thermal alteration	area [m2]	volume [m3]	masse volumique [kg/m3]	Cu [%]	enrichment	removed/added Cu		Cu in supergene zone	total removed/ added Cu of supergene zone	total Cu in supergene zone	largeur de la zone d'alteration	hypothetic high of the porphyry
N4400	sup-	po	2.26E+05	2.26E+07	2650	0.0126	0.0045	2.69E+08	2.69E+08	7.54E+08				
N4400	sup+	po	2.45E+04	2.45E+06	2650	**0.0273**	0.0192	1.25E+08	1.25E+08	1.77E+08				
N4400	zo	po	9.93E+04	9.93E+06	2650	0.0265	0.0184	4.84E+08	4.84E+08	6.98E+08	8.78E+08	1.63E+09	4.63E+02	884
N4400	prim	qs	1.59E+05	1.59E+07	2650	0.0073	0		0.00E+00					
N4400	sup-	qs	2.21E+05	2.21E+07	2650	0.0129	0.0056	3.27E+08	3.27E+08	7.54E+08				
N4400	sup+	qs	4.29E+04	4.29E+06	2650	0.0294	0.0221	2.52E+08	2.52E+08	3.35E+08				
N4400	zo	qs	3.78E+04	3.78E+06	2650	0.0039	-0.0034	-3.41E+07	0.00E+00	3.91E+07	5.45E+08	1.13E+09	2.18E+02	1292
N4500	prim	chl	8.00E+05	8.00E+07	2650	0.0017	0		0.00E+00					
N4500	sup+	chl			2650	0	0	0.00E+00	0.00E+00	0.00E+00				
N4500	zo	chl	5.05E+04	5.05E+06	2650	0.0053	0.0036	4.82E+07	4.82E+07	7.10E+07	4.82E+07	7.10E+07	4.05E+02	264
N4500	prim	po	4.06E+05	4.06E+07	2650	0.008	0		0.00E+00					
N4500	sup-	po	1.30E+05	1.30E+07	2650	0.0128	0.0048	1.66E+08	1.66E+08	4.42E+08				
N4500	sup+	po	1.64E+04	1.64E+06	2650	0.023	0.015	6.54E+07	6.54E+07	1.00E+08				
N4500	zo	po	7.66E+04	7.66E+06	2650	0.0095	0.0015	3.04E+07	3.04E+07	1.93E+08	2.61E+08	7.35E+08	4.07E+02	303
N4500	prim	qs	1.91E+05	1.91E+07	2650	0.007	0		0.00E+00					
N4500	sup-	qs	2.93E+05	2.93E+07	2650	0.0083	0.0013	1.01E+08	1.01E+08	6.44E+08				
N4500	sup+	qs	6.85E+04	6.85E+06	2650	0.0292	0.0222	4.03E+08	4.03E+08	5.30E+08				
N4500	zo	qs	8.13E+04	8.13E+06	2650	0.008	0.001	2.15E+07	2.15E+07	1.72E+08	5.26E+08	1.35E+09	4.00E+02	708
N4600	prim	chl	6.08E+05	6.08E+07	2650	0.0025	0		0.00E+00					
N4600	sup+	chl			2650	0	0	0.00E+00	0.00E+00	0.00E+00				
N4600	zo	chl	3.96E+04	3.96E+06	2650	0.0075	0.005	5.25E+07	5.25E+07	7.87E+07	5.25E+07	7.87E+07	3.66E+02	216
N4600	prim	po	5.15E+05	5.15E+07	2650	0.0072	0		0.00E+00					
N4600	sup-	po	1.02E+05	1.02E+07	2650	0.0085	0.0013	3.50E+07	3.50E+07	2.29E+08				
N4600	sup+	po	8.60E+03	8.60E+05	2650	0.0196	0.0124	2.83E+07	2.83E+07	4.47E+07				
N4600	zo	po	5.03E+04	5.03E+06	2650	0.0162	0.009	1.20E+08	1.20E+08	2.16E+08	1.83E+08	4.89E+08	3.57E+02	269
N4600	prim	qs	2.98E+05	2.98E+07	2650	0.0083	0		0.00E+00					
N4600	sup-	qs	3.15E+05	3.15E+07	2650	0.0095	0.0012	1.00E+08	1.00E+08	7.93E+08				

	supergene zones	hydro-thermal alteration	area [m2]	volume [m3]	masse volumique [kg/m3]	Cu [%]	enrichment	removed/added Cu		Cu in supergene zone	total removed/ added Cu of supergene zone	total Cu in supergene zone	largeur de la zone d'alteration	hypothetic high of the porphyry
N4600	sup+	qs	5.65E+04	5.65E+06	2650	0.0242	0.0159	2.38E+08	2.38E+08	3.62E+08				
N4600	zo	qs	9.96E+04	9.96E+06	2650	0.0035	-0.0048	-1.27E+08	0.00E+00	9.24E+07	2.12E+08	1.25E+09	5.76E+02	167
N4700	prim	chl	5.81E+05	5.81E+07	2650	0.0011	0		0.00E+00					
N4700	sup-	chl	5.30E+03	5.30E+05	2650	0.0094	0.0083	1.17E+07	1.17E+07	1.32E+07				
N4700	sup+	chl			2650	0	0	0.00E+00	0.00E+00	0.00E+00				
N4700	zo	chl	6.79E+04	6.79E+06	2650	0.0099	0.0088	1.58E+08	1.58E+08	1.78E+08	1.70E+08	1.91E+08	4.11E+02	1420
N4700	prim	po	6.22E+05	6.22E+07	2650	0.008	0		0.00E+00					
N4700	prim	po	9.79E+04	9.79E+06	2650	0.008	0		0.00E+00					
N4700	sup-	po	1.15E+05	1.15E+07	2650	0.0098	0.0018	5.48E+07	5.48E+07	2.99E+08				
N4700	sup+	po	4.23E+04	4.23E+06	2650	0.0221	0.0141	1.58E+08	1.58E+08	2.47E+08				
N4700	zo	po	9.12E+04	9.12E+06	2650	0.0243	0.0163	3.94E+08	3.94E+08	5.87E+08	6.07E+08	1.13E+09	4.69E+02	610
N4700	prim	qs	1.87E+05	1.87E+07	2650	0.0077	0		0.00E+00					
N4700	sup-	qs	1.75E+05	1.75E+07	2650	0.0127	0.005	2.32E+08	2.32E+08	5.89E+08				
N4700	sup+	qs	2.39E+04	2.39E+06	2650	0.0195	0.0118	7.46E+07	7.46E+07	1.23E+08				
N4700	zo	qs	7.87E+04	7.87E+06	2650	0.0135	0.0058	1.21E+08	1.21E+08	2.82E+08	4.27E+08	9.94E+08	4.46E+02	470
N4800	prim	chl	5.45E+05	5.45E+07	2650	0.0008	0		0.00E+00					
N4800	sup-	chl	1.95E+04	1.95E+06	2650	0.0018	0.001	5.16E+06	5.16E+06	9.29E+06				
N4800	sup+	chl			2650	0	0	0.00E+00	0.00E+00	0.00E+00				
N4800	zo	chl	3.45E+04	3.45E+06	2650	0.0075	0.0067	6.13E+07	6.13E+07	6.86E+07	6.65E+07	7.79E+07	2.89E+02	1085
N4800	prim	po	5.75E+05	5.75E+07	2650	0.0076	0		0.00E+00					
N4800	sup-	po	1.50E+05	1.50E+07	2650	0.009	0.0014	5.56E+07	5.56E+07	3.58E+08				
N4800	sup+	po	2.80E+04	2.80E+06	2650	0.0282	0.0206	1.53E+08	1.53E+08	2.09E+08				
N4800	zo	po	9.32E+04	9.32E+06	2650	0.0232	0.0156	3.85E+08	3.85E+08	5.73E+08	5.94E+08	1.14E+09	5.87E+02	502
N4800	prim	qs	3.84E+05	3.84E+07	2650	0.005	0		0.00E+00					
N4800	sup-	qs	1.47E+05	1.47E+07	2650	0.0103	0.0053	2.07E+08	2.07E+08	4.02E+08				
N4800	sup+	qs	3.70E+04	3.70E+06	2650	0.0097	0.0047	4.61E+07	4.61E+07	9.52E+07				
N4800	zo	qs	7.43E+04	7.43E+06	2650	0.0036	-0.0014	-2.76E+07	0.00E+00	7.09E+07	2.26E+08	5.68E+08	4.73E+02	360

	supergene zones	hydro-thermal alteration	area [m2]	volume [m3]	masse volumique [kg/m3]	Cu [%]	enrichment	removed/added Cu		Cu in supergene zone	total removed/ added Cu of supergene zone	total Cu in supergene zone	largeur de la zone d'alteration	hypothetic high of the porphyry
N4900	prim	chl	2.84E+05	2.84E+07	2650	0.0058	0		0.00E+00					
N4900	sup-	chl	8.26E+04	8.26E+06	2650	0.0022	-0.0036	-7.88E+07	0.00E+00	4.81E+07				
N4900	sup+	chl			2650	0	0	0.00E+00	0.00E+00	0.00E+00				
N4900	zo	chl	3.40E+04	3.40E+06	2650	0.0175	0.0117	1.05E+08	1.05E+08	1.57E+08	2.65E+07	2.06E+08	3.88E+02	45
N4900	prim	po	7.05E+05	7.05E+07	2650	0.0062	0		0.00E+00					
N4900	sup-	po	1.65E+05	1.65E+07	2650	0.0108	0.0046	2.01E+08	2.01E+08	4.73E+08				
N4900	sup+	po	3.43E+04	3.43E+06	2650	0.0207	0.0145	1.32E+08	1.32E+08	1.88E+08				
N4900	zo	po	1.00E+05	1.00E+07	2650	0.0274	0.0212	5.62E+08	5.62E+08	7.26E+08	8.95E+08	1.39E+09	5.67E+02	961
N4900	prim	qs	3.84E+05	3.84E+07	2650	0.007	0		0.00E+00					
N4900	sup-	qs	1.07E+05	1.07E+07	2650	0.0092	0.0022	6.24E+07	6.24E+07	2.61E+08				
N4900	sup+	qs	5.58E+03	5.58E+05	2650	0.0308	0.0238	3.52E+07	3.52E+07	4.55E+07				
N4900	zo	qs	5.64E+04	5.64E+06	2650	0.0079	0.0009	1.34E+07	1.34E+07	1.18E+08	1.11E+08	4.24E+08	3.88E+02	154
N5000	prim	chl	2.52E+05	2.52E+07	2650	0.0026	0		0.00E+00					
N5000	sup-	chl	5.15E+04	5.15E+06	2650	0.005	0.0048	6.55E+07	6.55E+07	6.82E+07				
N5000	sup+	chl	4.17E+03	4.17E+05	2650	0.0091	0.0089	9.85E+06	9.85E+06	1.01E+07				
N5000	zo	chl	5.21E+04	5.21E+06	2650	0.0123	0.0121	1.67E+08	1.67E+08	1.70E+08	2.42E+08	2.48E+08	3.67E+02	959
N5000	prim	po	1.26E+06	1.26E+08	2650	0.0043	0		0.00E+00					
N5000	sup-	po	1.84E+05	1.84E+07	2650	0.0081	0.0038	1.86E+08	1.86E+08	3.95E+08				
N5000	sup+	po	4.86E+04	4.86E+06	2650	0.0176	0.0133	1.71E+08	1.71E+08	2.27E+08				
N5000	zo	po	1.58E+05	1.58E+07	2650	0.0149	0.0106	4.44E+08	4.44E+08	6.24E+08	8.01E+08	1.25E+09	1.00E+03	700
N5100	prim	chl	2.48E+05	2.48E+07	2650	0.0032	0		0.00E+00					
N5100	sup-	chl	5.01E+04	5.01E+06	2650	0.0044	0.0012	1.59E+07	1.59E+07	5.85E+07				
N5100	sup+	chl	9.99E+02	9.99E+04	2650	0.0213	0.0181	4.79E+06	4.79E+06	5.64E+06				
N5100	zo	chl	4.05E+04	4.05E+06	2650	0.0088	0.0056	6.01E+07	6.01E+07	9.45E+07	8.09E+07	1.59E+08	3.28E+02	291
N5100	prim	po	1.25E+06	1.25E+08	2650	0.0063	0		0.00E+00					
N5100	sup-	po	2.34E+05	2.34E+07	2650	0.01	0.0037	2.29E+08	2.29E+08	6.19E+08				
N5100	sup+	po	7.25E+04	7.25E+06	2650	0.0167	0.0104	2.00E+08	2.00E+08	3.21E+08				

	supergene zones	hydro-thermal alteration	area [m2]	volume [m3]	masse volumique [kg/m3]	Cu [%]	enrichment	removed/added Cu		Cu in supergene zone	total removed/ added Cu of supergene zone	total Cu in supergene zone	largeur de la zone d'alteration	hypothetic high of the porphyry
N5100	zo	po	1.41E+05	1.41E+07	2650	0.0068	0.0005	1.87E+07	1.87E+07	2.54E+08	4.47E+08	1.19E+09	1.02E+03	262
N5200	prim	chl	2.00E+05	2.00E+07	2650	0.0031	0		0.00E+00					
N5200	sup-	chl	4.01E+04	4.01E+06	2650	0.0046	0.0043	4.57E+07	4.57E+07	4.88E+07				
N5200	sup+	chl	1.31E+03	1.31E+05	2650	**0.0168**	0.0165	5.74E+06	5.74E+06	5.84E+06				
N5200	zo	chl	3.63E+04	3.63E+06	2650	0.0078	0.0075	7.22E+07	7.22E+07	7.51E+07	1.24E+08	1.30E+08	2.80E+02	537
N5200	prim	po	6.47E+05	6.47E+07	2650	0.0086	0		0.00E+00					
N5200	sup-	po	2.59E+05	2.59E+07	2650	0.0079	-0.0007	-4.81E+07	0.00E+00	5.43E+08				
N5200	sup+	po	4.94E+04	4.94E+06	2650	0.0227	0.0141	1.85E+08	1.85E+08	2.97E+08				
N5200	zo	po	1.38E+05	1.38E+07	2650	0.0136	0.005	1.83E+08	1.83E+08	4.97E+08	3.19E+08	1.34E+09	9.86E+02	142
N5300	prim	chl	3.17E+05	3.17E+07	2650	0.0013	0		0.00E+00					
N5300	sup-	chl	5.43E+04	5.43E+06	2650	0.0045	0.0032	4.60E+07	4.60E+07	6.47E+07				
N5300	sup+	chl	5.13E+03	5.13E+05	2650	0.0123	0.011	1.49E+07	1.49E+07	1.67E+07				
N5300	zo	chl	5.24E+04	5.24E+06	2650	0.0017	0.0004	5.55E+06	5.55E+06	2.36E+07	6.65E+07	1.05E+08	3.96E+02	488
N5300	prim	po	6.05E+05	6.05E+07	2650	0.0051	0		0.00E+00					
N5300	sup-	po	2.38E+05	2.38E+07	2650	0.0069	0.0018	1.13E+08	1.13E+08	4.35E+08				
N5300	sup+	po	2.99E+04	2.99E+06	2650	**0.0186**	0.0135	1.07E+08	1.07E+08	1.48E+08				
N5300	sup+	po	7.47E+03	7.47E+05	2650	**0.0186**	0.0135	2.67E+07	2.67E+07	3.68E+07				
N5300	zo	po	1.34E+05	1.34E+07	2650	0.0053	0.0002	7.11E+06	7.11E+06	1.88E+08	2.54E+08	8.08E+08	9.97E+02	189
N5400	prim	chl	4.17E+05	4.17E+07	2650	0.0055	0		0.00E+00					
N5400	sup-	chl	6.88E+04	6.88E+06	2650	0.0047	-0.0008	-1.46E+07	0.00E+00	8.57E+07				
N5400	sup+	chl	9.99E+03	9.99E+05	2650	0.0095	0.004	1.06E+07	1.06E+07	2.52E+07				
N5400	zo	chl	6.36E+04	6.36E+06	2650	0.0065	0.001	1.68E+07	1.68E+07	1.10E+08	1.29E+07	2.20E+08	6.42E+02	14
N5400	prim	po	6.24E+05	6.24E+07	2650	0.0049	0		0.00E+00					
N5400	sup-	po	1.77E+05	1.77E+07	2650	0.0051	0.0002	9.36E+06	9.36E+06	2.39E+08				
N5400	sup+	po	4.79E+04	4.79E+06	2650	0.0145	0.0096	1.22E+08	1.22E+08	1.84E+08				
N5400	zo	po	9.43E+04	9.43E+06	2650	0.0061	0.0012	3.00E+07	3.00E+07	1.52E+08	1.61E+08	5.75E+08	7.55E+02	164
N5500	prim	chl	4.45E+05	4.45E+07	2650	0.0027	0		0.00E+00					

	supergene zones	hydro-thermal alteration	area [m2]	volume [m3]	masse volumique [kg/m3]	Cu [%]	enrichment	removed/added Cu		Cu in supergene zone	total removed/ added Cu of supergene zone	total Cu in supergene zone	largeur de la zone d'alteration	hypothetic high of the porphyry
N5500	sup-	chl	9.81E+04	9.81E+06	2650	0.0074	0.0047	1.22E+08	1.22E+08	1.92E+08				
N5500	sup+	chl	9.21E+03	9.21E+05	2650	0.0098	0.0071	1.73E+07	1.73E+07	2.39E+07				
N5500	zo	chl	6.51E+04	6.51E+06	2650	0.0022	-0.0005	-8.62E+06	0.00E+00	3.79E+07	1.31E+08	2.54E+08	6.52E+02	281
N5500	prim	po	6.86E+05	6.86E+07	2650	0.005	0		0.00E+00					
N5500	sup-	po	8.27E+04	8.27E+06	2650	0.0037	-0.0013	-2.85E+07	0.00E+00	8.11E+07				
N5500	sup+	po	4.68E+04	4.68E+06	2650	0.004	-0.001	-1.24E+07	0.00E+00	4.96E+07				
N5500	zo	po	8.26E+04	8.26E+06	2650	0.0057	0.0007	1.53E+07	1.53E+07	1.25E+08	**-2.56E+07**	2.56E+08	7.09E+02	-27
N5600	prim	chl	4.38E+05	4.38E+07	2650	0.0032	0		0.00E+00					
N5600	sup-	chl	6.22E+04	6.22E+06	2650	0.0021	-0.0011	-1.81E+07	0.00E+00	3.46E+07				
N5600	sup+	chl	3.10E+03	3.10E+05	2650	**0.0098**	0.0066	5.43E+06	5.43E+06	8.06E+06				
N5600	zo	chl	4.60E+04	4.60E+06	2650	0.0014	-0.0018	-2.19E+07	0.00E+00	1.71E+07	**-3.47E+07**	5.98E+07	5.22E+02	-78
N5600	prim	po	7.60E+05	7.60E+07	2650	0.003	0		0.00E+00					
N5600	sup-	po	6.74E+04	6.74E+06	2650	0.0045	0.0015	2.68E+07	2.68E+07	8.03E+07				
N5600	sup+	po	3.96E+04	3.96E+06	2650	0.007	0.004	4.20E+07	4.20E+07	7.35E+07				
N5600	zo	po	9.90E+04	9.90E+06	2650	0.006	0.003	7.87E+07	7.87E+07	1.57E+08	1.48E+08	3.11E+08	7.57E+02	245
N5700	prim	chl	4.55E+05	4.55E+07	2650	0.0012	0		0.00E+00					
N5700	sup-	chl	5.65E+04	5.65E+06	2650	0.0025	0.0013	1.95E+07	1.95E+07	3.74E+07				
N5700	sup+	chl			2650	**0**	0	0.00E+00	0.00E+00	0.00E+00				
N5700	zo	chl	4.60E+04	4.60E+06	2650	0.0009	-0.0003	-3.66E+06	0.00E+00	1.10E+07	1.58E+07	4.84E+07	4.60E+02	108
N5700	prim	po	7.58E+05	7.58E+07	2650	0.0024	0		0.00E+00					
N5700	sup-	po	1.06E+05	1.06E+07	2650	0.0042	0.0018	5.08E+07	5.08E+07	1.19E+08				
N5700	zo	po	1.22E+05	1.22E+07	2650	0.0022	-0.0002	-6.49E+06	0.00E+00	7.14E+07	4.43E+07	1.90E+08	8.36E+02	83
N5800	prim	chl	6.55E+05	6.55E+07	2650	0.0017	0		0.00E+00					
N5800	sup-	chl	5.16E+04	5.16E+06	2650	0.0019	0.0002	2.73E+06	2.73E+06	2.60E+07				
N5800	sup+	chl			2650	**0**	0	0.00E+00	0.00E+00	0.00E+00				
N5800	zo	chl	5.76E+04	5.76E+06	2650	0.0003	-0.0014	-2.14E+07	0.00E+00	4.58E+06	**-1.86E+07**	3.06E+07	5.43E+02	-76
N5800	prim	po	6.24E+05	6.24E+07	2650	0.0034	0		0.00E+00					

	supergene zones	hydro-thermal alteration	area [m2]	volume [m3]	masse volumique [kg/m3]	Cu [%]	enrichment	removed/added Cu		Cu in supergene zone	total removed/ added Cu of supergene zone	total Cu in supergene zone	largeur de la zone d'alteration	hypothetic high of the porphyry
N5800	sup-	po	9.63E+04	9.63E+06	2650	0.004	0.0006	1.53E+07	1.53E+07	1.02E+08				
N5800	zo	po	1.21E+05	1.21E+07	2650	0.0025	-0.0009	-2.90E+07	0.00E+00	8.05E+07	**-1.36E+07**	1.83E+08	7.76E+02	-20
N5900	prim	chl	8.05E+05	8.05E+07	2650	0.0017	0		0.00E+00					
N5900	sup-	chl	5.76E+04	5.76E+06	2650	0.0019	0.0002	3.05E+06	3.05E+06	2.90E+07				
N5900	sup+	chl			2650	**0**	0	0.00E+00	0.00E+00	0.00E+00				
N5900	zo	chl	6.16E+04	6.16E+06	2650	0.0015	-0.0002	-3.26E+06	0.00E+00	2.45E+07	**-2.11E+05**	5.35E+07	6.77E+02	-1
N5900	prim	po	5.29E+05	5.29E+07	2650	0.0042	0		0.00E+00					
N5900	sup-	po	8.17E+04	8.17E+06	2650	0.0023	-0.0019	-4.12E+07	0.00E+00	4.98E+07				
N5900	zo	po	1.13E+05	1.13E+07	2650	0.0031	-0.0011	-3.30E+07	0.00E+00	9.31E+07	**-7.42E+07**	1.43E+08	7.12E+02	-94
N6000	prim	chl	1.00E+06	1.00E+08	2650	0.0026	0		0.00E+00					
N6000	sup-	chl	7.03E+04	7.03E+06	2650	0.0022	-0.0004	-7.46E+06	0.00E+00	4.10E+07				
N6000	sup+	chl			2650	**0**	0	0.00E+00	0.00E+00	0.00E+00				
N6000	zo	chl	9.15E+04	9.15E+06	2650	0.0018	-0.0008	-1.94E+07	0.00E+00	4.37E+07	**-2.69E+07**	8.47E+07	9.78E+02	-40
N6000	prim	po	3.91E+05	3.91E+07	2650	0.0036	0		0.00E+00					
N6000	sup-	po	6.07E+04	6.07E+06	2650	0.0078	0.0042	6.75E+07	6.75E+07	1.25E+08				
N6000	zo	po	9.31E+04	9.31E+06	2650	0.005	0.0014	3.45E+07	3.45E+07	1.23E+08	1.02E+08	2.49E+08	5.42E+02	197
N6100	prim	chl	1.11E+06	1.11E+08	2650	0.0009	0		0.00E+00					
N6100	sup-	chl	1.15E+05	1.15E+07	2650	0.0033	0.0024	7.33E+07	7.33E+07	1.01E+08				
N6100	sup+	chl			2650	**0**	0	0.00E+00	0.00E+00	0.00E+00				
N6100	zo	chl	8.73E+04	8.73E+06	2650	0.0014	0.0005	1.16E+07	1.16E+07	3.24E+07	8.49E+07	1.33E+08	1.11E+03	320
N6100	prim	po	3.12E+05	3.12E+07	2650	0.0032	0		0.00E+00					
N6100	sup-	po	4.25E+04	4.25E+06	2650	0.0032	0	0.00E+00	0.00E+00	3.61E+07				
N6100	zo	po	8.49E+04	8.49E+06	2650	0.0042	0.001	2.25E+07	2.25E+07	9.45E+07	2.25E+07	1.31E+08	5.78E+02	46
N6200	prim	chl	1.15E+06	1.15E+08	2650	0.0009	0		0.00E+00					
N6200	sup-	chl	1.32E+05	1.32E+07	2650	0.0024	0.0015	5.23E+07	5.23E+07	8.37E+07				
N6200	sup+	chl			2650	**0**	0	0.00E+00	0.00E+00	0.00E+00				
N6200	zo	chl	1.90E+05	1.90E+07	2650	0.0015	0.0006	3.02E+07	3.02E+07	7.56E+07	8.26E+07	1.59E+08	1.26E+03	276

	supergene zones	hydro-thermal alteration	area [m2]	volume [m3]	masse volumique [kg/m3]	Cu [%]	enrichment	removed/added Cu		Cu in supergene zone	total removed/ added Cu of supergene zone	total Cu in supergene zone	largeur de la zone d'alteration	hypothetic high of the porphyry
N6200	prim	po	2.43E+05	2.43E+07	2650	0.0024	0		0.00E+00					
N6200	sup-	po	2.80E+04	2.80E+06	2650	0.0052	0.0028	2.08E+07	2.08E+07	3.86E+07				
N6200	zo	po	6.16E+04	6.16E+06	2650	0.0042	0.0018	2.94E+07	2.94E+07	6.85E+07	5.02E+07	1.07E+08	3.25E+02	243
							total copper	1.97E+10	2.16E+10	4.83E+10				
								19.7 Mt	**21.6 Mt**	**48.3 Mt**				

Annex 3.1

Results of the sequential extraction on chrysocolla (sample 3, 3 aliquots) and copper pitch (sample 4, 3 aliquots) samples obtained on the solvent after each sequential extraction step by ICP-MS and/or ICP optic.

ID	sample	step	Ag	Al	As	Ba	Bi	Ca	Cd	Co	Cr	Cu	Fe
			[ug]	[ug]	[ug]	[ug]	[ug]	[ug]	[ug]	[ug]	[ug]	[ug]	[ug]
			MS	*optic*	*MS*	*MS*	*MS*	*optic*	*MS*	*MS*	*MS*	*optic*	*mix*
Sample 3.1 step 1	3.1	1	2.041E-05	5.786E+00	2.684E-03	5.054E-03	0.000E+00	5.596E+01	5.753E-02	1.737E-01	6.116E-04	8.379E+01	1.702E-02
Sample 3.2 step 1	3.2	1	0.000E+00	5.984E+00	2.650E-03	3.829E-03	0.000E+00	5.670E+01	5.145E-02	1.606E-01	4.763E-04	8.601E+01	1.400E-02
Sample 3.3 step 1	3.3	1	8.660E-06	5.785E+00	2.514E-03	4.325E-03	0.000E+00	5.872E+01	5.575E-02	1.645E-01	5.121E-04	8.649E+01	1.909E-02
Sample 4.1 step 1	4.1	1	0.000E+00	5.231E+00	1.735E-04	5.725E-03	0.000E+00	4.147E+03	5.394E-03	6.552E-02	7.785E-05	4.140E+01	4.587E-01
Sample 4.2 step 1	4.2	1	0.000E+00	4.371E+00	2.154E-04	6.196E-03	0.000E+00	3.159E+03	5.626E-03	6.798E-02	5.677E-05	3.143E+01	4.695E-01
Sample 4.3 step 1	4.3	1	0.000E+00	4.445E+00	1.966E-04	7.022E-03	0.000E+00	4.031E+03	5.723E-03	6.866E-02	0.000E+00	3.942E+01	4.941E-01
Sample 3.1 step 2	3.1	2	4.364E-02	7.744E+01	2.072E-02	2.866E-02	2.229E-02	1.922E+02	1.856E-01	3.306E-01	0.000E+00	6.157E+02	9.969E-02
Sample 3.2 step 2	3.2	2	1.786E-02	6.940E+01	1.616E-02	3.081E-02	1.044E-02	1.892E+02	1.922E-01	3.519E-01	0.000E+00	6.110E+02	2.654E-02
Sample 3.3 step 2	3.3	2	1.234E-02	4.771E+01	1.466E-02	3.169E-02	5.584E-03	1.851E+02	1.656E-01	3.456E-01	0.000E+00	6.017E+02	3.513E-02
Sample 4.1 step 2	4.1	2	9.640E-03	6.980E+01	6.300E-03	7.098E-03	3.654E-03	3.559E+03	8.745E-03	7.550E-02	0.000E+00	5.407E+02	5.262E-01
Sample 4.2 step 2	4.2	2	1.010E-02	7.064E+01	3.833E-03	1.516E-02	3.263E-03	4.294E+03	1.143E-02	7.478E-02	0.000E+00	6.576E+02	5.882E-01
Sample 4.3 step 2	4.3	2	9.246E-03	6.464E+01	4.577E-03	1.902E-02	2.046E-03	4.057E+03	9.684E-03	7.532E-02	0.000E+00	6.500E+02	7.108E-01
Sample 3.1 step 3a	3.1	3a	1.613E-02	6.871E+01	6.480E-02	5.427E-01	5.946E-04	2.357E+01	1.499E-01	1.721E+00	0.000E+00	8.660E+02	2.092E+00
Sample 3.2 step 3a	3.2	3a	1.382E-02	7.282E+01	6.668E-02	7.123E-01	1.815E-04	3.479E+01	1.866E-01	2.469E+00	3.685E-03	1.203E+03	2.736E+00
Sample 3.3 step 3a	3.3	3a	2.611E-02	7.726E+01	7.218E-02	7.048E-01	4.874E-04	3.668E+01	1.891E-01	2.334E+00	0.000E+00	1.238E+03	2.754E+00
Sample 4.1 step 3a	4.1	3a	2.967E-02	5.940E+01	5.361E-02	9.273E+00	5.721E-04	6.860E+01	3.219E-01	1.116E+02	0.000E+00	3.573E+03	2.627E+01
Sample 4.2 step 3a	4.2	3a	1.003E-02	6.361E+01	5.572E-02	1.033E+01	0.000E+00	5.747E+01	3.676E-01	1.238E+02	0.000E+00	3.769E+03	2.982E+01
Sample 4.3 step 3a	4.3	3a	1.653E-02	6.612E+01	5.674E-02	1.033E+01	2.877E-04	5.933E+01	3.560E-01	1.229E+02	0.000E+00	4.038E+03	2.962E+01
Sample 3.1 step 3b	3.1	3b	1.136E-02	7.925E+02	4.439E-01	0.000E+00	3.020E-03	N.D.	1.262E-02	1.184E-01	9.391E-02	2.538E+02	5.077E+00
Sample 3.2 step 3b	3.2	3b	1.540E-02	7.104E+02	4.272E-01	0.000E+00	2.293E-03	N.D.	1.198E-02	1.295E-01	1.065E-01	3.318E+02	5.399E+00
Sample 3.3 step 3b	3.3	3b	1.962E-02	8.051E+02	5.594E-01	0.000E+00	2.686E-03	7.470E+00	6.555E-03	1.401E-01	1.223E-01	3.887E+02	8.942E+00
Sample 4.1 step 3b	4.1	3b	3.246E-02	2.613E+02	3.270E-01	1.523E-01	3.965E-03	N.D.	5.694E-03	6.403E+00	1.209E-02	6.111E+02	2.141E+01
Sample 4.2 step 3b	4.2	3b	2.838E-02	2.749E+02	3.502E-01	1.696E-01	4.199E-03	N.D.	6.181E-03	6.114E+00	1.229E-02	7.281E+02	2.376E+01
Sample 4.3 step 3b	4.3	3b	2.054E-02	2.733E+02	3.404E-01	2.049E-01	5.589E-03	2.985E+00	6.168E-03	5.999E+00	1.001E-02	4.419E+02	2.334E+01
Sample 3.1 step 4	3.1	4	2.338E-02	4.468E+02	1.391E-01	4.585E-03	1.940E-03	N.D.	4.247E-02	7.712E-03	2.061E-01	8.944E+02	2.378E+00
Sample 3.2 step 4	3.2	4	1.825E-02	4.820E+02	1.978E-01	0.000E+00	7.274E-04	N.D.	9.293E-03	1.387E-02	2.238E-01	1.242E+03	2.765E+00

ID	sample	step	Ag	Al	As	Ba	Bi	Ca	Cd	Co	Cr	Cu	Fe
			[ug]	[ug]	[ug]	[ug]	[ug]	[ug]	[ug]	[ug]	[ug]	[ug]	[ug]
			MS	*optic*	*MS*	*MS*	*MS*	*optic*	*MS*	*MS*	*MS*	*optic*	*mix*
Sample 3.3 step 4	3.3	4	1.957E-02	4.474E+02	1.374E-01	0.000E+00	1.609E-03	N.D.	4.840E-03	4.957E-03	2.198E-01	8.776E+02	2.529E+00
Sample 4.1 step 4	4.1	4	2.386E-02	2.537E+02	4.705E-02	1.278E-02	8.611E-04	N.D.	3.278E-04	2.304E-01	5.769E-03	1.353E+03	3.396E+01
Sample 4.2 step 4	4.2	4	2.288E-02	2.605E+02	5.029E-02	2.164E-02	8.429E-04	N.D.	1.064E-03	1.774E-01	5.953E-03	2.003E+03	3.568E+01
Sample 4.3 step 4	4.3	4	1.596E-02	2.530E+02	4.310E-02	1.529E-02	1.151E-03	N.D.	0.000E+00	2.067E-01	1.403E-02	6.644E+02	3.715E+01
Sample 3.1 step 5	3.1	5	N.A.	3.837E+00	N.A.	N.A.	N.A.	3.731E-01	N.A.	N.A.	N.A.	9.419E+00	5.430E-02
Sample 3.2 step 5	3.2	5	N.A.	3.035E+00	N.A.	N.A.	N.A.	3.275E-01	N.A.	N.A.	N.A.	7.221E+00	4.780E-02
Sample 3.3 step 5	3.3	5	N.A.	2.666E+00	N.A.	N.A.	N.A.	1.509E-01	N.A.	N.A.	N.A.	4.430E+00	2.428E+00
Sample 4.1 step 5	4.1	5	N.A.	3.604E+01	N.A.	N.A.	N.A.	N.D.	N.A.	N.A.	N.A.	1.456E+01	6.133E-01
Sample 4.2 step 5	4.2	5	N.A.	3.630E+01	N.A.	N.A.	N.A.	N.D.	N.A.	N.A.	N.A.	1.944E+01	7.900E-01
Sample 4.3 step 5	4.3	5	N.A.	3.588E+01	N.A.	N.A.	N.A.	N.D.	N.A.	N.A.	N.A.	1.755E+01	7.200E-01
Sample 3.1 step 6	3.1	6	1.072E-01	3.298E+02	7.166E-02	5.533E-02	4.117E-03	1.526E+02	2.688E-01	0.000E+00	7.219E-02	4.700E+03	9.956E+00
Sample 3.2 step 6	3.2	6	1.061E-01	7.402E+02	1.349E-01	6.915E-02	5.527E-03	2.956E+02	5.332E-01	2.392E-03	1.358E-01	1.079E+04	1.584E+01
Sample 3.3 step 6	3.3	6	1.194E-01	5.725E+02	1.095E-01	6.806E-02	5.233E-03	2.046E+02	5.113E-01	0.000E+00	1.643E-01	8.524E+03	1.595E+01
Sample 4.1 step 6	4.1	6	1.085E-01	2.772E+02	6.825E-02	7.633E-02	3.762E-03	2.155E+01	1.349E-02	9.840E-02	1.119E-01	2.944E+03	9.473E+01
Sample 4.2 step 6	4.2	6	1.251E-01	3.522E+02	1.635E-01	5.182E-01	6.517E-03	1.494E+03	5.502E-02	4.597E-01	6.575E-02	4.047E+03	1.862E+02
Sample 4.3 step 6	4.3	6	1.188E-01	3.671E+02	9.832E-02	8.517E-02	3.402E-03	8.625E+00	1.658E-02	1.529E-01	1.078E-02	4.168E+03	1.350E+02

	sample	step	K	La	Li	Mg	Mn	Mo	Na	Ni	P	Pb	Sb
			[ug]	[ug]	[ug]	[ug]	[ug]	[ug]	[ug]	[ug]	[ug]	[ug]	[ug]
			optic	*MS*	*optic*	*MS*	*mix*	*MS*	*MS*	*MS*	*optic*	*mix*	*MS*
Sample 3.1 step 1	3.1	1	3.040E+01	7.263E-04	N.D.	5.664E+01	1.274E+01	4.886E-03	1.528E+02	1.123E-01	4.926E+00	7.201E-04	1.351E-04
Sample 3.2 step 1	3.2	1	3.161E+01	6.199E-04	N.D.	5.270E+01	1.182E+01	3.631E-03	1.433E+02	1.043E-01	5.134E+00	4.626E-05	1.036E-04
Sample 3.3 step 1	3.3	1	3.155E+01	6.956E-04	N.D.	5.407E+01	1.209E+01	3.129E-03	1.475E+02	1.066E-01	4.976E+00	5.840E-05	1.219E-04
Sample 4.1 step 1	4.1	1	1.934E+01	4.415E-04	N.D.	3.865E+01	1.769E+00	6.878E-03	1.087E+02	9.910E-03	4.817E+00	7.815E-05	5.462E-05
Sample 4.2 step 1	4.2	1	1.543E+01	4.376E-04	6.888E+00	4.058E+01	1.822E+00	7.087E-03	1.142E+02	9.496E-03	4.815E+00	0.000E+00	0.000E+00
Sample 4.3 step 1	4.3	1	1.854E+01	5.271E-04	N.D.	4.126E+01	1.845E+00	7.436E-03	1.160E+02	9.508E-03	4.811E+00	2.925E-07	7.248E-06
Sample 3.1 step 2	3.1	2	5.612E+01	7.617E-02	1.590E+02	1.368E+02	2.706E+01	2.549E-01	1.944E+01	1.726E-01	3.431E+02	0.000E+00	1.246E-01
Sample 3.2 step 2	3.2	2	4.976E+01	6.425E-02	1.728E+02	1.476E+02	2.922E+01	1.187E-01	1.921E+01	1.849E-01	3.418E+02	0.000E+00	6.096E-02
Sample 3.3 step 2	3.3	2	5.204E+01	6.053E-02	1.309E+02	1.486E+02	2.905E+01	7.351E-02	2.145E+01	1.821E-01	3.424E+02	0.000E+00	3.644E-02
Sample 4.1 step 2	4.1	2	5.184E+01	2.284E-03	1.452E+02	8.626E+00	2.434E+00	2.701E-02	2.000E+01	0.000E+00	3.415E+02	0.000E+00	2.623E-02
Sample 4.2 step 2	4.2	2	4.720E+01	2.823E-03	6.244E+01	9.085E+00	2.467E+00	1.410E-02	2.027E+01	0.000E+00	3.419E+02	0.000E+00	2.090E-02
Sample 4.3 step 2	4.3	2	4.264E+01	2.903E-03	4.602E+01	8.853E+00	2.646E+00	3.639E-03	1.938E+01	0.000E+00	3.412E+02	0.000E+00	1.546E-02
Sample 3.1 step 3a	3.1	3a	8.785E+00	1.289E-02	1.625E+02	2.119E+00	1.211E+02	1.055E-01	4.666E-01	1.420E-02	3.006E+02	0.000E+00	7.415E-03
Sample 3.2 step 3a	3.2	3a	1.855E+01	1.416E-02	1.208E+02	3.150E+00	1.697E+02	9.489E-02	6.749E-01	4.809E-02	3.003E+02	0.000E+00	5.255E-03
Sample 3.3 step 3a	3.3	3a	1.932E+01	1.469E-02	8.062E+01	4.307E+00	1.617E+02	8.471E-02	7.274E-01	3.722E-02	3.007E+02	0.000E+00	7.169E-03
Sample 4.1 step 3a	4.1	3a	4.660E+01	1.005E-02	2.155E+02	1.328E+00	4.287E+03	4.110E+00	9.556E+00	6.262E-02	2.993E+02	1.352E-01	9.679E-03
Sample 4.2 step 3a	4.2	3a	7.284E+01	1.167E-02	2.001E+02	1.491E+00	4.765E+03	4.461E+00	1.046E+01	6.978E-02	2.987E+02	1.659E-01	4.285E-03
Sample 4.3 step 3a	4.3	3a	7.525E+01	1.206E-02	1.469E+02	1.375E+00	4.700E+03	4.447E+00	1.059E+01	6.781E-02	2.989E+02	1.548E-01	6.560E-03
Sample 3.1 step 3b	3.1	3b	2.745E+01	2.752E-03	1.490E+02	5.548E+00	1.200E+01	7.269E-01	3.438E-01	0.000E+00	3.525E+02	0.000E+00	6.882E-03
Sample 3.2 step 3b	3.2	3b	2.601E+01	1.835E-03	1.499E+02	6.162E+00	1.115E+01	7.027E-01	1.473E+00	1.912E-01	3.432E+02	0.000E+00	7.519E-03
Sample 3.3 step 3b	3.3	3b	3.012E+01	2.168E-03	1.334E+02	7.025E+00	1.222E+01	8.919E-01	1.460E+00	3.749E-02	3.657E+02	0.000E+00	1.019E-02
Sample 4.1 step 3b	4.1	3b	3.381E+01	1.243E-03	1.673E+02	1.095E+00	2.017E+02	3.396E+00	2.860E-01	3.153E-02	2.767E+02	0.000E+00	1.512E-02
Sample 4.2 step 3b	4.2	3b	3.042E+01	9.788E-04	1.530E+02	1.232E+00	1.903E+02	3.718E+00	1.056E-01	1.344E-02	2.779E+02	0.000E+00	1.022E-02
Sample 4.3 step 3b	4.3	3b	3.078E+01	1.245E-03	2.824E+02	1.206E+00	1.958E+02	3.599E+00	6.144E-01	2.174E-02	2.771E+02	0.000E+00	1.424E-02
Sample 3.1 step 4	3.1	4	2.503E+01	6.313E-03	3.504E+02	4.397E+00	1.621E+00	1.227E-01	0.000E+00	8.783E-03	3.408E+02	0.000E+00	1.037E-02
Sample 3.2 step 4	3.2	4	3.780E+01	1.799E-03	1.451E+02	4.393E+00	2.168E+00	2.136E-01	0.000E+00	4.636E-04	3.602E+02	0.000E+00	8.956E-03
Sample 3.3 step 4	3.3	4	2.573E+01	1.567E-03	2.890E+02	4.434E+00	1.288E+00	1.412E-01	3.668E-03	0.000E+00	3.447E+02	0.000E+00	1.031E-02
Sample 4.1 step 4	4.1	4	3.857E+01	2.154E-03	1.543E+02	1.213E+00	1.333E+01	6.372E-01	0.000E+00	0.000E+00	3.015E+02	0.000E+00	1.186E-02
Sample 4.2 step 4	4.2	4	3.252E+01	3.786E-03	1.174E+02	1.298E+00	1.016E+01	7.675E-01	0.000E+00	0.000E+00	3.014E+02	0.000E+00	1.316E-02
Sample 4.3 step 4	4.3	4	3.283E+01	3.308E-03	1.262E+02	1.414E+00	1.146E+01	7.222E-01	0.000E+00	1.184E-01	3.003E+02	0.000E+00	9.363E-03

	sample	step	K	La	Li	Mg	Mn	Mo	Na	Ni	P	Pb	Sb
			[ug]	[ug]	[ug]	[ug]	[ug]	[ug]	[ug]	[ug]	[ug]	[ug]	[ug]
			optic	*MS*	*optic*	*MS*	*mix*	*MS*	*MS*	*MS*	*optic*	*mix*	*MS*
Sample 3.1 step 5	3.1	5	N.D.	N.A.	N.D.	N.A.	6.860E-02	N.A.	N.A.	N.A.	4.252E+01	2.000E-03	N.A.
Sample 3.2 step 5	3.2	5	N.D.	N.A.	N.D.	N.A.	1.000E-01	N.A.	N.A.	N.A.	4.982E+01	2.000E-03	N.A.
Sample 3.3 step 5	3.3	5	N.D.	N.A.	N.D.	N.A.	8.920E-02	N.A.	N.A.	N.A.	4.606E+01	1.200E-03	N.A.
Sample 4.1 step 5	4.1	5	1.810E+01	N.A.	1.809E+02	N.A.	5.900E+00	N.A.	N.A.	N.A.	2.082E+02	N.D.	N.A.
Sample 4.2 step 5	4.2	5	1.924E+01	N.A.	1.228E+02	N.A.	4.280E+00	N.A.	N.A.	N.A.	2.142E+02	N.D.	N.A.
Sample 4.3 step 5	4.3	5	2.128E+01	N.A.	1.253E+02	N.A.	6.300E+00	N.A.	N.A.	N.A.	2.118E+02	N.D.	N.A.
Sample 3.1 step 6	3.1	6	1.908E+04	1.595E-01	6.975E+02	3.360E+00	1.820E+00	5.468E-02	1.012E+01	0.000E+00	4.727E+02	1.031E-02	6.019E-02
Sample 3.2 step 6	3.2	6	2.304E+04	2.663E-01	1.757E+02	6.429E+00	4.713E+00	8.280E-02	1.569E+01	0.000E+00	4.841E+02	1.300E-02	6.563E-02
Sample 3.3 step 6	3.3	6	2.015E+04	2.624E-01	3.958E+02	5.486E+00	3.444E+00	6.501E-02	1.388E+01	0.000E+00	4.762E+02	1.745E-02	6.712E-02
Sample 4.1 step 6	4.1	6	2.169E+04	1.277E-02	3.538E+02	1.544E+00	6.020E+00	2.052E-01	1.113E+01	2.564E-01	4.323E+02	4.958E-02	5.605E-02
Sample 4.2 step 6	4.2	6	2.252E+04	2.361E-02	4.568E+02	3.133E+01	9.048E+00	2.497E-01	1.830E+01	3.650E-01	4.321E+02	3.654E-01	6.493E-02
Sample 4.3 step 6	4.3	6	2.159E+04	2.058E-02	3.775E+01	1.507E+00	8.510E+00	2.151E-01	1.311E+01	0.000E+00	4.329E+02	5.555E-02	5.672E-02

ID	sample	step	Se	Si	Sn	Sr	Ti	V	W	Y	Zn
			[ug]	[ug]	[ug]	[ug]	[ug]	[ug]	[ug]	[ug]	[ug]
			MS	*optic*	*MS*	*MS*	*MS*	*MS*	*MS*	*MS*	*MS*
Sample 3.1 step 1	3.1	1	1.736E-03	2.394E+01	1.660E-04	5.730E-01	4.408E-05	8.169E-03	2.713E-02	2.117E-03	1.416E+01
Sample 3.2 step 1	3.2	1	2.769E-03	2.455E+01	1.688E-04	5.323E-01	3.182E-04	8.257E-03	4.721E-02	1.837E-03	1.322E+01
Sample 3.3 step 1	3.3	1	2.593E-03	2.431E+01	1.406E-04	5.481E-01	1.739E-04	7.883E-03	3.528E-02	2.055E-03	1.352E+01
Sample 4.1 step 1	4.1	1	2.384E-03	2.023E+01	1.997E-04	2.397E+00	4.305E-04	5.063E-05	1.230E-01	3.301E-03	2.127E+00
Sample 4.2 step 1	4.2	1	1.908E-03	1.538E+01	1.187E-04	2.515E+00	3.804E-04	5.792E-05	5.515E-02	3.321E-03	2.212E+00
Sample 4.3 step 1	4.3	1	1.854E-03	1.991E+01	9.855E-05	2.555E+00	1.455E-04	5.468E-05	3.153E-02	3.386E-03	2.228E+00
Sample 3.1 step 2	3.1	2	2.448E-02	1.316E+01	1.304E-01	2.013E+00	5.772E-04	1.018E-02	4.676E-02	1.821E-01	3.295E+01
Sample 3.2 step 2	3.2	2	3.970E-02	1.138E+01	7.056E-02	2.133E+00	0.000E+00	8.965E-03	7.918E-02	1.804E-01	3.474E+01
Sample 3.3 step 2	3.3	2	2.666E-02	1.252E+01	3.837E-02	2.153E+00	9.784E-03	8.848E-03	0.000E+00	1.664E-01	3.516E+01
Sample 4.1 step 2	4.1	2	0.000E+00	1.668E+01	3.101E-02	1.719E+00	0.000E+00	0.000E+00	0.000E+00	2.162E-02	1.668E+00
Sample 4.2 step 2	4.2	2	6.027E-02	2.166E+01	2.512E-02	1.752E+00	0.000E+00	0.000E+00	0.000E+00	2.507E-02	1.689E+00
Sample 4.3 step 2	4.3	2	1.980E-02	2.302E+01	1.787E-02	1.767E+00	0.000E+00	0.000E+00	0.000E+00	2.290E-02	1.806E+00
Sample 3.1 step 3a	3.1	3a	0.000E+00	5.136E+01	9.021E-03	3.048E-01	0.000E+00	1.029E+00	1.157E-01	3.564E-02	1.202E+01
Sample 3.2 step 3a	3.2	3a	9.023E-04	6.916E+01	6.483E-03	4.306E-01	0.000E+00	1.412E+00	9.607E-03	4.550E-02	1.724E+01
Sample 3.3 step 3a	3.3	3a	4.153E-04	7.019E+01	1.009E-02	4.259E-01	0.000E+00	1.369E+00	1.887E-02	4.561E-02	1.700E+01
Sample 4.1 step 3a	4.1	3a	7.263E-02	2.483E+01	1.428E-02	1.983E+00	0.000E+00	5.150E-01	0.000E+00	2.139E-01	2.162E+01
Sample 4.2 step 3a	4.2	3a	6.393E-02	2.697E+01	4.786E-03	2.203E+00	2.244E-02	5.741E-01	1.350E-02	2.626E-01	2.431E+01
Sample 4.3 step 3a	4.3	3a	6.665E-02	2.916E+01	9.528E-03	2.207E+00	0.000E+00	5.645E-01	6.485E-03	2.525E-01	2.390E+01
Sample 3.1 step 3b	3.1	3b	4.697E-02	1.858E+02	1.264E-02	9.763E-03	2.006E-02	9.687E-01	6.677E-01	2.770E-01	4.580E+00
Sample 3.2 step 3b	3.2	3b	2.083E-02	1.430E+02	1.295E-02	8.368E-03	2.055E-02	9.606E-01	9.605E-01	2.214E-01	4.861E+00
Sample 3.3 step 3b	3.3	3b	3.631E-02	1.796E+02	2.344E-02	1.563E-02	0.000E+00	1.172E+00	7.529E-01	2.992E-01	5.098E+00
Sample 4.1 step 3b	4.1	3b	2.989E-02	2.745E+01	3.028E-02	7.044E-02	2.495E-01	7.328E-02	4.991E-01	1.815E-01	3.331E+00
Sample 4.2 step 3b	4.2	3b	5.187E-02	2.685E+01	2.204E-02	8.598E-02	2.597E-01	7.530E-02	5.668E-01	1.969E-01	3.594E+00
Sample 4.3 step 3b	4.3	3b	6.642E-02	2.678E+01	2.514E-02	9.424E-02	2.400E-01	7.188E-02	5.499E-01	1.937E-01	3.007E+00
Sample 3.1 step 4	3.1	4	2.762E-02	2.775E+02	2.566E-02	1.971E-02	5.537E-04	7.157E-01	4.500E-01	1.018E-01	9.794E+00
Sample 3.2 step 4	3.2	4	2.355E-02	2.588E+02	1.845E-02	1.778E-02	8.883E-03	6.984E-01	7.841E-01	1.095E-01	4.094E+00
Sample 3.3 step 4	3.3	4	1.965E-02	2.882E+02	1.960E-02	1.217E-02	1.502E-02	7.186E-01	6.013E-01	9.847E-02	3.396E+00
Sample 4.1 step 4	4.1	4	3.041E-02	1.653E+02	2.575E-02	3.981E-02	1.421E-01	2.390E-02	3.997E-01	5.285E-02	7.417E-01
Sample 4.2 step 4	4.2	4	2.069E-02	1.637E+02	2.148E-02	4.428E-02	1.348E-01	2.429E-02	1.564E-01	4.825E-02	8.616E-01
Sample 4.3 step 4	4.3	4	4.067E-02	1.516E+02	1.696E-02	3.883E-02	1.185E-01	2.256E-02	1.902E-01	4.465E-02	8.105E-01

ID	sample	step	Se	Si	Sn	Sr	Ti	V	W	Y	Zn
			[ug]	[ug]	[ug]	[ug]	[ug]	[ug]	[ug]	[ug]	[ug]
			MS	*optic*	*MS*	*MS*	*MS*	*MS*	*MS*	*MS*	*MS*
Sample 3.1 step 5	3.1	5	N.A.	1.249E+01	N.A.	N.A.	N.A.	N.A.	N.A.	N.A.	N.A.
Sample 3.2 step 5	3.2	5	N.A.	1.640E+01	N.A.	N.A.	N.A.	N.A.	N.A.	N.A.	N.A.
Sample 3.3 step 5	3.3	5	N.A.	7.299E+00	N.A.	N.A.	N.A.	N.A.	N.A.	N.A.	N.A.
Sample 4.1 step 5	4.1	5	N.A.	3.380E+00	N.A.	N.A.	N.A.	N.A.	N.A.	N.A.	N.A.
Sample 4.2 step 5	4.2	5	N.A.	4.960E+00	N.A.	N.A.	N.A.	N.A.	N.A.	N.A.	N.A.
Sample 4.3 step 5	4.3	5	N.A.	5.020E+00	N.A.	N.A.	N.A.	N.A.	N.A.	N.A.	N.A.
Sample 3.1 step 6	3.1	6	1.035E-01	1.253E+01	4.695E-01	2.186E-01	7.333E-02	7.408E-01	6.330E+00	2.981E-01	2.853E+01
Sample 3.2 step 6	3.2	6	5.813E-02	3.065E+01	9.357E-01	3.914E-01	8.560E-02	1.350E+00	5.619E-01	5.336E-01	5.597E+01
Sample 3.3 step 6	3.3	6	4.667E-02	2.310E+01	1.003E+00	3.344E-01	1.512E-01	1.244E+00	2.595E-01	4.885E-01	4.840E+01
Sample 4.1 step 6	4.1	6	6.045E-02	1.998E+01	7.297E-01	1.295E-01	1.776E-01	5.655E-02	3.902E+00	8.094E-02	5.264E+00
Sample 4.2 step 6	4.2	6	8.059E-02	1.993E+01	1.702E+00	3.762E+00	2.586E-01	9.846E-02	2.916E+00	1.189E-01	1.240E+01
Sample 4.3 step 6	4.3	6	2.611E-02	1.903E+01	9.881E-01	1.224E-01	2.855E-01	7.246E-02	4.913E-01	1.098E-01	7.265E+00